Metabolic processes and ecological adaptations of phytoplankton in oligotrophic environments

A Theoretical and Experimental Approach

Eleni Livanou

A thesis submitted in partial fulfillment of the requirements for the degree of Doctor of Philosophy

University of Crete
School of Sciences and Engineering
Department of Biology

Heraklion, June 2020

Διερεύνηση μεταβολικών διεργασιών και οικολογικών προσαρμογών του φυτοπλαγκτού στα ολιγοτροφικά περιβάλλοντα

Μία Θεωρητική και Πειραματική Προσέγγιση

Ελένη Λιβανού

Διδακτορική Διατριβή

Πανεπιστήμιο Κρήτης
Σχολή Θετικών και Τεχνολογικών Επιστημών
Τμήμα Βιολογίας

Ηράκλειο, Ιούνιος 2020

Επιβλέπουσα Καθηγήτρια

Κωνσταντία Λύκα (Αναπληρώτρια Καθηγήτρια, Πανεπιστήμιο Κρήτης)

Επιβλέπουσα Ερευνήτρια

Στέλλα Ψαρρά (Διευθύντρια Ερευνών, Ελληνικό Κέντρο Θαλασσίων Ερευνών)

Συμβουλευτική και Εξεταστική Επιτροπή

Κωνσταντία Λύκα (Αναπληρώτρια Καθηγήτρια, Πανεπιστήμιο Κρήτης)

Στέλλα Ψαρρά (Διευθύντρια Ερευνών, Ελληνικό Κέντρο Θαλασσίων Ερευνών)

Κυριάκος Κοτζαμπάσης (Καθηγητής, Πανεπιστήμιο Κρήτης)

Εξεταστική Επιτροπή

Ιωάννης Καρακάσης (Καθηγητής, Πανεπιστήμιο Κρήτης)

Παρασκευή Πήττα (Διευθύντρια Ερευνών, Ελληνικό Κέντρο Θαλασσίων Ερευνών)

Γεώργιος Πετυχάκης (Διευθυντής Ερευνών, Ελληνικό Κέντρο Θαλασσίων Ερευνών)

Ουρανία Χρηστάκη (Καθηγήτρια, Université du Littoral Côte d'Opale)

Πρόλογος

Με την ολοκλήρωση της παρούσας διδακτορικής διατριβής μια μακρά πορεία επιστημονικής (κάποιες φορές και εσωτερικής) αναζήτησης φτάνει στο τέλος της. Η πορεία αυτή ήταν γεμάτη μοναδικές εμπειρίες, αρκετές από αυτές ευχάριστες, κάποιες από αυτές διδακτικές αλλά ποτέ μοναχικές, καθώς σε κάθε βήμα είχα πάντα δίπλα μου δασκάλους, συνεργάτες, φίλους και συγγενείς. Για το λόγο αυτό θα ήθελα στις γραμμές που ακολουθούν να ευχαριστήσω τους ανθρώπους που χωρίς την βοήθεια και παρουσία τους στη ζωή μου δεν θα ήταν δυνατή η ολοκλήρωση της εργασίας αυτής.

Αρχικά, θα ήθελα να ευχαριστήσω θερμά το Ίδρυμα Μποδοσάκη για τη χορήγηση διετούς υποτροφίας για διδακτορικές σπουδές. Η διδακτορική αυτή διατριβή χρηματοδοτήθηκε επίσης μέσω υποτροφίας από το κληροδότημα "Μαρίας Μιχαήλ Μανασσάκη". Η οικονομική ενίσχυση μέσω των δύο αυτών υποτροφιών ήταν καθοριστική για την επιτυχή ολοκλήρωση της παρούσας διατριβής.

Μέρος της παρούσας διδακτορικής διατριβής πραγματοποιήθηκε στα πλαίσια της ωκεανογραφικής αποστολής LEVECO, η οποία έλαβε χώρα στα πλαίσια του προγράμματος "Διεπιστημονική ωκεανογραφική έρευνα του Λιβυκού Πελάγους νοτίως του Ελληνικού Τόξου: Θαλάσσιο περιβάλλον, ευαίσθητα/ακραία οικοσυστήματα και υποθαλάσσιοι ενεργειακοί πόροι" υποέργο του εθνικού προγράμματος "Αειφορική αξιοποίηση των οικοσυστημάτων των θαλασσών και εσωτερικών υδάτων της Α. Μεσογείου στο πλαίσιο της Γαλάζιας Ανάπτυξης" χρηματοδοτούμενο από τη Γενική Γραμματεία Έρευνας και Τεχνολογίας-ΓΓΕΤ, μέσω των Προγραμματικών Συμφωνιών Ερευνητικών Κέντρων–ΓΓΕΤ/ΙΚΥ/SIEMENS 2014–2016. Ιδιαίτερες ευχαριστίες απευθύνονται στον καπετάνιο, στους αξιωματικούς και στο πλήρωμα του ωκεανογραφικού πλοίου ΑΙΓΑΙΟ. Παράλληλα, η παρούσα μελέτη χρηματοδοτήθηκε από τα ακόλουθα εθνικά προγράμματα: 1) "Σύστημα περιβαλλοντικής παρακολούθησης των Ελληνικών θαλασσών με τη χρήση δορυφορικών τηλεπισκοπικών δεδομένων και *in-situ* μετρήσεων" με τη χρηματοδότηση της Ευρωπαϊκής Ένωσης και εθνικών πόρων μέσω του Ε.Π. Ανταγωνιστικότητα, Επιχειρηματικότητα & Καινοτομία (ΕΠΑνΕΚ, ΕΣΠΑ 2014–2020) του Υπουργείου Οικονομίας και Ανάπτυξης. 2) "SeaDataCloud–Further developing the pan-European infrastructure for marine and ocean data management" με τη χρηματοδότηση της Ευρωπαϊκής Ένωσης.

Ένα θερμό ευχαριστώ οφείλω στα μέλη της Τριμελούς Συμβουλευτικής Επιτροπής, Ντίνα Λύκα, Στέλλα Ψαρρά και Κυριάκο Κοτζαμπάση για την καθοδήγηση, τις συζητήσεις, τις συμβουλές τους και την άψογη συνεργασία. Ιδιαίτερα όμως θέλω να αναφερθώ στις δύο επιβλέπουσες της διατριβής αυτής. Η Ντίνα Λύκα ήταν αυτή που, από τις προπτυχιακές μου ακόμη σπουδές, μου έμαθε τον κόσμο της Μαθηματικής Βιολογίας. Ήταν πάντα δίπλα μου όλα αυτά τα χρόνια σαν δασκάλα αλλά και σαν φίλη. Την ευχαριστώ για την απεριόριστη διάθεση και υπομονή της να συζητήσει μαζί μου όλες τις απορίες και τους προβληματισμούς, για όσα μου έμαθε, γιατί με άφηνε να περιπλανηθώ και γιατί με βοηθούσε να βρω το δρόμο όταν χανόμουν. Η Στέλλα Ψαρρά ήταν αυτή που μου έδωσε το εισιτήριο

και μου έδειξε τον κόσμο της Βιολογικής Ωκεανογραφίας. Την ευχαριστώ γιατί με εμπιστεύθηκε και μου έμαθε από το μηδέν πως οργανώνεται και υλοποιείται ένα πείραμα. Με αστείρευτη αισιοδοξία και ενθουσιασμό, αφιερώνοντας χρόνο και ενέργεια, ενθάρρυνε και υποστήριξε πρακτικά και ηθικά κάθε μου προσπάθεια όλα αυτά τα χρόνια. Την ευχαριστώ επίσης γιατί πίστευε σε εμένα όταν δεν μπορούσα να το κάνω εγώ.

Ευχαριστώ θερμά τα μέλη της Εξεταστικής Επιτροπής, Ιωάννη Καρακάση και Γεώργιο Πετυχάκη, που δέχθηκαν να συμμετέχουν και να αφιερώσουν χρόνο στην αξιολόγηση της διδακτορικής αυτής διατριβής. Ευχαριστώ, επίσης, την Παρασκευή Πήττα, ως μέλος της Εξεταστικής Επιτροπής, αλλά και για τη βοήθεια και τις συμβουλές της στα πρώτα μου βήματα στον τομέα της θαλάσσιας μικροβιολογίας. Ένα μεγάλο ευχαριστώ οφείλω στην Ουρανία Χρηστάκη, ως μέλος της Εξεταστικής Επιτροπής, αλλά κυρίως για την αμέριστη βοήθεια και υποστήριξη στα πειράματα θήρευσης νανομαστιγωτών που, χωρίς την καθοδήγηση της, δεν θα ήταν δυνατό να ολοκληρωθούν. Ένα θερμό ευχαριστώ οφείλω επίσης τόσο στην Ουρανία Χρηστάκη όσο και στο συνεργάτη της, καθηγητή Ludwig Jardillier, για την ευκαιρία που μου έδωσαν να βρεθώ στη Γαλλία, στο Université Paris-Sud και για τα όσα μου έμαθαν σχετικά με τις σύγχρονες τεχνικές στη θαλάσσια μικροβιολογία. Ευχαριστώ επίσης την Ήρα Καραγιάννη για την καθοδήγηση και τις συμβουλές της για τα πειράματα θήρευσης νανομαστιγωτών.

Δύο άνθρωποι έπαιξαν καθοριστικό ρόλο στην επιτυχή ολοκλήρωση της εργασίας αυτής, τόσο ως επιστήμονες αλλά και ως φίλοι, η Άννα Λαγαρία και ο Ανδρέας Οικονόμου. Η Άννα ήταν ο καταλύτης για να ξεκινήσει αυτή η διεπιστημονική διδακτορική διατριβή. Την ευχαριστώ για όλα όσα μου έμαθε, για τον προσωπικό χρόνο που αφιέρωσε για να με βοηθήσει, για την φιλία της και γιατί ήταν πάντα δίπλα μου όλα αυτά τα χρόνια. Ο Ανδρέας ήρθε στο ΕΛΚΕΘΕ στη μέση του διδακτορικού μου, όταν όλα φαίνονταν ακόμη βουνό και με βοήθησε να ξαναδώ την αισιόδοξη πλευρά. Τον ευχαριστώ γιατί ήταν οργανωτικός και μεθοδικός όταν εγώ δεν μπορούσα να σκεφτώ καθαρά, για την αμέριστη βοήθεια και υποστήριξή του όλον αυτόν τον καιρό, για τις συζητήσεις μας και για τη φιλία του. Επίσης, είμαι ευγνώμων στη Βίβιαν Μάρα για τις επιστημονικές συμβουλές, την ανιδιοτελή βοήθεια και την ενθάρρυνση στα πρώτα στάδια της δουλειάς αυτής.

Ευχαριστώ, επίσης, τις συναδέλφους μου στο ΕΛΚΕΘΕ που μοιραστήκαμε το ίδιο γραφείο, Άννα Ζαχαριουδάκη και Ιλιάνα Σαντή και το συνάδελφό μου στο Πανεπιστήμιο, Ορέστη Σταυρακίδη για την καλή διάθεση, το χιούμορ και τις ευχάριστες κουβέντες στα διαλείμματα που έδιναν μία νότα αισιοδοξίας στην καθημερινότητα. Ιδιαίτερα στην Ιλιάνα, οφείλω ένα μεγάλο ευχαριστώ για τη βοήθεια της στα πρώτα μου βήματα στο εργαστήριο και την υπέροχη συνεργασία μας. Αν και η ίδια υποψήφια διδάκτορας εκείνη την περίοδο, πάντα έβρισκε το χρόνο να με βοηθήσει και να συζητήσει μαζί μου τις ατελείωτες απορίες μου.

Ιδιαίτερες ευχαριστίες απευθύνονται επίσης στις Ελένη Δαφνομήλη και Snezana Zivanovic για τις χημικές αναλύσεις και τους Νεκτάριο Σπυριδάκη, Μανώλη Πέττα και Δημήτριο Ανδρουλάκη για την τεχνική υποστήριξη κατά τη διάρκεια των δειγματοληψιών. Ευχαριστώ επίσης τον Μανώλη Μανδαλάκη για την άψογη συνεργασία και τις αναλύσεις HPLC και την Αλεξάνδρα Παυλίδου για τα δεδομένα θρεπτικών αλατών κατά την ωκεανογραφική αποστολή LEVECO.

Πέρα από την υποστήριξη που είχα από τους άμεσα εμπλεκόμενους, δεν θα μπορούσα να ολοκληρώσω αυτή την εργασία χωρίς την ηθική, ψυχολογική και πρακτική υποστήριξη των φίλων και της οικογένειας μου. Είμαι ευγνώμων που έχω στη ζωή μου φίλες σαν την Ελένη και τη Μαριάννα. Τις ευχαριστώ για τις ψυχοθεραπευτικές ατελείωτες συζητήσεις, την αλληλοϋποστήριξη, το χιούμορ,

τις αξέχαστες διακοπές και την υπέροχη ενέργεια τους. Ευχαριστώ επίσης όλους τους φίλους, ιστιοπλόους και δύτες, για τις όμορφες στιγμές στη θάλασσα που ανανέωναν τη διάθεση μου. Ένα μεγάλο ευχαριστώ πάει στον Μάνο για τους ιστιοπλοϊκούς αγώνες και τις θαλασσινές πορείες που κάναμε μαζί, τα οποία μου έδιναν την ενέργεια να συνεχίσω, αλλά και γιατί ήταν πάντα δίπλα μου από την αρχή μέχρι το τέλος αυτού του ταξιδιού.

Τέλος, ευχαριστώ όλη μου τη μεγάλη οικογένεια για την ανιδιοτελή αγάπη και υποστήριξη και για το μοναδικό δεσμό που έχουμε μεταξύ μας, ο οποίος μου δίνει δύναμη να προχωράω στη ζωή μου. Ιδιαίτερα, ευχαριστώ τους γονείς μου, Παναγιώτη και Φιλιώ, για όσα μου έμαθαν, για όσα έχουν κάνει για εμένα όλα αυτά τα χρόνια και για τη στήριξή τους σε κάθε μου προσπάθεια, καθώς και τα αδέλφια μου Κωνσταντίνο και Δέσποινα, γιατί υπάρχουν στη ζωή μου και την κάνουν ομορφότερη.

Περίληψη

Στην παρούσα διδακτορική διατριβή διερευνώνται δύο πτυχές της οικοφυσιολογίας του φυτοπλαγκτού, οι οποίες είναι ιδιαίτερα σημαντικές στα ολιγοτροφικά υδάτινα οικοσυστήματα. Η πρώτη σχετίζεται με το μηχανισμό της απέκκρισης διαλυτού οργανικού υλικού από τα φωτοσυνθετικά κύτταρα σε μεταβαλλόμενες συνθήκες διαθεσιμότητας θρεπτικών. Η δεύτερη αφορά τη μικτοτροφία στα φωτοσυνθετικά νανομαστιγωτά, δηλαδή το συνδυασμό αυτοτροφίας μέσω της φωτοσύνθεσης (φωτοτροφία) και ετεροτροφίας μέσω της φαγοκυττάρωσης βακτηρίων (φαγοτροφία). Τα αποτελέσματα της παρούσας μελέτης προκύπτουν από το συνδυασμό θεωρητικών και πειραματικών προσεγγίσεων.

Με σκοπό τη διερεύνηση και κατανόηση της διαδικασίας της απέκκρισης διαλυτού οργανικού υλικού από τα φωτοσυνθετικά κύτταρα σε συνθήκες υψηλής και χαμηλής διαθεσιμότητας θρεπτικών αναπτύχθηκε ένα μαθηματικό μοντέλο βασισμένο στη θεωρία Δυναμικού Ενεργειακού Ισοζυγίου (Dynamic Energy Budget, DEB). Στα πλαίσια της θεωρίας DEB προκύπτουν δύο εναλλακτικά μονοπάτια απέκκρισης οργανικού υλικού. Το πρώτο σχετίζεται με την αύξηση και τη λύση των κυττάρων και το δεύτερο με την απόρριψη υποστρωμάτων λόγω στοιχειομετρικών περιορισμών. Τα δύο αυτά μονοπάτια αντιστοιχούν στους δύο θεωρητικούς μηχανισμούς απέκκρισης οργανικού υλικού, οι οποίοι είναι η παθητική διάχυση και η ενεργός απέκκριση. Η σχετική συνεισφορά των δύο μηχανισμών στην απέκκριση του οργανικού υλικού από τα φωτοσυνθετικά κύτταρα εξαρτάται από τη διαθεσιμότητα των θρεπτικών και επηρεάζει ποιοτικά το παραγόμενο διαλυτό οργανικό υλικό, σε ότι αφορά τη στοιχειακή και μοριακή σύσταση αλλά και το μοριακό βάρος. Οι ιδιότητες αυτές με τη σειρά τους μπορεί να έχουν σημαντικές επιπτώσεις στη βιοδιαθεσιμότητα του παραγόμενου διαλυτού οργανικού υλικού για τα βακτήρια.

Εστιάζοντας στη μικτοτροφία στα φωτοσυνθετικά νανομαστιγωτά, αναπτύχθηκε ένα πλαίσιο μοντελοποίησης για τις διαφορετικές στρατηγικές θρέψης των μικτότροφων φωτοσυνθετικών νανομαστιγωτών. Τα μοντέλα που προέκυψαν περιγράφουν, για πρώτη φορά, τη λειτουργική ποικιλότητα της ομάδας των φωτοσυνθετικών νανομαστιγωτών, λαμβάνοντας υπόψη την δυναμική αλληλεπίδραση μεταξύ φωτοτροφίας και φαγοτροφίας σε τέσσερις διαφορετικούς τύπους μικτότροφων φωτοσυνθετικών νανομαστιγωτών. Οι προσομοιώσεις του μοντέλου υποδεικνύουν ότι η διαθεσιμότητα των φυσικών πόρων (φως, συγκέντρωση διαλυμένων ανόργανων θρεπτικών και βακτηρίων) επιδρά με διαφορετικό τρόπο στις δυναμικές των ρυθμών αύξησης των επιμέρους τύπων φωτοσυνθετικών νανομαστιγωτών. Παράλληλα, με βάση τις προσομοιώσεις του μοντέλου, η σύγκριση των ρυθμών παραγωγής οργανικού άνθρακα και κατανάλωσης βακτηρίων για τους τέσσερις τύπους φωτοσυνθετικών νανομαστιγωτών δείχνει ότι ο λειτουργικός τους ρόλος ως παραγωγοί ή καταναλωτές εξαρτάται από τον τύπο μικτοτροφίας και μπορεί να ποικίλει ως συνάρτηση των περιβαλλοντικών συνθηκών που επικρατούν την εκάστοτε χρονική στιγμή.

Επίσης, στην παρούσα διατριβή, παρουσιάζεται, μια εμπεριστατωμένη μελέτη της μικτοτροφίας στα φωτοσυνθετικά νανομαστιγωτά στην υπερ-ολιγοτροφική και ιδιαίτερα φτωχή σε φώσφορο ανατολική Μεσόγειο θάλασσα. Η μελέτη αυτή περιλάμβανε πειράματα θήρευσης βακτηρίων από τα νανομαστιγωτά στο πεδίο αλλά και σε εργαστηριακές βιοδοκιμές. Όσον αφορά τα πειράματα πεδίου, καταγράφηκε η αφθονία και η επίδραση της θήρευσης των φωτοσυνθετικών και ετερότροφων νανομαστιγωτών στους πληθυσμούς του προκαρυωτικού πικοπλαγκτού (*Synechococcus* και ετερότροφα βακτήρια). Τα πειράματα έλαβαν χώρα τον Απρίλιο 2016 σε τέσσερις σταθμούς στη βορειοδυτική Λεβαντινή θάλασσα και σε δύο επιλεγμένα βάθη, τα οποία ήταν αντιπροσωπευτικά για το επιφανειακό και βαθύτερο (βαθυμέγιστο χλωροφύλλης) στρώμα της εύφωτης ζώνης. Τα αποτελέσματα έδειξαν ότι τα ετερότροφα νανομαστιγωτά ήταν οι κυρίαρχοι θηρευτές του προκαρυωτικού πικοπλαγκτού στο επιφανειακό στρώμα, ενώ τα φωτοσυνθετικά νανομαστιγωτά ήταν οι κυρίαρχοι θηρευτές του προκαρυωτικού πικοπλαγκτού στο βαθύτερο στρώμα της εύφωτης ζώνης. Παρατηρήθηκε επίσης αρνητική συσχέτιση μεταξύ της συγκέντρωσης φωσφορικών αλάτων και του ρυθμού θήρευσης των φωτοσυνθετικών νανομαστιγωτών. Τα επακόλουθα πειράματα μικρόκοσμων πραγματοποιήθηκαν με δείγμα νερού από το Κρητικό πέλαγος, εξαιρετικά φτωχό σε θρεπτικά, κατά την περίοδο της ύστερης στρωμάτωσης της υδάτινης στήλης. Τα πειράματα μικρόκοσμων είχαν σκοπό να διερευνήσουν την απόκριση του ρυθμού θήρευσης των ετερότροφων και φωτοσυνθετικών νανομαστιγωτών στην αύξηση της διαθεσιμότητας του ανόργανου φωσφόρου. Επιβεβαιώνοντας τις ενδείξεις από τα πειράματα πεδίου, ο ρυθμός θήρευσης των φωτοσυνθετικών νανομαστιγωτών επί των ετερότροφων βακτηρίων μειώθηκε σημαντικά στους μικρόκοσμους όπου πραγματοποιήθηκε προσθήκη φωσφόρου, ενώ για τα ετερότροφα νανομαστιγωτά ο ρυθμός αυτός δεν επηρεάστηκε από την αύξηση της διαθεσιμότητας του φωσφόρου. Τα φωτοσυνθετικά νανομαστιγωτά ήταν οι κυρίαρχοι θηρευτές των βακτηρίων στους μικρόκοσμους όπου δεν πραγματοποιήθηκε προσθήκη φωσφόρου (μάρτυρες). Αντίθετα, στους μικρόκοσμους όπου πραγματοποιήθηκε προσθήκη φωσφόρου η συνεισφορά των φωτοσυνθετικών και ετερότροφων νανομαστιγωτών στη συνολική θήρευση επί των βακτηρίων ήταν παρόμοια. Τα αποτελέσματα των πειραματικών δοκιμών αναδεικνύουν το σημαντικό ρόλο των φωτοσυνθετικών νανομαστιγωτών ως καταναλωτών των βακτηρίων στην ανατολική Μεσόγειο, ο οποίος φαίνεται να εξαρτάται από τη διαθεσιμότητα του φωσφόρου.

Τα αποτελέσματα της θεωρητικής και πειραματικής μελέτης συνδυάζονται σε ένα θεωρητικό μοντέλο που προσομοιάζει ένα απλοποιημένο τροφικό πλέγμα. Η θεωρητική αυτή ανάλυση έχει σκοπό την περαιτέρω ποιοτική διερεύνηση της επίδρασης της διαθεσιμότητας του φωσφόρου στις τροφικές αλληλεπιδράσεις και φυσιολογικές διεργασίες των ετερότροφων βακτηρίων και των ετερότροφων και φωτοσυνθετικών νανομαστιγωτών στην ανατολική Μεσόγειο. Οι προσομοιώσεις του μοντέλου υποδεικνύουν εναλλακτικά μονοπάτια μεταφοράς φωσφόρου διαμέσου του μικροβιακού τροφικού πλέγματος σε περιόδους υψηλής και χαμηλής διαθεσιμότητας φωσφόρου. Τα φωτοσυνθετικά νανομαστιγωτά κατέχουν σημαντικό ρόλο στη μεταφορά του φωσφόρου μέσω του μονοπατιού που ορίζεται ως "by-pass" από τους Thingstad et al. (2005) [Thingstad et al., 2005. *Science*, 309:1068–1071] σε συνθήκες περιορισμένης διαθεσιμότητας φωσφόρου ενώ ο σχετικός ρόλος των ετερότροφων νανομαστιγωτών ενισχύεται σε συνθήκες υψηλής διαθεσιμότητας φωσφόρου. Οι πολύπλοκες αλληλεπιδράσεις μεταξύ φωτοσυνθετικών νανομαστιγωτών και ετερότροφων βακτηρίων στην ανατολική Μεσόγειο θάλασσα θα μπορούσαν να περιγραφούν εννοιολογικά ως ένας εναλλακτικός μικροβιακός βρόχος, ως προς το καθιερωμένο παράδειγμα που αναφέρεται στα ετερότροφα βακτήρια και τη θήρευση τους από τα ετερότροφα νανομαστιγωτά. Στον εναλλακτικό αυτό μικροβιακό βρόχο, τα φωτοσυνθετικά νανομαστιγωτά έχουν το λειτουργικό ρόλο των πρωτογενών παραγωγών διαλυτού οργανικού υλικού, κυρίως

μέσω του μηχανισμού της ενεργούς απέκκρισης, ενώ ταυτόχρονα μοιράζονται με τα ετερότροφα νανομαστιγωτά το ρόλο των καταναλωτών των βακτηρίων μέσω της μικτοτροφίας. Η λειτουργία αυτού του εναλλακτικού μικροβιακού βρόχου στην υπερ-ολιγοτροφική Μεσόγειο θάλασσα εξαρτάται από τη διαθεσιμότητα του φωσφόρου.

Τα αποτελέσματα της διδακτορικής αυτής διατριβής αναδεικνύουν τη σημασία της ευέλικτης φυσιολογίας των φωτοσυνθετικών μονοκύτταρων οργανισμών για τη λειτουργία των ολιγοτροφικών οικοσυστημάτων καθώς και την ανάγκη να λαμβάνεται υπόψη η προσαρμοστική αυτή συμπεριφορά στα βιογεωχημικά μοντέλα έτσι ώστε να προβλεφθεί η απόκριση των ολιγοτροφικών οικοσυστημάτων στις περιβαλλοντικές αλλαγές.

Abstract

The present thesis investigates two aspects of phytoplankton ecophysiology, which are particularly important in oligotrophic aquatic ecosystems. The first aspect is related to the mechanism of excretion of dissolved organic matter by photosynthetic cells, under varying nutrient availability conditions. The second aspect refers to mixotrophy in pigmented nanoflagellates (PNF) which is defined as the combination of autotrophy through photosynthesis (phototrophy) and heterotrophy through phagocytosis of bacteria (phagotrophy). The results of the present study emerge from the combination of theoretical and experimental approaches.

In order to better understand the processes of dissolved organic matter (DOM) release by photosynthetic cells under nutrient-replete and nutrient-limited conditions, a model based on Dynamic Energy Budget (DEB) theory is developed. In the context of DEB theory, two alternative pathways of DOM release emerge from the theory; one relates to growth and lysis of the cells and one to rejection of unprocessed substrates due to stoichiometric constraints. These pathways represent the two conceptual mechanisms of DOM release, which are the passive diffusion and active exudation, respectively. The relative contribution of the two mechanisms to DOM excretion depends on nutrient availability and affects the quality of produced DOM in terms of elemental and molecular composition and size fractionation, which, in turn, may have implications for the bioavailability of the produced DOM to bacteria.

Focusing on mixotrophy among PNF, a general modelling framework is developed for describing the nutritional strategies in four types of mixotrophic PNF. The resulting mathematical expressions are incorporated in the aforementioned DEB model for photosynthetic cells. The resulting models describe explicitly, for the first time, the functional diversity of the PNF assemblage taking into account the dynamic interaction of phototrophy and phagotrophy within the four types of PNF. Simulations suggest that the growth dynamics of the four types of PNF are affected differently by the availability of resources (light, dissolved inorganic nutrients and bacteria). A comparison of the rates of organic carbon production and prey consumption by the various PNF types shows that their net ecosystem role, as producers or consumers, depends on the mixotrophic strategy and it can vary as a function of the prevailing environmental conditions.

Moreover, in the present thesis, an in-depth investigation of mixotrophy among PNF

in the ultra-oligotrophic, phosphorus (P)-limited Eastern Mediterranean Sea (EMS) is performed, employing a two-phase experimental study that combined both field and laboratory nanoflagellates grazing experiments. During the field experiments, the abundance, and grazing effect of pigmented (PNF) and heterotrophic (HNF) nanoflagellates on prokaryotic picoplankton stock (i.e., heterotrophic bacteria (HB) and *Synechococcus*) were assessed in April 2016 at four stations in the NW Levantine sea and at two selected depths representing the surface and the deeper (deep chlorophyll maximum) euphotic layer. Results showed that HNF dominated prokaryotic picoplankton consumption in the surface layer, whereas, PNF were the dominant grazers of prokaryotic picoplankton in the deeper euphotic layer. A negative relationship between phosphate concentration and ingestion rate of PNF on prokaryotic picoplankton was observed. Subsequent microcosm experiments were performed with nutrient depleted water from the Cretan Sea (EMS) during the late stratified season, in order to asses the responses of heterotrophic and pigmented nanoflagellates, in terms of bacterial grazing, when relaxing the observed P-limitation. In accordance with the results of the field experiments, PNF ingestion rate of heterotrophic bacteria (HB) was significantly reduced in the P-amended treatment, whereas for HNF this rates remained unaffected by P-addition. PNF dominated bacterivory in the unperturbed (control) bottles, whereas, in the P amended treatment HNF and PNF contributed equally to total bacterivory. The experimental results obtained in the present study emphasize the significant and P-dependent role of PNF as consumers of HB in the EMS.

The results of the theoretical and experimental work undertaken in the present thesis are synthesized into an idealized microbial food web model. This theoretical analysis aims to further explore qualitatively the effect of phosphorus availability on the trophic interactions and physiological processes of heterotrophic bacteria, heterotrophic and pigmented nanoflagellates in the EMS. The model simulations suggest alternating pathways of P transfer through the microbial food web components during P-replete and P-limited conditions. Pigmented nanoflagellates hold a key role in P transfer through the trophic "by-pass" pathway *sensu* Thingstad et al. (2005) [Thingstad et al., 2005. *Science*, 309:1068–1071] under P-limited conditions, whereas the relative role of heterotrophic nanoflagellates in this pathway is more prominent at P-replete conditions. The complicated interactions between PNF and HB in the EMS could be conceptually described as an alternative microbial loop, in respect to the established paradigm involving heterotrophic bacteria and HNF. In this alternative microbial loop, PNF have the functional role of DOM primary producers, mainly through the active exudation mechanism, and, at the same time, share with HNF the functional role of bacterial consumers via mixotrophy. This alternative microbial loop in the oligotrophic system of the EMS operates in a phosphorus-dependent way.

The results of this thesis emphasize the importance of the adaptive physiology of photosynthetic protists for the functioning of oligotrophic systems and the importance of taking into account this adaptive behaviour in biogeochemical models in order to predict the response of oligotrophic systems to environmental changes.

Contents

List of Abbreviations

BP: Bacterial Production

DEB theory: Dynamic Energy Budget theory

DOM: Dissolved Organic Matter

DOC: Dissolved Organic Carbon

DON: Dissolved Organic Nitrogen

DOP: Dissolved Organic Phosphorus

EMS: Eastern Mediterranean Sea

FLB: Fluorescently Labelled Bacteria

HNF: Heterotrophic Nanoflagellates

HB: Heterotrophic Bacteria

LDOM: Labile DOM

PER: Percentage Extracellular Release

PNF: Pigmented Nanoflagellates

PP: Primary Production

RDOM: Refractory DOM

SLDOM: Semi-labile DOM

SRDOM: Semi-refractory DOM

SU: Synthesizing Unit

Chapter 1

General Introduction

Phytoplankton refers to single-celled microorganisms, both prokaryotes and eukaryotes, capable of photosynthesis. These organisms, transform the light energy into chemical energy in the form of organic carbon compounds through photosynthesis, fuelling the growth and metabolic demands of all other living organisms in aquatic ecosystems. Phytoplankton are responsible for most of the marine primary production, which constitutes approximately 45% of the global annual primary production (Field et al., 1998). Photosynthesis supplies carbohydrates which can be used to cover the respiration requirements of the photosynthetic cell. In order to build new biomass and grow, photosynthetic cells require a combination of carbohydrates and inorganic nutrients. Therefore, aquatic primary producers are equally depended upon the availability of light and inorganic nutrients for their growth. However, these two resources, have an inverse relationship in the euphotic layer. Light intensity reduces exponentially with increasing depth (Kirk, 2011), while nutrient concentrations are much higher in the deeper layers, which act as an accumulation site of nutrients, due to the mineralization of organic matter sunken from the euphotic layer and the absence of autotrophs (Falkowski and Raven, 2007). This spatial difference in the distribution of light and nutrients is intensified in oligotrophic waters where strong thermal stratification, prevailing for long periods of time, limits the flux of nutrients to the euphotic layer. In such systems, although there is sufficient light, primary production is limited by the availability of inorganic nutrients. Among these nutrients, nitrogen (N) and phosphorus (P) are of major importance as they are necessary building blocks of essential macromolecules, such as proteins and nucleic acids, while their concentration can often drop down to levels which can limit biomass production (Riebesell and Wolf-Gladrow, 2002).

Almost 60% of the global ocean, primarily the central oceans' anticyclonic gyres, are characterised as oligotrophic systems (Antoine et al., 1996; Longhurst et al., 1995; Guieu et al., 2014) due to the low concentrations of N and P, which in turn result in low chlorophyll α (Chlα) concentrations ($<$0.05 µg L^{-1}) (Lalli and Parsons, 1997) and low rates of primary production (typically below 0.3 to 0.4 g C m^{-2} d^{-1}) (Longhurst et al., 1995). Despite their low productivity status, oligotrophic systems in the Mediterranean Sea and the

Atlantic and Pacific subtropical gyres comprise 40% of the earth's surface, while evidence suggests that they are currently expanding, as a result of the increased stratification due to global warming (Polovina et al., 2008; Capotondi et al., 2012). Therefore, these systems contribute significantly to marine primary production and, consequently, to biogeochemical cycles on a global scale. The extensive oligotrophic oceanic areas are commonly referred to as Low Nutrient Low Chlorophyll (LNLC) areas (Guieu et al., 2014). The microbial food web mediates most of the carbon and nutrient fluxes in LNLC areas (Legendre and Rassoulzadegan, 1996). In this food web bacteria and small sized phytoplankton are dominant in terms of biomass, photosynthetic prokaryotes and nanoflagellates (<20 µm) are the principal primary producers (Cho and Azam, 1990; Uitz et al., 2010) and microbial grazing rather than herbivorous grazing is the main pathway of algal and bacterial carbon transfer to mesozooplankton (Legendre and Rassoulzadegan, 1996).

A central aspect to the functioning of microbial food web is the microbial loop, which refers to a set of processes where photosynthetically produced dissolved organic matter (DOM) is channelled to the food web via the heterotrophic bacteria - nanoflagellates - microzooplankton food chain (Azam et al., 1983). DOM is defined as the organic matter that is less than 0.7 μm, thus passing through the pores of glass-fiber filters (Carlson and Hansell, 2015). According to its reactivity, DOM is partitioned into labile (LDOM), semi-labile (SLDOM), semi-refractory (SRDOM), refractory (RDOM) and ultra-refractory (URDOM) (Hansell, 2013; Carlson and Hansell, 2015). Of these compartments, the refractory pools have a turnover time ranging from years to centuries or even millennia as they resist microbial degradation, whereas only the pools of LDOM and SLDOM are considered biologically reactive with lifetimes of hours to days and of weeks to months, respectively (Hansell, 2013).

LDOM and SLDOM can be distinguished on the basis of chemical composition. LDOM is mostly comprised of dissolved free amino acids (DFAA) and dissolved free neutral sugars (DFNS) both being of major importance for bacterial production. SLDOM is mostly comprised of dissolved combined neutral sugars (DCNS) and dissolved combined amino acids (DCAA), N-acetyl amino polysaccharides (N-AAPs) and acyl heteropolysaccharides (APS)(Carlson and Hansell, 2015, and references therein). DOM can also be characterized on the basis of size. Low molecular weight (LMW) DOM is defined as the DOM passing through ultrafiltration membranes with a pore size of ca. 1 nm (molecular weight cutoff of 1 kDa) whereas DOM higher than 1 kDa is defined as high molecular weight (HMW) DOM (Benner and Amon, 2015).

A significant part of the organic carbon fixed by phytoplankton ends up in the DOM pool, as LDOM or SLDOM, constituting a major carbon source for heterotrophic prokaryotes (Carlson and Hansell, 2015; Hansell et al., 2009). Although LDOM may be produced at high rates on an annual basis, in terms of organic carbon, LDOC represents only a small portion (<0.2 Pg C) of total oceanic dissolved organic carbon (DOC) since the tight coupling of its production and consumption processes prevents its accumulation (Repeta, 2015; Hansell, 2013). In this respect, LDOM does not have, at least directly, a significant role in carbon

export and redistribution of nutrients, as most of the regenerated elements are retained within the euphotic layer (Carlson and Hansell, 2015). On the other hand, the low reactivity of SLDOM allows its accumulation in the surface waters, particularly in the subtropical gyres, where it can be exported to depths of a few hundred meters via convective mixing, constituting the most important route for DOM export from the epipelagic zone. However, most of the exported SLDOM is mineralized within the mesopelagic zone (100-500 m) via bacterial degradation and eventually it is returned to the atmosphere within a timescale of months to years (Carlson and Hansell, 2015; Hansell et al., 2009).

Several processes may result in the transformation of particulate matter into the dissolved fraction such as grazing and sloppy feeding (Møller, 2007), viral lysis (Fuhrman, 1999), cell death and lysis (Orellana et al., 2013). Moreover, extracellular release of recently fixed carbon, commonly referred to as dissolved primary production (López-Sandoval et al., 2011), is a significant source of fresh DOM to aquatic systems (Fogg, 1983; Bjørnsen, 1988; Borchard and Engel, 2015). Extracellular release is a normal function of healthy photosynthetic cells occurring at all stages of growth (Fogg, 1983; Mague et al., 1980; Bjørnsen, 1988; Myklestad, 2000; Borchard and Engel, 2012). Production rates of DOM by phytoplankton are usually expressed as Percentage Extracellular Release (PER) (Thornton, 2014), which is the relative rate of dissolved primary production to total primary production (dissolved and particulate). Values of PER as high as 60% have been reported in phytoplankton cultures (Myklestad, 2000). Data from field studies show that PER is usually between 4-9% in eutrophic marine environments, whereas in oligotrophic systems up to 46% (Fogg, 1983; Teira et al., 2001a,b; Lagaria et al., 2013) of total primary production ends up in the DOM pool. Many studies suggest an inverse relationship between PER and total primary production (Teira et al., 2001a; Morán et al., 2002; López-Sandoval et al., 2011; Lagaria et al., 2013) implying that as primary production decreases the relative importance of DOC production increases. Therefore, in oligotrophic pelagic systems, autochthonously produced DOM is the primary organic carbon source for heterotrophic bacteria (Morán et al., 2002). The DOM consumed may be either mineralized (Ducklow et al., 1986) or transformed into POM and, thus, channelled towards heterotrophic protists, forming a link to higher trophic levels (Azam et al., 1983) or even transformed through heterotrophic microbial processes into recalcitrant forms of DOM, fuelling the Microbial Carbon Pump (MCP) (Jiao et al., 2010), which is particularly important for carbon sequestration and long term storage of carbon in oligotrophic systems where POC export is low (Jiao et al., 2014).

Although phytoplankton provide bacteria with DOM, mainly through extracellular release, at the same time they compete with bacteria for inorganic nutrients. However, bacteria have a higher affinity and they are better competitors than phytoplankton for dissolved inorganic nutrients (Thingstad et al., 1996; Moutin et al., 2002), which gives rise to an apparent paradoxical ecological relationship where phytoplankton provide organic substrates that fuel bacterial metabolism, while at the same time phytoplankton compete rather unequally with bacteria for inorganic nutrients (Bratbak and Thingstad, 1985). A possible explanation to this paradox is the predatory control of bacterial biomass exerted by heterotrophic nanoflagellates (HNF) (Azam et al., 1983; Sherr and Sherr, 1994; Caron et al., 1999; Christaki et al.,

2001). At the same time, HNF may return some of the nutrients back to the dissolved phase through mineralization and phytoplankton can, in turn, take up the mineralized nutrients (Thingstad and Rassoulzadegan, 1995, 1999). The combination of nutrient limitation and predatory control of bacterial growth may result in a situation referred to as the "malfunction of the microbial loop", which is a term that describes the inability of heterotrophic bacteria to consume all the primary production released as DOC from food web processes, resulting in the accumulation of degradable DOC in the surface layers (Thingstad et al., 1997).

Apart from HNF, photosynthetic pigmented nanoflagellates (PNF) cells, which are also capable of phagotrophy, can be important consumers of prokaryotic picoplankton (heterotrophic bacteria and cyanobacteria) (Stoecker et al., 2017). The ability of photosynthetic cells to consume other organisms is termed mixotrophy and it is defined as the combination of phagotrophy and phototrophy in a single cell (Sanders, 1991). In particular, PNF are of major importance in oligotrophic systems, where they can account for more than 50% of total flagellate bacterivory (e.g., Havskum and Riemann, 1996; Unrein et al., 2007) while, at the same time, they are significant contributors to primary production (Li, 1994; Jardillier et al., 2010). Thus, a situation emerges where photosynthetic cells provide organic carbon that fuels bacterial metabolism and in turn take advantage of the higher affinity of bacteria for nutrients through their consumption, a strategy that has been termed as "eating your competitor" (Thingstad et al., 1996). In such cases, PNF, functioning both as primary producers and consumers, have a significant effect on the fluxes of carbon and nutrients in microbial food webs (Thingstad et al., 1996; Mitra et al., 2014; Ward and Follows, 2016).

The aforementioned observations suggest that in oligotrophic environments, interactions between phytoplankton and bacteria are complex, including competition for mineral nutrients, commensalism through DOM release by phytoplankton and through provision of nutrients to phytoplankton by bacteria via mineralization, as well as predation on bacteria by mixotrophic organisms. Moreover, our current understanding of functioning of these systems in terms of metabolism, ecological adaptations and trophic interactions of the main plankton groups is still limited (Marañón et al., 2007). This doctoral thesis examines two important aspects of phytoplankton metabolism which offer insights to the otherwise paradoxical situation, where phytoplankton through the release of organic matter stimulate their competitors (Bratbak and Thingstad, 1985). The first aspect is the ability of phytoplankton to produce DOM of variable quality which may affect bacterial growth. The second aspect is the ability of photosynthetic cells to consume bacteria, through mixotrophy. As such, both the physiological mechanism of DOM release by photosynthetic cells and the trophic adaptation of mixotrophy among PNF are the focus of the present study.

1.1 Excretion of Dissolved Organic Matter

Phytoplankton-derived DOM mostly comprises polysaccharides (Myklestad, 1995; Mühlenbruch et al., 2018) which mainly consist of the neutral monosaccharides glucose, mannose,

fucose, arabinose, xylose, rhamnose and galactose (Aluwihare and Repeta, 1999; Borchard and Engel, 2015; Mühlenbruch et al., 2018). The monomer composition of excreted polysaccharides depends on the phytoplankton growth phase (Borchard and Engel, 2015) and it is also species-specific (Urbani et al., 2005; Mühlenbruch et al., 2018). Excreted polysaccharides may also include uronic acids, such as galacturonic acid and glucuronic acid and amino-sugars, like glucosamine and galactosamine (Borchard and Engel, 2012, 2015). Besides carbohydrates, phytoplankton produce dissolved organic nitrogen (DON) in the form of proteins and free amino acids, which may also constitute a significant part of DOM released by phytoplankton (Mague et al., 1980; Myklestad et al., 1989; Granum et al., 2002; Nagao and Miyazaki, 2002; Saad et al., 2016; Pujo-Pay et al., 1997). Finally, under P replete conditions phytoplankton excrete dissolved organic phosphorus (DOP), mainly in the form of P esters (>90% of dissolved organic phosphorus) (Saad et al., 2016). In terms of size, both HMW and LMW DOM are released by phytoplankton (Biddanda and Benner, 1997). To date, two conceptual processes have been proposed to describe the extracellular release of DOM by healthy phytoplankton cells; that is the passive leakage by diffusion through the cell membrane and active exudation (Thornton, 2014).

The passive diffusion describes the leakage of LMW compounds from photosynthetic cells (Bjørnsen, 1988). This leakage is due to a 10^6–fold concentration difference of LMW products of photosynthesis across the cell membrane. This concentration gradient promotes the diffusive transport of DOM from the cells to their surroundings and it is maintained due to the immediate uptake of the LMW compounds by heterotrophic bacteria (Bjørnsen, 1988; Carlson and Hansell, 2015). According to the passive diffusion model, the released DOM should consist of LMW uncharged molecules that are able to pass through the cell membrane, the leakage rate should increase with the surface-to-volume ratio of the cells and it should correlated to phytoplakton biomass (Bjørnsen, 1988; Myklestad, 2000; Carlson and Hansell, 2015; Borchard and Engel, 2015). Moreover, it has been suggested that the lowest size fraction of HMW DOM, the 1–10 kDa size fraction, can also pass through the cell membrane via passive diffusion (Borchard and Engel, 2015). Thus, the passive diffusion mechanism has been described as a "property tax", which can be translated into a daily loss rate of ca. 5% of carbon biomass (Bjørnsen, 1988). Nevertheless, a significant fraction of the DOM excreted by phytoplankton are of HMW, > 10kDa in particular, that cannot passively diffuse through the cell membrane (Borchard and Engel, 2015). This implies that the HMW compounds are actively excreted (Myklestad, 2000; Engel et al., 2004).

The overflow model describes a physiological mechanism of active exudation of photosynthetically produced DOM by healthy cells and constitutes a physiological response of photosynhthetic cells to nutrient-limitation (Fogg, 1983; Borchard and Engel, 2015). In phytoplankton the pathways of carbon and nutrients assimilation are uncoupled since organic carbon production depends upon the rate of photosynthesis, which is primarily regulated by light availability, whereas, inorganic nutrients are taken up from the surrounding environment. Therefore, balanced growth is only possible when the influx rates of the essential nutrients are proportional to carbon assimilation rates according to the ratios determined by biomass stoichiometry (Berman-Frank and Dubinsky, 1999). Phytoplankton cells growing

under light saturated and nutrient replete conditions, usually display a relatively constant molar ratio of the major nutrients that can be approximated by the Redfield ratio (C:N:P = 106:16:1), yet significant taxon-specific variations may be observed, particularly regarding the N:P ratio which can vary between 5 and 19 (Geider and La Roche, 2002). On the other hand, under sufficient inorganic carbon concentration and saturating light conditions, when inorganic nutrients are limiting, carbohydrates, produced through photosynthesis are in excess of what can be used for the biosynthesis of the structural components of the cell, resulting in a situation where photosynthesis and growth are uncoupled (Fogg, 1983; Berman-Frank and Dubinsky, 1999; Thornton, 2014; Carlson and Hansell, 2015). The photosynthetic cell responds to this stressing condition in various ways. For example, in response to nutrient limitation, many phytoplankton species have been shown to accumulate carbon in the form of storage compounds (Geider and La Roche, 2002). In diatoms the principal storage polysaccharide is chrysolaminarin, a glucan molecule consisting of $\beta 1 \rightarrow 3$- and $\beta 1 \rightarrow 6$ linked glucose units in a ratio of 11:1 with a total length of 12 glucose monomers, although species-specific differences in the branching and number of glucose monomers' length do exist (Mühlenbruch et al., 2018, and references therein).

The cellular glucan content accumulates markedly under nutrient deficiency in both eukaryotic (Myklestad, 2000; Granum et al., 2002) and prokaryotic phytoplankton (De Philippis et al., 1996). However, a significant part of this excess carbon is excreted outside the cell. This overflow mechanism is thought to be beneficial for the cell as it allows for the maintenance of active photosynthetic machinery and at the same time for the dissipation of the excess light energy (Wood and Van Valen, 1990; Berman-Frank and Dubinsky, 1999). It is hypothesized that this strategy minimizes the time required to resume growth when nutrients become available (Wood and Van Valen, 1990; Berman-Frank and Dubinsky, 1999), allowing photosynthetic cells to take full advantage of intermittent nutrient pulses associated either with atmospheric deposition or with mesoscale physical structures that promote deep vertical mixing and nutrient upwelling. A basic assumption of the overflow model is that the compounds excreted through active exudation should contain a minimum amount of the limiting elements, since this mechanism is supposed to be a physiological adaptation of phototosynthetic cells to sequester the surplus of energy stored as carbohydrates under nutrient limiting condition (Engel et al., 2004).

The production of polysaccharides and their active exudation are energy demanding processes that require specific biosynthetic pathways and exocytosis mechanisms (Thornton, 2014). Regulated exocytosis involving the formation of secretory vesicles containing densely packed polysaccharides, through the Golgi apparatus and their active release from the cell, has been demonstrated for *Phaeocystis globosa* (Chin et al., 2004), whereas the prokaryotic cyanobacteria exudation of polymeric substances involves the activity of membrane proteins (Pereira et al., 2009). Since the release of DOM has a cost in terms of energy and carbon loss, one may expect that it should be serving a specific function. Yet, why phytoplankton cells actively excrete a portion of their photosynthates is not fully understood (Thornton, 2014). Most likely, photosynthetic overflow is a mechanism allowing the photosynthetic cell to maintain cellular homeostasis and dispose any material that is in excess of its growth ca-

pacity. However, during evolution, secondary functions may have been added to this cellular process (Berman-Frank and Dubinsky, 1999). These may include exudation of exoenzymes that facilitate the acquisition of nutrients, release of secondary metabolites that can act as infochemicals or growth inhibiting factors as well as exudation of compounds serving functions related to defense against predators or infectious agents or density reduction (Thornton, 2014).

Findings from numerous field- and culture-based studies have supported the existence of either one or both conceptual processes of DOM release (Myklestad, 2000; Chin et al., 2004; Marañón et al., 2004; Lagaria et al., 2013; Thornton, 2014; Teira et al., 2015), indicating that these two mechanisms are not mutually exclusive and they probably operate simultaneously (Thornton, 2014). Therefore, DOM release by phytoplankton is the sum of passive diffusion and active exudation. However, the relative importance of these two processes depends on the physiological state and growth status of phytoplankton with implications for the quantity (Fogg, 1983; Myklestad et al., 1989; Obernosterer and Herndl, 1995; Granum et al., 2002) and the quality in terms of size, elemental and molecular composition (Biddanda and Benner, 1997; Granum et al., 2002; Underwood et al., 2004; Urbani et al., 2005; Saad et al., 2016) of the produced DOM.

At the same time, the quality of excreted DOM is an important determinant of the DOM availability to heterotrophic bacteria. For example, polysaccharides, rich in glucose, are easily consumed by bacteria, while heteropolysaccharides are more resistant to bacterial degradation and can accumulate in the water column (Obernosterer and Herndl, 1995; Hama and Yanagi, 2001; Urbani et al., 2005). Moreover, when heterotrophic bacteria were provided with organic carbon derived from P-limited phytoplankton, bacterial growth rates were significantly lower compared to those achieved when provided with organic carbon derived from P-replete phytoplankton (Puddu et al., 2003). The size of DOM may have also implications for its consumption by heterotrophic bacteria, as HMW DOM should be first hydrolyzed to monomers by extracellular enzymes prior to transport and utilization by the bacteria (Arnosti, 2011). The time lag between production of HMW by phytoplankton and synthesis of the hydrolytic enzymes by heterotrophic bacteria may result in a temporal uncoupling between production and consumption processes, leading to the accumulation of SLDOM and facilitating its export from the euphotic zone through convective mixing (Hansell, 2013). Also, excreted HMW compounds, due to their large size and, consequently, their lower diffusion rates, have a higher residence time in the phycosphere, which is defined as the phytoplanktonic cell surface and the directly surrounding space (Mühlenbruch et al., 2018). This may increase the time that bacteria are staying close to the phycosphere, which allows phytoplankton cells to benefit from the mineralization of nutrients by bacteria (Seymour et al., 2017; Mühlenbruch et al., 2018). The distinct pools of HMW and LMW DOM, produced by phytoplankton have also different composition with HMW DOM having a C:N ratio of ca. 21, reflecting its C-rich nature. On the other hand, LMW DOM produced was found to be N-rich with an average C:N ratio of ca. 6 (Biddanda and Benner, 1997), which is close to the Redfield ratio of 6.6. The compositional differences between HMW and LMW DOM produced by phytoplankton seem to be reflected in varying microbial reactivity, as

HMW DOM is related to high rates of bacterial respiration, whereas LMW DOM supports higher bacterial growth efficiencies (Amon and Benner, 1996). Therefore, it is important to resolve the physiological processes that regulate DOM production by phytoplankton, as they influence the degree and the nature of coupling between bacteria and phytoplankton, with implications for the carbon cycling in the ocean.

1.2 Mixotrophy

The widespread occurrence of mixotrophy and its importance for planktonic food web dynamics and elemental cycling has been rigorously demonstrated in a series of recent studies (reviewed in Worden et al., 2015; Selosse et al., 2017). As a result, mixotophy is now widely recognized as an inherent trait of many planktonic protists, rather than an occasional observation among certain organisms, as it was previously considered to be (Flynn et al., 2013). As already defined, mixotrophy refers to the the combination of phototrophy and phagotrophy in a single cell. This definition excludes the uptake and use of DOM via osmotrophy since this is an inherent trait of most prokaryotic and eukaryotic planktonic microbes (Flynn et al., 2013). Moreover, osmotrophy alone does not have important implications for trophic dynamics, contrary to phagotrophy which involves the death of another organism (Thingstad et al., 1996; Flynn et al., 2013).

Among mixotrophic planktonic protists, pigmented nanoflagellates, particularly in the smaller size fraction (<5 μm), constitute a very important group in oligotrophic ecosystems, where they are the dominant group of nanophytoplankton in terms of abundance (Zubkov and Tarran, 2008; Siokou-Frangou et al., 2010; Hartmann et al., 2013) and they are responsible for a significant fraction of marine primary production (Jardillier et al., 2010; Duhamel et al., 2019). Experimental work, conducted in coastal and pelagic oligotrophic ecosystems over large oceanic areas (Mediterranean Sea, Pacific Ocean, Atlantic ocean), has shown that small PNF are major consumers of bacteria, often accounting for $>50\%$ of total bacterivory (Unrein et al., 2007; Zubkov and Tarran, 2008; Tsai et al., 2011; Hartmann et al., 2012; Sato et al., 2017). PNF comprise a diverse group of various phylogenetic lineages such as chrysophytes, haptophytes, cryptophytes and chlorophytes (Stoecker et al., 2017), however, they all share a common trait that is a "constitutive" (inherent) ability to photosynthesize (Mitra et al., 2016) as their plastids are well integrated both physiologically and evolutionarily (Stoecker, 1998). Therefore, mixotrophic nanoflagellates are collectively termed as "constitutive mixotrophs" (CM) *sensu* Mitra et al. (2016).

Phagotrophy is a prerequisite for the evolution of mixotrophy and it is considered the primitive state of constitutive mixotrophic protists (Raven, 1997). The capacity for oxygenic photosynthesis in eukaryotes was acquired by endosymbiosis, with ingested cyanobacteria being retained by the phagotrophic protist as photosynthetic endosymbionts. Subsequently, the symbiotic cyanobacterium lost its ability to exist independently from its host and most of photosynthesis related genes were transferred to the host's nucleus. This primary en-

dosymbiosis event gave rise to the plastids of chlorophytes (including higher plants) and rhodophytes. The phylogenetic groups of heterokonta (including diatoms and chrysophytes), cryptophytes, haptophytes and dinophytes acquired their plastids through secondary endosymbiosis by the ingestion of another plastid-bearing protist belonging to the group of chlorophytes or rhodophytes (Raven, 1997; Delwiche, 1999; Keeling, 2013). In most cases, these lineages retained their capacity for phagotrophy along with phototrophy. The multiple and independent events that led to the acquisition of photosyntetic capability under various selection pressures are reflected in the wide range of mixotrophic strategies in planktonic protists, representing a spectrum of nutritional strategies (Jones, 1997; Stoecker, 1998). Strict phototrophs and strict phagotrophs are placed to the two extremes of this spectrum (Flynn et al., 2013), whereas, the complete loss of phagotrophic capability seems to be restricted to very few groups of photosynthetic protists, with diatoms being the most representative example (Wilken et al., 2019).

Despite the view that PNF can be placed along a continuum of phagotrophy and phototrophy, research has shown that certain species have a distinct set of responses to environmental cues, while they display a certain dependence and preference to each of the trophic modes, i.e., phototrophy and phagotrophy, for growth and energy derivation (Liu et al., 2016; McKie-Krisberg et al., 2015). As such, the PNF assemblage encompasses great functional diversity, which, additionally, does not always vary systematically with phylogeny (Jones, 1997; Stoecker, 1998; Mitra et al., 2016). For example, in two chrysophytes of the genus *Ochromonas* it was found that the isolate CCMP1393 is an obligate mixotroph, since it simultaneously requires light and prey as complementary resources for its growth, whereas, the coastal isolate CCMP2951 uses phototrophy and phagotrophy in a substitutable way, allowing for heterotrophic growth when light is limiting (Wilken et al., 2020). The effect of mixotrophic PNF on carbon and nutrient cycling in aquatic systems can vary greatly as a function of their photosynthetic and feeding capabilities, their physiological state and the environmental conditions prevailing at a certain moment (Worden et al., 2015; Wilken et al., 2018).

Despite the global significance of mixotrophy in PNF and the associated important ecological implications for the functioning of marine food webs (Mitra et al., 2014; Ward and Follows, 2016), the factors controlling the occurrence of mixotrophy as a mode of nutrition or the extent of mixotrophic activity, particularly among small PNF, have not yet been exhaustively resolved (Wilken et al., 2020). The ability of prey ingestion by photosynthetic organisms may be of use as energy and carbon supplement in light-limiting conditions (McKie-Krisberg et al., 2015). However, in oligotrophic conditions, it is the acquisition of the limiting inorganic forms of nutrients that is mostly related to mixotrophy (Unrein et al., 2007; Tsai et al., 2011; Sato et al., 2017).

Defining the ecological role of PNF as net consumers or net producers is difficult, not only due to the great diversity of nutritional strategies, but also due to the fact that most of the methods used to quantify grazing and primary production cannot differentiate between the contribution of pure autotrophs and mixotrophs. Among the methodologies used for

investigating mixotrophy among PNF, the most commonly used approach involves short incubations using fluorescently labelled bacteria (FLB) and the observation of FLB ingestion by nanoflagellates with epifluorescence microscopy (Sherr et al., 1987; Christaki et al., 1999; Unrein et al., 2007; Tsai et al., 2011; Sanders and Gast, 2012; Sato et al., 2017). Zubkov and Tarran (2008) and Hartmann et al. (2012) used labelled bacterioplankton cells with a pulse chase of two amino acids, [35S]methionine and [3H] leucine and they performed flow cytometric sorting of the labelled prey and predator cells to examine digestion of prey biomass by protist predators. These approaches allow the quantification of PNF ingestion rates but do not provide any information about the phylogenetic identity of the active mixotrophic grazers. On a different approach, Frias-Lopez et al. (2009) used prey marked with stable isotopes in order to taxonomically identify mixotrophic phytoplankton but they could not estimate the ingestion rates. Due to these difficulties, PNF are usually considered as a single group of mixotrophic organisms. Only very few studies tried to resolve the different functional groups (Gerea et al., 2019) or the different phylogentic groups (Unrein et al., 2014), highlighting the importance of haptophytes in terms of abundance and bacterivory. Resolving the ecological role of this diverse group is a complicated task, while the plasticity in nutritional behaviour creates great uncertainty when attempting to include mixotrophic PNF in ecosystem models. Nevertheless, mixotrophic PNF are ubiquitous in the euphotic zone of both marine and freshwater ecosystems, which implies that it is critical to understand and model their ecological role in order to describe accurately the biogeochemical cycles in these systems.

1.3 Modelling phytoplankton physiology

Understanding the functioning of pelagic ecosystems is a major challenge for oceanographers, yet it is absolutely necessary in order to predict the response of these systems to the ongoing environmental change. Mathematical models combining hydrodynamics and biogeochemical processes are an excellent tool towards such predictions (Baklouti et al., 2006; Doney et al., 2001). Applications of mathematical models are essential in analysing historic trends and forecasting changes relevant to management purposes and in assessing the potential impacts of climate change on the functioning of marine food webs and biogeochemical cycles (Gehlen et al., 2015). However, compared to physical ocean models, biogeochemical models are still at the early stages of development while they exhibit high uncertainty (Franks, 2009; Fennel et al., 2019)

Phytoplankton growth and ecophysiology plays an integral role in marine biogeochemical cycling (Falkowski et al., 2008) as described in the previous sessions. Realistic models describing phytoplankton growth are essential in understanding aquatic food webs and the flows of carbon and nutrients in these systems (Cullen et al., 1993). Over the years, considerable scientific effort has been put into developing conceptual and numerical models that capture the controls and drivers of phytoplankton production, resulting in a variety of alternative formulations for phytoplankton growth. Early models of phytoplankton growth used

Monod/Michaelis-Menten kinetics, where the relationship between organism growth and the limiting substrate are described by a rectangular-hyperbolic term. These models assumed a constant stoichiometry of the major elements, i.e., C, N, P, which could be approximated by the Redfield ratio of 106:16:1 (Redfield, 1958). Such models, however, do not account for the variable stoichiometry observed in phytoplankton when growing under non-steady state conditions (Goldman et al., 1979; Geider and La Roche, 2002; Flynn, 2010). This variable stoichiometry stems from the ability of phytoplankton to form internal stores of nutrients and energy in the form of carbohydrates (Berman-Frank and Dubinsky, 1999). A more appropriate description of phytoplankton growth was given by Droop (1968) who introduced the quota function where the intracellular concentration of the limiting nutrient (named quota) rather than the environmental concentration determines phytoplankton growth, stimulating a new generation of phytoplankton models that allowed variable biomass stoichiometry (e.g., Baretta-Bekker et al., 1997; Geider et al., 1998; Spitz et al., 2001; Baklouti et al., 2006; Flynn, 2008).

The existence of alternative formulations to describe phytoplankton growth is due to the fact that the modeled processes are described based on empirical observations (Baird and Suthers, 2007; Baklouti et al., 2006). In contrast to physical oceanography, where the governing equations are well known, in biogeochemical modelling, the terms for the various processes are calculated using empirical functions derived either from limited field data or laboratory experiments (Doney et al., 2001; Kriest and Oschlies, 2007), while the physiological mechanisms are not fully understood (Flynn, 2010). This lack of a solid mechanistic description in biogeochemical modelling, along with the unavailability of appropriate data to constrain the simulations, have been identified as major pitfalls, limiting the ability of models to reproduce the observed patterns, particularly in under-sampled marine systems and to predict ecosystem response under environmental change (Doney et al., 2001; Gehlen et al., 2015; Fennel et al., 2019; Rocha et al., 2019).

Due to the limitations of existing models for phytoplankton growth some authors have stressed the need for a new generation of plankton models. These models should describe a generic cell, they should be based on a robust physiological formulation and they should be able to capture key physiological processes (Flynn, 2010; Allen and Polimene, 2011; Glibert et al., 2013; Sharma and Steuer, 2019). Only such models, based on mechanistic rather than empirical formulations, will be able to reproduce and predict the ecosystem dynamics as emergent properties under current and future environmental conditions (Allen and Polimene, 2011). Creating a general model for phytoplankton growth is particularly challenging as it should be based on a well defined set of physiological and ecological principles that are common for all levels of biological organization (Marques et al., 2014).

Dynamic Energy Budget (DEB) theory comprises a set of simple physical and chemical rules that govern metabolic processes and they are applicable to all organisms. The theory provides a general mathematical framework to describe physiological cellular processes regarding the uptake and the use of energy and nutrients by the individual organism (Sousa et al., 2010; Kooijman, 2010). In DEB theory the individual is taken as the basis

for metabolic organization because, at this level, energy and mass balances can be made. Therefore, DEB theory is rigorous in specifying mass and energy balances, thus, conforming with the conservation law for energy and mass which is one of the few laws available in biology (Kooijman, 2010). As a result, DEB theory allows to link the physiological processes occurring at the individual level to the population and ecosystem level, through matter and energy fluxes (Sousa et al., 2008; Kooijman, 2010; Marques et al., 2014).

In DEB theory differential equations are used to describe the rates of uptake of energy and elemental matter and their utilization for the maintenance, growth, maturation or reproduction/division of the individual organism. According to the theory, the state of an organism can be fully described by the volume of structural mass and the energy in the reserves. Conversions between structural volume, energy in the reserves and mass can easily be made. The biomass of the organism has contributions from both structural and reserves mass. The use of volume as a state variable allows description of size related measurements of the organism according to the shape of the organism. For example, for isomorphic organisms, the surface area is proportional to volume$^{2/3}$ and the weight is proportional to volume to the power of one, whereas, for V1-morphs the surface area is proportional to volume to the power of one. Moreover, it allows to specify size related processes. Thus, the uptake of energy and elemental matter by the organism is taken proportional to its surface area, while the maintenance costs are taken proportional to volume of structural mass (Kooijman, 2010). According to DEB theory structure and reserves have a constant stoichiometry, an assumption called "strong homeostasis", however, the proportion of an element in the total biomass may vary due to variation in the relative amount of reserves and structure (Lika and Nisbet, 2000; Sousa et al., 2008; Kooijman, 2010).

DEB theory has been thoroughly tested and successfully applied in modelling the energetics of a variety of organisms, mostly animals, spanning from fish (Pecquerie et al., 2009, 2011) to mussels (Rosland et al., 2009), oysters (Bernard et al., 2011) and birds (Teixeira et al., 2014). These models employ one reserve and one structure DEB model (Kooijman, 2010). Furthermore, several studies demonstrate the capability of DEB theory to model autotrophy (Papadakis et al., 2005; Lorena et al., 2010; Muller et al., 2011; Papadakis et al., 2012; Grossowicz et al., 2017a) and even to combine the two traditionally distinct strategies of autotrophy and heterotrophy (Kooijman et al., 2002; Troost et al., 2005b; Lika and Papadakis, 2009). There are, however, certain features that differentiate the phytoplankton model from the standard DEB model. Among those features is the need to consider multiple reserves and multiple substrates (Lorena et al., 2010).

The need to consider multiple reserves arises from the fact that the assimilation pathways of essential resources, i.e., inorganic nutrients and carbohydrates from photosynthesis, are essentially independent in phototrophic cells. As such, the assumption of "strong homeostatsis" can only be ensured if there are different reserves for each independent assimilation pathway (Lorena et al., 2010). The advantage of using DEB models when working with phototrophic cells lies in the formulation of DEB theory, with the distinction between reserves and structure being a core assumption of the theory. The dependence of growth on

reserve dynamics and the variation in stoichiometry with changing environmental conditions are both emergent properties of the model and have been already mathematically formulated. Interestingly, the empirical model introduced by (Droop, 1968) for algal growth turns out to be a special case of DEB theory (Kooijman, 2010). Additionally, in the context of DEB theory, unicellular organisms that propagate through division, such as phytoplankton cells, can be considered as V1-morphs, which implies that the surface area is proportional to volume to the the power of 1. Consequently, the distinction between a single cell and a population is eliminated in the expressions of mass fluxes and the whole population can be described by state variables that are the sum of the state variables of each individual cell (Kooijman, 2010; Lorena et al., 2010; Marques et al., 2014). Considering unicellular organism as V1-morphs is possible due to the narrow range of size during cell growth, which implies that the deviations from the V1-morph are irrelevant when investigating population growth (Kooijman, 2010; Lorena et al., 2010).

In DEB theory, all transformations of substrates are performed using the concept of synthesizing unit introduced by Kooijman (1998, 2010). Synthesizing Units (SUs) can be described as generalized enzymes that bind arriving molecules of one or more substrates to form one or more products (Kooijman, 1998; Brandt et al., 2003). One of the main advantages of the SU is that it operates at multiple levels of biological organization from the molecular to the ecosystem level. Therefore, SUs handle a variety of substrates such as food items, macromolecules or simple molecules and they may produce other macromolecules or biomass (Kooijman, 1998; Muller et al., 2019). A SU, at its simplest form, is a one substrate–one product enzyme with steady state kinetics similar to those originating from the Michaelis–Menten formulation. The main difference between a SU and Michaelis–Menten kinetics is that in the former the substrate arrival fluxes are used as input variables, whereas in the latter the concentration or densities of substrates are used as input variables. In homogeneous environments this difference is not important since arrival rates of substrate molecules to the enzymes are proportional to the substrate concentration, on the basis of diffusive transport. However, in spatially structured environments, such as cells, it is difficult to determine concentrations of substrates and so is the linking of transformations to concentrations. In DEB theory growth dynamics are modelled based on mobilised reserve fluxes and, therefore, the mobilised reserve flux rather than diffusive transport determines the arrival rate. Moreover, using fluxes instead of concentrations allows the perception of light availability in a similar way to substrates, by using the light flux, quantified in mole photons per second, along with stoichiometric coupling coefficients in the light reactions of photosynthesis (Kooijman, 2010; Muller et al., 2019).

SU mediated transformations can be classified based on the basis of presence or absence of interaction between the substrates and according to their relative role in the formation of the product. Thus, a parallel transformation occurs when there is no interaction between the two substrates, whereas, a sequential transformation occurs when the binding of one substrate either promotes or disables the binding of the other. Moreover, two substrates can be complementary when both are needed at fixed stoichiometric proportions for the formation of the product and the absence of one substrate prevents the uptake of the other,

whereas they are called substitutable when they can be separately transformed into product. The potential combinations of these four classes give rise to the four basic schemes of SU mediated transformations namely sequential–substitutable, sequential–complementary, parallel–substitutable and parallel–complementary (Brandt et al., 2003; Kooijman, 2010). The equations that describe the SU kinetics on the basis of these four rules of transformation offer a general mathematical framework that can be used to study many biological processes involving two or more substrates, such as photosynthesis and photoinhibition (Muller et al., 2011; Papadakis et al., 2012), multiple nutrient limitation of phototrophic cells (Grossowicz et al., 2017a), multiple substrate utilization and co-metabolism in bacterial (Brandt et al., 2003) and algal growth (Lika and Papadakis, 2009), as well as mixotrophy (Kooijman et al., 2002).

In conclusion, DEB theory and the concept of SU provide a consistent, mechanistic framework for describing the physiological processes occurring in a photosynthetic cell and also has enough flexibility to allow the incorporation of the alternative nutritional strategies of mixotrophs.

1.4 The Eastern Mediterranean Sea

The Eastern Mediterranean Sea (EMS) has been identified as one of the most oligotrophic areas in the world (Krom et al., 2003). It is characterized by very low concentration of dissolved inorganic nitrogen and especially phosphorus, with an unusual nitrate to phosphate ratio (N:P) in the deep waters of ca. 28:1 (Krom et al., 1991), resulting in extremely low primary production rates averaging 60 – 80 g C m^{-2} y^{-1} (Psarra et al., 2000). In the EMS it is the microbial food web that mostly mediates carbon and nutrient fluxes throughout the year (Siokou-Frangou et al., 2002, 2010). Thus, small-sized nano- and picoplankton dominate the phytoplankton community both in terms of biomass and production (Vidussi et al., 2001; Siokou-Frangou et al., 2002; Psarra et al., 2005), there is a strong coupling between HNF grazing and heterotrophic bacteria production (Christaki et al., 2001), whereas, microheterotrophs, especially ciliates, are responsible for channelling energy and nutrients to higher trophic levels (Pitta et al., 2016). The peak of primary production occurs during late winter-early spring after the enrichment of the euphotic layer with inorganic nutrients due to winter mixing. The main phytoplankton bloom takes place during this period and larger cells, such as diatoms and dinoflagellates, may increase their numbers enhancing the relative importance of the classical food web (Psarra et al., 2000; Ignatiades et al., 2002). During the winter bloom, the surface euphotic layer becomes depleted in phosphate, while, some residual nitrate concentrations still remain (Krom et al., 1991). As a strong thermal stratification develops from May on-wards, both phosphate and nitrate are depleted in the surface layers, until the next winter mixing occurs that will fertilize the euphotic layer (Krom et al., 2003).

In the EMS, during the stratified period, DOC release by phytoplankton is a significant

process accounting for ca. 37% of total primary production (López-Sandoval et al., 2011), while both phytoplankton and bacteria are severely P-limited (Krom et al., 1991; Zohary and Robarts, 1998; Moutin and Raimbault, 2002; Van Wambeke et al., 2002). Despite an apparent high N:P ratio in the EMS, N and P co-limitation has also been reported for phytoplankton (Thingstad et al., 2005; Zohary et al., 2005) or for both heterotrophic bacteria and phytoplankton (Tanaka et al., 2011; Lagaria et al., 2011). Nevertheless, P-flux through the microbial food web is an important pathway that significantly affects productivity in the EMS. During the nutrient depleted stratification periods episodic nutrient enrichment pulses through dust deposition from the adjacent Saharan Desert is an important process that fertilises the euphotic layer in the EMS and supports primary and bacterial production (Lagaria et al., 2017b; Pitta et al., 2017; Rahav et al., 2018). Thus, it is important to understand how the trophic relationships and the P-flux through the microbial food web are affected during such enrichment events.

The CYCLOPS Lagrangian experiment, where phosphate was added to P-depleted surface waters of the EMS provided some insight on the P-flow through the components of the microbial food web after a fertilization event (Thingstad et al., 2005). These results were validated later by a mesocosm experiment ("NUTRITUNNEL" project) (Pitta et al., 2016). According to the paradigm established by these two projects, two, non mutually exclusive mechanisms, mediate the rapid transfer of P through the microbial food web to copepods; i) P is rapidly taken up by bacteria, and transferred efficiently up to copepods, "by-passing" the phytoplankton ("by-pass" mechanism) and ii) P is taken up by both bacteria and phytoplankton in excess of their needs for immediate growth ("luxury consumption") transforming them into P rich prey, which ultimately enhances copepods growth ("tunneling mechanism") (Thingstad et al., 2005). Both mechanisms indicate a tight coupling between production and consumption processes and tight predator-prey relationships where the microbial heterotrophs transfer efficiently the limiting element to higher trophic levels, without obvious biomass oscillations (Tanaka et al., 2007).

During the ADAMANT project, a mesocosm experiment with Cretan Sea water during the stratified season (May) was carried out in order to investigate the effect of Saharan dust deposition on the microbial food web of the Eastern Mediterranean Sea (Pitta et al., 2017). The pathways of the added nutrients in the food web were further examined through a comprehensive biogeochemical model describing the nutrient uptake by the organisms, and the effect of dust addition to the food web interactions and the carbon and nutrient fluxes (Tsiaras et al., 2017). This study showed that dust addition enhances bacterial and phytoplankton primary production, however the effect of dust addition was not evident in the biomass of the intermediate trophic levels of the microbial food web, until it was again visible in mesozooplankton, which presented a higher density in the dust-amended mesocosms (Lagaria et al., 2017b; Pitta et al., 2017). These results highlight the importance of multiple grazing processes in the microbial food web for transferring energy and nutrients to higher trophic levels in the EMS. Moreover, dust addition did not cause a shift from a microbial food web to a more classical food web, but just increased its trophic status, with more carbon circulating in the entire food web (Tsiaras et al., 2017).

Despite the occurrence of enrichment events, the euphotic layer of EMS remains P depleted for long periods, during the stratified season when up to 90–95 % of primary production is supported by efficient internal recycling of organic matter (Moutin and Raimbault, 2002). The understanding of the functioning of the microbial food web during these prolonged P depleted periods is still limited. For example, studies investigating P uptake in the EMS during the CYCLOPS experiment have shown that the smallest size fraction $0.2 - 1$ µm, including both heterotrophic bacteria and *Synechococcus* dominated P uptake, while the >2 µm size fraction was responsible for only 4% of P uptake (Flaten et al., 2005). Nevertheless, in terms of contribution to total primary production, the >2 µm fraction, mostly consisting of nanoflagellates, was responsible for the 45% of total primary production (Flaten et al., 2005; Psarra et al., 2005). During the "NUTRITUNNEL" P-enrichment experiment it was also observed that, in the control, unperturbed treatment, 57% of PP was due to nanophytoplankton which, at the same time, were responsible for only 4 – 13% of total inorganic phosphorus uptake (Pitta et al., 2016). These observations suggest that the >2 μm fraction should obtain a significant part of their phosphorus requirements through other processes, with mixotrophy among PNF being the most possible one (Flaten et al., 2005). The three aforementioned major projects (CYCLOPS, NUTRITUNNEL, ADAMANT) thoroughly examined the effects of nutrient addition on the nutrient and carbon fluxes through the microbial food web in the EMS. Yet, the effect of mixotrophy among pigmented nanoflagellates was not taken into account during these studies, leaving the functional role of pigmented nanoflagellates in this system poorly resolved.

1.5 Aim and outline of the thesis

This doctoral thesis examines the metabolic processes and ecological adaptations of phytoplankton in oligotrophic ecosystems. The core aim of this work is to contribute towards understanding the metabolism and biogeochemical role of photosynthetic organisms, focusing particularly on pigmented nanoflagellates, since their functional role in the microbial food webs of oligotrophic systems has not been extensively resolved, to date. More specifically, two aspects of phytoplankton ecophysiology are investigated. The first aspect concerns the mechanism of excretion of dissolved organic matter by photosynthetic cells, and how this mechanism is affected by nutrient availability. The second aspect deals with the nutritional strategies employed by mixotrophic pigmented nanoflagellates and the implications of these strategies for carbon and nutrient fluxes in aquatic ecosystems. The present study combines both theoretical and experimental approaches by using mathematical models as well as field and laboratory experiments, to investigate the effect of resources' availability on phytoplankton ecophysiology and to resolve the functional role of mixotrophic pigmented nanoflagellates as producers and/or consumers in the microbial food web of oligotrophic aquatic systems, focusing specifically in the ultra-oligotrophic Eastern Mediterranean Sea.

In Chapter 2, a DEB model for photosynthetic growth under varying availability of nutrients is developed and validated quantitatively, providing mechanistic formulations for DOM

release. Chapter 3 presents a modelling framework for describing the various nutritional strategies in mixotrophic pigmented nanoflagellates. The resulting mathematical formulations are incorporated in the DEB model for photosynthetic cells that was developed in Chapter 2 to describe the growth kinetics of four distinct types of mixotrophic pigmented nanoflagellates. In Chapter 4 the results of a series of grazing experiments performed in the field are presented with the aim to elucidate the relative importance of PNF and HNF as consumers of prokaryotic picoplankton cells in the EMS. Additionally, the results of subsequent microcosm experiments with P-depleted water from the Cretan Sea are presented. These experiments were performed in order to assess the grazing responses of HNF and PNF on bacteria, when relaxing the observed P-limitation and to confirm or reject the indications from the aforementioned field study in the EMS, that mixotrophy is used by PNF as a strategy to acquire the limiting phosphorus. In Chapter 5, in a synthesizing context, the results of the theoretical and experimental work are combined into a simplified food web model in order to further explore the implications of the studied ecophysiological responses of PNF on the phosphorus and carbon fluxes between heterotrophic bacteria and nanoflagellates in the ultra-oligotrophic EMS under varying P availability. Finally, in Chapter 6 the main conclusions of this doctoral thesis are summarized.

Chapter 2

A DEB-based approach of modeling dissolved organic matter release by phytoplankton

2.1 Introduction

DOM release by phytoplankton is the sum of passive diffusion and active exudation. These two mechanisms are not mutually exclusive and they probably operate simultaneously (Thornton, 2014). The relative importance of the two processes of DOM release depends on the physiological state and growth status of phytoplankton, while, the physiological mechanism of the photosynthetic cells responsible for the production and release of DOM affects its consumption and minreralization by heterotrophic bacteria (see Chapter 1 for further details). Thus, linking phytoplankton physiology with the composition and subsequent bacterial utilization of photosynthetically-derived DOM is an important step in understanding the patterns of DOM fluxes in the ocean and the relationships between phytoplankton and bacteria. As a result DOM production has been the focus of many experimental studies (e.g., Teira et al., 2001a; Marañón et al., 2004; Lagaria et al., 2011). However, it is very difficult to elucidate the underlying cell mechanisms based solely on the empirical observations of these studies, as for example, correlations of dissolved organic carbon (DOC) release with primary production (PP). Thus, in order to explore these mechanisms, other tools such as mathematical models are also needed.

Table 2.1 summarizes the main features of selected, representative models that include

This work is published in: **Livanou, E.**, A. Lagaria, S. Psarra, and K. Lika. 2019. A DEB-based approach of modeling dissolved organic matter release by phytoplankton. Journal of Sea Research 143, 140–151.

Table 2.1: Representative models on DOM release.

References	Biomass stoichiometry	Excreted DOM stoichiometry	DOM release
Baretta-Bekker et al. (1997)	C:N:P (v)	C	R_{PP}, $R^{\star}_{PP}$
Anderson and Williams (1998)	C:N (f)	C:N (v)	R_{PP}, $R_{GR(lim)}$
Bissett et al. (1999)	C:N (v)	C	$R_{biomass}$
Vallino (2000)	C:N (f)	C:N (f)	R_{PP}
Spitz et al. (2001)	C:N (f)	C:N (f)	$R_{biomass}$, R_{GR}, $R_{GR(lim)}$
Anderson and Pondaven (2003)	C:N (f)	C:N (v)	R_{PP}
Mongin et al. (2003)	C:N (v)	C:N (v)	$R_{biomass}$, $R_{N_{upt}}$, $R^{\star}_{PP}$
Van Den Meersche et al. (2004)	C:N (v)	C:N (v)	$R_{PP,N_{upt}}$, $R^{\star}_{PP}$
Baklouti et al. (2006)	C:N:P (v)	C:N:P (v)	$R^{\star}_{PP}$
Schartau et al. (2007)	C:N (v)	C:N (v)	$R_{biomass}$
Vichi et al. (2007)	C:N:P (v)	C	R_{PP}, $R^{\star}_{PP}$
Pahlow et al. (2008)	C:N (v)	C:N (f)	$R^{\star}_{PP}$
Flynn et al. (2008)(DOM3)	C:N (v)	C:N (v)	$R^{\star}_{PP,N_{upt}}$, R_{conc}
Druon et al. (2010)	C:N (f)	C:N (v)	R_{GR}, $R_{GR(lim)}$
Lorena et al. (2010)	C:N (v)	C	$R_{reserves}$, R_{GR}, R_{maint}
Keller and Hood (2011)	C:N (f)	C:N (v)	R_{PP}
Hasumi and Nagata (2014)	C:N (f)	C:N (f)	$R_{biomass}$, R_{GR}, $R_{GR(lim)}$
Kreus et al. (2014)	C:N:P (v)	C:N:P (v)	$R_{biomass}$
Grossowicz et al. (2017a)	C:N:P (v)	C:N:P (v)	$R_{reserves}$
Ghyoot et al. (2017)	C:N:P (v)	C	$R_{reserves}$
Grossowicz et al. (2017b)	C:N (v)	C:N (v)	$R_{biomass}$

(f) = fixed stoichiometry; (v) = variable stoichiometry.

Biomass stoichiometry: C= Carbon; N= Nitrogen; P = Phosphorus.

Excreted DOM stoichiometry: C = only DOC exudation is considered; C:N = exudation of DOC, DON or C:N:P = exudation of DOC, DON, DOP are considered.

DOM release: $R_{biomass}$ = proportional to biomass; R_{PP}, $R_{N_{upt}}$, $R_{PP,N_{upt}}$ = fixed fraction of primary production, N uptake, and both, respectively (the $\star$ indicates that the rates are multiplied by a factor related to nutrient status of biomass (various formulations)); R_{GR} = proportional to growth rate; $R_{GR(lim)}$ = proportional to the difference between nutrient-limited and nutrient-saturated growth rates; $R_{reserves}$ = proportional to internal reserves; R_{conc} = rate of leakage depends on the external concentration of DOM; R_{maint} = proportional to maintenance.

the process of DOM release. The simplest formulation assumes fixed biomass stoichiometry and DOM release rate as a fixed fraction of primary production with a fixed DOC:DON ratio (Vallino, 2000), while some models include an additional term of DOC release as a fixed fraction of primary production, resulting in the production of DOM with high DOC:DON ratio (Anderson and Pondaven, 2003; Keller and Hood, 2011). Many models with fixed biomass stoichiometry, in addition to fixed DOM release rate that is proportional to biomass

or growth rate or primary production or nitrogen uptake, assume an extra process of DOC release, proportional to the difference between nutrient-limited and nutrient-saturated growth rates (Anderson and Williams, 1998; Spitz et al., 2001; Druon et al., 2010; Hasumi and Nagata, 2014). The latter formulation results in the production of DOM with high DOC:DON ratio under nutrient-limiting conditions. Other models, although assuming fixed rate of DOM release proportional to biomass, allow the elemental stoichiometry of biomass (C:N or C:N:P) to vary (Schartau et al., 2007; Kreus et al., 2014; Grossowicz et al., 2017b). An alternative approach is to relate DOM release to the nutrient status of the cell, using elemental ratios (Baretta-Bekker et al., 1997; Mongin et al., 2003; Van Den Meersche et al., 2004; Baklouti et al., 2006; Vichi et al., 2007; Flynn et al., 2008). Therefore, in the last two model categories, the stoichiometry of DOM produced varies dynamically with the physiological state of cells (Table 2.1).

Variations of biomass stoichiometry are mainly due to variations of the stored cellular nutrients and carbon reserves, while the structural composition should be relatively constant (Geider and La Roche, 2002; Ross and Geider, 2009). Thus, distinguishing in the physiological model between reserves and structural components of the cell is a key step towards the development of purely mechanistic models. The idea of explicitly representing stored and structural components has been employed by modelers using various formulations (Shuter, 1979; Geider et al., 1996; Flynn et al., 2008; Ross and Geider, 2009; Lorena et al., 2010; Talmy et al., 2014). However, DOM exudation has been rarely modeled in relation to reserve dynamics, with the exception of Lorena et al. (2010); Grossowicz et al. (2017a); Ghyoot et al. (2017). Moreover, some models make explicit distinction between the two modes of release, with passive diffusion of DOM being described as a fixed percentage of PP and/or biomass and active exudation of "extra carbon" (DOC) being represented as a fraction of primary production, either fixed (Anderson and Pondaven, 2003) or dependent on nutrient limitation of phytoplankton (Baretta-Bekker et al., 1997; Anderson and Williams, 1998; Spitz et al., 2001; Mongin et al., 2003; Van Den Meersche et al., 2004; Vichi et al., 2007; Druon et al., 2010) employing various formulations (Table 2.1).

Dynamic Energy Budget (DEB) theory (Kooijman, 2010) provides an alternative and consistent quantitative framework for modeling phytoplankton physiology and mechanistically deriving formulations of DOM release. The advantage of using DEB models when working with phytoplankton physiology lies in the formulation of DEB theory, with the distinction between reserves and structure being a core assumption of the theory, and the link between exudation and reserve dynamics being already mathematically specified, but not quantitatively validated, in Lorena et al. (2010) and Grossowicz et al. (2017a) (Table 2.1). Moreover, DEB theory is rigorous in specifying mass and energy balances, a feature of paramount importance for describing excretion processes. Finally, DEB theory allows for generality as it is based on physicochemical first principles and, as such, implies mechanistic rules for energy uptake and use by the organism, that apply to all organisms (Sousa et al., 2010).

In this Chapter, a phytoplankton model, based on DEB theory, with multiple reserves that links the reserve dynamics with DOM release is presented. The model includes explicitly

the uptake, use and excretion of carbon and nitrogen by the individual cell. The aims of this chapter are to: 1) investigate the effects of nitrogen availability on DOM release by phytoplankton and on the relationship between primary production and DOC release and 2) elucidate the mechanisms under the two conceptual processes of DOM production, namely, passive diffusion and active exudation.

2.2 Methods

2.2.1 Model overview

The phytoplankton model is based on the modeling framework provided by DEB theory (Kooijman et al., 2002; Kooijman, 2010). DEB theory focuses on the individual organism, using differential equations to describe the rates of uptake of energy and elemental matter and their utilization. According to DEB theory the organism's biomass is partitioned in structural mass and reserves, the uptake of energy and elemental matter is taken proportional to its surface area while the maintenance costs are taken proportional to volume of structural mass. Moreover, unicellular organisms that propagate through division, such as phytoplankton cells, can be considered as V1-morphs which implies that surface area is proportional to volume (Kooijman, 2010; Lorena et al., 2010) (see Chapter 1, Section 1.3 for details).

First, the metabolic processes that occur at the individual level are presented. Subsequently, the dynamics at the population level are described. The model takes into account inorganic nitrogen (N) as the limiting nutrient and inorganic carbon (IC), each taken up independently. According to DEB theory, biomass is partitioned into structural mass M_V and a number of reserves masses M_i (here $i = E$ (generalized reserves), E_N (N-reserves), E_C (C-reserves)) and each pool is assumed to have constant chemical composition as the "strong homoeostasis" assumption indicates. Elemental composition of biomass is monitored in terms of Carbon (C) and Nitrogen (N). Although both reserves and structure have constant stoichiometry, the proportion of an element in the total biomass may vary due to variation in the relative amount of reserves and structure. All transformations of substrates are performed using the concept of synthesizing unit (SU) (Kooijman, 1998, 2010), which has been already used for modeling the uptake of substrates and synthesis of products in phytoplankton (Papadakis et al., 2005; Lika and Papadakis, 2009; Lorena et al., 2010; Grossowicz et al., 2017a).

A schematic presentation of the metabolic processes and the transformation of substrates in an individual cell is given in Fig. 2.1. The model describes the formation of carbohydrates from light and inorganic carbon, while phytoplankton growth is controlled by the availability of nitrogen. Inorganic carbon (CT) and nitrogen (NT) transporters are simple one-substrate SUs that take up inorganic carbon and nitrogen from the environment. Photosystems (PSU) harvest light (L) and produce photo-generated reductant that is combined with inorganic carbon by SU_C to produce organic carbon (C) in the form of carbohydrates. Then, nitrogen

and carbohydrates, each with its corresponding assimilation flux, are merged by SU_1 to form the generalized reserves (E). The generalized reserves can be described as mixtures of soluble precursors, such as amino acids, carbohydrates, nucleotides, proteins etc, that collectively have a fixed stoichiometry. Thus, the generalized reserves are considered as intermediate steps prior to structure formation.

SU dynamics imply some substrate rejection fluxes due to stoichiometric constraints. Each rejected substrate "molecule" by SU_1 is channeled to the corresponding reserves (E_N,

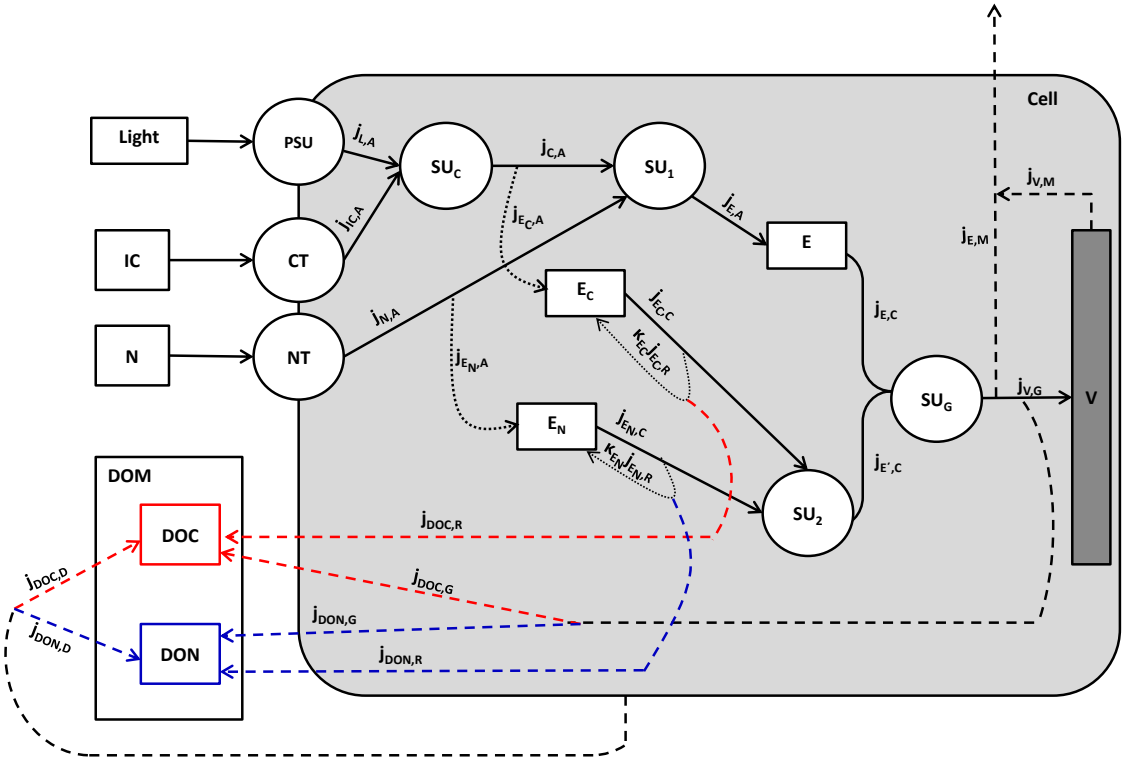

Figure 2.1: Schematic presentation of the model. Boxes represent concentrations, circles synthesizing units/transporters and arrows mass fluxes. CT, NT: carbon–, nitrogen–transporter, PSU: photosynthesizing unit, $SU_{1,2}$ synthesizing units/generalized enzymes, SU_C : synthesizing unit for carbohydrates, SU_G : growth SU, V: structure, E and E_i : reserves. $j_{i,k}$ denotes the flux of compound i associated with process k (k = A (Assimilation), C (Catabolism), G (Growth), R (Rejection), M (Maintenance), D (Death)). Solid arrows denote incoming fluxes, dotted arrows denote rejection fluxes fed to the reserves, dashed arrows denote fluxes excreted to the environment. For simplicity, only the excretion fluxes contributing to DOM are shown; excretion of DOC (red) and DON (blue).

E_C) where they are assumed to be converted in a stored form of C and N. A second synthesis (SU_2) occurs due to the catabolic flux from E_N- and E_C-reserves and the rejected molecules from SU_2 are either directed back to the reserves or excreted outside the cell. Mobilized reserves are combined to increase structure (V) and pay the maintenance costs (M) of the cell, with maintenance taking priority over growth (G). In addition to the rejected reserve "molecules", that are excreted in an organic form, the release of organic matter by phytoplankton is also associated with growth (G) and death (D). The combining rules of substrates by the SUs are discussed later in this Chapter (Section 2.2.2).

Because of the V1-morphy assumption of phytoplankton cells, the dynamics of an individual and that of a population are mathematically equivalent (Kooijman, 2010; Lorena et al., 2010). Therefore, the proposed population model has four state variables for the organism (structure–V, nitrogen–E_N, carbon–E_C and generalized–E reserves) and two for the environment (inorganic carbon, IC, and inorganic nitrogen, N) (light, L is assumed to be constant). In addition, two more variables are monitored to account for the excreted dissolved organic matter (DOM): DOC to account for the C component of DOM and DON for the N component of DOM. Thus, a fraction of DOC can be either free of nitrogen, or it should be linked with DON. The rates of change in the state variables are given by the following differential equations:

Environment-related state variables

$$\begin{aligned}
\frac{d}{dt}X_{IC} &= (-j_{C,A} + j_{IC,E})X_V \\
\frac{d}{dt}X_N &= (-j_{N,A} + j_{N,E})X_V
\end{aligned} \tag{2.1}$$

The organism-related state variables

$$\begin{aligned}
\frac{d}{dt}X_E &= (j_{E,A} - j_{E,C})X_V - \dot{h}X_E \\
\frac{d}{dt}X_{E_C} &= (j_{E_C,A} - j_{E_C,C} + \kappa_{E_C} j_{E_C,R})X_V - \dot{h}X_{E_C} \\
\frac{d}{dt}X_{E_N} &= (j_{E_N,A} - j_{E_N,C} + \kappa_{E_N} j_{E_N,R})X_V - \dot{h}X_{E_N} \\
\frac{d}{dt}X_V &= (\dot{r} - \dot{h})X_V
\end{aligned} \tag{2.2}$$

DOM-related state variables

$$\begin{aligned}
\frac{d}{dt}X_{DOC} &= j_{DOC,E}X_V + \dot{h}(X_E + X_{E_C}) \\
\frac{d}{dt}X_{DON} &= j_{DON,E}X_V + \dot{h}(n_{N,E}X_E + X_{E_N})
\end{aligned} \tag{2.3}$$

where X_i is the concentration of compound i and $j_{i,k}$ is the specific (i.e., per unit of structural mass) flux of compound i associated with process k, where k = A (assimilation), R (rejection), E (excretion), or C (catabolism). $\dot{r}$ denotes the net growth rate and $\dot{h}$ denotes the death rate. Finally, the total particulate organic matter (POM) is expressed in terms of carbon (POC) and nitrogen (PON), that comprise the sum of organic carbon and nitrogen in cell's structure and reserves. The reserves of a dead cell contribute to the dissolved organic pool (Eq 2.3), while its structure is added to the particulate organic compartment. Thus, the rate of change for POC is $\frac{d}{dt}X_{POC} = \frac{d}{dt}(X_V + X_E + X_{E_C}) + \dot{h}X_V$ and for PON is $\frac{d}{dt}X_{PON} = \frac{d}{dt}(n_{N,V}X_V + X_{E_N}) + \dot{h}n_{N,V}X_V$. Variables and parameters in the above and the following model equations are introduced in Table 2.2.

Table 2.2: Table of frequently used symbols. Dimensions: t means time and l length.

Symbol	Interpretation (Dimensions)
t	Time (t)
M_V, M_{E_i}	Mass of structure, reserves (mol)
m_{E_i}	Density of reserve $E_i = M_{E_i}/M_V$ (mol/mol)
X_i	Concentration of compound i (mol i l^{-3})
L	Incident light intensity (mol photons l^{-2} t^{-1})
$j_{i,k}$	Specific flux of compound i associated with process $k^{(a)}$ (mol i (mol V)$^{-1}$ t^{-1})
α_L	Specific photons' arrival cross section (l^2 (mol V)$^{-1}$)
ρ_L	Photon's binding probability (–)
K_i	Half-saturation constants for compound i (mol i l^{-3})
$\dot{k}_i$	Turnover rate of compound i (t^{-1})
κ_{E_i}	Fraction of rejected flux of E_i returning to reserves (–)
$y_{i,j}$	Stoichiometric coefficients (mol i (mol j)$^{-1}$)
$n_{*_1,*_2}$	Chemical index of element $*_1$ in compound $*_2$ (#/#)
$j_{E,M}$	Maintenance rate (t^{-1})
$\dot{r}$	specific growth rate of structural mass (t^{-1})
$\dot{h}$	Death rate (t^{-1})

[(a)] k refers to process: A (assimilation), R (rejection), E (excretion), or C (catabolism).

2.2.2 Formulation of processes

Assimilation rates and photosynthesis

The photosynthetic units (PSUs) of phytoplankton convert light and inorganic carbon into autotrophic assimilate. Photons arrive at PSUs at a rate proportional to incident light intensity L and bind to PSUs with a probability ρ_L. The specific binding rate of photons equals $j_{L,A} = \rho_L \alpha_L L$, with α_L the specific photons arrival cross section. The binding probability

ρ_L captures the quantum yield of PSII, which declines under nitrogen starvation (Parkhill et al., 2001; Kamalanathan et al., 2016), and the allocation of excitation energy to the Calvin-Benson cycle, which may also decline under nutrient-limiting conditions in favor of the cyclic electron flow and the production of ATP (Berges et al., 1996). It is assumed that ρ_L decreases from a maximum value, $\rho_{L_{max}}$, to a minimum value, $\rho_{L_{min}}$, as the N status of the cell declines (see Appendix A for details).

The uptake rates of inorganic carbon and nitrogen follow classic Michaelis-Menten kinetics and are given by

$$j_{i,A} = j_{i,A_m} \frac{X_i}{X_i + K_i}, \quad (i = IC, N) \tag{2.4}$$

where j_{i,A_m} is the maximum uptake rate of substrate i and K_i is the half-saturation constant.

Phytoplankton cells produce carbohydrates through inorganic carbon and reductant that is supplied by the light reactions of photosynthesis. SU_C (Fig. 2.1) processes the two complementary substrates in parallel, meaning that both substrates are required to form the product and that the binding of one substrate to the SU is independent from the binding of the other (see for example Lika and Papadakis (2009)). Thus, the specific carbohydrates assimilation flux is given by

$$j_{C,A} = \left(\frac{1}{j_{C,A_m}} + \frac{1}{j'_{IC,A}} + \frac{1}{j'_{L,A}} - \frac{1}{j'_{IC,A} + j'_{L,A}} \right)^{-1} \tag{2.5}$$

where $j'_{i,A} = j_{i,A}/y_{i,C}$ is the specific arrival rate of substrate i (IC or L), $y_{i,C}$ is the stoichiometric coefficient that denotes the amount of compound i consumed per amount of organic C produced, and j_{C,A_m} is the maximum assimilation rate of carbohydrates.

Reserves formation

Generalized reserves, E, are formed directly from the assimilation fluxes of C and N given by Eqs. (2.4) and (2.5). In this transformation, C and N are complementary substrates and their binding is parallel. The specific assimilation flux of generalized reserves is

$$j_{E,A} = \left(\frac{1}{j_{E,A_m}} + \frac{1}{j'_{C,A}} + \frac{1}{j'_{N,A}} - \frac{1}{j'_{C,A} + j'_{N,A}} \right)^{-1} \tag{2.6}$$

where $j'_{i,A} = j_{i,A}/y_{i,E}$ denotes the specific arrival rate of substrate i (C, N), $y_{i,E}$ the yield coefficient that represents the mole of the compound i required to form one mole of the generalized reserves, E, and j_{E,A_m} the structure-specific maximum assimilation rate of generalized reserves. The metabolic costs of biosynthesis are taken into account in the model

by the stoichiometric coefficient $y_{C,E}$ that couples carbohydrates to the generalized reserves yield.

Since the nutrients are taken up independently, one or more assimilation fluxes can limit the synthesis of the generalized reserves. In that case, the non-limiting assimilated "molecules" will occupy the binding sites of the SU but they will not be processed further due to the absence of the limiting flux (Lorena et al., 2010) and, thus, they will be rejected by the SU. The "molecules" of the compound i rejected from SU_1 (Fig. 2.1) are stored in the corresponding reserves at rates

$$j_{E_i,A} = j_{i,A} - y_{i,E} j_{E,A} \qquad (i = C, N)$$

Growth rate

All reserves are mobilized to allocate energy to growth and maintenance. According to DEB theory, reserve densities $m_E = M_E/M_V$ and $m_{E_i} = M_{E_i}/M_V$ with i = C, N follow first-order kinetics, which means that the structure-specific catabolic fluxes $j_{E,C}$ and $j_{E_i,C}$ are given by

$$j_{E,C} = m_E(\dot{k}_E - \dot{r}) \qquad \text{and} \qquad j_{Ei,C} = m_{E_i}(\dot{k}_{E_i} - \dot{r}) \tag{2.7}$$

with $\dot{k}_E, \dot{k}_{E_i}$ the reserves turnover rates, which are constant, and $\dot{r}$ the net specific growth rate of structural mass. The specific catabolic fluxes represent the mobilized reserves per unit of structural mass that will be used for growth and maintenance, with maintenance taking priority over growth.

E_i–reserves send their specific catabolic fluxes, $j_{Ei,C}$, to synthesizing unit SU_2 (Fig. 2.1) to form a compound E' identical to the generalized reserve E, in an analogous transformation as for E. E' will be also used for covering the metabolic needs of the cell (maintenance and growth). The specific catabolic flux, $j_{E',C}$, can be calculated from Eq. (2.6) by replacing $j_{*,A}$ with $j_{*,C}$ (Kooijman, 2010).

The two resulting catabolic fluxes, $j_{E,C}$ and $j_{E',C}$ are combined together by the growth SU_G, which is assumed to be fast enough to avoid spoiling of reserves, to form the flux for growth j_{VG}

$$j_{VG} = y_{E,V}^{-1}(j_{E,C} + j_{E',C} - j_{E,M})_+ \tag{2.8}$$

The term $j_{E,M}$ stands for the structure specific maintenance flux and it is assumed to be constant. The subscript '+' means that the growth rate j_{VG} is zero when the term within parentheses is negative. When the catabolic fluxes $j_{E,C} + j_{E',C}$ are not enough to cover the maintenance requirements, the remainder will be paid from structure at a rate $j_V^M = (j_{E,M} - \min(j_{E,C} + j_{E',C}, j_{E,M}))y_{E,V}^{-1}$. The net specific growth rate, $\dot{r}$, is calculated numerically

from $\dot{r} = j_{VG} - j_V^M$. The inclusion of the term j_V^M allows the net specific growth rate to be negative. Note that losses from death are not included in the net specific growth rate.

Excretion fluxes

In the context of DEB theory, exudation of DOM by phytoplankton can be described when considering the two possible contributing fluxes: rejection flux and product synthesis (Lorena et al., 2010). The catabolic fluxes from the E_C and E_N that cannot be used for synthesis will be rejected by the SU_2 at rates

$$j_{E_i,R} = j_{E_i,C} - y_{i,E'} j_{E',C} \qquad (i = C, N) \tag{2.9}$$

These $j_{E_i,R}$ rejection fluxes are further divided into two types of fluxes: a fixed fraction κ_{E_i} that is fed back to the respective reserve and the rest $(1 - \kappa_{E_i})$ that is excreted in the environment (Kooijman, 2010; Marques et al., 2014). This rejection flux, directed outside the cell, is dynamic and depends on the nutrient status of the cell. The $(1 - \kappa_{E_i})$ fraction of the rejection flux from the E_C-reserves, $j_{DOC,R}$, is fed to the DOC pool, while the rejection flux from E_N-reserves, $j_{DON,R}$, is fed to the DON pool

$$j_{\ell,R} = (1 - \kappa_{E_i}) j_{E_i,R} \quad (\ell = DOC, DON) \text{ and } (i = C, N) \tag{2.10}$$

According to DEB theory product synthesis must be a weighted sum of the basic fluxes: assimilation, maintenance and growth (Kooijman, 2010; Lorena et al., 2010). No direct evidence exists for DOM excretion related either to assimilation or maintenance. However, DOM can be excreted from growing cells in the exponential phase of culture (Lomas et al., 2000; Myklestad, 2000; Urbani et al., 2005; Saad et al., 2016) and the specific DOM release is proportional to the specific growth rate (Myklestad et al., 1989; Underwood et al., 2004). Therefore, in this work, it is assumed that the growth flux contributes to DOM production at a specific rate

$$j_{\ell,G} = y_{\ell,V} j_{VG} \quad (\ell = DOC, DON) \tag{2.11}$$

where, $y_{\ell,V}$ stoichiometrically couples DOM production to the growth rate according to the relationship: $y_{\ell,V} = y_{E,V} n_{i,E} - n_{i,V}$ (i = C, N). Therefore, from Eq. (2.10) and Eq. (2.11) the excretion flux of DOM from phytoplankton is: $j_{\ell,E} = j_{\ell,R} + j_{\ell,G}$, with ($\ell = DOC,\ DON$). Finally, inorganic carbon and nitrogen are released as by-products from the maintenance processes according to the stoichiometric relationship

$$j_{i,M} = n_{*,E} j_{E,M} + j_V^M (n_{*,V} - y_{E,V} n_{*,E}) \tag{2.12}$$

where $i = IC, N$. Thus, the excretion flux of inorganic nitrogen is $j_{N,E} = j_{N,M}$, while for the inorganic carbon excretion rate, in addition to $j_{IC,M}$ (Eq. 2.12) there are two extra

sources of inorganic carbon production associated with the costs of biosynthesis (see Section 2.2.2). Thus, the excretion fluxes of inorganic carbon is $j_{IC,E} = (y_{C,E} - n_{C,E})j_{E,A} + (y_{C,E'} - n_{C,E'})j_{E',C} + j_{IC,M}$.

2.2.3 Linking the model to experimental data

The model was first calibrated to published experimental data for *Thalassiosira pseudonana* grown with ammonium as the nitrogen source (Clark, 1999; Flynn et al., 2008). Data were digitized from Fig. 4 in Flynn et al. (2008) using the WebPlotDigitalizer (Rohatgi, 2017). These data allowed tracking of carbon and nitrogen in the inorganic and organic pools. The calibration of the model with the experimental data was done by using the freely downloadable DEBtool software (http://www.bio.vu.nl/thb/deb/deblab/). Model simulations were implemented in MATLAB. The parameter estimation procedure (Marques et al., 2019) uses the Nead-Melder simplex method and filters that prevent the parameter values to be outside the boundaries of the physically allowed values. All parameters were constrained to take positive values and probabilities ($\rho_{L_{max}}$ and $\rho_{L_{min}}$) and fractions (κ_{E_C}, κ_{E_N}) are constraint in the interval [0,1]. The yield coefficient y_{EV} (C-mol of E required per C-mol of V) must be larger than the chemical index n_{CV}. The reserve turnover rates were all assumed to have the same value which was estimated from the data. The maximum specific uptake rate of inorganic carbon, j_{IC,A_m}, and the maximum specific assimilation rate of carbohydrates, j_{C,A_m}, were assumed to be equal and their values were taken from the literature (Table A1 in Appendix A). Furthermore, molecular elemental ratios of biomass were used in order to constrain the parameter values. The molecular elemental ratio of biomass C:N is calculated by n_C/n_N, where $n_C = n_{C,E}M_E + M_{E_C} + n_{C,V}M_V$ is the total C-mol content of the cells and $n_N = n_{N,E}M_E + M_{E_N} + n_{N,V}M_V$ is the total N-mol content. The C:N ratio was restricted in the interval (5.7, 26) (Perry, 1976; Claquin et al., 2002; Flynn et al., 2008).

2.3 Results

The model (Eqs. 2.1–2.3) has a close qualitative and quantitative correspondence with the experimental data (Fig. 2.2). The overall goodness of fit of the model, quantified by the Mean Relative Error (MRE) (Marques et al., 2018, 2019), has the value of 0.23. MRE can take values in the interval [0, ∞); values close to 0 mean that predictions match the data exactly (Marques et al., 2019). The total particulate carbon (POC) and nitrogen (PON) in the system comprise the sum of each element in the structural mass, reserves and dead structural mass. POC and PON in the system increase exponentially and reach a stationary phase when nitrogen is consumed and eventually is depleted. Two phases of growth are distinguished: an exponential phase with sufficient supply of nitrogen (N-replete phase) and a stationary phase when nitrogen in the medium has been depleted (N-limited phase). The end of N-replete phase is marked when PON reaches its maximum. The model predictions

for the inorganic carbon fit rather well the experimental data (Fig. 2.2 a). Model predictions for POC and DOC agree with the data up to day five, but from day six onwards the data show a continuous increase in POC and a significant decrease in DOC, both of which are not captured by the model (Fig. 2.2 c). The model predicts a faster depletion of inorganic nitrogen than the one observed (Fig. 2.2 b). The model output for the particulate (PON) and dissolved (DON) organic nitrogen (Fig. 2.2 d) describes adequately the experimental data although there is an overestimation of DON produced at some time points.

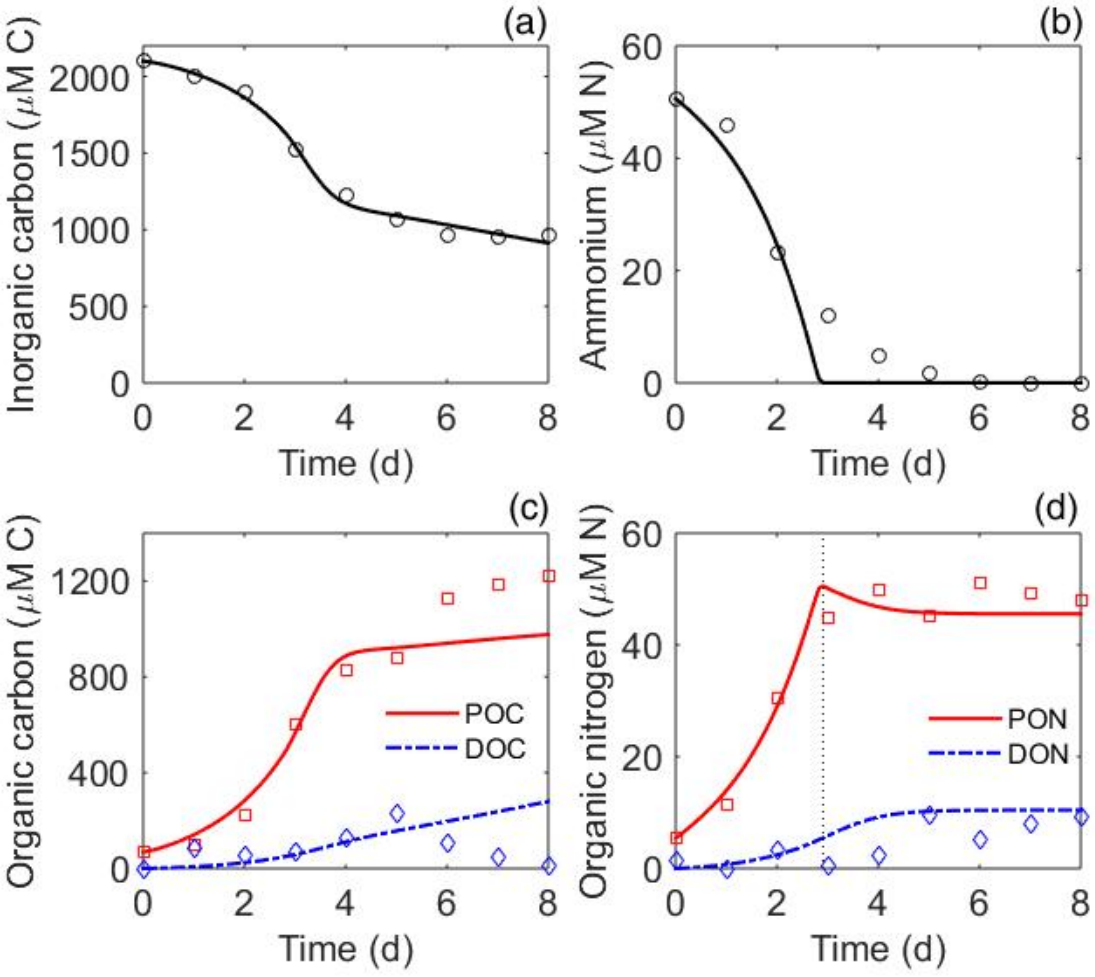

Figure 2.2: Model fits (lines) to data (symbols) from Flynn et al. (2008) for *Thalassiosira pseudonana*. (a) Dissolved inorganic carbon, (b) ammonium, (c) organic carbon (particulate–POC and dissolved–DOC), (d) particulate organic nitrogen (PON) and dissolved organic nitrogen (DON). Vertical dotted line marks the two phases of nutrient availability (N-replete, N-limited).

In order to explore the effects of nitrogen limitation on DOM release additional simulations were performed using the parameters given in Table A1 of Appendix A. Thus, structural

mass-specific metabolic rates are presented in Fig. 2.3. The net growth rate, $\dot{r}$, (see Section 2.2.2) is responsible for the production of new structural mass, after maintenance and growth costs having been paid (Fig. 2.3 a). Specific primary production (PP) rate relates to the photosynthetically produced organic carbon (Fig. 2.3 b) and is given by the carbohydrates assimilation flux $j_{C,A}$ (Eq. 2.5). Specific DOC release rate corresponds to the sum of fluxes that contribute to the release of dissolved organic carbon from the cell (Fig. 2.3 c). Percentage Extracellular Release (PER) is calculated as the percentage of DOC release over PP (Fig. 2.3 d).

High specific growth (Fig. 2.3 a) and primary production (Fig. 2.3 b) rates are observed during the N-replete phase where both reach their maximum ($\dot{r}_{max} = 0.67$ d^{-1}, PP$_{max} = 1.69$ d^{-1}) and decrease to minimum values in the N-limited phase. Specific DOC release rate presents a maximum value (0.15 d^{-1}) in the N-replete and declines during the N-limited phase (Fig. 2.3 c). PER remains approximately constant with a mean value of 8.2% during the N-replete period and increases abruptly with the onset of the N-limited phase reaching a maximum value of 65% at the end of the N-limited phase (Fig. 2.3 d).

DOC release rate is analysed into the contributing fluxes that are presented in Fig. 2.4 a. DOC release has contributions from three fluxes: $j_{DOC,R}$, the rejection flux from the E_C-reserves due to nutrient limitation, given in Eq. (2.10), $j_{DOC,G}$, which is proportional to growth rate, given in Eq. (2.11), and the flux $j_{DOC,D} = \dot{h}(m_E + m_{E_C})$ that relates to the release of DOC due to cell death and subsequent lysis. Fig. 2.4 a illustrates the relative contribution of the three fluxes to DOC release. The flux $j_{DOC,G}$, has the highest contribution to DOC release during the N-replete phase (Fig. 2.4 a, solid line). With the onset of the N-limited phase the relative contribution of $j_{DOC,G}$ to the DOC release flux decreases, while the relative contribution of $j_{DOC,R}$ flux increases to become the most significant flux of DOC release towards the end of the simulation (Fig. 2.4 a, dashed line), when growth has ceased, as specific growth rate approaches zero (Fig. 2.3 a). Finally, the maximum relative contribution of $j_{DOC,D}$ flux to total DOC release rate is always less than 10% (Fig. 2.4 a, dash-dot line).

The fluxes associated with growth ($j_{DOC,G}$) and death ($j_{DOC,D}$) processes receive an input from the reserves, via catabolism and cell lysis, respectively. Thus, the DOC produced as a result of these two fluxes, denoted as DOC$_L$, should have a composition similar to the cellular material. On the other hand, $j_{DOC,R}$ corresponds to the rejection flux of unprocessed substrates by the SU, that are channeled outside the cells, and it is a result of nutrient limitation and unbalanced growth. Therefore, $j_{DOC,R}$ should be associated to a regulated excretion of the excess carbon in response to nutrient limitation. Regulated excretion involves complex physiological processes related to the transformation, transport and release of these compounds through the cell membrane (Chin et al., 2004; Borchard and Engel, 2015). Thus, it is assumed that the DOC produced through this flux, denoted as DOC$_H$, should have a distinct composition from the cellular material. Fig. 2.4 b illustrates the DOC composition in DOC$_L$ and DOC$_H$. Note that the dynamics of DOC$_L$ and DOC$_H$ are not explicitly shown in Eq. 2.3. According to model results, during the N-replete phase DOC is almost entirely comprised by DOC$_L$ (mean value throughout the N-replete phase: 99%, Fig. 2.4 b, solid

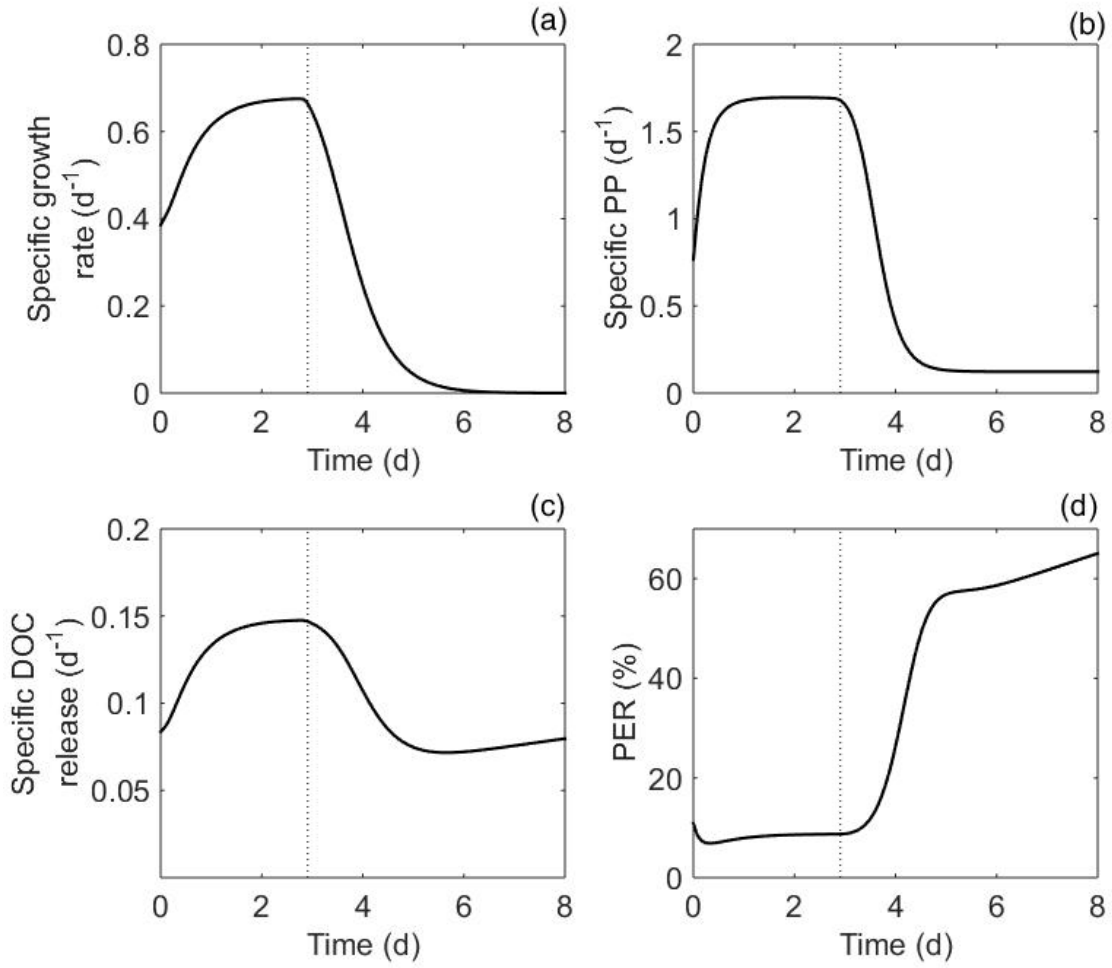

Figure 2.3: Structural mass-specific rates. (a) Net specific growth rate, (b) specific primary production (PP) rate, (c) specific DOC release rate and (d) Percentage Extracellular Release (PER). Vertical dotted line marks the two phases of nutrient availability (N-replete, N-limited).

line). As nutrient limitation progresses, the fraction of DOC_H (Fig. 2.4 b, dashed line), progressively increases, as a result of the increased relative importance of the $j_{DOC,R}$ flux (Fig. 2.4 a, dashed line). At the end of the simulation, DOC is composed by 46% and 54% of DOC_L and DOC_H, respectively.

The relationship between log-transformed total (calculated at the population level) DOC release and total primary production (PP) rate, is often reported in oceanographic studies and it is also presented here (Fig. 2.5 a) for comparison. Total DOC release and PP rates in the model are calculated by multiplying the specific DOC release and the specific PP rate with X_V. During the N-replete phase there is a positive linear relationship between DOC

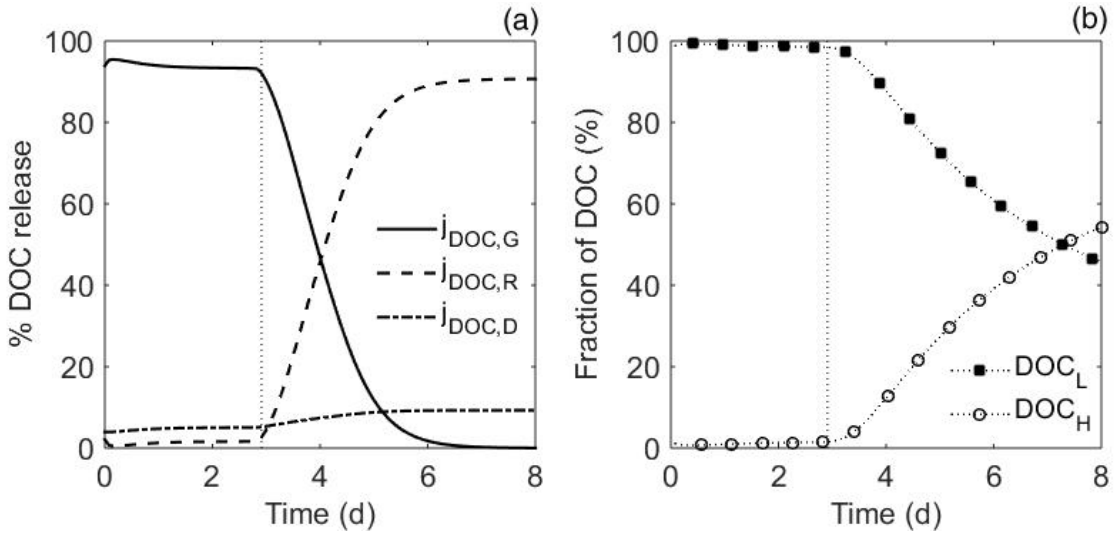

Figure 2.4: (a) Analysis of the DOC release rate into the contributing fluxes ($j_{DOC,G}$: solid line, $j_{DOC,R}$: dashed line, $j_{DOC,D}$: dash-dot line). (b) Composition of DOC produced by phytoplankton: the DOC produced via $j_{DOC,G}$ and $j_{DOC,D}$ fluxes (DOC_L, line with squares) and the DOC produced via $j_{DOC,R}$ flux (DOC_H, line with circles). Vertical dotted line marks the two phases of nutrient availability (N-replete, N-limited).

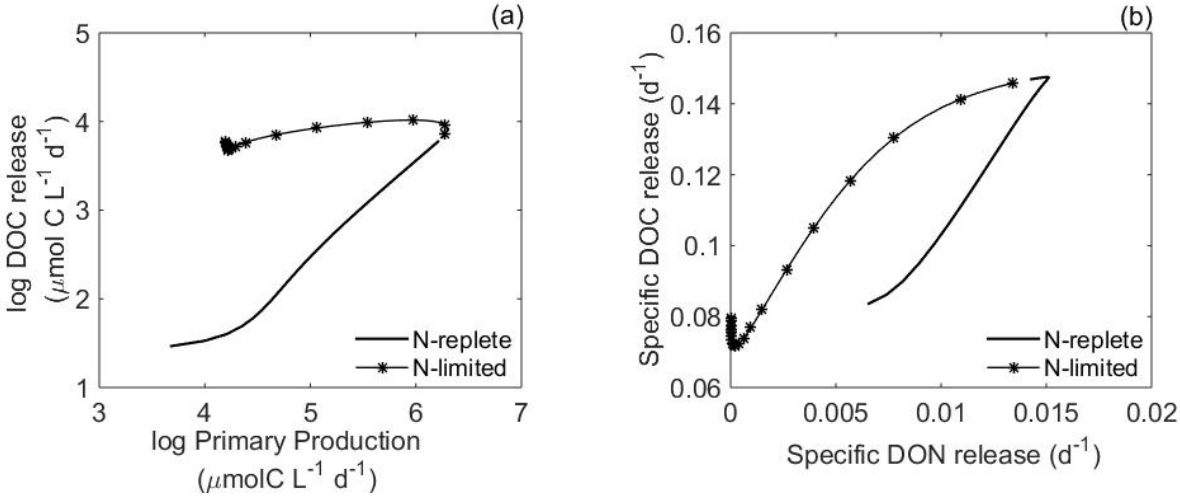

Figure 2.5: Relationships between (a) log-transformed total DOC release rate and total primary production and (b) structural-mass specific DOC release and DON release rate. Solid line denotes the N-replete phase and asterisks marks the N-limited phase.

release and PP rates (Fig. 2.5 a, solid line). In the N-limited phase, the linearity between PP and DOC release rate is lost because PP rate has a more rapid decrease to a minimum value than DOC release rate (Fig. 2.5 a, asterisks). The decrease in PP rate is due to the effect of nitrogen limitation on the photosynthetic rate (see Section 2.2.2). Comparing the

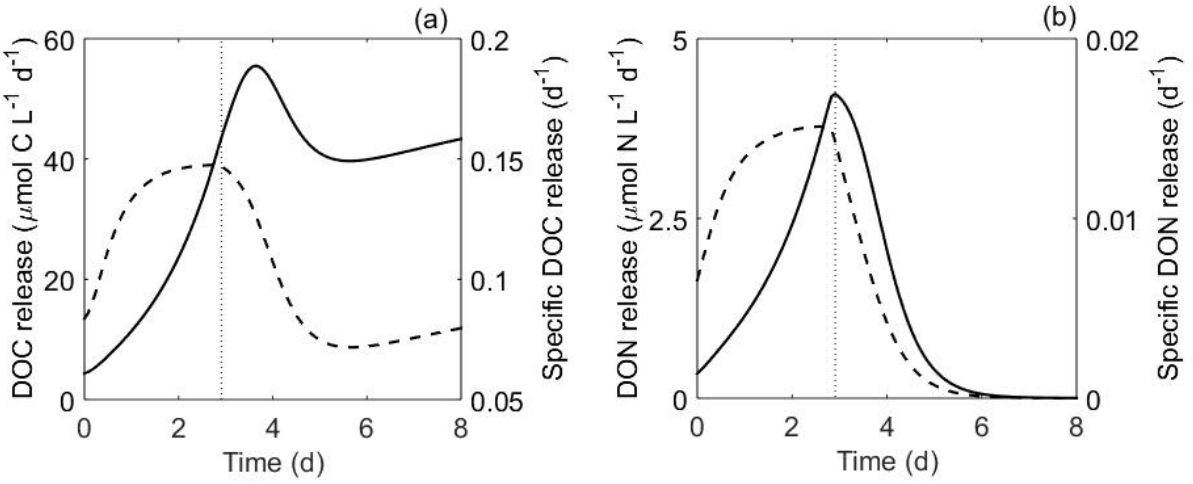

Figure 2.6: (a) Total DOC release rate (solid line) and structural-mass specific DOC release rate (dashed line). (b) Total DON release rate (solid line) and structural-mass specific DON release rate (dashed line). Vertical dotted line marks the two phases of nutrient availability (N-replete, N-limited).

log-transformed total DOC release with total net primary production, which in the model is calculated by multiplying the specific net growth rate, $\dot{r}$, with X_V, the same patterns described above for total DOC release and PP rates are observed (figure not shown).

Figure 2.5 b shows the relationship between structural mass-specific DOC release and DON release rate. During the N-replete phase the specific DOC and DON release are linearly linked (Fig. 2.5 b, solid line), thus a large fraction of DOC is combined with DON, in reality this probably being in the form of dissolved amino acids. In the N-limited phase, DOC and DON excretion rates are decoupled, as DON excretion declines to zero while DOC exudation declines more slowly and remains above zero throughout the N-limited phase (Fig. 2.5 b, asterisks). Thus, during this phase, DOC should be mainly composed of carbohydrates that do not contain nitrogen.

Temporal dynamics of total (calculated at the population level) and structural mass-specific DOC and DON release rates were plotted together for comparison (Fig. 2.6). Total DOC release is higher in the N-limited phase than in the N-replete phase. However, the structural mass specific DOC release has the opposite pattern presenting an increase during the N-replete phase (Fig. 2.6 a) and a decrease during the N-limited phase. On the other hand, both the total and the specific rate of DON release rates increase during the N-replete phase and decrease to zero during the N-limited phase (Fig. 2.6 b)

Elemental ratios of C and N of phytoplankton biomass and of produced DOM are shown in Fig. 2.7. During the N-replete phase, C:N of biomass and DOM are relatively constant, both presenting a mean value of 10 mol C mol N^{-1} (Fig. 2.7). In the N-limited phase, nitrogen depletion induced significant alterations in the physiological status of the cells, with the C:N

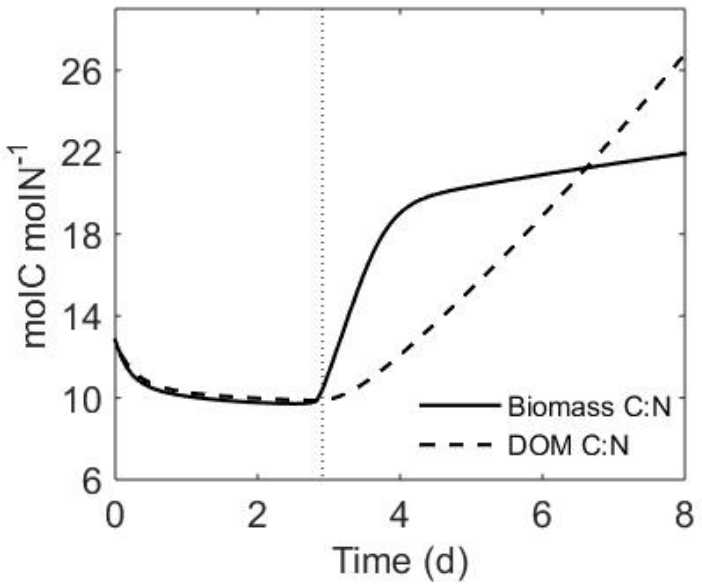

Figure 2.7: Time-course evolution of C:N ratio of biomass (solid line) and DOM (dashed line). Vertical dotted line marks the two phases of nutrient availability (N-replete, N-limited).

ratio of biomass being almost double, up to 22 mol C mol N^{-1}, at the end of the simulation. This decoupling of carbon and nitrogen dynamics in phytoplankton also affected DOM C:N ratio which rapidly deviated to reach its maximum, 27 mol C mol N^{-1} at the end of the simulation. The variations of elemental ratios of biomass is due to the variations of reserve densities, while the variation of the DOM elemental ratio is due to the different physiological processes of phytoplankton that contribute to the production of DOM in the two phases of N-availability, as shown in Fig. 2.4, and the decoupling of the DOC and DON release rate during the N-limited phase, as shown in Fig. 2.5 b.

2.4 Discussion

In this study, a dynamic model of phytoplankton growth has been developed, in order to elucidate the physiological mechanisms that govern the release of dissolved organic matter during the different growth phases of phytoplankton. The model explicitly includes nitrogen as the limiting nutrient and carbon reserves, therefore allowing one to follow the variable biomass stoichiometry, and also to account for the uncoupling between carbon and inorganic nutrients assimilation. Although the present study focuses only on one limiting substrate, namely nitrogen, because of the generality of DEB theory and in particular of the concept of synthesizing units, the model can be extended to include also phosphorus (e.g., Grossowicz et al. (2017a)). In Appendix A, the extended equation for the generalized reserves formation, considering both nitrogen and phosphorus as the limiting substrates is given (Eq. A.2).

Moreover, here only a purely autotrophic mode of nutrition is considered. However, because of the inclusion of the generalized reserves in the present formulation, the model can be extended to accommodate mixotrophic nutrition by combining autotrophy with either osmotrophy (uptake of DOM) or phagotrophy without altering the structure of the model, other than including the rules of merging the different assimilatory pathways (Kooijman et al., 2002). Furthermore, being based on the general framework for metabolic organization provided by DEB theory, the model, although calibrated against the diatom *T. pseudonana*, is applicable to other phytoplankton species. DEB theory provides the framework and the tools to obtain and systematically compare parameter values and properties derived from them for different phytoplankton species. For example, DEB theory has led to the development of the Add-my-Pet (AmP) online database (Marques et al., 2018) of DEB parameters and implied properties for animals.

Overall, the model was in agreement with the data retrieved from Flynn et al. (2008). However, towards the end of the N-limited phase, the increase in POC and the significant decrease in DOC observed in the data were not accurately reproduced by the model. Given that a further reduction was not observed in the inorganic carbon compartment, the increase in POC was not due to phytoplankton photosynthesis. Thus, a possible explanation would be the coagulation of the extracellular dissolved polysaccharides (DOC) to form transparent exopolymer particles (TEP) that would be measured as POC, as has been observed previously in cultures of *T. pseudonana* (Urbani et al., 2005). In addition, DON in the model is overestimated at certain time points. This could be possibly explained by the fact that diatoms may be able to utilize, to a certain extent, organic forms of nitrogen, mostly in the form of dissolved amino acids (Flynn et al., 2008); a process that is not accounted for in the current model.

Model results showed that specific growth and PP rates were higher during the N-replete phase and that both rates decreased to minimum values in the N-limited phase. DOC and DON were also produced at high structural mass-specific rates during the N-replete period of growth, while they were reduced to a minimum value in the N-limited phase. Conversely, PER, calculated as DOC release over PP rate, had lower values in the N-replete phase (mean throughout the N-replete phase: 8.2%) and higher values, up to 65%, in the N-limited phase, as a result of the progressive reduction of PP with the development of nutrient limitation. The pattern of specific PP and DOC release rates and the range of PER values predicted by the present model is in accordance with many experimental and field studies. For example, in nutrient-limited diatom cultures, maximum extracellular production of carbohydrates has been observed at the transition phase between the exponential and the stationary phase (Alcoverro et al., 2000; Urbani et al., 2005), while higher specific (per cell) carbohydrates and amino acids release rates have been observed in the exponential phase than in the stationary phase (Myklestad et al., 1989; Myklestad, 1995; Granum et al., 2002; Flynn et al., 2008). Furthermore, in a study with the diatom *Chaetoceros affinis* it was found that the specific photosynthetic rate was reduced by 50% in the transition phase to reach 10% of the exponential phase value during the stationary phase (Myklestad et al., 1989). Moreover, PER has been found to vary between 2–10% in the exponential phase and to reach up to

60% in the stationary, nutrient-limited phase, depending on the species and the condition of the culture (Myklestad, 2000). Field studies have also reported average PER values less than 10% in productive areas under nutrient-replete conditions and average values up to 46% under oligotrophic conditions (Teira et al., 2001a,b; Lagaria et al., 2013). Finally, total DOC release rate, that is the specific production rate of DOC multiplied by the total structural biomass, was higher in the N-limited phase than in the N-replete phase. This was a result of the higher population size during this phase, as well as due to the accumulation of E_C-reserves that are actively excreted from the cells. On the other hand, total DON release rate was higher during the N-replete phase and reduced, approximating zero, during the N-limited phase. This was the result of the reduction of the growth rate and the associated production flux of DON ($j_{DON,G}$, Eq. 2.11) and also due to the decline of the E_N reserves.

In the present study it was assumed that the DOC released due to growth and death processes (DOC_L) will have a composition similar to the cellular material. In addition, during the N-replete phase, most DOC is in the form of DOC_L and DOC and DON release rates are stoichiometrically coupled. Therefore, part of DOC_L should be associated with DON probably in the form of dissolved amino acids, that are known to be released at high rates from N-replete cells (Myklestad et al., 1989; Flynn et al., 2008). On the other hand, it was assumed that DOC produced under N-limiting conditions, associated with the mechanism of rejection of unprocessed substrates by the SU (DOC_H), should have a more distinct composition from the cellular material. Furthermore, the reduction of DON release rate during the N-limited phase and the subsequent increase in the C:N ratio of produced DOM, indicates that DOC_H produced under N-limiting conditions should be mainly in the form of nitrogen-free compounds, such as carbohydrates.

In accordance with the model assumptions and results, cell structural material of various phytoplankton species has been characterized by high mole percentages of glucose (Biersmith and Benner, 1998), while in cultures of marine diatoms glucose has been also identified as the most abundant monomer during the exponential, nutrient-replete phase of growth in the extracellular carbohydrates. A pronounced decrease of glucose and increase of heteropolysacharides, containing various monomers, has been observed in the stationary phase (Underwood et al., 2004; Urbani et al., 2005). In addition, in N-replete cultures of *T. pseudonana* amino acids accounted for 70% of total DOC while carbohydrates accounted for the rest 30%. On the other hand, extracellular release of amino acids decreased markedly in the stationary phase of N-limited cultures of the diatom *Chaetoceros affinis* (Myklestad et al., 1989). Moreover, in P-limited cultures of *Emiliania huxleyi* at steady-state, it was found that glucose was the dominant monomer in both the small size fraction (1–10 kDa) of dissolved polysacchrides and the particulate fraction (cell content), while it was less significant in the larger size fractions (>10 kDa) that had a more distinct composition than the cellular material (Borchard and Engel, 2015). Furthermore, Pete et al. (2010) found that high molecular weight polysaccharides (>1400 kDa) formed a major component of the DOM produced by N-limited cultures of *Skeletonema costatum*, while increased C:N ratios of DOM upon nitrogen limitation have been also observed (Wetz and Wheeler, 2004; Conan et al., 2007; Pete et al., 2010). Thus, it has been suggested that the release of DOC with size < 10 kDa

is associated with the passive diffusion mechanisms since these small molecules can passively cross the cell membrane. Larger DOC (>10 kDa), due to its size and distinct molecular composition, should be released via active trans-membrane release and ,thus, via the active exudation mechanism (Borchard and Engel, 2015).

In the present study, using the DEB model for phytoplankton (Kooijman, 2010) and without making further assumptions, two alternative pathways of DOM release emerge from the theory, one relating to growth and one to excretion of the non-limiting compound. These pathways represent the two conceptual mechanisms of DOM release, i.e., passive diffusion and active exudation, respectively. Release of the cellular material due to cell lysis can be also seen as another path related to the passive diffusion mechanism. One of the the most rigorous attempts to mechanistically model DOM release to date was performed by Flynn et al. (2008). In that work, the authors explored alternative formulations of DOM release with increasing levels of complexity and concluded that DOM release rate should be related to the nutrient status of the cells. Thus, in the most complex model presented in Flynn et al. (2008), the authors employed an empirical description that related the relative rate of leakage of DOC and DON to the N:C status of the cells. On the other hand, the DEB model for phytoplankton growth and the theory of SU provides a formulation that allows one to model the active exudation process of the non-limiting compounds as a function of reserve dynamics. The advantage of this approach is that the latter process is an emergent property of the DEB model that nicely reproduces the experimental evidence related to the active exudation of the non-limiting nutrient under unbalanced growth. Moreover, in the Flynn et al. (2008) model there is another empirical formulation that assumed a higher rate of leakage until the external concentration attained a critical value, in order to account for the rapid accumulation of DOM observed during the initial stages of the culture (Flynn and Berry, 1999). On the other hand, in the model presented here, on the basis of DEB theory's assumptions for product formation, a second process of DOM excretion is described, which is stoichiometrically coupled to the growth rate and results in high rates of DOM production during the initial nutrient-replete phase of the culture. This can be seen as an overhead for growth as this material is passively leaked outside the cell.

The model results presented in this work indicate that nutrient availability determines which pathway of DOM release will dominate, as has been previously suggested (Mueller et al., 2016). The relative importance of each of the two pathways, will have implications for the size and quality of DOM produced and its subsequent utilization by bacteria. According to model results, during the phase of unlimited growth the physiological mechanism responsible for DOM production is mainly related to the growth rate of phytoplankton and, thus, to the passive diffusion hypothesis (Bjørnsen, 1988; Mueller et al., 2016). DOM produced via the passive diffusion mechanism should be composed of low molecular weight compounds with a high content of glucose and amino acids and should have a low C:N ratio, a characteristic of labile DOM (Hopkinson and Vallino, 2005). This organic matter is efficiently utilized by bacteria (Hama and Yanagi, 2001; Puddu et al., 2003; Pete et al., 2010; Wear et al., 2015b). As a result, a tight coupling is expected between phytoplankton production and bacterial production. This expectation is actually confirmed from field studies that report

a direct coupling of phytoplankton–bacteria dynamics in productive, upwelling ecosystems (Teira et al., 2015; Wear et al., 2015a) or in microcosms after nutrient additions (Lagaria et al., 2011; Fouilland et al., 2014). On the contrary, model results showed that under nutrient limiting conditions carbon assimilation continues, while the carbohydrates' incorporation into structural material slows down due to limited supply of N. The extra carbon is stored in the E_C-reserves and as a result the C:N ratio of biomass rapidly increases. As N-limitation continues, the photosynthetic ability of the cells is diminishing, while the accumulated intracellular carbohydrates are partially released in the environment due to the rejection flux of the non-limiting compound (i.e., organic carbon) and, thus, the active exudation mechanism (Fogg, 1983; Mueller et al., 2016). The active exudation of C-rich DOM causes an increase in the DOC:DON ratio with a time lag of about one day, relative to the increase of the C:N ratio of biomass, and eventually, by the time that growth has stopped, the C:N ratio of DOM becomes higher than that of biomass. Similar results were reported in Van Den Meersche et al. (2004). DOM produced via this mechanism has a high C:N ratio, a characteristic of recalcitrant DOM (Hopkinson and Vallino, 2005; Carlson and Hansell, 2015), and should be mainly composed of high molecular weight heteropolysacharides. This type of DOM may escape bacterial degradation and, thus, accumulate in the water column (Obernosterer and Herndl, 1995; Thingstad et al., 1997; Hama and Yanagi, 2001). Consequently, the lack of correlation between phytoplankton PP or DOC release and bacterial production often documented in nutrient poor conditions (Lagaria et al., 2011; Fouilland et al., 2014; Teira et al., 2015) may be related, at least to some extent, to the prevalence of the rejection flux and, thus, the active exudation mechanism.

The relationship between primary production and DOC release is of great interest in the field studies but to date it has not been fully understood, since, based on empirical and experimental observations, both linear and non-linear relationships have been observed. For example, Teira et al. (2001a) showed that there was a linear relationship between log-transformed primary production and DOC release rates for three upwelling regions (Benguela (SW Africa), Mauritania (NW Africa) and NW Spain) while for data from the oligotrophic North Atlantic subtropical gyre no significant relationship was found. The present model study revealed that these two rates, DOC release and PP, present a linear relationship only in the nutrient-replete phase of growth, while this relationship is lost during the nutrient-limited phase. This deviation is a result of the prevalence of the active exudation mechanism and the reduction of PP rate due to nutrient limitation. Under this point of view, the variability found in field data may be better understood. For example, in the experiments of Lagaria et al. (2011), a strong linear relationship can only be observed when the data corresponding to the double nitrogen and phosphorus additions are considered, while no apparent relationship is observed, when taking into account the separate nutrient additions, since the system was most probably co-limited by nitrogen and phosphorus. However, from an ecosystem point of view, other food web processes of indirect release of DOM by phytoplankton, such as sloppy feeding by zooplankton and viral lysis, may also contribute to the patterns between primary production and DOM release observed in oligotrophic environments (Teira et al., 2001a).

In this Chapter, a dynamic model has been developed that explicitly describes the release

of DOM by phytoplankton under N-replete and N-limiting conditions and captures common patterns observed in various phytoplankton cultures. The model presented here is based on the general framework provided by DEB theory and, although calibrated with data for the diatom *T. pseudonana*, it can describe the growth and DOM release of any phytoplankton species. Testing the model's performance with a variety of phytoplankton species, representative of the major taxa in marine ecosystems and ideally grown in axenic cultures, will further improve its accuracy and prediction power. The model allows for the distinction and assessment of the two conceptual mechanisms of DOM release: the passive diffusion, which is related to growth and lysis of the cells, and the active exudation, which is related to rejection of unprocessed substrates by the SUs. Based on the findings of the present study, these two mechanisms are not mutually exclusive but their relative importance depends on the nutrient-status of the cells. In addition, the assumption that these two mechanisms will produce DOM of distinct quality and size fractionation is supported by observations from phytoplankton cultures. However, to quantitatively test this assumption a mass-balanced data set describing the dynamics of nitrogen and carbon and also the different size fractions of produced DOM would be needed. Finally, the present model suggests that the prevalence of the active exudation mechanism may be a possible explanation for the decoupling of primary production and DOC release and of primary production and bacterial production, observed in oligotrophic conditions.

Chapter 3

Modelling the nutritional strategies in pigmented nanoflagellates

3.1 Introduction

Pigmented nanoflagellates (PNF) have been identified as major consumers of bacteria particularly in oligotrophic systems where they can be responsible for more than half of total bacterivory (Unrein et al., 2007; Zubkov and Tarran, 2008). In addition, the significance of mixotrophy as a trophic mode in PNF and the associated important ecological implications for the functioning of marine food webs has been demonstrated by ecological models (Mitra et al., 2014; Ward and Follows, 2016; Leles et al., 2018). In most of these studies, PNF are regarded as a single group. However, PNF comprise a diverse phylogenetic group, displaying high variability in terms of the relative contribution of phototrophy and phagotrophy to their growth. In addition, PNF display great variation in their ability to adjust their nutritional strategy in response to environmental conditions. This huge metabolic plasticity has been demonstrated by many laboratory studies (e.g., Liu et al., 2016; Lie et al., 2018; Wilken et al., 2020) and results in great functional diversity in the group of PNF, which has important implications for the fluxes of matter and energy through the microbial food web under changing environmental conditions.

A first attempt to systematically describe the various physiological types of PNF was made by Jones (1997) who classified mixotrophic protists into four groups based on their nutritional behavior. Stoecker (1998) proposed conceptual models for the different physiological types of mixotrophic flagellates based on functional responses. Stoecker (1998) identified

This work is published in: **Livanou, E.**, Barsakis, K., Psarra, S. and Lika, K. 2020. Modelling the nutritional strategies in mixotrophic nanoflagellates. Ecological Modelling 428, 109053.

three physiological types of phagotrophic "algae" which are primarily phototrophic and can assimilate dissolved inorganic nutrients, while i) feeding is initiated in response to nutrient limitation (e.g., N, P or Fe) (Type IIA), ii) feeding is a strategy to obtain organic compounds necessary for growth (Type IIB), and iii) feeding is a response to low light in order to obtain energy and carbon (Type IIC). Furthermore, mixotrophic nanoflagellates that are primarily phagotrophic, are termed as Type IIIA in Stoecker (1998) and they are characterized by the ability to engage in phototrophy through carbon fixation and inorganic nutrients assimilation when prey are scarce.

To date, diverse approaches in modelling the nutrition of constitutive mixotrophs have been developed with a varying level of complexity. Simpler approaches use additive descriptions of phototrophy and phagotrophy, with no reference to the dynamic interchange of the two modes of nutrition (Thingstad et al., 1996; Stickney et al., 2000; Hammer and Pitchford, 2005). Kooijman and colleagues (Kooijman et al., 2002; Troost et al., 2005b) were the first that attempted to model mixotrophic organisms with reference to the physiological mechanisms of energy assimilation and usage by the individuals. In their work, however, they did not resolve the dynamic interaction between the phototrophic and phagotrophic nutritional strategy. On the other hand, Flynn and colleagues (Flynn and Mitra, 2009; Mitra et al., 2014; Ghyoot et al., 2017; Leles et al., 2018) incorporated the interactions between the alternating energy and nutrient acquisition pathways using regulatory functions that modulate the rates of phototrophy and phagotrophy under certain physiological conditions. Nevertheless, the spectrum of nutritional strategies found in the PNF group, as was conceptualized by Stoecker (1998), has not been mathematically described to date. However, a mechanistic modelling framework for the different functional types of mixotrophic nanoflagellates is necessary, in order to understand how their role in biogeochemical processes is affected by the prevailing environmental factors and, therefore, to predict how carbon and nutrients cycles will respond to the global climate change.

The aim of this study is to develop mathematical models that describe the functional responses for the four groups of PNF proposed by Stoecker (1998) (Types IIA, IIB, IIC, IIIA). This chapter is organized as follows: Section 3.2 presents the general modelling framework for describing the dynamic combination of phototrophy and phagotrophy by the different types of PNF. Then, these mathematical expressions are incorporated in the Dynamic Energy Budget (DEB) model for photosynthetic cells, presented in Chapter 2, in order to describe the growth kinetics of the four PNF types. Section 3.3 presents the resulting functional responses as well as the growth kinetics for the different PNF types under varying availability of the three regulating resources, namely, irradiance, dissolved inorganic nutrients, and prey availability. Finally, in Section 3.4 the modelling approach is discussed and comparisons are made between the model output and qualitative observations compiled from experiments performed with organisms representative of each one of the four PNF types.

3.2 Methods

3.2.1 Formulation of processes

PNF combine light, inorganic nutrients and microbial prey to form new biomass. In DEB theory context, biomass is partitioned into reserves and structural mass. The assimilated substrates are first transformed into generalized reserves (E) which are described as mixtures of soluble structural biomass precursors with a fixed stoichiometry. Generalized reserves are then catabolized to cover maintenance and to increase the structure (V) of the cells (Kooijman et al., 2002, Chapter 2 of the present thesis).

A schematic presentation of the processes taking place within the four different types of PNF during the assimilation (A) of resources into E-reserves is shown in Fig. 3.1. Inorganic carbon (IC), inorganic nutrients (N) and bacterial prey (F) are taken up from the environment by a simple one-substrate SU (Eq. B.1). Photosynthetic units (PSU) harvest light (L) and produce reductant (Eq. B.2), which is combined with inorganic carbon in a complementary and parallel transformation to form photosynthetically produced organic carbon (C). In the next step, generalized reserves are formed from the combination of carbon and nutrients obtained via the two pathways of phototrophy and phagotrophy. Phototrophy is defined as the process of assimilating organic carbon from photosynthesis and nutrients into reserves, while phagotrophy is defined as the process of prey consumption. Figure 3.2 shows schematically the merging of the assimilates from the phototrophic and phagotrophic pathways into E-reserves for the four types of PNF. In the following subsections the different types of PNF are presented. Table 3.1 introduces the symbols of variables and parameters used in the models' equations, while their derivations are given in Appendix B.

Table 3.1: Table of frequently used symbols. (V: structure, E: generalised reserves)

Symbol	Interpretation (Units)
θ	Fraction of synthesizing units (–)
$\hat{\theta}$	Fraction of synthesizing units in quasi-steady state (–)
j_*	Specific arrival / production rate of compound $*$ (mol $*$ (mol V)$^{-1}$ d^{-1})
j_*^+	Specific consumption rate of compound $*$ (mol $*$ (mol V)$^{-1}$ d^{-1})
$j_{E,A}$	Specific generalised reserves formation rate (mol E (mol V)$^{-1}$ d^{-1})
$\dot{k}_*$	Handling rate of compound(s) $*$ by SU (d^{-1})
y_{ij}	Stoichiometric coefficients (amount of compound i required per compound j formed) (mol i (mol j)$^{-1}$)

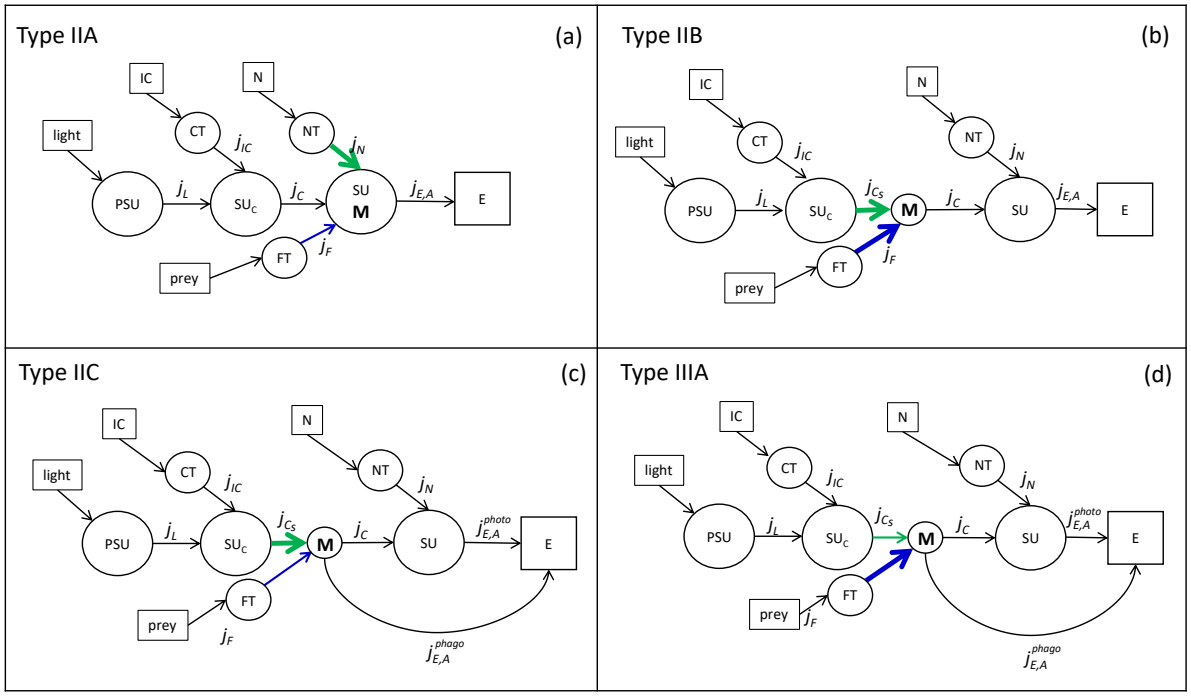

Figure 3.1: Schematic presentation of the model for the four types of mixotrophic strategies. Boxes represent concentrations, circles synthesizing units/transporters and arrows fluxes. CT, NT, FT: carbon–, nutrients–, prey–transporter, PSU: photosynthetic unit. SU_C: synthesizing unit for photosynthetically produced organic carbon. Bold coloured arrows denote the preference for substrates obtained via each of the two trophic pathways (i.e., phototrophy (green) and phagotrophy (blue)), M denotes the point of merging of the two pathways. E: reserves. j_* denote fluxes (normalized to structural mass) of arriving substrates ($* = $ IC, inorganic carbon; N, inorganic nutrients; L, light) or production fluxes ($* = $ C, photosynthetically produced organic carbon; C_S, intermediate product during photosynthesis). $j_{E,A}$ denotes the reserves assimilation flux. (a) Type IIA mixotrophy: algae that are primary phototrophic but consume prey to obtain limiting nutrients. (b) Type IIB mixotrophy: algae that use phagotrophy to obtain a required organic compound necessary for growth. (c) Type IIC mixotrophy: algae that are primarily phototrophic but consume prey in order to obtain organic carbon under light-limiting conditions. (d) Type IIIA mixotrophy: algae that are primarily phagotrophic but photosynthesize under prey-limiting conditions.

Type IIA

In type IIA PNF, such as *Prymnesium parvum* (Carvalho and Granéli, 2010) and *Isochrysis galbana* (Anderson et al., 2018), phototrophy is the dominant mode of nutrition, whereas phagotrophy is initiated in response to inorganic nutrient (e.g., nitrogen, phosphorus) limitation (Stoecker, 1998). In this mode of mixotrophy, inorganic nutrients and nutrients

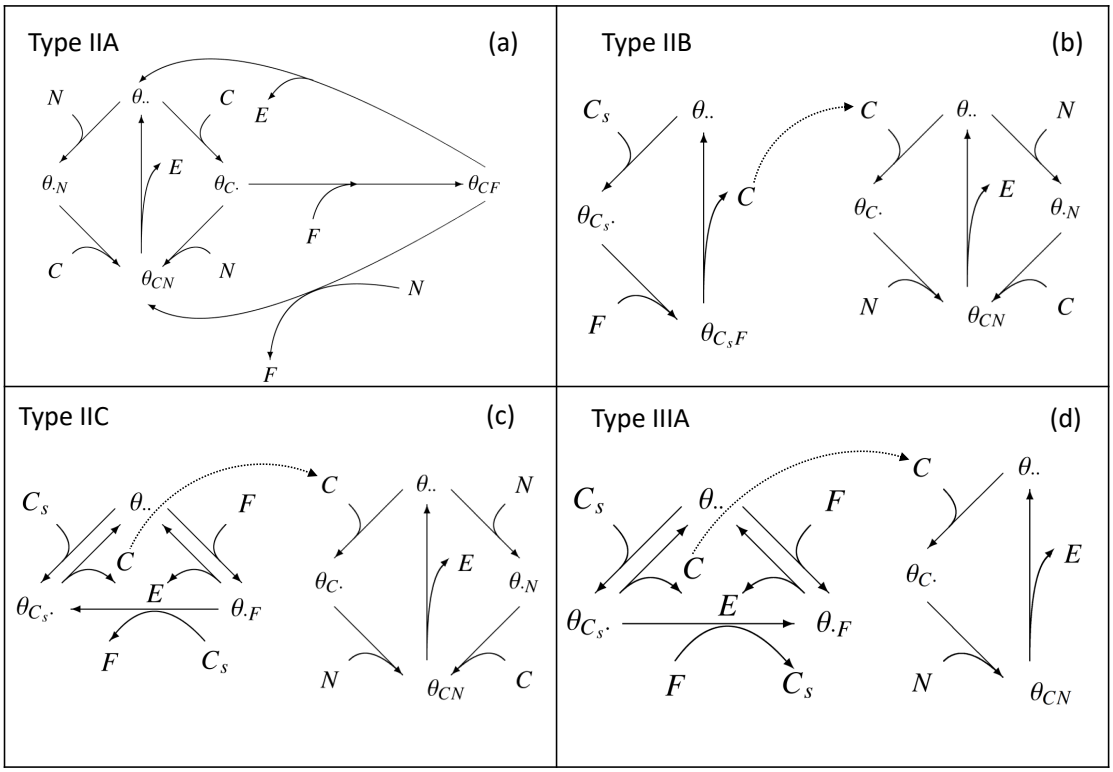

Figure 3.2: Scheme of the transformations of substrates, showing the merging of the assimilates from the phototrophic and phagotrophic pathways into E-reserves for the four mixotrophic strategies. Following the standard notation of DEB theory, θ_{*1*2} represents the fraction of SU that have bound both substrates $*_1$ and $*_2$, $\theta_{..}$ represents the fraction of free SU that haven't bound any substrate, while $\theta_{*1.}$ and $\theta_{.*_2}$ denote SU that have bound either $*_1$ or $*_2$ substrates, respectively. Arriving substrates: N, inorganic nutrients; C, photosynthetically produced organic carbon; C_s, intermediate product during photosynthesis; F, bacterial prey.

obtained via phagotrophy are considered substitutable substrates and interact at the level of E-reserves synthesis after the formation of photosynthetically derived organic carbon by the SU_C (Eq B.3) (Fig. 3.1 a). It is assumed that only the nutrients from prey are used for E-reserve formation, whereas the organic carbon from prey is excreted to the environment. These model assumptions are supported by observations showing that in *Prymnesium parvum* chlorophyll α content in feeding and non-feeding cells is constant, which suggests that carbon fixation rate is not downregulated as a result of prey consumption (Carvalho and Granéli, 2010) and that cellular carbon is mostly derived from photosynthesis, whereas the carbon from prey is not assimilated at any substantial level (Liu et al., 2015a; Carpenter et al., 2018). In addition, inorganic nutrients are preferred over nutrients obtained

from prey. Thus, a free SU can bind the arriving organic carbon molecules C in parallel with arriving inorganic nutrients N, and proceed to E-reserve formation. Moreover, a SU that has already bound a C-molecule may bind the arriving nutrient molecules, F, from the phagotrophic pathway, and then proceed to E-reserve formation, or reject it if a N-molecule arrives (Fig. 3.2 a).

The dynamics of the fractions of SUs at the five different states ($\theta_{..}$, $\theta_{.N}$, $\theta_{C.}$, θ_{CN}, θ_{CF}, in Fig. 3.2 a) are described in detail in Appendix B (Eq. B.4). According to the transformation rules of type IIA mixotrophy, the rate of E-reserves assimilation is proportional to the fractions of SUs at quasi-steady state $\hat{\theta}_{CN}$ and $\hat{\theta}_{CF}$ (Eq. B.5). Thus, E-reserves are formed at a rate $j_{E,A} = \dot{k}_{CN}\hat{\theta}_{CN} + \dot{k}_{CF}\hat{\theta}_{CF}$ (Eq. B.6). The explicit solutions of $\hat{\theta}_{CN}$ and $\hat{\theta}_{CF}$ are lengthy and their substitution in Eq. (B.6) does not result in a simpler expression. For this type of nutritional strategy, the rates of organic carbon (j_C^+), prey (j_F^+) and inorganic nutrients (j_N^+) used for E-reserves formation are

$$j_C^+ = y_{CE}(\dot{k}_{CN}\hat{\theta}_{CN} + \dot{k}_{CF}\hat{\theta}_{CF}) \qquad j_F^+ = y_{FE}\dot{k}_{CF}\hat{\theta}_{CF} \qquad j_N^+ = y_{NE}\dot{k}_{CN}\hat{\theta}_{CN} \tag{3.1}$$

where $\hat{\theta}_{CN}$ and $\hat{\theta}_{CF}$ are given by (Eq. B.5). Phototrophy rate and phagotrophy rate are quantified by j_C^+ and j_F^+, respectively. All respiratory costs of the phototrophic or the phagotrophic pathways, quantified by y_{CE}, are paid by photosynthesis. Unassimilated carbon and nutrients from prey are excreted to the environment.

Type IIB

PNF of type IIB use phagotrophy as a nutritional strategy to obtain organic compounds necessary for growth such as various forms of organic carbon (e.g., phospholipids) or essential micronutrients (e.g., vitamins) (Fig. 3.1 b) (Stoecker, 1998). An example of type IIB mixotroph is some chrysophytes of the genus *Dinobryon* (Caron et al., 1993; Liu et al., 2016). In this mode of mixotrophy, during photosynthesis, the two complementary substrates light and inorganic carbon form an intermediate product, C_s, at a rate j_{C_s}, which is given by Eq. (B.3) with $\dot{k}_C = 0$, since the two substrates are bound to the SU_C but not processed yet. Then, a free SU binds first the arriving product of photosynthesis C_s (Fig. 3.2 b, left) and subsequently binds the complementary substrate from phagotrophy F to form organic carbon, C, at rate j_C (Eq. B.9) in a complementary-sequential transformation. Apart from organic carbon type IIB PNF can also assimilate nutrients contained in prey. These assumptions are based on experiments with *Dinobryon cylindricum* showing that this species can obtain up to 50% of its cellular carbon through prey ingestion and up to 100% of its cellular nitrogen and phosphorus from bacteria (Bird and Kalff, 1987; Caron et al., 1993). Consequently, the organic carbon in combination with inorganic nutrients and nutrients from prey will form the generalized E-reserves (Fig. 3.2 b, right) in a complementary and parallel transformation, at a rate $j_{E,A}$ given by Eq. (B.10). The derivation of the rates of product formation is described in Appendix B. For this type of nutritional strategy, the rates of organic

carbon (j_C^+), prey (j_F^+) and nutrients (j_N^+) (inorganic and from prey) used for E-reserves formation are

$$j_C^+ = y_{CE} j_{E,A} \qquad j_F^+ = y_{FC} j_C \qquad j_N^+ = y_{NE} j_{E,A} \tag{3.2}$$

where j_C is given by Eq. (B.9) and $j_{E,A}$ is given by Eq. (B.10). Phototrophy rate and phagotrophy rate are quantified by j_C^+ and j_F^+, respectively. The respiratory costs of assimilation are included in the stoichiometric coefficient y_{CE} while the costs of phagotrophy are included in the stoichiometric coefficient y_{FC}. Unassimilated carbon and nutrients from prey are excreted to the environment.

Type IIC

In type IIC PNF, phototrophy is the dominant mode of nutrition, while phagotrophy is initiated in response to light limitation as a strategy to obtain energy and carbon (Fig. 3.1 c) (Stoecker, 1998). *Chrysochromulina brevifilum* is a species exhibiting this type of nutrition using phagotrophy as a means to obtain carbon along with nutrients when light availability limits photosynthesis (Jones, 1997). In this type of mixotrophic strategy the substrates from phototrophy and phagotrophy are substitutable and their binding to the SU is parallel but with a preference for phototrophy (Fig. 3.2 c, left). The two complementary substrates light, L, and inorganic carbon, IC, are arriving to the SU_C to form an intermediate product, C_s, at a rate j_{C_s} (Eq. B.3, with $\dot{k}_C = 0$). A free SU may bind C_s and proceed to the formation of organic carbon, which will be combined with inorganic nutrients (N) in a complementary and parallel transformation to form reserves (Fig. 3.2 c, right), or it may bind the substrate F and proceed to the phagotrophic pathway (Fig. 3.2 c, left). The two pathways combined produce E-reserves at a rate $j_{E,A} = j_{E,A}^{phago} + j_{E,A}^{photo}$ (Eqs. B.14 and B.16). The derivation of the rates of product formation is described in Appendix B. For this type of nutritional strategy, the rates of organic carbon (j_C^+), prey (j_F^+) and inorganic nutrients (j_N^+) used for E-reserves formation are

$$j_C^+ = y_{CE} j_{E,A}^{photo} \qquad j_F^+ = y_{FE} j_{E,A}^{phago} \qquad j_N^+ = y_{NE} j_{E,A}^{photo} \tag{3.3}$$

where $j_{E,A}^{phago}$ is given by Eq. (B.14) and $j_{E,A}^{photo}$ is given by Eq. (B.16). Phototrophy rate and phagotrophy rate are quantified by j_C^+ and j_F^+, respectively. The costs of phagotrophy, quantified by the stoichiometric coefficient y_{FE}, are paid by carbon obtained from prey while the costs of phototrophy, quantified by the stoichiometric coefficient y_{CE}, are paid by photosynthetically produced carbon. Unassimilated carbon and nutrients from prey are excreted to the environment.

Type IIIA

PNF of type IIIA are primarily heterotrophic that use phototrophy when prey is limiting (Fig. 3.1 d) (Stoecker, 1998). *Ochromonas* sp. strain BG-1 is an example of type IIIA mixotroph (Lie et al., 2017). As in types IIB and IIC mixotrophy, the two complementary substrates light, L, and inorganic carbon, IC, form the intermediate substance C_s at a rate j_{C_s} (Eq. B.3, with $\dot{k}_C = 0$), which then interacts with the substrate obtained from phagotrophy, F, in a parallel and substitutable transformation, with preference for phagotrophy (Fig. 3.2 d, left). A free SU may bind the substrate F and proceed to the phagotrophic pathway or the substrate C_s and proceed to the phototrophic pathway. The phototrophic pathway proceeds in the formation of organic carbon, which will be combined with inorganic nutrients in a complementary and sequential transformation to form E-reserves (Fig. 3.2 d, right). The two pathways combined produce E-reserves at a rate $j_{E,A} = j_{E,A}^{phago} + j_{E,A}^{photo}$ (Eqs. B.20 and B.22). The derivation of the rates of product formation is described in Appendix B. For this type of nutritional strategy, the rates of organic carbon (j_C^+), prey (j_F^+) and inorganic nutrients (j_N^+) used for E-reserves formation are

$$j_C^+ = y_{CE} j_{E,A}^{photo} \qquad j_F^+ = y_{FE} j_{E,A}^{phago} \qquad j_N^+ = y_{NE} j_{E,A}^{photo} \tag{3.4}$$

where $j_{E,A}^{phago}$ is given by Eq. B.20 and $j_{E,A}^{photo}$ is given by Eq. B.22. Phototrophy rate and phagotrophy rate are quantified by j_C^+ and j_F^+, respectively. The costs of phagotrophy (quantified by y_{FE}) are paid by carbon obtained from prey while the costs of phototrophy (y_{CE}) are paid by photosynthetically produced carbon.

Experiments with *Ochromonas* sp. have shown that this algae releases dissolved inorganic nutrients when grown heterotrophically in both light and dark conditions (Rothhaupt, 1997; Sanders et al., 2001) while it consumes inorganic nutrients only when prey is unavailable (Rothhaupt, 1997). Moreover transcriptomics studies with the same organism suggest that ammonium transporters are not always expressed but their expression is upregulated only when prey is not available (Lie et al., 2017). These evidence suggest that inorganic nutrients should be taken up based on a demand rather than a supply system and, therefore, the uptake rate is quantified as $j_N = j_N^+$. Any unassimilated carbon and nutrients from prey or any surplus of organic carbon from photosynthesis quantified from the relationship $(j_C - j_C^+)$ (with j_C given in Eq. (B.21)) is excreted outside the cell.

3.2.2 Modelling mixotrophic growth

In order to study their growth dynamics under varying availability of the regulating resources, namely inorganic nutrients, prey and irradiance, the models developed above for the four types of PNF are incorporated into the DEB model for photosynthetic cells presented in detail in Chapter 2. A brief description of the model can be found in Appendix B and model equations are presented in Table B1 in the Appendix B.

Parameterization of mixotrophic models requires detailed information on their physiology and although considerable effort has been placed towards this direction (McKie-Krisberg et al., 2015; Terrado et al., 2017; Carpenter et al., 2018; Anderson et al., 2018) complete data sets covering all physiological processes (e.g., nutrient acquisition, ingestion rate, photosynthesis rate, growth rate) that are necessary for model validation are still lacking. As such, here, emphasis is placed on the qualitative rather than the quantitative results during model analysis and interpretation of model output. Thus, the focus of this study is the development of theoretical models for the functional responses and analyze the growth dynamics of the four types of PNF under varying availability of irradiance, inorganic nutrients and prey using parameters given in Table B2 in the Appendix B. In addition, Appendix B provides justification on parameter choices. The limiting inorganic nutrient could be either nitrogen or phosphorus, however for the purposes of this work the models have been parameterized for inorganic nitrogen.

3.3 Results

3.3.1 Functional responses

Figures 3.3 – 3.6 show for the four types of PNF, how the rates of phototrophy (j_C^+) and phagotrophy (j_F^+) are varying as functions of the three regulating substrate fluxes, namely, inorganic nutrients, prey and photons arrival fluxes to the SU.

In type IIA mixotrophs, phototrophy increases with inorganic nutrients flux (Fig. 3.3 a). Phototrophy has also a positive relationship with prey availability (Fig. 3.3 b) as inorganic nutrients are substituted by nutrients contained in prey; the increase in phototrophy is enhanced under inorganic nutrient limitation. Phagotrophy decreases when inorganic nutrients flux increases (Fig. 3.3 c), while it has a positive relationship with photons arrival flux (Fig. 3.3 d). The latter means that when photosynthetic carbon production increases, and inorganic nutrients availability is low, feeding is enhanced to supplement nutrients. In type IIB mixotrophy, phototrophy increases with both inorganic nutrients and prey arrival flux (Fig. 3.4 a, b). On the other hand, phagotrophy does not depend on inorganic nutrients availability (Fig. 3.4 c) but it increases with photons arrival flux (Fig. 3.4 d). In mixotrophs of type IIC, phototrophy increases with inorganic nutrients flux (Fig. 3.5 a) but it does not depend on prey availability (Fig. 3.5 b). Phagotrophy decreases with photons arrival flux (Fig. 3.5 d), as the organism prefers phototrophy over phagotrophy when light for photosynthesis is available, however, phagotrophy does not depend on the inorganic nutrients arrival flux (Fig. 3.5 c). In type IIIA mixotrophs, phototrophy increases with inorganic nutrients arrival flux (Fig. 3.6 a), whereas, it decreases with prey availability (Fig. 3.6 b), as the organism prefers phagotrophy over phototrophy when prey is available. Finally, phagotrophy rate is irrelevant to inorganic nutrients as well as to photons arrival flux (Fig. 3.6 c, d).

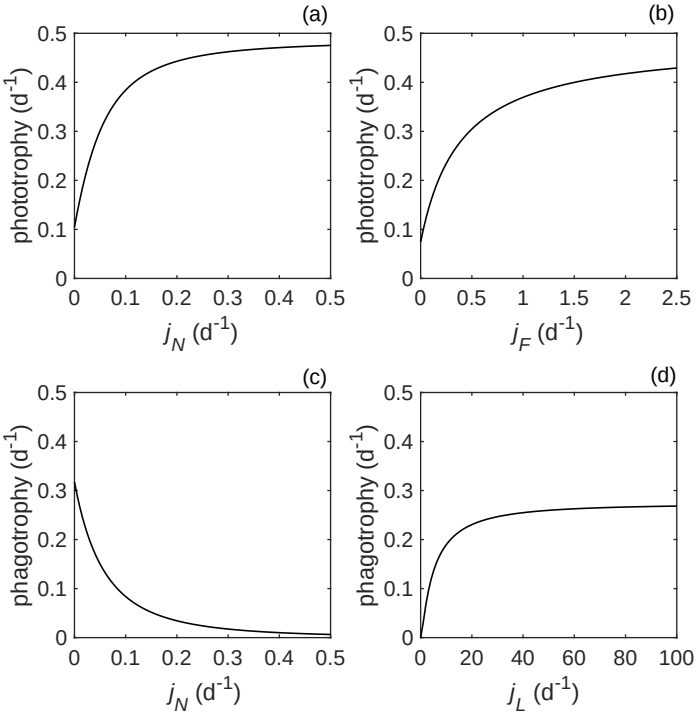

Figure 3.3: Type IIA mixotrophy. Phototrophy rate as a function of a) inorganic nutrients arrival flux (j_N) and b) prey arrival flux (j_F) . Phagotrophy rate as a function of c) inorganic nutrients arrival flux (j_N) and d) photons arrival flux (j_L).

3.3.2 Growth predictions

The models describing the four mixotrophic strategies with a DEB model for algal growth presented in Chapter 2 were combined in order to examine the growth kinetics of the four types of mixotrophs (see Appendix B for details). The simulations were performed for varying concentrations of prey and varying irradiance under low and high inorganic nutrients concentration (Fig. 3.7). For all simulations, it is assumed that inorganic carbon is not limiting growth.

In type IIA PNF, when inorganic nutrients concentration is high, prey availability does not affect the growth rate which only depends on irradiance (Fig. 3.7 a). Under low inorganic nutrients availability, the organisms use bacterial prey to obtain nutrients which are combined with organic carbon produced from photosynthesis to form E-reserves. As a result there is a positive relationship between the growth rate and both prey concentration and irradiance (Fig. 3.7 b). Finally, irrespective of inorganic nutrients availability, growth in these mixotrophs is inhibited in the dark even when prey concentration is high (Fig. 3.7 a, b).

In type IIB PNF, the substrates from phototrophy and phagotrophy are complementary.

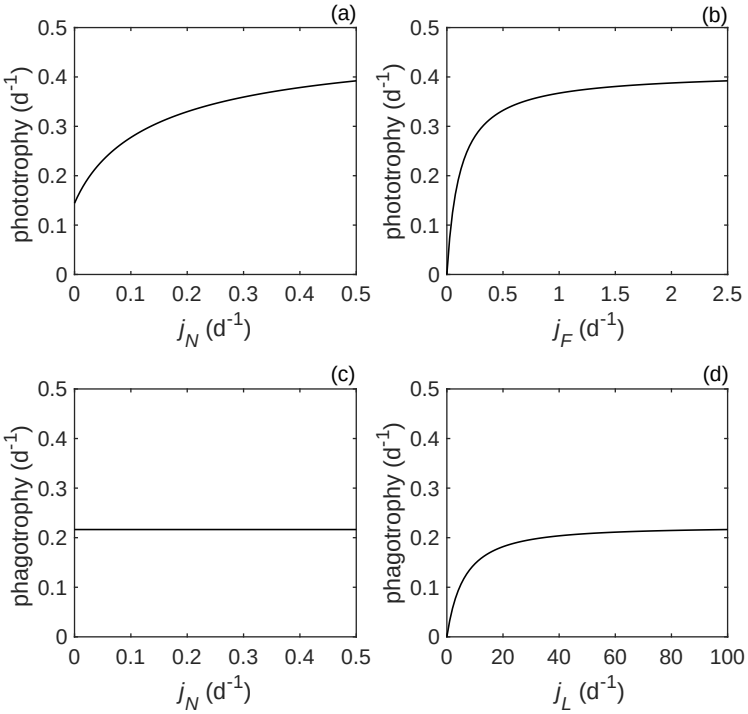

Figure 3.4: Type IIB mixotrophy. Phototrophy rate as a function of a) inorganic nutrients arrival flux (j_N) and b) prey arrival flux (j_F). Phagotrophy rate as a function of c) inorganic nutrients arrival flux (j_N) and d) photons arrival flux (j_L).

Therefore, the growth rate depends on the availability of both prey and light and when either one of these resources is not available the organism does not grow (Fig. 3.7c, d). Under low inorganic nutrients concentration growth rate decreases, however, the organism can maintain positive growth by using the nutrients contained in the ingested prey (Fig. 3.7 d).

Type IIC PNF can use phototrophy and phagotrophy in a substitutable way. Under high inorganic nutrients concentration, growth rate increases with irradiance, whereas for low irradiance the organisms can use prey as a source of energy and nutrients to grow (Fig. 3.7 e). Under low inorganic nutrients concentration and for low irradiance values, type IIC mixotrophs use phagotrophy as the feeding strategy and, therefore, the growth rate increases with increasing prey concentration (Fig. 3.7 f). However, as irradiance increases a decrease in growth rate is observed. This results from the assumptions about the regulation of mixotrophy in type IIC mixotrophs, i.e., the trigger for phagotrophy is energy deprivation. Therefore, since light for photosynthesis is available the organisms have to use phototrophy as their main feeding strategy, which, due to the low availability of inorganic nutrients, results in lower growth rate than the one achieved when using phagotrophy as their main feeding strategy (Fig. 3.7 f).

Type IIIA PNF are primarily phagotrophic. Therefore, when prey is available, irrespec-

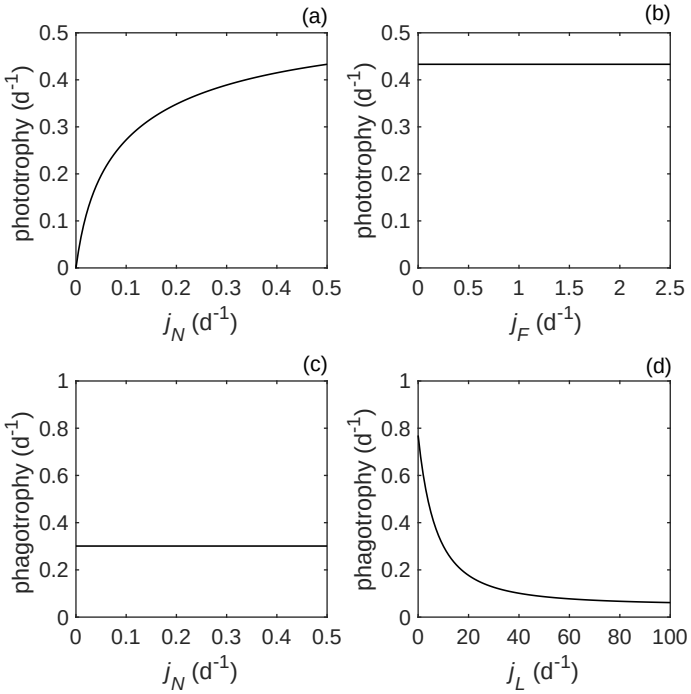

Figure 3.5: Type IIC mixotrophy. Phototrophy rate as a function of a) inorganic nutrients arrival flux (j_N) and b) prey arrival flux (j_F). Phagotrophy rate as a function of c) inorganic nutrients arrival flux (j_N) and d) photons arrival flux (j_L).

tive of inorganic nutrients availability, phagotrophy is the main feeding mode and growth rate increases mostly with prey concentration (Fig. 3.7g, h). On the other hand, for low concentrations of prey when inorganic nutrients concentration is high, type IIIA mixotrophs use phototrophy as their main feeding strategy and their growth rate increases with irradiance (Fig. 3.7 g). However, under low inorganic nutrients availability, this type of mixotrophs cannot use efficiently phototrophy and therefore an increase in irradiance does not have any significant effect on their growth rate (Fig. 3.7 h).

Fig. 3.8 shows the relationship between structural mass specific rates of organic carbon production via photosynthesis (j_C) and organic carbon consumption via phagotrophy (j_F^+) for the four different types of PNF. The simulations for each type were performed for various levels of the regulating environmental factor (Type IIA: varying nutrients, Type IIB: varying prey, Type IIC: varying irradiance, Type IIIA: varying prey) and by keeping all other resources constant. Points above the line $y = x$ indicate that C-consumption is higher than C-production. According to the model, in type IIA mixotrophs, as inorganic nutrient concentration decreases, the rate of phagotrophy increases relative to the rate of photosynthesis. However, even at very low inorganic nutrients concentrations, these organisms continue to photosynthesize at relatively high rates as there is an obligatory need for photosynthetically derived carbon. In type IIB organisms, phagotrophy and photosynthesis covary in response

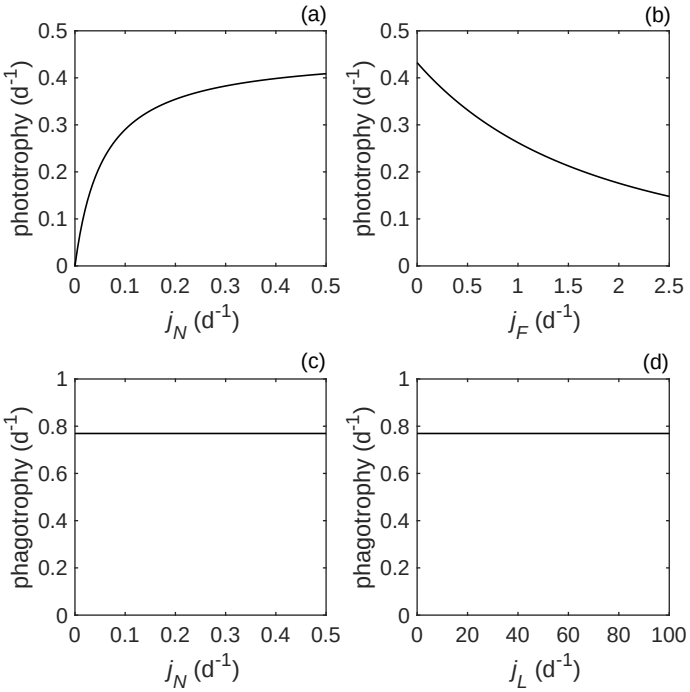

Figure 3.6: Type IIIA mixotrophy. Phototrophy rate as a function of a) inorganic nutrients arrival flux (j_N) and b) prey arrival flux (j_F). c) Phagotrophy rate as a function of c) inorganic nutrients arrival flux (j_N) and d) photons arrival flux (j_L).

to increasing prey concentration (and irradiance (results not shown)), as both physiological processes are necessary for the growth of these organisms. Type IIC mixotrophs, under high irradiance, may consume prey at low rates but the rate of carbon production is much higher than the rate of prey consumption. However, when light is limiting the rate of organic carbon consumption through phagotrophy can be significantly higher than the rate of organic carbon production from photosynthesis. Finally, in type IIIA mixotrophs, only at low concentrations of prey organic carbon production through photosynthesis may exceed organic carbon consumption.

3.4 Discussion

In this work a modelling framework able to capture the diverse nutritional strategies of mixotrophic nanoflagellates is presented. The models developed here are based on the DEB theory and the concept of the Synthesizing Unit, that has been previously used to describe the mixotrophic nutrition (Kooijman et al., 2002; Troost et al., 2005b). Here a step forward is made, by accounting for the dynamic interaction of the two energy and nutrient assimilation pathways, i.e., phototrophy and phagotrophy within the different types of PNF. This new

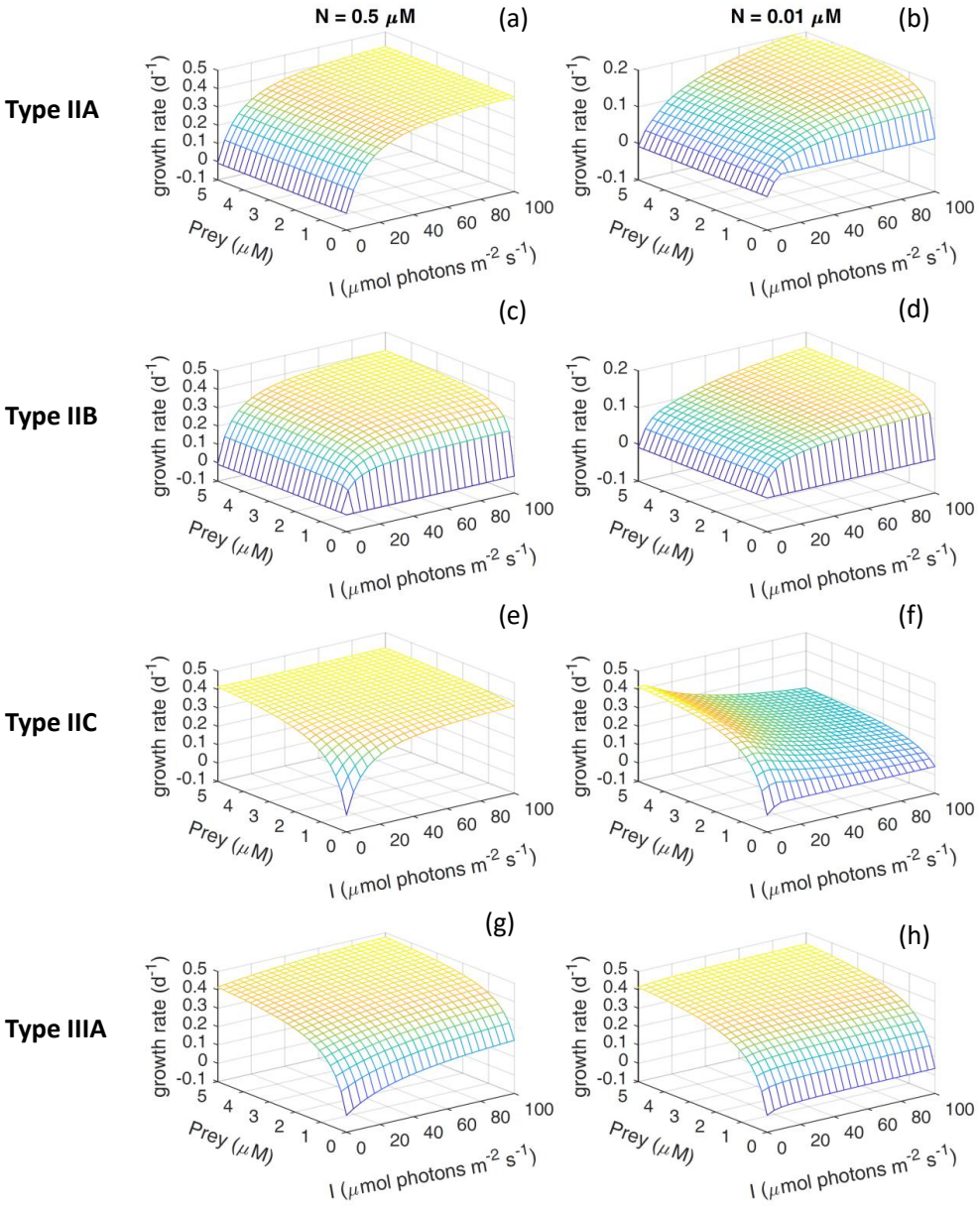

Figure 3.7: Growth rate as a function of prey and irradinace under high (0.5 μM) and low (0.01 μM) inorganic nutrients availability for the four types of PNF.

approach allows to explicitly describe the functional diversity within the group of PNF and to explore the contributions of phagotrophy and phototrophy to the metabolism and growth of mixotrophs under varying availability of resources. Overall, the functional responses of the different types of PNF are in agreement with the conceptual models for PNF developed by Stoecker (1998).

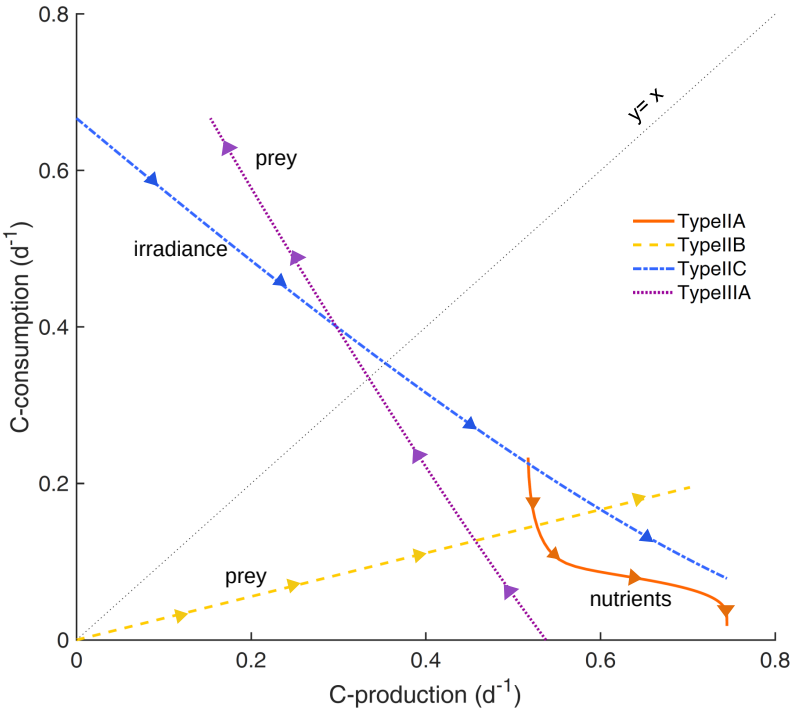

Figure 3.8: Relationship between structural mass specific rate of organic carbon production through photosynthesis and organic carbon consumption through phagotrophy for the four types of PNF. The simulations for each type where performed for various levels of their respective regulating environmental factor and by keeping all other resources constant. Arrow heads point to the direction of increasing availability of the regulating resource (Type IIA: inorganic nutrient, Type IIB: prey, Type IIC: irradiance, Type IIIA: prey). Points above the line $y = x$ indicate that C-consumption is higher than C-production.

The advantages of using SU mediated transformations to describe mixotrophic growth are two fold. Firstly, they offer a common modelling framework with enough flexibility to describe mechanistically the various nutritional strategies of PNF. In this study, the mathematical formulations describing mixotrophy were incorporated into a DEB model for algal growth, in order to study the dynamic response of the four types of PNF under varying availability of light, inorganic nutrients and prey. However, the mathematical formulations described here can be embedded within any model of algal growth as long as it accounts for the inorganic nutrient uptake and photosynthetic carbon production pathways. Secondly, the rate of phototrophy and phagotrophy can be described with a single function with no need to formulate extra assumptions, such as threshold values, in order to describe the regulation of photorophy and phagotrophy. Thresholds are generally difficult to evaluate and metabolically not very realistic. For example, experiments with *Prymnesium parvum*, a type IIA mixotroph show that when both prey and nutrients are available the organism continues to feed in order to obtain nutrients from prey but the frequency of feeding cells in the population decreases, which suggests a preference for phototrophy (Carvalho and Granéli,

2010). Moreover, in *Chrysochromulina ericina*, a prymnesiophyte with typical type IIC behaviour, phagotrophy continued when prey concentration was high, even though light was readily available (Hansen and Hjorth, 2002). These findings indicate that there is a continuum rather than abrupt switches between phagotrophy and phototrophy in mixotrophic organisms. In the present approach, by using the SU concept to merge the substrates from phagotrophy and phototrophy, there is no need to define switches in the model structure. This means that there are no either-or situations where the organisms can use only one mode of nutrition in a given moment, but both pathways can operate simultaneously. However, the relative importance of each of the two pathways will depend on the type of mixotrophy, the organism-specific parameters and the availability of the regulating resources. Thus, SU mediated transformations provide a parameter sparse approach (Kooijman, 1998) that allows for smooth transitions from one nutritional mode to the other when resources availability in the environment is changing.

Light dependency of both growth and prey ingestion has been observed in several constitutive mixotrophs such as the chlorophytes of the genus *Nephroselmis*, the haptophytes *Isochrysis galbana* (Anderson et al., 2018) and *Prymnesium parvum* (Brutemark and Granéli, 2011) and the chrysophyte *Dinobryon cylindricum* (Caron et al., 1993). It seems that in these organisms there is an obligatory demand for photosyntehtically derived carbon that cannot be substituted from carbon obtained via phagotrophy. In reflection of these observations, a common approach when modelling the growth dynamics of these organisms is to impose a minimum level of phototrophy (Flynn and Mitra, 2009; Berge et al., 2016; Ghyoot et al., 2017).The models for types IIA and IIB developed in the present study are able to adequately reproduce the observed patterns of covariation of phagotrophy rate and light availability and of the light-depended growth, even when prey is available at high concentrations. At the same time, in the present modelling formulation for types IIA and IIB the observation of low growth and low phagotrophy rate when photosynthesis is inhibited emerges from SU kinetics and the rules of the sequential-complementary transformation without the need to formulate extra assumptions.

Despite the similarity regarding the light dependent growth for types IIA and IIB, there is an important difference between the two mixotrophic strategies. Model simulations show that in type IIA mixotrophs, under high inorganic nutrients concentration, phagotrophy rate decreases while the growth rate does not depend on prey concentration, suggesting that these organisms can fully substitute phagotrophy with phototrophy when inorganic nutrients are not limiting. These findings are consistent with patterns observed in experimental cultures of *Nephroselemis* sp. and *Isochrysis galbana* (Anderson et al., 2018) showing that the percentage of feeding cells and the ingestion rates drastically decreased when nutrient limitation was alleviated.

On the other hand, type IIB mixotrophs require both light and prey in order to grow. In the present model formulation, they consume prey to obtain a portion of their organic carbon, probably an organic compound necessary for growth, that they cannot synthesize, while they can also assimilate the nutrients that are contained in prey. This allows them to grow, when

both prey and light are available, even when inorganic nutrients are limiting. The covariation of C-consumption and C-production in response to both irradianace and prey availability in type IIB mixotrophs, shown by the model, is a consequence of the complementary role of the two pathways for the growth of this type of PNF. Carbon fixation and ingestion rates have been shown to covary in response to light availability for *Ochromonas* CCMP1393 (Wilken et al., 2020) and this is also reflected in the transcriptomic response of the strain in varying availability of light and bacterial prey (Lie et al., 2018). It is important to note that such a response could not have been modelled if a trait-based approach using differential investment in the two nutritional pathways, i.e., phototrophy and phagotrophy, would be used (Berge et al., 2016; Wilken et al., 2020). Overall, these findings indicate that Type IIB mixotrophs are obligate mixotrophs as opposed to type IIA mixotrophs, which are obligate phototrophs but facultative mixotrophs.

Type IIC mixotrophs use phagotrophy as an alternative strategy to obtain energy when growing under sub-optimum irradiance. The inverse relationship between C-production via photosynthesis and C-consumption via phagotrophy in response to irradiance shown by the model simulations corroborate well with observations in *Ochromonas* CCMP2951 isolate (Wilken et al., 2020). These patterns derive from the substitutable nature of the substrates from phototrophy and phagotrophy and highlight the facultative mixotrophic potential of type IIC PNF. It is worth mentioning that despite the inverse relationship between light availability and phagotrophy in the present model, phagotrophy rate will never become zero when prey is available (Eq. B.14). In that way, model behaviour is in agreement with experiments showing that phagotrophy rate decreases with increasing irradiance in *Chrysochromulina ericina* and *Ochromonas* CCMP2951, yet remaining above zero as long as prey is available (Hansen and Hjorth, 2002; Wilken et al., 2020). In the present model, the ratio between phototrophy and phagotrophy when both light and prey are available will depend on parameter values that are specific to the organism of interest. Moreover, according to the model output, these organisms benefit from phagotrophy only at low irradiances that do not allow maximum photosynthetic rates to be reached. As irradiance increases, the positive effect of phagotrophy on the growth rate is less significant as the organism relies more on phototrophy for energy derivation and growth. These results are consistent with experimental studies with *Chrysochromulina ericina* (Hansen and Hjorth, 2002) and *Chrysochromulina brevifilum* (Jones, 1997) showing that the growth rate increased in response to prey addition for algae grown at low irradiances, whereas, at high irradiances prey availability did not affect the growth rate in *Chrysochromulina ericina* (Hansen and Hjorth, 2002). Nevertheless, exceptions from this behaviour have been reported, as for example with *Ochromonas* CCMP2951 that always exhibited higher growth rates when prey was available, irrespective of light availability (Wilken et al., 2020).

Although in type IIC mixotrophs energy deprivation is the stimulus that enhances phagotrophy, the organism may also benefit from the nutrients contained in their prey. In the present approach it was assumed that, when type IIC mixotrophs ingest prey, they can directly form reserves as they can use both carbon and nutrients contained in prey. Thus, model simulations show that under nutrient limiting conditions, growth rate increases as a function of

prey concentration. However, this increase is more pronounced at low irradiances, when the flux of organic carbon to the SU_C is diminished, allowing the substrates from phagotrophy to bind to the free SU. Observations of increasing abundance of *Chrysochromulina brevifilum* with increasing availability of prey, under nutrient and light limiting conditions, are in agreement with the model output (Jones, 1997). Conversely, the model shows that under nutrient limiting conditions, when irradiance levels are high, type IIC mixotrophs are obliged to use phototrophy, which results in lower growth rate than the one achieved when using phagotrophy as their main feeding strategy. This prediction may appear strange since one can hypothesize that an organism that has the ability to feed would do so when it is nutrient–limited. In support of the model predictions come the experimental observations on the species *Mantoniella antarctica* and *Geminigera cryophila* showing that ingestion rates were increased in response to light limitation but not in response to nutrient limitation (McKie-Krisberg et al., 2015). On the other hand, the flagellate *Pyramimonas tychotreta* consumed bacteria only when inorganic nutrient concentration was low, irrespective of light availability, yet under nutrient limitation ingestion rates were also inversely related to light availability (McKie-Krisberg et al., 2015). These findings suggest that a combination of inorganic nutrients concentration, primarily, and light availability secondarily stimulates phagotrophy in this species. Since the development of formulations for the four types of PNF as were defined by Stoecker (1998) was the aim of the present study, the current version of the model cannot resolve situations where a combination of resources is involved in the regulation of assimilation pathways in PNF. Nevertheless, on the strength of the SU approach such a response could easily be resolved by assuming a similar transformation as in type IIC but with three interacting substrates and with the point of merging of phototrophy and phagotrophy positioned after the assimilation of both organic carbon from photosynthesis and nutrients into E-reserves precursor molecules.

For type IIIA PNF, model output suggests that phototrophy is beneficial to these organisms only for low concentrations of available prey while there is an inverse relationship between C-production and C-consumption in response to prey availability. *Ochromonas* sp. strain BG-1 is an example of type IIIA mixotrophs. In this organism, phagotrophy is the dominant mode of nutrition, while Chl*a* synthesis and, therefore, photosynthesis as well as ammonium uptake is upregulated once prey is depleted (Lie et al., 2017). These observations are in agreement with the results of the present study and they highlight the substitutable role of phototrophy and phagotrophy and, thus, the facultative mixotrophic potential in type IIIA mixotrophs. For these PNF, phototrophy is a survival strategy to cope with prey concentrations lower than those that allow efficient heterotrophic growth (Rothhaupt, 1996b; Lie et al., 2017). The capability for phototrophy may allow these mixotrophs to coexist with pure heterotrophs. For example, *Ochromonas* sp. coexisted with the pure heterotroph *Bodo* sp. when light was available, however it was excluded by *Bodo* sp. when photosynthesis was disabled (Rothhaupt, 1996a).

Mixotrophic organisms have to invest in the synthesis and maintenance of both a phototrophic and a phagotorophic apparatus, which can lead to an increased metabolic cost (Raven, 1997). The costs of maintaining a photosynthetic apparatus has been estimated to

be up to 50% of the total energy, carbon and nutrients of the cell, whereas, the costs of synthesis and maintenance of the phagotrophic machinery has been estimated to be 10% of the cell's total energy, carbon and nutrients (Raven, 1997). These combined energetic costs may result in lower growth rates compared to pure photo- or phagotrophs (Rothhaupt, 1996a; Raven, 1997; Tittel et al., 2003; Ward et al., 2011). Moreover, mixotrophic organisms have to partition their finite cell surface between uptake sites for dissolved inorganic and particulate organic resources (Ward et al., 2011), which should result in a reduced ability to take up resources in comparison to specialists (pure photo- and phago-trophs). This suggests that, when resources are not limiting, specialists should be able to outcompete generalists (i.e., mixotrophs). Mathematical models that account for these trade-offs are useful tools to perform such a costs-benefit analysis to understand the ecological aspects of mixotrophy (e.g., Thingstad et al., 1996; Crane and Grover, 2010; Troost et al., 2005b,a; Ward et al., 2011; Våge et al., 2013). Although the aim of this study was not to conduct such a cost-benefit analysis on the trade-offs of mixotrophy, the modelling framework presented here, allows to account for the costs of mixotrophy. These costs can be incorporated in the stoichiometric coefficients y_{*1*2}, in line with previous models of mixotrophy in the context of DEB theory (Troost et al., 2005b,a). These coefficients quantify the amount of substrate (either photosynthetically produced carbon or prey) required to form one mol of E-reserve. The value of y_{*1*2} depends on the operating assimilation pathway and it may be higher for the phototrophic than for the phagotrophic pathway on the basis of Raven (1997). Moreover, the trade-offs of mixotrophy can be incorporated in the values of maximum assimilation rates and half saturation constants (Ward et al., 2011) or in mixotrophs stoichiometric requirements which should be higher than specialists (Crane and Grover, 2010; Ward et al., 2011). Finally, the maintenance rate of constitutive mixotrophs may also be higher than pure phototrophs or pure phagotrophs, as constitutive mixotrophs have to maintain both assimilation machineries. It should be noted, however, that these theoretical assumptions remain hypothetical and cannot be adequately constraint by the available experimental data (Ward et al., 2011; Våge et al., 2013). Moreover, the ability of the different types of mixotrophic nanoflagellates to control, to a certain extent, the relative investment on each of the two pathways on the basis of the prevailing environmental conditions, may be also a cost effective way to reduce the costs of maintaining the apparatus for both trophic pathways simultaneously (Stoecker, 1998).

Using the models developed here to compare the rates of organic carbon production and prey consumption, it was shown that the different nutritional strategies result in different functional roles of PNF within the planktonic food webs. Moreover, these functional roles are not fixed but they can change in response to varying resources availability. For example, according to model output, type IIA mixotrophs increase their prey consumption as inorganic nutrient availability decreases. However, type IIA PNF continue to produce organic carbon, as photosynthesis is the only way for these organisms to cover their energy and carbon requirements. This strategy has important implications in terms of primary production, especially for oligotrophic systems, as this type of mixotrophs can maintain high rates of carbon fixation and new biomass production even when inorganic nutrients

are limiting. Indeed, field studies conducted in the oligotrophic, P–depleted Mediterranean Sea have revealed a negative correlation between ingestion rates of PNF and phosphorus (Unrein et al., 2007, Chapter 4 of the present thesis), suggesting that, type IIA mixotrophs may dominate the PNF community in this and, possibly, other oligotrophic environments. Interestingly, the competitive advantage of type IIA PNF over the strict phototrophs and heterotrophs under oligotropihc conditions, is regulated by light availability (Ptacnik et al., 2016). Moreover, model results for type IIB mixotrophs suggest that prey consumption increases proportionally to carbon fixation in response to both prey availability and photons arrival flux, but in all cases these mixotrophs are functioning as net primary producers as the rate of organic carbon production is always higher than the rate of prey consumption. In agreement with these findings, in *Ochromonas* strain CCMP1393, a type IIB PNF, it has been shown that phagotrophy enhances photosynthesis and, therefore, organic carbon production, suggesting a role of net producer for this strain (Lie et al., 2018; Wilken et al., 2020). Of course the net effect of type IIB PNF will depend on the relative magnitude of the rate of phagotrophy as compared to the rate of carbon fixation that may vary in different species. On the other hand, the model results suggest that the ecological role of type IIC mixotrophs is depended on light availability and suggests a role of net consumers under light limiting conditions. Indeed, increased grazing activity in the dark, comparable to purely phagotrophic nanoflagellates, has been observed in the Antarctic PNF *Geminigera cryophila* and *Mantoniella antarctica* (McKie-Krisberg et al., 2015). Thus, type IIC mixotrophy may have important implications for the carbon fluxes in polar seas where photosynthetic organisms have to deal with the long periods of darkness during the austral winter. Finally, type IIIA mixotrophs have the role of net producers only for low concentrations of prey. However, as prey availability increases, type IIIA PNF switch from being net producers to being net consumers. Such pattern of increased phagotrophy rate and decreased photosynthesis when prey is readily available has been observed in *Ochromonas* strain BG-1, suggesting a role of net consumer for this PNF of type IIIA (Lie et al., 2017).

In conclusion, this modelling study is among the few that take into account the variety of nutritional strategies within PNF. The mathematical framework developed here allows to model the functional roles of PNF within the microbial community and to study how these roles are affected by resources availability. The present study shows that the range of energy and nutrient acquisition strategies, in combination with the variety of metabolic responses of the different types of PNF to environmental drivers, determine the net ecosystem impact of PNF in terms of carbon fluxes.

Chapter 4

Mixotrophy in pigmented nanoflagellates in the ultra-oligotrophic Eastern Mediterranean Sea

4.1 Introduction

The Eastern Mediterranean Sea (EMS) is among the most oligotrophic water bodies in the world, being characterized by very low nitrogen concentrations and, more importantly, very low phosphorus concentrations (Krom et al., 1991), low values of primary production and phytoplankton abundance (Moutin and Raimbault, 2002; Ignatiades et al., 2009) as well as exceptionally low bacterial production and abundance (Robarts et al., 1996; Christaki et al., 2001). In this environment, small-sized (<5 μm) pigmented and heterotrophic nanoflagellates dominate the eukaryotic assemblage in terms of abundance (reviewed by Siokou-Frangou et al., 2010) and the microbial food web mostly mediates the carbon and nutrient fluxes throughout the year (Siokou-Frangou et al., 2002, 2010). Therefore, in this environments, grazing on prokaryotic picoplankton (i.e., hereafter, heterotrophic bacteria and *Synechococcus*) by nanoflagellates should represent an important energy pathway within the planktonic food web.

This work is published in:

1. **Livanou, E.**, Lagaria, A., Santi, I., Mandalakis, M., Pavlidou, A., Lika, K., Psarra. S. 2019. Pigmented and heterotrophic nanoflagellates: Abundance and grazing on prokaryotic picoplankton in the ultra-oligotrophic Eastern Mediterranean Sea. Deep Sea Research Part II. Topical Studies in Oceanogrophy 164, 100–111.

2. Oikonomou, A., **Livanou, E.**, Mandalakis M., Lagaria, A., Psarra, S. 2020. Grazing effect of flagellates on bacteria in response to phosphate addition in the oligotrophic Cretan Sea, NE Mediterranean. FEMS Microbiology Ecology 96, fiaa086

Studies focusing on nanoflagellate grazing in the EMS have revealed a strong coupling between HNF grazing and heterotrophic bacteria (HB) production (Christaki et al., 2001). Studies investigating the grazing effect of PNF on prokaryotic picoplankton have provided partly contradicting results. For example, Christaki et al. (1999) found that mixotrophic nanoflagellates in the Aegean Sea (EMS), accounted for only 5% of nanoflagellate bacterivory. In a subsequent longitudinal study conducted in the Mediterranean Sea, heterotrophic protists <3 μm were identified as the dominant grazers of prokaryotic picoplankton, while the grazing activity of PNF was of minor importance (Christaki et al., 2001). Pachiadaki et al. (2016) also found that PNF were less important consumers of heterotrophic bacteria in comparison to HNF. On the other hand, a mesocosm experiment conducted in the Cretan Sea (EMS) showed that PNF exerted significant top-down control on prokaryotic picoplankton under non-limiting light conditions (Ptacnik et al., 2016). Moreover, in the EMS, prymnesiophytes are the dominant group of pigmented nanoplankton in terms of diagnostic pigments (Psarra et al., 2005; Siokou-Frangou et al., 2010), and they are also well known for their significant mixotrophic potential and grazing effect on heterotrophuc bacteria (Unrein et al., 2014). Although PNF seem to have the potential to significantly control prokaryotic populations, the relevance of PNF grazing on picoplankton in the EMS has not been extensively studied, obscuring the understanding on the role of PNF in the microbial food web of this oligotrophic environment.

Previous field (Arenovski et al., 1995; Christaki et al., 1999; Tsai et al., 2011) and laboratory (Nygaard and Tobiesen, 1993; Mckie-Krisberg and Sanders, 2014; Anderson et al., 2018) studies have shown that the phagotrophic activity of PNF increases with decreasing availability of inorganic nutrients, suggesting that mixotrophy may allow PNF to cope with nutrient stress under oligotrophic conditions. These findings suggest that the functional role of PNF as net consumers or net producers depends on P availability. In the EMS episodic nutrient enrichment through dust deposition from the adjacent Saharan Desert is a significant process fertilizing the EMS and supporting primary and bacterial production (Pitta et al., 2017; Rahav et al., 2018). Moreover, intermittent nutrient pulses associated with dynamic mesoscale physical structures, such as the numerous permanent or semi-permanent eddies, that favour deep vertical mixing and turnover of water masses may affect biological activity in the EMS (Petihakis et al., 2009; Moutin and Prieur, 2012; Varkitzi et al., 2020). Thus, it is crucial to understand how phosphate availability affects the abundance of nanoflagellates and their grazing effect on bacteria. Yet, quantitative data on nanoflagellate ingestion rates as a response to phosphorus addition to an apparent P-limited environment are not available from the EMS, leaving the role of heterotrophic and mainly of pigmented nanoflagellates poorly resolved.

The aim of the work presented in this Chapter is 1) to assess the relative importance of pigmented and heterotrophic nanoflagellates as consumers of prokaryotic picoplankton cells in a wide offshore area south of Crete (NW Levantine Sea, EMS) and 2) to investigate the functioning of nanoflagellate community in terms of their grazing potential as a response to episodic phosphate inputs. For this reason a two-phase study, employing both field and laboratory experiments, was designed. First, the abundance, ingestion rates and grazing effect

of pigmented and heterotrophic nanoflagellates on heterotrophic bacteria and *Synechococcus* stock were estimated during a multidisciplinary oceanographic cruise in April 2016 (9–17 Apr.) on board the R/V AEGAEO in the framework of the LEVECO cruise. The sampling design involved vertical samplings at selected stations with varying nutrient and light conditions, along a longitudinal transect, allowing for a better understanding of the nanoflagellate grazing activity and the significance of mixotrophy as a trophic mode for PNF in one of the most oligotrophic and phosphorus-starved marine environments. Secondly, P-addition microcosms experiments were performed with nutrient depleted water from a coastal site of the Cretan Sea (EMS) to assess whether the grazing effect of heterotrophic and pigmented nanoflagellates on bacteria changes with phosphate availability.

4.2 Methods

4.2.1 Methodology for estimating nanoflagellate ingestion rates

In order to determine the ingestion rates for heterotrophic and pigmented nanoflagellates, short term experiments were performed using Fluorescently Labeled Bacteria (FLB) as prey analogues (Sherr et al., 1987). Fluorescently Labelled Bacteria (FLB) were prepared following the protocol of Vázquez-Domínguez et al. (1999) from *Brevundimonas diminuta*, obtained from the Spanish Type Culture Collection (València, Spain). After 2 weeks of incubation at 20 °C, starved small-sized cells were harvested by scrapping cells from the agar plates and suspending them in 0.2-µm filtered carbonate-bicarbonate buffer (Na_2CO_3/$NaHCO_3$, pH 9.5). The dye 5-([4,6-Dichlorotriazin-2-yl]amino)fluorescein hydrochloride (DTAF, Sigma-Aldrich) was added at a final concentration of 0.2 µg mL^{-1} (Sherr et al., 1987). The cell suspension was vortexed and incubated for 2 h at 60 °C. The stained cells were centrifuged and rinsed with 0.2-µm filtered carbonate-bicarbonate buffer multiple times to remove excess DTAF and sonicated for 5 min, in order to avoid clump formation. The prey analogues were stored at −20 °C until their use.

Ingestion rates of pigmented (PNF) and heterotrophic (HNF) nanoflagellates on heterotrophic bacteria (HB) were determined by short-term grazing experiments using 1L of the sampled seawater, where FLB were added as prey analogues. Prior to grazing experiments, FLB aliquots were thawed and sonicated for 5 min in a sonication bath. Samples were taken at three time-points, (i) before the addition of FLB to measure the initial concentration of HB and *Synechococcus*, (ii) immediately after the addition of FLB (T_0) to measure the initial concentration of FLB and nanoflagellates, and (iii) after 40 minutes (T_{40}), to enumerate ingested FLB by grazers over time. The incubation period of 40 minutes was selected based on previous studies in marine ecosystems that have shown a constant number of FLB $ind.^{-1}$ beyond that time point (Unrein et al., 2007; Tsai et al., 2011; Anderson et al., 2017). FLB ingestion rates (FLB $ind.^{-1}$ h^{-1}) for HNF and PNF were calculated from the total number of ingested FLB at T_{40} after subtracting the value of T_0 counts for all samples.

The cell-specific ingestion rates of HNF and PNF on HB (HB ind.$^{-1}$ h^{-1}) were calculated by multiplying the ingestion rate of FLB with the ratio of HB to FLB abundance, assuming no selective feeding for or against FLB. The grazing effect of HNF and PNF on HB (HB mL $^{-1}$ h^{-1}) was estimated by multiplying the ingestion rates (HB ind.$^{-1}$ h^{-1}) with the respective abundance of each nanoflagellate group. The percentage of the HB standing stock removed per day (%d^{-1}) by HNF and PNF was calculated by dividing the grazing effect by the corresponding HB abundance and multiplying by 24. Bacterial ingestion rates of HNF and PNF were also expressed in terms of daily bacterial biomass removal (fg C HB ind^{-1} d^{-1}), which was divided by the mean PNF and HNF biomass (fg C ind.$^{-1}$), in order to calculate the daily acquired carbon from HB as percentage of grazer carbon biomass (% d^{-1}).

Ingestion rates of HNF and PNF, on naturally occurring *Synechococcus*, were estimated following Dolan and Šimek (1998) and Christaki et al. (2001). Thus, ingested Synechococcus were examined at T_{40} filters under blue light excitation and the cell-specific ingestion rates of HNF and PNF on *Synechococcus* (*Syn.* ind.$^{-1}$ h^{-1}) were calculated based on the presence of naturally occurring *Synechococcus* in the food vacuoles of nanoflagellates and using a digestion rate of 1.1% cell content min^{-1} as determined by Dolan and Šimek (1998) for a mixture of marine nanoflagellates feeding on marine *Synechococcus*. For PNF, it was assumed that the assumption that digestion rate would be the same as HNF. The grazing effect of HNF and PNF on *Synechococcus* (*Syn.* mL^{-1} h^{-1}) was estimated by multiplying the ingestion rates (*Syn.* ind.$^{-1}$ h^{-1}) with the respective abundance of each group. The percentage of the *Synechococcus* standing stock removed per day (% d^{-1}) by HNF and PNF was calculated by dividing the grazing effect by the corresponding *Synechococcus* abundance and multiplying by 24. *Synechococcus* ingestion rates of HNF and PNF were also expressed in terms of daily *Synechococcus* biomass removal (fg C *Syn.* ind.$^{-1}$ d^{-1}), which was divided by the mean PNF and HNF biomass (fg C ind.$^{-1}$), in order to calculate the daily acquired carbon from *Synechococcus* as percentage of grazer carbon biomass (% d^{-1}).

It should be noted that constant ingestion rates of nanoflagellates on HB and *Synechococcus* over the diel cycle were assumed. However, significant daily shifts of ingestion rates have been observed for PNF feeding on HB (Pålsson and Granéli, 2003) and *Synechococcus* (Tsai et al., 2007) as well as for HNF feeding either on HB (Ng and Liu, 2016) or *Synechococcus* (Dolan and Šimek, 1999). Therefore, the percentage of HB and *Synechococcus* standing stock removed daily by nanoflagellates should be considered a rough estimate.

4.2.2 Study site and sampling for the field experiments

Physical oceanographic properties of the study area located south of Crete (western Levantine Sea, Eastern Mediterranean) and samples for the assessment of biogeochemical properties were collected during a multidisciplinary oceanographic cruise in April 2016 (9–17 Apr.) on board the R/V AEGAEO in the framework of the LEVECO cruise. Four stations (LV3 (35.0333N, 23.4667E), LV10 (34.6667N, 24.3667E), LV13 (34.25N, 25.4833E), LV18 (34.4333N, 26.3833E)) situated along a longitudinal transect (Fig. 4.1) were visited in the

morning (between 07:00 - 08:00 UTC). Station numbers follow the naming pattern of LEVECO cruise to keep in line with the rest of publications from this multidisciplinary project. Vertical profiles of temperature and salinity were obtained using a Sea-Bird Electronics CTD System. Photosynthetically Active Radiation (PAR) was determined using a hyperspectral radiometer (TriOS). Seawater sampling for biogeochemical parameters was performed with 10 L Niskin bottles attached to a 24-position rosette sampler. Grazing experiments were performed with samples taken from two selected depths, the first representing surface water (5 m) and the second representing the deeper euphotic layer (75 m) targeting the Deep Chlorophyll Maximum (DCM) zone at the sampling stations. All sampling bottles and carboys used in this study were prewashed in 10% (v/v) HCl acid and were thoroughly rinsed with deionized water before usage.

Seawater from 5 m and 75 m at the 4 sampling stations (LV3, LV10, LV13 and LV18) was collected in 4 L plastic carboys. After collection, water samples were gently filtered through a 50-µm net mesh to remove large predators. Subsequently, triplicate 1 L Nalgene-containers were filled with the filtered seawater from each depth. Prior to the FLB addition, the experimental containers were left undisturbed for 30 min in on-deck thermo-regulated incubators with a constant flow of surface-layer pumped water. Based on *in situ* PAR profiles obtained prior to grazing experiments, the following combinations were selected as an optimal approximation of ambient light conditions: the 5-m incubator was coated with one layer of

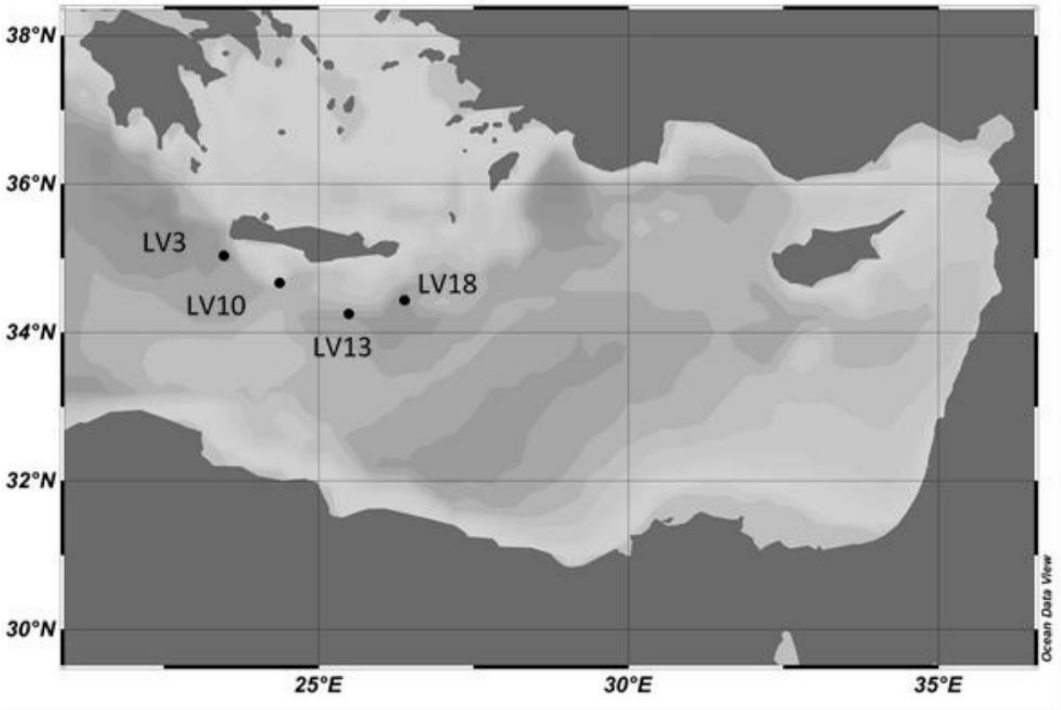

Figure 4.1: Sampling stations in the Eastern Mediterranean Sea during the LEVECO cruise.

filter type Eighth CTB (#218, LEE filters), lowering the light to 80% of incident irradiance. Respectively, the 75-m incubator was coated with a double layer of Mist Blue filter type (#061, LEE filters) and one layer of ND 0.6 filter type (#210, LEE filters) lowering the irradiance to 5% of incident irradiance. The grazing experiments were always run between 8:15 - 10:20 UTC.

For the grazing experiments, FLB were added to the experimental containers of 1 L at a concentration of ca. 30% of natural bacterial abundance. For determination of HB, *Synechococcus* and FLB abundance, 1960 µl aliquots were fixed with 0.2-µm filtered glutaraldehyde (0.5% final concentration). After fixation, samples were kept at 4 °C for 30 minutes, then frozen in liquid nitrogen and stored in -80 °C for later analysis. Initial abundances of HB, *Synechococcus* and FLB were determined by flow cytometry using a FACS-CaliburTM flow cytometer (Becton Dickinson) equipped with a 488-nm argon laser. For HB, SYBR Green I (Molecular Probes) diluted at 4×10^4 of the commercial stock was used. HB were distinguished and enumerated based on the different characteristics in the side scatter (SSC) and the green fluorescence from the stained nucleic acid (FL1). *Synechococcus* cells were distinguished according to the side scatter (SSC) and their orange auto-fluorescence from phycoerythrin (FL2). FLB, stained with DTAF, were counted from T_0 samples in plots of SSC versus FL1 (Vázquez-Domínguez et al., 1999; Gasol and Del Giorgio, 2000; Unrein et al., 2007). Yellow-green microspheres of 1 µm diameter were added as internal standard during all analyses. Data from flow cytometry were analysed using BD Cell Quest Pro software. Biomass in terms of carbon of heterotrophic bacteria and *Synechococcus*, was calculated from cell counts assuming a carbon content of 16.3 fg C cell^{-1} for HB (mean value from Robarts et al. (1996)) and 151 fg C cell^{-1} for *Synechococcus* (mean values from Bertilsson et al. (2003); Worden et al. (2004); Denis et al. (2010); Marañón et al. (2013)).

For the enumeration of nanoflagellates and the estimation of nanoflagellate ingestion rates on heterotrophic bacteria, 45 ml of each experimental container were fixed with 0.2 µm filtered glutaraldehyde (2% final concentration) at T_0 and T_{40} and kept at 4 °C for 3 h. The fixed samples were concentrated on 25 mm diameter, 0.6 µm black polycarbonate filters and stained with 4,6- diamidino-2-phenylindole (DAPI, 2 µg mL^{-1}) for 10 min. The filters were mounted on slides and stored at −20 °C until analysis. Filters were examined by an Olympus BX60 epifluorescence microscope at 1000X. Nanoflagellates stained with DAPI were enumerated under UV excitation. Chlorophyll autofluorescence of pigmented protists and ingested FLB were detected under blue light excitation. Non-plastidic protists were characterized as heterotrophic nanoflagellates (HNF) and protists showing plastidic structures were characterized as pigmented nanoflagellates (PNF). Nanoflagellates abundance was established by examining at least 100 fields while a minimum of 150 nanoflagellates cells were inspected for FLB ingestion in each sample. Filters from triplicate samples in station LV3 at 5m were flawed and thus were excluded from the analysis. One replicate from each depth at LV18 was also excluded because T_0 filters were flawed, thus in LV18 duplicate counts were made. Nanoflagellates were classified in 4 different size categories (<2 µm, 2–3 µm, 3–5 µm and 5–10 µm) using an ocular scale. However, the low number of individuals represented in the latter size fraction (HNF and PNF 5–10 µm) in the sampled volume did not allow for

accurate grazing estimates. Thus, grazing parameters were calculated only for the <5 µm size fraction defined hereafter as small nanoflagellates. Cell biovolume was calculated using approximate geometric shapes and the measurements of cell length and width. A conversion factor of 183 fg C µm $^{-3}$ was used to convert biovolume into C biomass (Caron et al., 1995).

4.2.3 Experimental design and sampling for the microcosm experiments

Seawater was collected on October 18, 2018 from the Cretan Sea (NE Mediterranean), three nautical miles offshore the Hellenic Centre for Marine Research (HCMR) facilities in Heraklion (35.38N, 25.27E) using the HCMR research inflatable Iolkos. The water column profile of conductivity, temperature and depth was assessed by deploying an SBE 19 profiler (Sea-Bird Electronics) down to 68 meters. Consecutive casts to the depth of 10 meters were performed in order to collect 180L of seawater, which was randomly distributed from each 5-L Niskin bottle (Hydro-Bios GmbH, Germany) to the six 30L microcosm units to ensure homogeneity among them prior to initiating the experiment. When filling the microcosm carboys on board, sea water was gently filtered through a 50-µm mesh to remove large predators. All sampling equipment and microcosm units were aged with seawater for a week before sampling, prewashed with 10% (v/v) HCl acid and thoroughly rinsed with deionized water prior to sampling. Then, the microcosm units were transferred within an hour to HCMR facilities. Immediately upon arrival at HCMR facilities the first samples were collected in order to determine initial (Day (-1)) nutrient concentrations and bacterial abundance for adjusting prey analogue percentage (see below). The microcosm units were allowed to acclimate overnight in a constant-temperature room at ambient temperature (22 °C).

The experimental set-up was designed with the aim to record the grazing responses of heterotrophic and pigmented nanoflagellates on bacteria, when relaxing the observed P-limitation and it consisted of six 30L microcosm units made of High Density Polyethylene (HDPE). The light:dark period was set as 12.5:11.5 hours (following ambient conditions at the time of sampling). Light intensity, confirmed by means of a hyperspectral photometer (Trios Ramses series), was adjusted close to the *in situ* conditions (214 µmol m^{-2} s^{-1}) using an array of TLD lamps (6×18Watt) mounted on a board parallel to the microcosm units. After overnight acclimation, three of the microcosm units were amended with 14.26 nM of PO_4^{-3} in the form of KH_2PO_4 (+P) and the other three were left as control treatments (Cnt). The experiment lasted five days and grazing experiments were performed at three time points (Day 0 (sampled after the addition), Day 2 and Day 4).

For the grazing experiments, 1 L of seawater was sampled from each microcosm unit, transferred to 1 L polyethylene bottles (Nalgene) and immediately inoculated with FLB to a concentration of 11–15% of the *in situ* bacterial abundance based on bacterial counts of Day (-1). A 150-mL subsample was taken at time 0 and 40 min and fixed with 0.2-µm filtered cold glutaraldehyde (2% final concentration). For the enumeration of nanoflagellates (T_0) and average ingested FLB by nanoflagellates (T_0 and T_{40}), 100 mL of the fixed sample were

filtered on 0.6-µm polycarbonate filters. A 1 mL aliquot of fixed sample was filtered on 0.2-µm polycarbonate filters for enumeration of bacterial abundance and actual concentration of added FLB at T_0. Filters were stained with DAPI (2 µg mL^{-1}) and examined by an Olympus BX60 epifluorescence microscope at 1000× magnification. A minimum of 25 fields were examined for flagellate abundance and at least 150 flagellates were inspected for ingested FLB. During counting HF and PF were sized by using an ocular and divided into 4 size categories (<3, 3–5, 5–10, >10 µm) according to their longer axes. Ingestion rates were determined for the whole HNF and PNF community respectively, without accounting for distinct size classes.

4.2.4 Biogeochemical parameters

Mineral nutrients

Mineral nutrients concentrations were assessed from seawater samples kept frozen (−20 °C) until their analysis. Nitrate (NO_3^-) and nitrite (NO_2^-) were measured at the laboratory according to Strickland and Parsons (1977). The determination of ammonium (NH_4) and phosphate (PO_4) was performed according to (Koroleff, 1970) and Rimellin and Moutin (2005), respectively. The dissolved inorganic nitrogen (DIN) was calculated as the sum of NO_3, NO_2 and NH_4.

Chlorophyll *a*, phytoplankton accessory pigments and CHEMTAX analysis

Chlorophyll *a* and phytoplankton accessory pigments were determined by High Performance Liquid Chromatography analysis (HPLC) and phytoplankton functional groups were estimated through CHEMTAX analysis. For the determination of pigments, 2L seawater samples were filtered through GF/F filters (25 mm) under low vacuum pressure (<150 mm Hg). The filters were immediately placed in liquid nitrogen and stored at −80 °C until analysis in the laboratory. The complete analysis description and the applied chromatographic conditions are provided in Lagaria et al. (2017a). Pigment data were further processed with the CHEMTAX software (Mackey et al., 1996) in order to calculate the relative contributions of the different functional phytoplankton groups to the total phytoplankton assemblage (in chlorophyll units). CHEMTAX algorithm is able to break down phytoplankton composition by considering a large suite of pigments simultaneously; the detailed procedure is described in (Lagaria et al., 2017a,b). Among the identified groups PRAS/CHLO (Prasinophytes and Chlorophytes), PRYMN (Prymnesiophytes), PELA/CHRYS (Pelagophytes and Chrysophytes) and CRYPTO (Cryptophytes) are considered as those mostly associated with the pigmented nanoflagellates (Unrein et al., 2014; Ptacnik et al., 2016, and references therein).

Primary production

Primary production (PP) rates were determined only during the field experments for the total phytoplankton community and the different size classes (pico-phytoplankton [0.2–2.0 µm], small nano-phytoplankton (snano-) [2.0–5.0 µm] and larger nano (lnano-) and micro-phytoplankton [>5.0 µm]) were assessed in the field experiments during the LEVECO cruise according to the 14C incorporation method (Steemann-Nielsen, 1952) with *in situ* incubations at 6 selected depths in the euphotic zone (from 5 to 120 m). The data presented here are from the 2 selected depths (5 m, 75 m) where PNF and HNF grazing experiments were performed. Details on the method can be found in (Lagaria et al., 2017a). Size classes selected here conformed to the generally established microbial size classes (Sieburth et al., 1978) as representative of the functional groups of pico-, snano- and lnano+micro-phytoplankton. Detailed classification as followed for microscopic counts is not feasible for the 14C method, particularly in such oligotrophic environments due to its insufficient sensitivity and logistic constraints.

4.2.5 Statistical analysis

Field experiments

To test differences between abundances and grazing parameters of HNF and PNF, two-tailed t-tests or non parametric Mann-Whitney tests (when normality assumption was not met) were used. Welch-ANOVA and Games-Howell post-hoc test was used to test for significant differences of the grazing parameters of HNF and PNF among stations at each of the two sampled depths. When differences were non-significant, samples from each depth were pooled together. To test correlation between parameters, Pearson's correlation coefficient was used or the non-parametric Spearman's rank-order coefficient (when normality assumption was not met). The normality assumption was tested with the Shapiro-Wilk test and homogeneity of variances with the Levene's test. The aforementioned statistical analyses were performed using SPSS version 22. In addition, principal component analysis (PCA) with standardized data was used in order to identify putative relationships between ingestion rates of nanoflagellates, environmental variables and community composition of PNF (in terms of chemotaxonomic groups). Several environmental parameters (i.e., PAR, Salinity, Temperature, DIN and PO_4), and biological parameters (i.e., biomass of Cryptophytes, Prymnesiophytes, Prasinophytes/Chlorophytes and Pelagophytes/Chrysophytes in chlorophyll units as derived from CHEMTAX analysis, ingestion rates of PNF and HNF on heterotrophic bacteria and Synechococcus) were included in the PCA. PCA analysis was performed using the R (R Core Team, 2019), package: factoextra (Kassambara and Mundt, 2017).

Microcosm experiments

A Mixed Design ANOVA (MD-ANOVA) was used to test for differences between the variables (abundance of bacteria and nanoflagellates, flagellate grazing rate, biomass of chemotaxonomic groups) across the different time points of the experiment (within-groups factor) and between the two treatments (between-groups factor) and also for interactions between the two factors (time × treatment). The Bonferroni post-hoc test was used to identify significant differences across the experimental days and between the two treatments when a significant interaction between time and treatments was observed. MD-ANOVA was also used to test for differences between the grazing parameters of HNF and PNF (between-groups factor) across the different time points of the experiment (within-groups factor) in each of the two treatments. The assumption of sphericity was tested with the Mauchly's test of sphericity. The homogeneity of variances was tested with Levene's test. Normality assumption was tested with the Shapiro-Wilk test. The aforementioned statistical analyses were performed using SPSS version 22.

4.3 Results

4.3.1 Field experiments

Hydrography and nutrients

Generally, the water column at all stations was weakly stratified. At 5 m temperature varied in a limited range (17.7 – 18.1 °C), while temperature at 75 m was ca. 16 °C. The ca. 2 °C temperature difference from surface to 100 m revealed the onset of seasonal thermal stratification (Fig. 4.2). Salinity varied within a relatively wide range across all stations and between the two depths, from 38.84 – 39.13 (Fig. 4.2). Moreover, within the 0–40 m layer, a west-east gradient of increasing salinity towards the east was observed. The lowest salinity values recorded at 5 m of station LV10 were attributed to Modified Atlantic Water (MAW) advected in the area by a dipole of gyres (Velaoras et al., 2018), from the main MAW course recorded at the southernmost study area. Overall, DIN in the sampled depths ranged from 0.071 to 1.420 µM (Table 4.1). Station LV13 presented the lowest DIN concentrations and station LV18 the highest. DIN concentration was always ca. 2-fold higher at 75 m in comparison to the 5 m. PO_4 concentrations were very low, ranging from 3.1 to 8 nM and generally they were similar or slightly lower at 75 m in comparison to the 5 m (Table 4.1). Although PO_4 values are at the lower limits of the ultra-sensitive analytical method Rimellin and Moutin (2005) for phosphate analysis and the range is narrow, a spatial pattern of a ca. 1.5 – 2-fold increase of PO_4 concentration from west to east was obvious when examining the two sampling depths (Table 4.1). With the exception of LV3, N/P ratio was 2–3-fold higher at 75 m, essentially associated to the higher concentrations of DIN, pointing at more pronounced phosphorus limitation at this depth. Photosynthetically Active Radiation (PAR)

was high at 5 m, ranging between 1202 – 1637 µmol photons m^{-2} s^{-1} and low (<60 µmol photons m^2 s^{-1}) at 75m (Table 4.1).

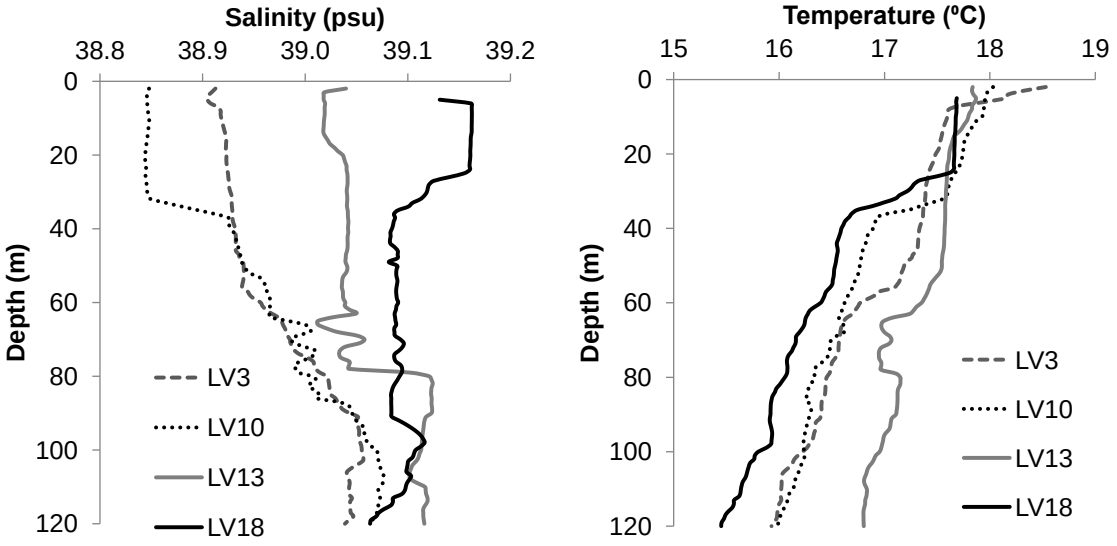

Figure 4.2: Vertical profiles of salinity and temperature at the four sampling stations.

Table 4.1: Biogeochemical parameters at the four sampling stations. PAR: Photosynthetic Active Radiation, DIN: Dissolved inorganic nitrogen (NO_3^- + NO_2^- + NH_4^+), PO_4^{3-}: Phosphate.

Station	**Depth (m)**	**Chlα (µg L^{-1})**	**PAR (µmol photons m^{-2} s^{-1})**	**DIN (µM)**	**PO_4^{3-} (nM)**	**N/P**
LV3	**5**	0.042	1246	0.138	3.1	44.3
	75	0.243	59	0.17	4.2	41
LV10	**5**	0.039	1202	0.169	4.7	36
	75	0.278	56	0.403	5.2	77
LV13	**5**	0.031	1637	0.071	7.4	10
	75	0.111	48	0.154	5.6	27
LV18	**5**	0.091	1594	0.587	8	74
	75	0.225	30	1.42	6.1	232

Chlorophyll α and primary production

Total Chlα concentrations at the two sampling depths, assessed by HPLC. ranged from 0.031 to 0.278 µg L^{-1} and higher values were always observed at 75 m (Table 4.1). Overall, primary production rates (PP) ranged from 0.013 (LV18, 120 m) to 0.672 (LV10, 50 m) µg C L^{-1} h^{-1}, presenting maximum values at 50 – 75 m depth layers at all sampling stations (data not shown). Primary production (PP) rates that corresponded to <2 µm cells were the highest, followed by rates of cells >5 µm. Considering the two representative depths studied, total PP rates were consistently higher at 75 m (from 1.5 to 2.5-fold than the 5 m values) and, with few exceptions, this was also true for all size fractions (Fig. 4.3 a, b). Average values of total PP rates were 0.50 ± 0.12 and 0.24 ± 0.04 µg C L^{-1} h^{-1} (mean ± sd), at 75 m and 5 m, respectively (Fig. 4.3 a, b). The relative contribution of each size fraction was rather balanced at 5 m (45, 21 and 35% for pico-, snano- and lnano+microphytoplankton, respectively) (Fig. 4.3 c), while pico-fraction dominated at 75 m (62, 13 and 25% the respective contributions) (Fig. 4.3 d). In addition, the only consistent W-E pattern was observed at 75 m, with a decreasing trend of PP rate values attributed to the >5 µm cells (Fig. 4.3 b), coupled to a similar decreasing trend in their relative contribution to total PP rates (Fig. 4.3 d).

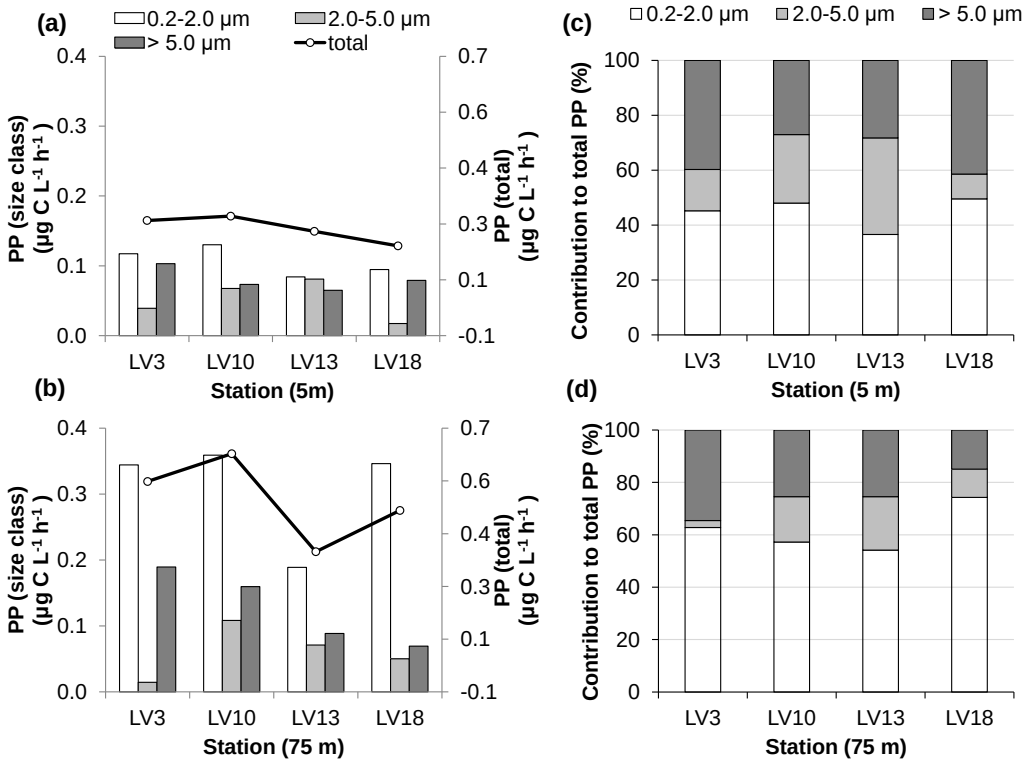

Figure 4.3: Primary production (PP) rate by size fractions and total at 5 m (a) and 75 m (b), and relative contributions of each size fraction to total PP at 5 m (c) and 75 m (d).

Abundance and size fractions of nanoflagellates

Abundance of HNF <5 µm ranged from 246 to 765 cells mL^{-1} and, station-wise, presented no significant difference between the two depths (t-tests, p >0.05) (Fig. 4.4 a, b). PNF <5 µm abundance differed significantly between the two depths at all stations (t-tests, p <0.05) presenting low values at 5 m (300 – 390 cells mL^{-1}) and higher values at 75 m (763 – 2463 cells mL^{-1}) (Fig. 4.4 a, b).

The small (<5 µm) nanoflagellate community was dominated by cells <3 µm in size at both depths which represented 84 ± 8.2% and 73 ± 12.2% (mean ± sd) of the total HNF <5 µm and of the total PNF <5 µm assemblage, respectively (Fig. 4.4 c, d). Interestingly, cells in the smallest size fraction <2 µm, accounted for 76.5% of the total PNF <5 µm at station LV18-75 m, where the maximum abundance of PNF was observed (Fig. 4.4 b). HNF and PNF of size 5 – 10 µm were always a minor component of the nanoflagellate community representing only 6 ± 1.8% and 3 ± 2.5% (mean ± sd) of the total HNF and of the total PNF abundance, respectively (data not shown).

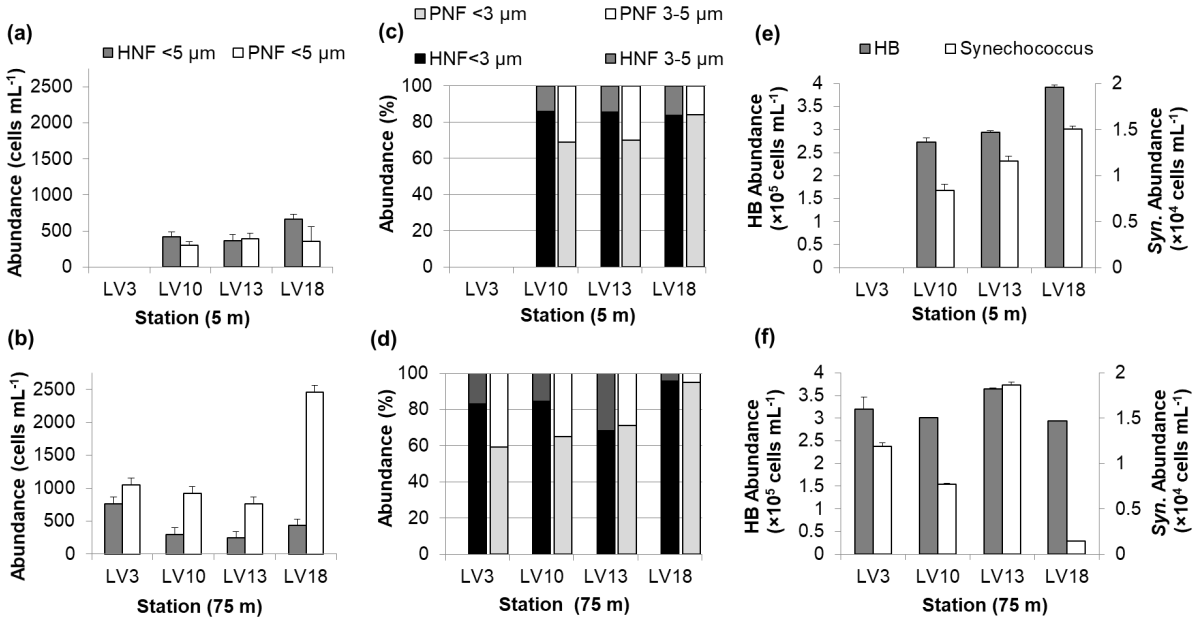

Figure 4.4: Abundance of small heterotrophic (HNF) and pigmented (PNF) nanoflagellates at 5 m (a) and 75 m (b), relative contribution of the two size classes <3 µm and 3 – 5 µm in HNF and PNF abundance at 5 m (c) and 75 m (d) and abundance of heterotrophic bacteria (HB) and *Synechococcus* (*Syn.*) at 5 m (e) and 75 m (f). Error bars represent standard error of the mean of the replicate samples.

Grazing on heterotrophic bacteria by small nanoflagellates

HB abundances ranged from 2.72×10^5 to 3.92×10^5 HB mL^{-1} presenting a maximum at 5 m of LV18 and a minimum at 5 m of LV10 (Fig. 4.4 e, f). At each depth, no significant differences were observed among stations for any of the parameters related to HB grazing, neither for HNF nor for PNF (Welch ANOVA, $p > 0.05$). Ingestion rates of HNF and PNF on HB ranged from 0.2 to 0.81 HB $ind.^{-1}$ h^{-1} and from 0.04 to 0.65 HB $ind.^{-1}$ h^{-1}, respectively (Fig. 4.5 a, b). At 5 m, ingestion rates of HNF exceeded those of PNF and the difference was significant (t-test, $p = 0.013$) (Fig. 4.5 a), while at 75 m ingestion rates of the two groups were similar (t-test, $p > 0.05$) (Fig. 4.4 b). Furthermore, ingestion rates of HNF did not differ between the two depths (t-test, $p > 0.05$). On the other hand, a ca. 3.5-fold significant increase in ingestion rates of PNF was observed at 75m (t-test, $p = 0.018$). Moreover, a significant negative correlation was observed only for phosphate concentration and PNF ingestion on HB (Pearson's $r = -0.829$, $p = 0.021$, $n = 7$) whereas, HNF ingestion rates did not show any significant relationship, neither with DIN nor with phosphate.

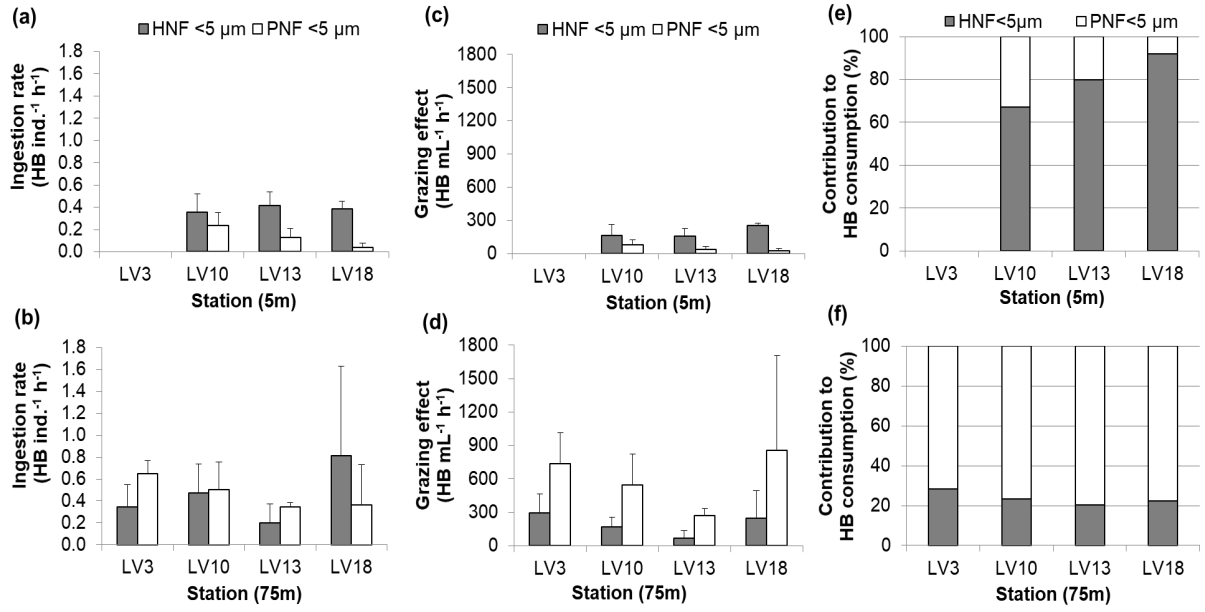

Figure 4.5: Ingestion rate of small heterotrophic (HNF) and pigmented (PNF) nanoflagellates on heterotrophic bacteria (HB) at 5 m (a) and 75 m (b), grazing effect of HNF and PNF on HB at 5 m (c) and 75 m (d) and contribution to HB consumption by HNF and PNF at 5 m (e) and 75 m (f). Error bars represent standard error of the mean of the replicate samples.

The grazing effect of HNF and PNF on HB ranged from 69 to 293 HB mL^{-1} h^{-1} and from 22 to 853 HB mL^{-1} h^{-1}, respectively (Fig. 4.5 c, d). At the surface, HNF accounted for 67 – 92% of total HB consumption (Fig. 4.5 e), whereas, at 75 m, PNF were the dominant HB consumers, accounting for 72 – 80% of total HB consumption (Fig. 4.5 f). The grazing

effect of HNF was not affected by depth (t-test, p >0.05) while the grazing effect of PNF was significantly affected by depth (t-test, p = 0.015) with 12-fold higher grazing effect of PNF being observed at 75 m (Fig. 4.5 c, d), as a result of the combined effect of higher ingestion rates (Fig. 4.5 a, b) and abundances (Fig. 4.4 a, b) of PNF. HNF removed 0.5 – 2.4% d^{-1} of the HB standing stock and this rate was similar at the two depths (t-test, p >0.05) (Table 2). Accordingly, PNF removed 0.1 – 6.9% d^{-1} of HB standing stock and this rate showed a significant 12-fold increase at 75 m (t-test, p = 0.023) (Table 2). HNF and PNF cumulatively consumed 4.4 ± 3.2% d^{-1} (mean ± sd) of the HB standing stock. Moreover, the daily acquired carbon from HB as percentage of HNF carbon biomass ranged from 3.5 to 35.4% d^{-1} (overall mean: 12.2% d^{-1}) and it was similar at both depths (t-test, p >0.05) whereas for PNF this rate ranged from 1.5 to 22.4% d^{-1} (overall mean: 9.6% d^{-1}), presenting, on average, a significant 4-fold increase at 75 m (t-test, p = 0.031) (Table 4.2).

Grazing on *Synechococcus* by small nanoflagellates

Synechococcus abundances ranged from 0.14 × 10^4 *Syn.* mL^{-1} to 1.87 × 10^4 *Syn.* mL^{-1} presenting a maximum at 75 m of station LV13 and minimum value at 75 m of station LV18 (Fig. 4.4 e, f). Regarding grazing parameters of HNF and PNF among stations and within each depth, significant differences were observed for PNF ingestion rates at 75 m (Welch ANOVA, p = 0.001) (Fig. 4.6 a, b). Games-Howel post-hoc test showed no significant differences between LV3-75 m, LV10-75m and LV13-75 m, while station LV18-75m had an overall minimum value of PNF ingestion rate, that differed significantly from stations LV3 (p = 0.004) and LV10 (p = 0.045). Generally, PNF ingestion rates on *Synechococcus* ranged from 0.006 to 0.104 *Syn.* ind.$^{-1}$ h^{-1}, and excluding station LV18, a significant increase of PNF ingestion rate on *Synechococcus* was observed at 75 m (t-test, p = 0.012). HNF ingestion rate on *Synechococcus* ranged from 0.03 to 0.09 *Syn.* ind.$^{-1}$ h^{-1} and they did not differ between the two depths (Mann-Whitney U test, p = 0.289) (Fig. 4.6 a, b). Correlations between inorganic nutrients and grazing parameters of HNF and PNF on *Synechococcus* were non-significant.

The grazing effect on *Synechococcus* by HNF and PNF, ranged from 7.88 to 73.55 *Syn.* mL^{-1} h^{-1} and from 2.61 to 108.79 *Syn.* mL^{-1} h^{-1}, respectively (Fig. 4.6 c, d). The grazing effect on *Synechococcus* was not significantly affected by depth for HNF (t-test, p >0.05), whereas, for PNF, it was, on average, 13-fold higher at 75 m, however, the difference was marginally significant (t-test, p = 0.05). At 5 m, HNF accounted for 71 – 90% of the total *Synechococcus* consumption (Fig. 4.6 e), while, at 75 m, PNF accounted for 60 – 74% of the total *Synechococcus* consumption (Fig. 4.6 f). HNF removed 2.9 – 14.8% d^{-1} of the *Synechococcus* standing stock and this rate was not affected by depth (t-test, p >0.05) (Table 4.2). On the other hand, *Synechococcus* standing stock removed by PNF ranged from 0.4 to 26.4% d^{-1} and a significant 17-fold increase was observed for this rate at 75 m (t-test, p = 0.015) (Table 4.2). HNF and PNF together removed 19.7±16% d^{-1} (mean ± sd) of the *Synechococcus* standing stock. Daily acquired carbon as percentage of HNF carbon from *Synechococcus* ranged from 6.9 to 19.7% d^{-1} (overall mean: 14.2% d^{-1}) and it was similar at

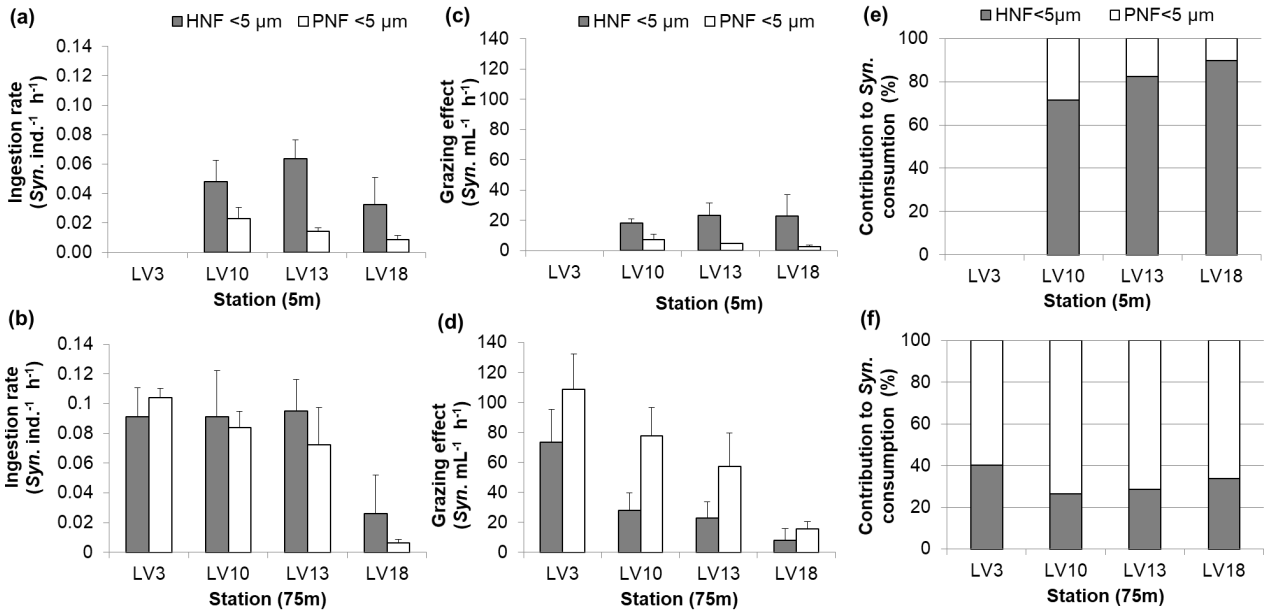

Figure 4.6: Ingestion rate of small heterotrophic (HNF) and pigmented (PNF) nanoflagellates on *Synechococcus* (*Syn.*) at 5 m (a) and 75 m (b), grazing effect of HNF and PNF on *Syn.* at 5 m (c) and 75 m (d) and contribution to *Syn.* consumption by HNF and PNF at 5 m (e) and 75 m (f). Error bars represent standard error of the mean of the replicate samples.

both depths (Mann-Whitney test, $p = 0.229$) (Table 4.2). For PNF, this rate ranged between 3.6 – 20.4% d^{-1} (overall mean: 12.1% d^{-1}) (Table 4.2) and when excluding the sample from LV18 at 75 m, where a minimum value for this depth was recorded, significantly higher values at 75 m were observed compared to the samples from 5 m (t-test, $p = 0.022$).

CHEMTAX analysis

Among accessory pigments that are related to flagellate taxa, 19′-hexanoyloxyfucoxanthin, 19′-butanoyloxyfucoxanthin and fucoxanthin (associated with Prymnesiophytes and Pelagophytes/ Chrysophytes) were the most abundant ones in the study area. Pigment data were further processed with CHEMTAX software in order to determine the distribution of chemotaxonomic phytoplankton groups (in chlorophyll units) of the flagellate community. According to CHEMTAX analysis, the major flagellate groups were Prymnesiophytes followed by Pelagophytes/Chrysophytes. Cryptophytes and Prasinophytes/ Chlorophytes showed much lower concentrations than the rest of the identified groups (Fig. 4.7). Overall, biomass (in chlorophyll units) of major PNF groups was consistently several-fold higher at 75 m compared to 5m with Prasinophytes/Chlorophytes and Cryptophytes presenting the most pronounced increase (Fig. 4.7). At 5 m of station LV18, a considerable increase of all groups was ob-

Table 4.2: Summarized means and ranges (in parenthesis) of small nanoflagellates (HNF and PNF) consumption parameters on heterotrophic bacteria (HB) and *Synechococcus* (*Syn.*) at the two sampled depths.

	HNF <5 µM		**PNF <5 µM**	
Depth (m)	**5**	**75**	**5**	**75**
HB stock removed (% d^{-1})	1.4 (1.3 – 1.5)	1.6 (0.5 – 2.4)	0.4 (0.1 – 0.7)	4.8 (1.8 – 6.9)
Carbon from HB (% d^{-1})	9.1 (8.4 – 9.9)	14.5 (3.5 – 35.4)	3.5 (1.5 – 5.8)	14.2 (9.0 – 22.4)
***Syn.* stock removed** (% d^{-1})	4.7 (3.7 – 5.4)	10.1 (2.9 – 14.8)	1.2 (0.4 – 2.3)	19.9 (7.4 – 26.4)
Carbon from *Syn.* (% d^{-1})	10.6 (6.9 – 14.0)	17.0 (10.5 – 19.7)	8.4 (4.3 – 13.4)	14.9 (3.6 – 20.4)
Prok.Pico (HB + *Syn.*) stock removed (% d^{-1})	1.5 (1.4 – 1.6)	1.7 (0.6 – 2.6)	0.4 (0.1 – 0.8)	5.0 (2.0 – 7.1)
Carbon from prok. pico (HB + *Syn.*) (% d^{-1})	19.7 (16.0 – 23.9)	31.5 (21.9 – 45.9)	12.0 (5.8 – 19.2)	29.1 (26.0 – 34.0)

served compared to the other stations. Particularly, Pelagophytes/Chrysophytes in LV18, when compared to the rest of the stations, showed an average 3.5- and 2.5- fold increase at 5 m and 75 m, respectively. Meanwhile, at 75 m layer, while overall higher values were recorded at all stations, Prymnesiophytes presented an opposite horizontal trend with an eastward decrease from station LV3 to LV18 (Fig. 4.7).

Ingestion rates analysis through PCA

Patterns between ingestion rates, nutrients and community composition of PNF (in terms of chemotaxonomic groups) at the four stations and the two depths were assessed with Principal Component Analysis (PCA) (Fig. 4.8). The variables used were: PAR, Salinity, Temperature, DIN and Phosphate concentration, biomass (in chlorophyll units as derived from CHEMTAX analysis) of Cryptophytes, Prymnesiophytes, Prasinophytes/Chlorophytes and Pelagophytes/Chrysophytes and ingestion rates of PNF and HNF on HB and *Synechococcus*. The first two principal components, PC1 and PC2 explained 54.5% and 30.2% of the total variance, respectively. The variables PAR, Temperature, ingestion rates of PNF on HB and

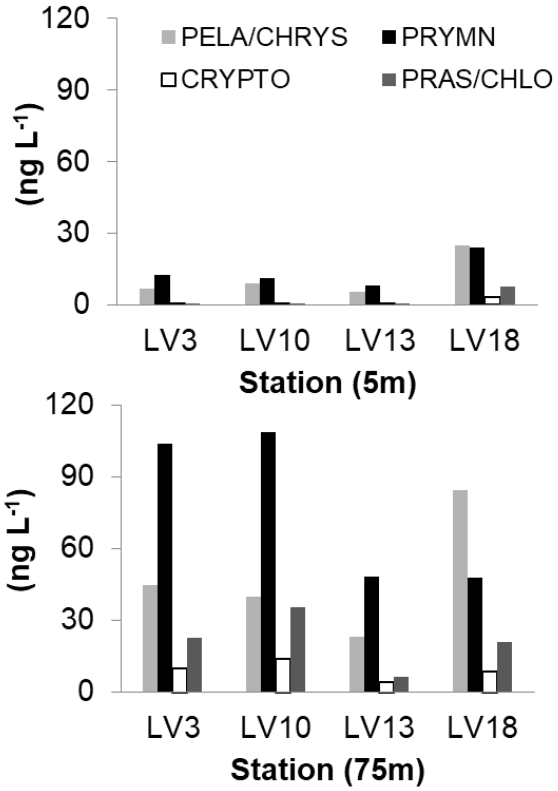

Figure 4.7: Community composition of flagellate community at the different stations and depths, as determined by pigment/CHEMTAX analysis (in chlorophyll units, ng L^{-1}). PRYMN: Prymnesiophytes, CRYPTO: Cryptophytes; PRAS/CHLO: Prasinophytes/Chlorophytes; PELA/CHRYS: Pelagophytes/Chrysophytes.

the biomass of Cryptophytes, Prymnesiophytes, Prasinophytes/Chlorophytes contributed >10% on PC1 formation. DIN concentration, the biomass of Pelagophytes/Chrysophytes and the ingestion rates of HNF on HB and *Synechococcus* were the variables contributing >10 % on the PC2 formation. Figure 4.8 a describes the relationships among samples, while the relationships among variables are displayed in the loading plot (Fig. 4.8 b). According to PCA results, all 5 m samples were well separated from the 75 m samples along the first principal component (PC1) (Fig. 4.8 a) Thus, as shown in Fig. 4.8 b, all 5 m samples were characterized by higher PAR and temperature and lower ingestion rates of PNF on HB. Samples from the 75 m of stations LV3, LV10 and LV13 denoted by 3D, 10D, 13D, respectively, were grouped together (Fig. 4.8 a) and they were associated mainly to low PAR, high ingestion rates of PNF on HB and high concentrations of Prymnesiophytes, Cryptophytes and Prasinophytes/Chlorophytes (Fig. 4.8 b). Moreover, samples from station LV18 were well separated from the rest of the samples along the second principal component (Fig. 4.8 a). Thus, LV18 was characterized mainly by high DIN concentration, high ingestion rates of HNF on HB and lower ingestion rate of HNF on *Synechococcus* as well as higher concentra-

tion of Pelagophytes/Chrysophytes (Fig. 4.8 b). Finally, as indicated from the position of the variables in the loading plot (Fig. 4.8 b) ingestion rates of PNF on HB and *Synechococcus* were negatively correlated to phosphorus concentration and positively correlated mostly to Prymnesiophytes concentration.

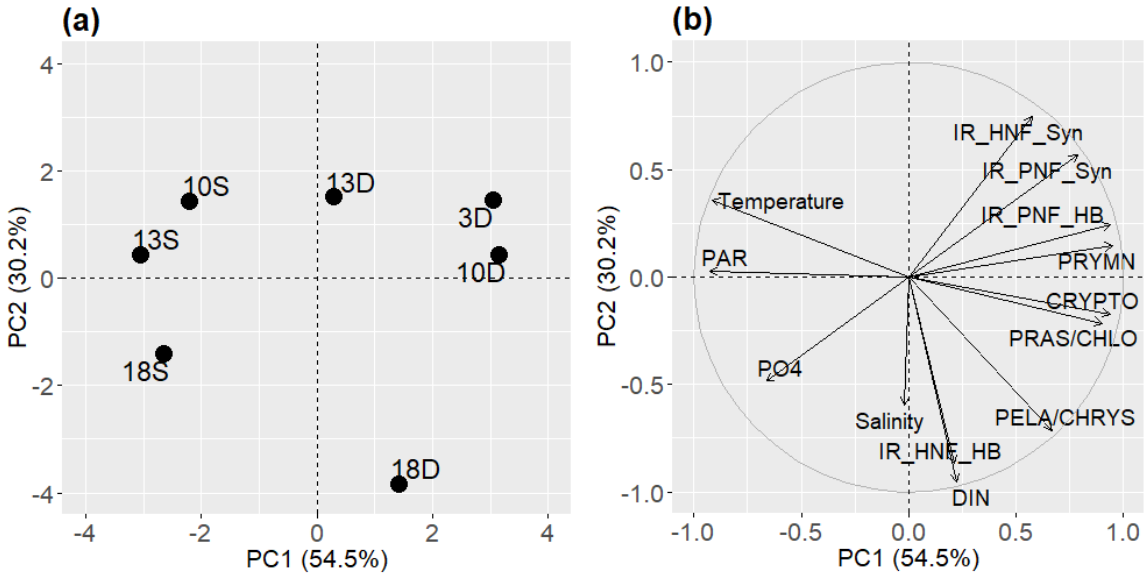

Figure 4.8: Principal Component Analysis (PCA) representing the relationships between (a) samples and (b) variables. (a): 10S, 13S, 18S denote samples from 5 m of stations LV10, LV13, LV18, respectively. 3D, 10D, 13D, 18D denote samples from 75 m of stations LV3, LV10, LV13 and LV18, respectively. (b): variables: IR_HNF_HB/IR_HNF_Syn: Small heterotrophic nanoflagellates ingestion rate on heterotrophic bacteria /*Synechococcus*; IR_PNF_HB/IR_PNF_Syn: Small pigmented nanoflagellates ingestion rate on heterotrophic bacteria/*Synechococcus*, PRYMN: Prymnesiophytes, CRYPTO: Cryptophytes, PRAS/CHLO: Prasinophytes, PELA/CHRYS: Pelagophytes/Chrysophytes.

4.3.2 Microcosm experiments

Initial conditions

At the time of sampling, temperature and salinity profiles showed that the water column presented characteristics of the late stratification period with a well mixed surface layer propagating down to 50 m, followed by the seasonal thermocline at the 50 – 70 m layer. At the sampling depth of 10 m temperature was 22.84 °C, salinity was 39.56 psu and light intensity was 269 µmol m^{-2} s^{-1} (Appendix C, Fig. C.1). Initial concentration of PO_4 and DIN at all microcosms containers was typically <2.67 nM and <0.371 µM, respectively

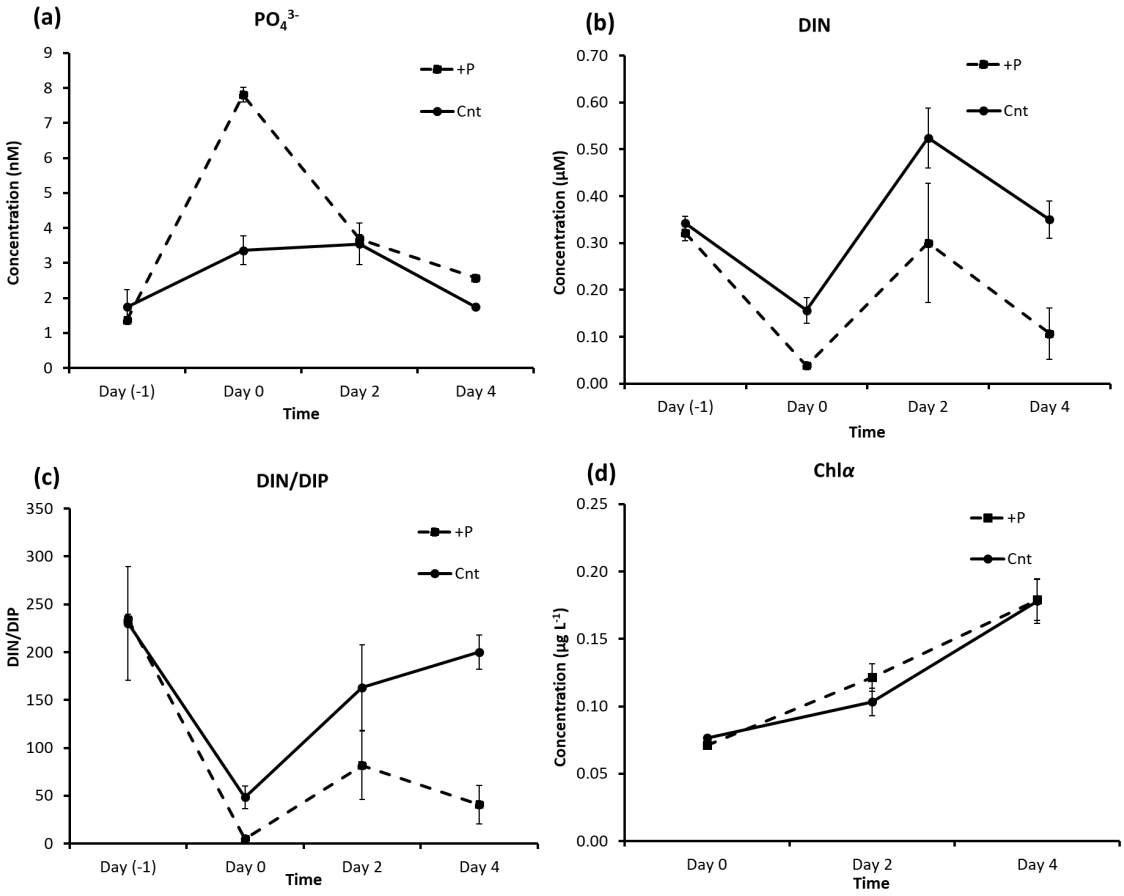

Figure 4.9: Nutrients concentrations of (a) Phosphate (PO_4^{3-}, DIP), (b) Dissolved Inorganic Nitrogen (DIN), (c) DIN/DIP ratio and (d) Chlorophyll α concetration over the course of the experiment for the P-addition (+P) and the control treatments (Cnt). Error bars represent standard error of the mean of the three replicates of each treatment.

(Fig. 4.9 a, b), while an average DIN/DIP ratio of 232/1 ± 66/1 (mean ± sd) was found across all microcosm containers, indicating severely P-depleted waters (Fig. 4.9 c). Chlα in the control treatments at Day 0, prior to P-addition was low (76.46 ± 1.81 ng L^{-1}) and characteristic of the oligotrophic status in the region (Fig 4.9 d).

Nutrients and Chlorophyll α

The addition of 14.26 nM of phosphate (Day 0) in the P-amended microcosms resulted in a 2.3-fold increase of phosphate compared to the control treatments (Fig.4.9). At the beginning of the experiment (Day 0), the concentration of PO_4^{3-} in the P-amended microcosms reached 7.81 nM ± 0.37 (mean ± sd), indicating that ca. 50% of the added phosphate was either rapidly taken up by the biota or elsewhere chemically absorbed within 1.5 hour from the time

point of P-addition to the filling of the nutrient bottles. Within two days after P-addition, all added phosphate was fully consumed in the P-amended treatment and its concentration dropped to levels similar to the control treatment but always higher than the initial ones (Day (-1), Fig. 4.9 a)). DIN followed a similar trend in both treatments (Fig. 4.9 b) however DIN concentrations after P addition were always lower in the P-amended treatment compared to the control. At Day 0, immediately after P-addition DIN concentration was 4-fold lower in the +P treatment compared to the control (Fig. 4.9 b). Average DIN/DIP ratio prior to P-addition was 232/1 and dropped to 200/1 in the control treatment and 41/1 in the P-amended treatment at the end of the experiment (Day 4, Fig. 4.9 c). Chlα concentration followed a similar increasing pattern in the two treatments over the course of the experiment with slightly higher values in the P-amended treatment at Day 2. (Fig. 4.9 d).

Microbial community response to P addition

Initial abundance (Day 0) of Heterotrophic Bacterial (HB) across all replicates and both treatments was $6.01 \pm 5.54 \times 10^5$ cells mL^{-1} (mean $\pm$ sd) whereas *Synechococcus* abundance ($3.01 \pm 1.02 \times 10^4$ cells mL^{-1} (mean $\pm$ sd)) was an order of magnitude lower. HB abundance was not significantly affected by time over the course of the experiment (MD-ANOVA, $F(2, 8) = 2.711$, $p = 0.126$), whereas phosphate addition had a significant positive effect on HB abundance (MD-ANOVA, $F(1,4) = 13.603$, $p = 0.021$) (Fig. 4.10 a, b). Similarly to HB, P-addition significantly affected *Synechococcus* abundance (MD-ANOVA, $F(1,4) = 8.9$, $p = 0.041$) which was higher at Day 2 and Day 4 in the P-amended treatment compared to the control (Bonferroni tests, $p < 0.05$) (Fig. 4.10 a, b). Moreover, *Synechococcus* abundance did not change significantly over time in the control (Bonferroni tests, $p > 0.05$), whereas in the P-amended treatment, a significant 2.5-fold increase was observed from Day 0 to Day 2 (Bonferroni test, $p = 0.02$) (Fig. 4.10 a, b).

Abundance of HNF did not change significantly over time in the control treatment, ranging from 754 cells mL^{-1} (Day 0) to 883 cells mL^{-1} (Day 4, Fig. 4.10 c) (Bonferrroni tests, $p > 0.05$). On the contrary, in the P-amended treatment HNF abundance ranged from 620 to 1454 cells mL^{-1}, thus presenting a significant 2.3-fold increase over time (Bonferroni test, $p = 0.009$). Phosphate addition resulted in significantly higher abundance of HNF, particularly at Days 2 and 4 compared to the respective days of the control treatment (Bonferroni tests, $p < 0.05$). Contrary to HNF, phosphate addition did not affect significantly the abundance of PNF (MD-ANOVA, $F(1, 4) = 7.266$, $p = 0.054$), which ranged from 648 to 2009 cells mL^{-1} when considering both treatments. However, a significant increase of PNF abundance from Day 0 to Day 4 was observed in both treatments (2.7-fold and 2.9-fold in the Cnt and +P, respectively) (MD-ANOVA, $F(2,8) = 70.105$, $p < 0.001$).

The nanoflagellate assemblage consisted mostly of small nanoflagellates (ca. 98% <10 µm). In both treatments, the HNF community was dominated by nanoflagellates <3 µm, while the dominant size fraction of the PNF community was nanoflagellates 3 – 5 µm (Fig. 4.10 e, f)). There was not a remarkable shift in size distribution of HNF or PNF

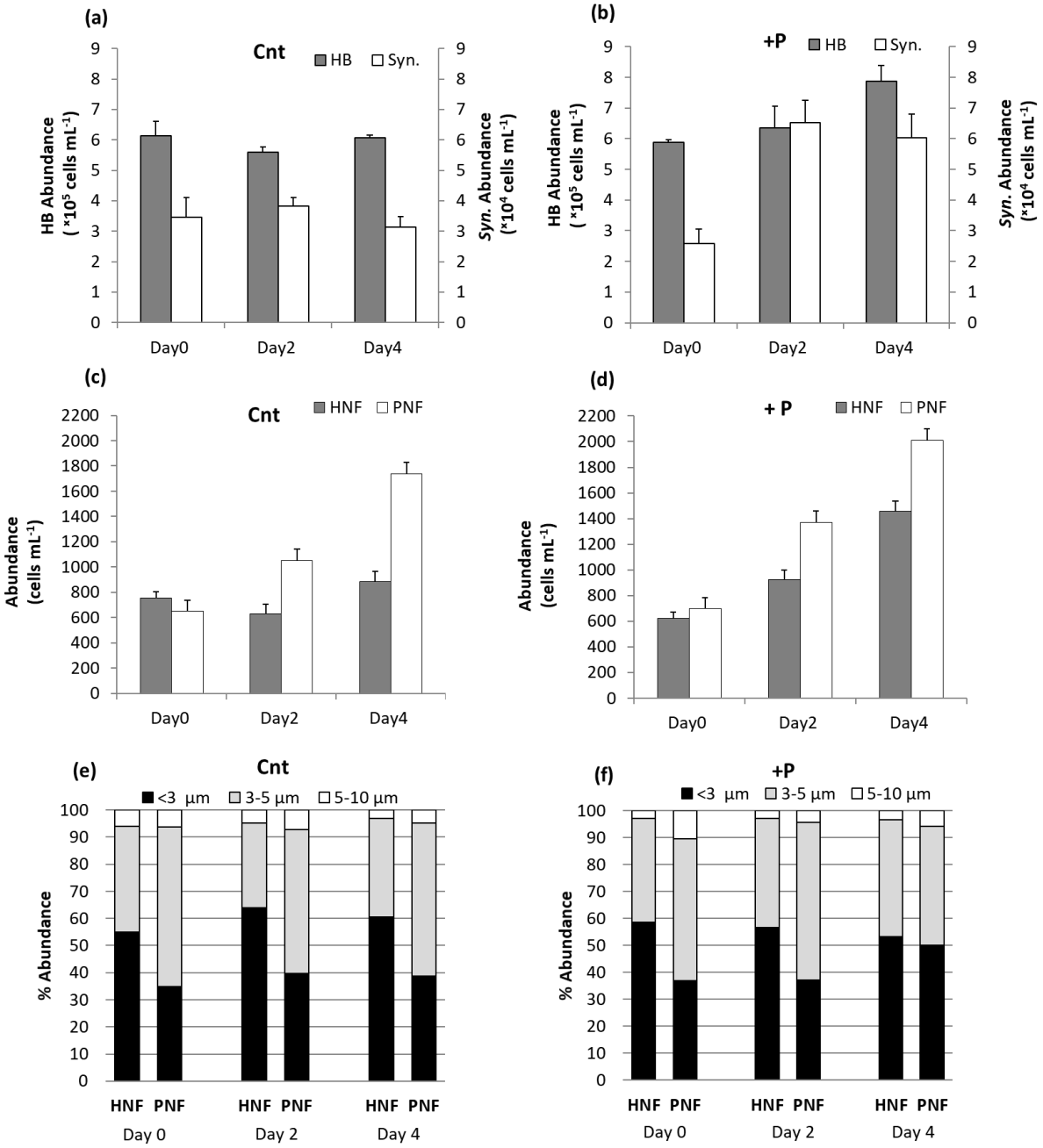

Figure 4.10: Mean abundance of Heterotrophic bacteria (HB) and *Synechococcus* (*Syn.*) in the control (Cnt) (a) and the P-addition (+P) (b) and of Heterotrophic (HNF) and of pigmented (PNF) nanoflagellates in the control (Cnt) (c) in the P-addition (+P) treatments (d). Error bars represent standard error of the mean of abundance values of the three replicates of each treatment. Percent contribution of size classes to the nanoflagellate assemblage in the control (Cnt)(e) and in the P-addition (+P) treatments (f).

after the P-addition, apart from a moderate increase of the PNF <3 µm size fraction at the end of the experiment in the P-amended treatment (Day4, +P) (Fig. 4.10 e, f)). The contribution of the size fraction >10 µm to total HNF and PNF abundance was negligible. HNF belonging to the size fraction >10 µm showed a maximum of 2% of total HNF abundance (Day0, Cnt), while for PNF (>10 µm) the respective percentage was 1% (Day4, Cnt).

Effect of P-addition on ingestion rates and bacterial removal rates

The ingestion rate of HNF was not affected by phosphate addition (Fig. 4.11 a, b), since no significant differences were observed between the two treatments (MD-ANOVA, $F(1,4) = 0.038$, $p = 0.855$) and it did not change significantly over time (MD-ANOVA, $F(2,8) = 0.289$, $p = 0.756$). Phosphate addition had a significant effect on PNF ingestion rate (MD - ANOVA $F(1,4) = 25.59$, $p=0.007$) resulting in lower ingestion rate in +P compared to Cnt treatments at all time points, whereas their ingestion rate did not change significantly over time (MD - ANOVA $F(2,8) = 3.747$, $p = 0.071$) (Fig. 4.11 a, b). Considering all days, in the control treatment, PNF ingestion rate was significantly higher compared to that of HNF (MD-ANOVA, $F(1,4) = 8.228$, $p = 0.046$) (Fig. 4.11 a), whereas the opposite pattern was observed in the P-amended treatment where HNF ingestion rate was significantly higher

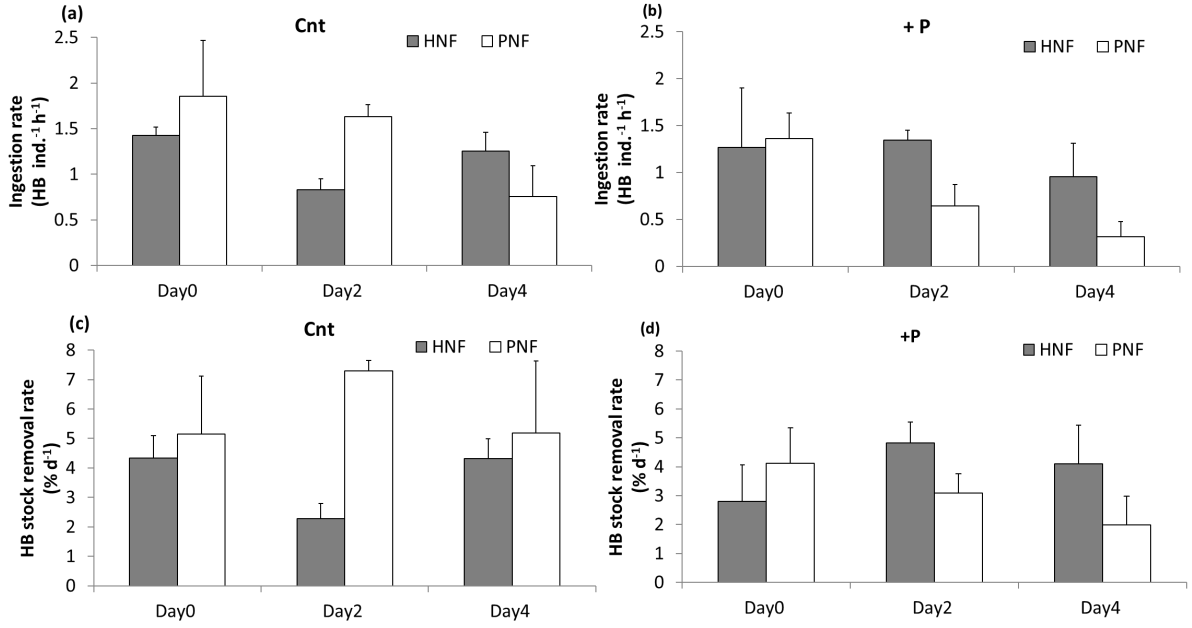

Figure 4.11: Mean ingestion rate of the Heterotrophic (HNF) and Pigmented nanoflagellates (PNF) groups in the control (Cnt) (a) and the P-addition (+P) treatment and (b) mean Heterotrophic Bacterial (HB) removal rate of HNF and PNF expressed as a percentage of the removed bacteria out of the bacterial stock. Error bars represent standard error of the mean values of the three replicates of each treatment.

than that of PNF (MD-ANOVA, F(1,4) = 9.408, p = 0.037) (Fig. 4.11 b).

In terms of HB daily removal rates (Fig. 4.11 c,d) the results show a significant effect of P-addition on HB daily removal rate of PNF (MD-ANOVA, F(1,4) = 42.681, p = 0.003), with lower rates being recorded in the P-amended treatment. No significant effect was observed for the HB removal rate of HNF due to P addition (MD-ANOVA F(1, 4) = 0.588, p = 0.486). Time had no significant effect on the bacterial removal rates either of HNF or PNF. In the control, bacterial removal rate by PNF was significantly higher than that of HNF (MD-ANOVA, F(1, 4) = 41.079, p = 0.003) (Fig. 4.11 c), whereas in the P-amended treatment the bacterial removal rates by HNF and PNF were similar (MD-ANOVA, F(1, 4) = 3.942, p = 0.118) (Fig. 4.11 d).

4.4 Discussion

4.4.1 Methodological considerations

In order to quantify the grazing effect of pigmented and heterotrophic nanoflagellates on HB the surrogate prey method was used. Uptake of FLB in short-term experiments is a commonly used technique to estimate nanoflagellate grazing in a variety of aquatic ecosystems (e.g., Unrein et al., 2007; Anderson et al., 2017; Vaqué et al., 2017; Gerea et al., 2019). The main benefit of the method is that it allows for grazer categorization through optical observation of cell morphology and pigmentation, which is a prerequisite to identify mixotropic grazers. However, the use of heat killed *B.diminuta*, results in prey analogues with altered cell surface properties and motility. Moreover, the size distribution of the prey analogues may deviate from the size distribution of the natural bacterial assemblage. Inevitably, these limitations of the FLB method introduce some uncertainty to the ingestion rate estimates. Nanoflagellates have been found to discriminate between living and dead cells (Landry et al., 1991), while their prey preferences can be affected by prey size (Epstein and Shiaris, 1992). The *B.diminuta* strain used in the present study, has the advantage of relatively small size and along with the starvation protocol that was followed, allows for prey surrogates within the size range of marine natural bacterial population (Vázquez-Domínguez et al., 1999; Unrein et al., 2007; Karayanni et al., 2008). Although FLB are a rather simplified version of natural prey, the application of the same methodology in the field and in the microcosm experiments, is a realistic tool for assessing the relative grazing potential and the relative differences in grazing responses of the nanoflagellates.

In order to estimate the daily stock removal rate of HB and *Synechococcus*, constant ingestion rates of nanoflagellates on HB and *Synechococcus* over the diel cycle were assumed. However, significant daily shifts of ingestion rates have been observed for PNF feeding on HB (Pålsson and Granéli, 2003) and *Synechococcus* (Tsai et al., 2007) as well as for HNF feeding either on HB (Ng and Liu, 2016) or *Synechococcus* (Dolan and Šimek, 1999). Therefore, the percentage of HB and *Synechococcus* standing stock removed daily by nanoflagellates should

be considered a rough estimate.

4.4.2 Field experiments

In the ultra-oligotrophic NW Levantine Sea (E. Mediterranean), under spring conditions, mixotrophy was found to be a relatively important trophic mode among pigmented small nanoflagellates, especially in the vicinity of the DCM layer (75 m) were PNF were the dominant grazers of prokaryotic picoplankton (HB and *Synechococcus*). In the study area, the nanoflagellate community was dominated by cells of small size <5 µm, most of them being even smaller than 3 µm, which is a common characteristic of the Mediterranean Sea (Christaki et al., 2001; Siokou-Frangou et al., 2010). Moreover, the present study showed that HNF and PNF <5 µm obtained 26.5±9.9% d^{-1} and 21.7±10.3% d^{-1} (mean±sd) of their carbon biomass from prokaryotic picoplankton (HB + *Synechococcus*), respectively, while, HNF and PNF, together, removed up to 9.1% (4.7±3.3%, mean±sd) of picoplankton standing stock per day. Thus, the results of this study highlight the role of small nanoflagellates (<5µm) as picoplankton consumers, and the importance of mixotrophy as a trophic strategy for PNF belonging to the lowest size fraction (<5 µm). Other potential grazers of prokaryotic picoplankton are larger nanoflagellates and ciliates. Although, on an individual basis, nanoflagellates in the 5–10 µm size class can have higher ingestion rates than those <5 µm, the very low abundance of 5–10 µm recorded in the present study implies a small grazing effect on prokaryotic picoplankton by this group, as has been previously shown in oligotrophic marine (Unrein et al., 2007; Tsai et al., 2011) as well as freshwater systems (Pernthaler et al., 1996; Callieri et al., 2002). Ciliates may also present higher ingestion rates than nanoflagellates (Unrein et al., 2007), however their abundance during the study period was low (0.51±0.16 cells mL^{-1} (mean±sd), I. Santi, unpublished data). Therefore, it is expected that their grazing effect on prokaryotic picoplankton would be moderate as has been previously reported in studies conducted in the Mediterranean Sea (Christaki et al., 2001; Pitta et al., 2001; Unrein et al., 2007) and on *Synechococcus* in a deep subalpine lake (Callieri et al., 2002). The observations reported in the present study are in line with the view that small pigmented and heterotrophic nanoflagellates are major contributors to the flow of energy and nutrients in oligotrophic systems (Unrein et al., 2007; Zubkov and Tarran, 2008; Hartmann et al., 2012).

HNF ingestion rates on HB were among the lowest ($\leqslant$ 0.81 HB ind.$^{-1}$h $^{-1}$) recorded in the Mediterranean Sea so far (Christaki et al., 2001; Unrein et al., 2007; Pachiadaki et al., 2016). However, this is not strange since values <1.5 HB $^{-1}$h $^{-1}$ are typical for HNF of <3 µm in size (Tsai et al., 2011), which dominated in the present study the small heterotrophic nanoflagellate community (84±8.2%). Moreover, the low HB concentrations (2.72 – 3.9 × 10^5 HB mL^{-1}) and the low HNF abundance ($\leqslant$ 765 cells mL^{-1}) may have contributed to the low HNF ingestion rates reported here. This explanation is further supported by a study conducted in the Weddell Sea, that found a positive relationship between the ingestion rates of HNF and the concentration of both HB and HNF (Vaqué et al., 2002). As with HNF, PNF

community in the present study was dominated by cells <3 µm and showed low ingestion rates on HB ($\leqslant$ 0.65 HB ind.$^{-1}$ h^{-1}) typical for this size class (Zubkov and Tarran, 2008; Tsai et al., 2011). Nevertheless, the present study showed that HNF and PNF together consumed, on average, 4.4±3.2% d^{-1} of HB standing stock, which is within the typical range reported in oligotrophic systems (Christaki et al., 2001; Unrein et al., 2007; Zubkov and Tarran, 2008; Tsai et al., 2011).

In the present study, depth affected the relative importance of HNF and PNF as consumers of heterotrophic bacteria since significant higher PNF abundance, ingestion rates and grazing effect were recorded at 75 m in comparison to 5 m while no difference was observed for HNF. At surface (5m), HNF ingestion rates and grazing effect exceeded those of PNF and, as a result, HNF dominated bacterivory. On the other hand, in the vicinity of the DCM layer (75 m) PNF were numerically dominant while their ingestion rates matched those of HNF and, thus, PNF accounted for most of the nanoflagellate bacterivory in this depth. Interestingly, N:P ratio was, on average, 2-fold higher at 75 m suggesting pronounced phosphorus limitation at this depth (Table 4.1). Moreover, a significant negative correlation between phosphorus concentration and the ingestion rates of PNF on HB was observed. Therefore, these observations are consistent with the prevailing view of mixotrophy as a strategy to obtain limiting nutrients. In support of this view, similar trends of increasing ingestions rates of PNF on HB with decreasing phosphate availability have been reported in time-series studies taking place in coastal oligotrophic waters (Unrein et al., 2007; Tsai et al., 2011, e.g), whereas others have reported significant declines in the proportion of actively feeding PNF in phosphate enrichment experiments conducted in oligotrophic systems (Arenovski et al., 1995; Christaki et al., 1999).

Ingestion rates on *Synechococcus* and the percentage of *Synechococcus* standing stock consumed daily by HNF did not vary with depth and they were similar to those reported previously for the Mediterranean Sea (Dolan and Šimek, 1999; Christaki et al., 2001). Moreover, HNF have been identified as dominant *Synechococcus* consumers in both marine (Caron et al., 1999; Christaki et al., 2001) as well as freshwater (Šimek et al., 1997; Callieri et al., 2002) systems as was the case of the surface samples in the present study. On the other hand, *Synechococcus* consumption by PNF has previously been found to be of minor importance in the Mediterranean Sea (Christaki et al., 2001). However, the results reported here showed that PNF ingestion rates on *Synechococcus*, although they were low ($\leqslant$ 0.02 *Syn.* ind.$^{-1}$ h^{-1}) at the surface, they were high at 75 m, where PNF were the dominant grazers, accounting for 60 – 74% of *Synechococcus* consumption. This finding suggests a key role of PNF as *Synechococcus* consumers as has been reported in various marine (Hall et al., 1993; Safi and Hall, 1999; Tsai et al., 2007; Chan et al., 2009) and freshwater (Gerea et al., 2019) systems. Moreover, PCA analysis indicated a negative relationship between phosphorus concentration and ingestion rates of PNF on *Synechococcus* implying that phosphorus limitation should trigger PNF grazing on *Synechococcus*. In the Mediterranean Sea, it has been shown that *Synechococcus* are far more efficient than eukaryotic phytoplankton and heterotrophic bacteria in obtaining phosphate, especially under nutrient limiting conditions (Moutin et al., 2002). Therefore, ingestion of *Synechococcus* by PNF may be an efficient way to obtain

phosphorus, thus employing a strategy of "eating your competitor", *sensu* Thingstad et al. (1996). Overall, in the present study, HNF and PNF consumed 19.7 ± 16% d^{-1} (mean ± sd) of *Synechococcus* standing stock, which suggests that *Synechococcus* may constitute an important energy and nutrients source for nanoflagellates under spring conditions in the E. Mediterranean Sea.

The mean carbon biomass obtained by PNF and HNF from HB and *Synechococcus* was in accordance with previous studies conducted in the Mediterranean (Christaki et al., 2001). For PNF, mean percentages of carbon biomass from HB and *Synechococcus* were somewhat lower than for HNF, though still comparable (Table 4.2). This suggests that HNF and PNF in the EMS are more or less equally dependent on prokaryotic picoplankton consumption for their growth, especially in the vicinity of the DCM layer. Moreover, light might have affected the phagotrophic behaviour of PNF, since, according to PCA analysis, samples from 75 m were subjected to lower PAR and presented significantly higher ingestion rates of PNF on prokaryotic picoplankton. This is not unexpected since there are some mixotrophic protists that increase their ingestion rates in response to light limitation in order to obtain organic carbon (e.g., McKie-Krisberg et al., 2015). However, in the present study, the ca. 2-fold higher primary production rates recorded at 75 m, comparing to the surface, particularly attributed to picoplankton cells (Fig. 4.3 a, b), indicate that light should not have been the major limiting factor. Thus, in the vicinity of the DCM layer (75 m), the light conditions, although corresponding to approximately 2 – 3% of surface irradiance, combined with the relatively high DIN concentrations recorded, were enough to sustain photosynthesis and production. Consequently, in the ultra-oligotrophic E. Mediterranean, low particle concentrations in the water column allow penetration of light in relatively large depths and when enough light reaches the nutricline layers, significant *in situ* growth may occur, as was the case in this experiment during spring in the NW Levantine area. As a result, the recorded increased ingestion rates of PNF on prokaryotic picoplankton should rather be a response to phosphorus limitation as suggested above.

Pigment/CHEMTAX analysis showed that Prymnesiophytes and Pelagophytes/Chrysophytes were the most important groups at both depths, at all stations, while Cryptophytes and Prasinophytes contributed more to the total pigmented nanoflagellate community at 75 m. Previous studies have confirmed the dominance of Prymnesiophytes in terms of diagnostic pigments in the Eastern Mediterranean (Psarra et al., 2005; Lagaria et al., 2017b) while Prymnesiophytes (<3 μm) have been identified among the most photosynthetically active small PNF in these waters (Man-Aharonovich et al., 2010). Interestingly, PCA analysis revealed a positive relationship between Prymnesiophytes and PNF ingestion rates on both HB and *Synechococcus* and a negative relationship of these rates with phosphorus concentration, suggesting that Prymnesiophytes were the most important grazers in the area. In accordance with the findings reported here, a study that analysed 16S rRNA gene sequences across the world ocean revealed a negative relationship between small (<3 μm) Prymnesiophytes and phosphorus concentration (Kirkham et al., 2013). Moreover, Unrein et al. (2014) showed that Prymnesiophytes in the size class 3 – 5 μm were the most important mixotrophic group, being responsible for up to 20.8 % of the total protist bacterivory. Prymnesiophytes have been

also identified as important grazers of cyanobacteria (*Synechococcus* and *Prochlorococcus*) (Frias-Lopez et al., 2009). Consequently, the dominance of Prymnesiophytes in phosphorus limited environments may be related to their mixotrophic potential (Liu et al., 2016).

Finally, PCA analysis showed that the easternmost station LV18, especially at 75 m, was distinguished from the rest of the stations, mainly due to the high DIN concentration, high ingestion rates of HNF on HB and lower ingestion rate of HNF on *Synechococcus*. Additionally, the marked increase of Pelagophytes/ Chrysophytes recorded at station LV18-75 m coincided with an increased contribution of the <2 µm size class of PNF confirming previous studies in the E. Mediterranean arguing that this group is abundant within the smallest (<2 µm) size class of phytoplankton (Lagaria et al., 2017b). Overall, these findings suggest a different structure and function of the small nanoflagellate community in the easternmost station LV18 that may be related to the proximity of this station to the Rhodes gyre, a permanent hydrographic structure of the E. Mediterranean that carries nutrient enriched waters from the deep layers to the euphotic zone (Velaoras et al., 2018).

The results of these field experiments pinpoint the role of small nanoflagellates both pigmented and heterotrophic as prokaryotic picoplankton consumers. Moreover, the negative relationship between phosphate concentration and ingestion rates of PNF on prokaryotic picoplankton implied that mixotrophy may be an ecological adaptation of small PNF to phosphate limitation which prevails in the in the ultra-oligotrophic EMS. This finding has important implications for the functioning of the microbial food web as it suggest that in periods of P-depletion, as for example during the stratified period, PNF are significant, even dominant, consumers of picoplankton. Moreover, it suggests that the role of PNF as picoplankton consumers is not fixed but it depends on P availability. Thus, these findings indicated that the functioning of the microbial food web in the EMS is complicated and warrants further investigation. Therefore, the follow up microcosm experiments were designed in order to better understand the trophic relationships between the components of the microbial food web in the EMS when P availability varies.

4.4.3 Microcosm experiments

In order to examine the grazing response of the nanoflagellate community to phosphate addition, microcosm experiments with nutrient depleted and P-starved surface water from the Cretan Sea (Eastern Mediterranean) during the late stratified season were performed. Pigmented nanoflagellates responded immediately to phosphate addition by lowering their ingestion rates, whereas P availability had no effect upon the ingestion rates of heterotrophic nanoflagellates. The present study is the first to quantitatively assess the heterotrophic and pigmented nanoflagellates ingestion rates on bacteria as a response to phosphate addition in the EMS in surface nutrient-depleted waters during the late stratified season.

The present study showed that PNF ingestion rate was significantly higher than that of HNF in the control treatment and lower than that of HNF in the P-amended treatment, considering the whole duration of the experiment. PNF in the control treatment were ca-

pable of removing more bacteria than HNF, as shown by the corresponding daily bacterial removal rate. Phosphate addition had a negative effect on PNF daily bacterial removal rate, suggesting that the importance of PNF relative to HNF as bacterial grazers, in stratified and phosphorus depleted surface waters in the EMS, is diminished as soon as phosphate is added to the system. PNF were found to be the dominant grazers in the deep chlorophyll maximum of the NW Levantine basin, as was shown and discussed in Section 4.4.2 and also in a coastal oligotrophic site of the Western Mediterranean Sea (Unrein et al., 2007). Previous grazing studies report that HNF harvested most of the bacterial production in an East-to-West transect (Christaki et al., 2001), and that bacterivory of heterotrophic flagellates roughly balanced bacterial production in NE Mediterranean (Christaki et al., 1999), whereas, mixotrophic nanoflagellates played a minor role as bacterivores in waters of Levantine origin (SE Mediteerranean) (Christaki et al., 1999). Such partly contradicting findings could result from the interplay of nutrient availability and PNF grazing.

The results presented here experimentally confirm that phosphate addition in P-depleted surface waters of the Cretan Sea, in the EMS has a negative effect on the ingestion rates as well as on the bacterial removal rate of PNF. These results are also supported by the negative correlations between phosphate concentrations and nanoflagellate grazing in the Mediterranean (finding of this study as presented in Section 4.3 and Unrein et al., 2007), as well as by phosphorus enrichment experiments with natural populations that showed marked declines in phagotrophically active pigmented nanoflagellates in the Aegean Sea (Christaki et al., 1999) and in the Sargasso Sea (Arenovski et al., 1995). A similar experiment in the subtropical Atlantic Ocean indicated a potential regulation of pigmented flagellate feeding rates by phosphate availability (Duhamel et al., 2019). Culture experiments have produced similar results and have demonstrated that ingestion of prey by mixotrophic nanoflagellates is stimulated by phosphorus deficiency (Carvalho and Granéli, 2010; Anderson et al., 2018).

In the present study, phosphate addition had a significant effect on the physiology of PNF by causing a reduction of their ingestion rates, however, it had no significant effect on their abundance, showing an increase over time in both treatments, despite the apparent P-limitation in the control treatment. These results might be better understood if the alternative trophic strategies of PNF are considered. In the P-limited conditions of the control treatment, PNF covered their need in phosphorus by consuming HB. On the other hand, in the P-amended treatment the ingestion rate of PNF was drastically reduced, suggesting that the observed increase in their abundance should have been supported by autotrophy. The lower PNF ingestion rates in the phosphate addition along with no significant difference in abundances between the two treatments, imply that PNF are able to maintain a steady growth by switching from phosphate uptake by prey ingestion to inorganic phosphate acquisition by osmotrophy. Moreover, Chlα at the end of the experiment displayed similar values for both treatments indicating that photosynthesis was not downregulated even though the organisms were consuming prey. This may suggest an obligatory demand for photosynthetically produced carbon which is combined with either inorganic nutrients or nutrients obtained from prey, depending on the phosphate acquisition pathway taking place in the PNF. Similar dependence on photosynthetically produced carbon has been reported

for *Prymnesium parvum* in which Chlα content in feeding and non-feeding cells was constant (Carvalho and Granéli, 2010) and carbon obtained through phagotrophy was not assimilated at any substantial level (Liu et al., 2015b; Carpenter et al., 2018).

Heterotrophic nanoflagellates increased in abundance due to phosphate addition with an obvious response after Day 2 of the experiment, however, their ingestion rates were similar in both treatments, thus P addition had no significant effect on HNF in terms of physiology. The steady ingestion rates combined with an increase in abundance may indicate a potential qualitative response of HNF to phosphate addition implying ingestion of higher quality P-rich food in their available prey (HB +*Synechococcus*). The measured prokaryotes abundance in the control treatment at Day 0, as representative of the natural population, is in accordance with values reported for the same region (Van Wambeke et al., 2000; Siokou-Frangou et al., 2002). The microcosm experiments showed that both heterotrophic bacteria and *Synechococcus* abundances were enhanced by phosphate addition. The enhancement of bacterial abundance observed in the P-amended microcosm supports the view of phosphorus-limited heterotrophic bacteria and *Synechococcus* in the oligotrophic Mediterranean Sea, as it has been demonstrated by previous studies (Zohary and Robarts, 1992; Vaulot et al., 1996; Krom et al., 2005).

In the EMS, HB are known to be under tight control of both phosphorus availability and grazing by HNF (Thingstad and Rassoulzadegan, 1995; Siokou-Frangou et al., 2010, and references therein). However, the findings of the present study suggest that the relaxation of both P-limitation and grazing pressure by PNF on HB, coupled to a stable grazing pressure by HNF, in the phosphate addition treatment, must have allowed the proliferation of HB and *Synechococcus* in the P-amended series. Thus, in light of the results reported here, it seems that grazing activity of PNF may be another important process contributing to the control of HB population under P-limited conditions. Despite the findings from the field experiments (Section 4.3) and from previous studies (Dolan and Šimek, 1999; Christaki et al., 2001), where it was shown that *Synechococcus* was grazed by flagellates in P-depleted Mediterranean waters, in the microcosm experiments of this study, ingested *Synechococcus* by heterotrophic or pigmented flagellates was rare, not allowing for accurate estimations of nanoflagellate grazing on *Synechococcus*.

In conclusion, the combination of field and laboratory grazing experiments provided a better understanding of the regulation of mixotrophy among PNF in the EMS. The significant negative relationship between P availability and ingestion rates of PNF observed during the field experiments performed in the NW Levantine Sea (EMS) indicated that P-deficiency promotes phagotrophy among PNF. This observation was verified by the microcosm experiments and the observed significant decrease of the ingestion rates of PNF in the P-amended treatment. Moreover, the present study revealed the significant role of PNF as bacterial consumers in the EMS under P depleted conditions. However, increase of phosphate concentration alters the functioning of the food web and leads to an immediate response of PNF by lowering their ingestion rates, and thus limiting their contribution to bacterial grazing, enhancing the relative importance of HNF as bacterial grazers. The phosphorus depen-

dent trophic relationships revealed by the present study are particularly relevant for the ecosystem functioning in the EMS with its pulsed atmospheric nutrient inputs from Saharan dust storms and the intermittent nutrient pulses associated with the intense mesoscale and sub-mesosacale activity that favour the turnover of water masses through cyclonic and anti-cyclonic circulation.

Chapter 5

Synthesis: A conceptual framework of nanoflagellates-bacteria interactions in the Eastern Mediterranean Sea

5.1 Introduction

Accumulated evidence gathered from the present and previous studies suggest a pivotal role of PNF as both primary producers and consumers in P-limited marine ecosystems and particularly in the EMS. The experimental study presented in Chapter 4 showed that pigmented nanoflagellates (PNF) contributed significantly to the total bacterial consumption in the vicinity of the deep chlorophyll maximum layer of the NW Levantine (EMS) and also in the unperturbed (control), P-depleted treatment of the P addition microcosm experiments performed with surface water from a coastal site of the Cretan sea (EMS). These findings are in agreement with recent studies in other oligotrophic, P-limited environments, such as the Atlantic ocean (Hartmann et al., 2012; Duhamel et al., 2019) and the NW Mediterranean (Unrein et al., 2007), that have revealed a major role of mixotrophic PNF as heterotrophic bacteria (HB) consumers. Prymnesiophytes, in particular, are the dominant group among nanoplankton in the EMS, in terms of diagnostic pigments (Psarra et al., 2005; Lagaria et al., 2017b, this study (Chapter 4)), but they are also well known for their phagotrophic potential (Unrein et al., 2014, this study (Section 4.3)), as well as their important contribution to primary production (Man-Aharonovich et al., 2010). Additionally, PNF were found responsible for 45–57% of total primary production in the P-depleted EMS waters (Flaten et al., 2005; Pitta et al., 2016). To date, however, the phagotrophic activity of PNF has not been conceptually integrated in the functioning of the microbial food web of the EMS. The lack of a collective effort to combine consistent field and experimental observations with hypothesis-based predictions hampers our understanding of ecosystem functioning and of biogeochemical cycles, especially in the oligotrophic EMS.

The findings presented in Chapter 4 confirm that P deficiency promotes phagotrophy among PNF in the EMS. The inverse relationship between P-availability and ingestion rates of PNF along with the similar concentrations of Chlα in both treatments in the microcosm experiments (Section 4.3.2) suggests that PNF in the EMS can be primarily described as type IIA mixotrophs according to the classification system of Stoecker (1998) (see Chapter 3). The presence of type IIA mixotrophic PNF in the EMS implies that their phagotrophic activity strongly depends on P-availability. Apart from the regulating role of P-availability on the phagotrophic activity of PNF, nutrient availability is also related to the mechanism of dissolved organic matter (DOM) release by photosynthetic cells as it was shown in Chapter 2. In turn, the quality of the released DOM seems to be affected by the physiological mechanism responsible for its production, being either passive diffusion or active exudation (Borchard and Engel, 2015; Mueller et al., 2016), with implications for the efficiency of this DOM assimilation into bacterial biomass (Obernosterer and Herndl, 1995; Mühlenbruch et al., 2018).

Thus, phosphate availability affects directly and simultaneously three interrelated and co-dependent processes, that is a) the excretion of DOM by photosynthetic cells, in terms of quantity and quality (Chapter 2), b) bacterial growth, and c) bacterial grazing by mixotrophic PNF (Chapter 4). The fact that these key ecosystem processes are affected by nutrient availability implies that different carbon and nutrients pathways are operating before and after nutrient enrichment events. This is particularly important for the understanding of the microbial food web functioning in the EMS, as pulsed atmospheric nutrient enrichment through dust deposition from the adjacent Saharan Desert occurs frequently in the region (Pitta et al., 2017; Rahav et al., 2018). Moreover, numerous mesoscale structures, such as permanent or semi-permanent eddies, that favour vertical exchange of water masses have a significant effect on biological activity in the EMS (Petihakis et al., 2009; Moutin and Prieur, 2012; Varkitzi et al., 2020).

In this chapter, a simplified model of microbial food web interactions is built that integrates the findings presented in the previous chapters of this thesis. The aim is to qualitatively explore the pathways of P and C flow through the heterotrophic bacteria-nanoflagellates (pigmented and heterotrophic) link of the EMS microbial food web. The model considers varying availability of phosphorus and takes into account mixotrophy among PNF and two mechanisms of DOM release, i.e., passive diffusion and active exudation.

5.2 Methods

5.2.1 Model formulation

In this theoretical study, a zero-dimensional mathematical model is implemented. The model describes the dynamics of carbon (C) and phosphorus (P), as the latter is the primarily limiting nutrient in the EMS both for heterotrophic prokaryotes and phytoplankton growth. The

environment is modeled with 8 state variables; the inorganic carbon (IC) and phosphorus (IP), the dissolved organic matter, which is expressed in carbon (DOC_x) and phosphorus (DOP_x) units and it is partitioned into three compartments comprising the labile ($x = L$), semi-labile ($x = S$) and semi-refractory pools ($x = R$), each having different mineralization rates by HB and different production pathways. The semi-refractory DOM fraction is defined as the less biologically reactive fraction of DOM (Polimene et al., 2006; Carlson and Hansell, 2015). Plankton growth dynamics results from the interplay between gains through assimilation of organic and inorganic phosphorus and carbon and losses due to maintenance and growth overheads, excretion due to stoichiometric constraints of growth, predation and non-predatory mortality. All organisms are modelled based on DEB theory, as it allows for detailed description and quantification of the metabolic processes taking part within the organisms.

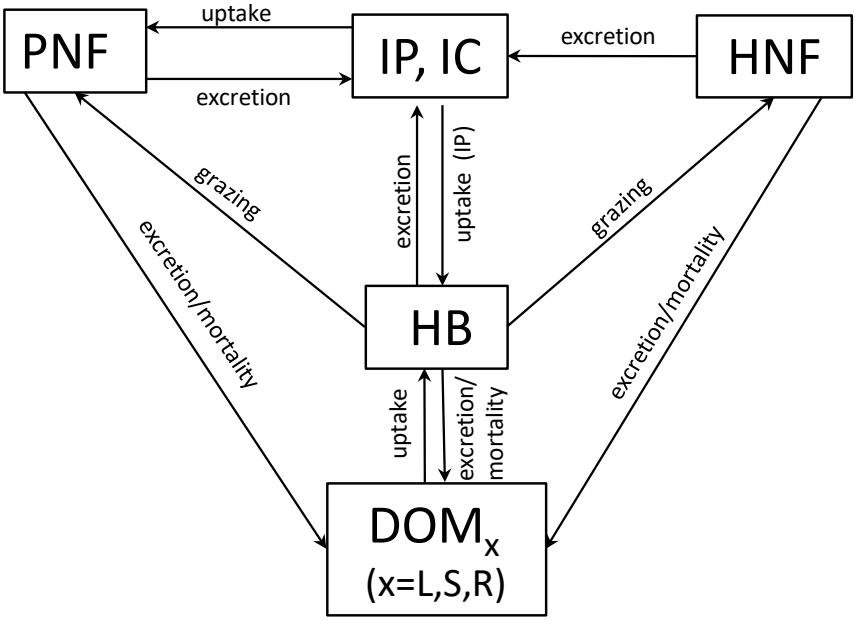

Figure 5.1: Conceptual diagram of the biogeochemical interactions between the organisms and the environment. PNF: Pigmented Nanoflagellates, HNF: Heterotrophic Nanoflagelaltes, HB: Heterotrophic Bacteria, IP: Inorganic Phosphorus, IC: Inorganic Carbon, DOM$_x$: Dissolved Organic Matter (x = L (labile), S (semi-labile), R (semi-refractory)), DOM refers to both Dissolved Organic Carbon (DOC) and Dissolved Organic Phosphorus (DOP).

Figure 5.1 summarizes the interactions between the three functional groups of organisms (i.e., Heterotrophic Bacteria (HB), Heterotrophic Nanoflagellates (HNF) and Pigmented Nanoflagellates (PNF)) and the environment through the biogeochemical processes. The conceptual model implemented in this study consists of complex interactions among the plankton compartments as PNF and HNF are competing for bacterial prey. On the other hand,

HB and PNF are simultaneously linked together through commensalism, providing DOM originated from photosynthesis for bacterial growth, through competition for phosphate and through a predator-prey relationship, where PNF consume bacterial prey to obtain phosphorus. The dynamics of the state variables of the system are given in Table 5.1, while the equations for production and consumption fluxes (j) of the state variables are presented in the following subsections.

Table 5.1: Model state variables. X_i is the concentration of compound i (in µmol L^{-1}) and j_{i,k_*} is the specific flux (in mol i (mol $V*)^{-1}$ d^{-1}) of compound i associated with process k and organism $*$, with $k \in \{U, A, R, Ex, D\}$[1], $* \in \{P, B, H\}$[2], and $i \in \{IC, IP, V*, E*, EP_C, EP_P, DOi_L, DOi_S, DOi_R\}$[3]. j_{i,k_*} are given in Tables 5.2, 5.3 and 5.4. See the Methods section for details.

No	Equation
5.1	$\frac{d}{dt}X_{IC} = -(j_{C,A_P} + j_{IC,Ex_P})\ X_{VP} + j_{IC,Ex_B}\ X_{VB} + j_{IC,Ex_H}\ X_{VH}$
5.2	$\frac{d}{dt}X_{IP} = (-j_{IP,U_P} + j_{IP,Ex_P})\ X_{VP} + j_{IP,Ex_B}\ X_{VB} + j_{IP,Ex_H}\ X_{VH}$
5.3	$\frac{d}{dt}X_{VB} = (\dot{r}_B - j_{VB,D_B})\ X_{VB} - j_{B,U_H}\ X_{VH} - j_{B,A_P}\ X_{VP}$
5.4	$\frac{d}{dt}X_{EB} = (j_{EB,A_B} - m_{EB}(\dot{k}_{EB} - \dot{r}_B))\ X_{VB} - m_{EB}\ (j_{B,U_H}\ X_{V_H} + j_{B,A_P}\ X_{VP}) - j_{VB,D_B}\ X_{EB}$
5.5	$\frac{d}{dt}X_{VH} = (\dot{r}_H - j_{VH,D_H})\ X_{VH}$
5.6	$\frac{d}{dt}X_{VP} = (\dot{r}_P - j_{VP,D_P})\ X_{V_P}$
5.7	$\frac{d}{dt}X_{EP} = (j_{EP,A_P} - j_{EP,C_P})\ X_{VP} - j_{VP,D_P}\ X_{EP}$
5.8	$\frac{d}{dt}X_{EP_C} = (j_{EP_C,A_P} - j_{EP_C,C_P} + \kappa_{EP}\ j_{EP_C,R_P})\ X_{VP} - j_{VP,D_P}\ X_{EP_C}$
5.9	$\frac{d}{dt}X_{EP_P} = (j_{EP_P,A_P} - j_{EP_P,C_P} + \kappa_{EP}\ j_{EP_P,R_P})\ X_{VP} - j_{VP,D_P}\ X_{EP_P}$
5.10	$\frac{d}{dt}X_{DOi_L} = j_{DOi_L,Ex_P}\ X_{VP} + j_{VP,D_P}\ (n_{i,EP}\ X_{EP} + X_{EP_i}) + (0.5\ j_{VH,D_H}\ n_{i,VH} + j_{DOi_L,Ex_H})\ X_{VH}$ $+(j_{DOi_S,U_B} + j_{DOi_R,U_B} - j_{DOi_L,U_B})\ X_{VB} + j_{VB,D_B}\ n_{i,EB}\ X_{EB}$, where $i = C, P$
5.11	$\frac{d}{dt}X_{DOi_S} = j_{DOi_S,Ex_P}\ X_{VP} - j_{DOi_S,U_B}\ X_{VB}$, where $i = C, P$
5.12	$\frac{d}{dt}X_{DOi_R} = (j_{DOi_R,Ex_B} + j_{VB,D_B}\ n_{i,VB})\ X_{VB} - j_{DOi_R,U_B}\ X_{VB}$ $+j_{VP,D_P}\ \ n_{i,VP}\ X_{VP} + 0.5\ \ n_{i,VH}\ j_{VH,D_H}\ X_{VH}$, where $i = C, P$

[1] U: uptake, A: assimilation, R: rejection, Ex: excretion, D: death

[2] P: PNF, B: Bacteria, H: HNF.

[3] IC: inorganic carbon, IP: inorganic phosphorus, $V*$: structural mass of organism $*$, $E*$ generalized reserve of organism $*$, EP_C: Carbon-reserves of PNF , EP_P: Phosphorus reserves of PNF, DOi_L, DOi_S, DOi_R: labile, semi-labile and semi-refractory pools of dissolved organic matter in terms of carbon ($i = C$) and phosphorus ($i = P$).

Pigmented nanoflagellates

PNF are modeled as type IIA mixotrophs on the basis of the experimental evidence presented in Chapter 4. The model for type IIA PNF was described in Chapter 3 and it was built on

Table 5.2: Equations that describe the physiological processes occurring in PNF.

No	Equation	Explanation
5.13	$j_{i,U_P} = j_{i,U_{P_m}} \dfrac{X_i}{X_i + KP_i}, \quad (i = IP)$	IP uptake
5.14	$j_{i,U_P} = j_{i,U_{P_m}} \dfrac{X_i}{X_i + KP_i}, \quad (i = IC, B)$	Potential uptake
5.15	$j_{L,U_P} = \alpha_L L$	Photons' arrival rate
5.16	j_{C,A_P}	C-formation rate[1]
5.17	j_{EP,A_P}	E- reserve formation[2]
5.18	$j_{B,A_P} = j_B^+$	Bacterial uptake[3]
5.19	$j_{EP_C,A_P} = j_{C,A_P} - j_C^+$	EP_C-reserve formation[3]
5.20	$j_{EP_P,A_P} = j_{IP,U_P} - j_P^+$	EP_P-reserve formation[3]
5.21	$j_{EP_i,C_P} = m_{EP_i}(\dot{k}_{EP} - \dot{r}_P) \quad (i = -, C, P)$	Catabolic rate
5.22	$j_{EP',C_P} = 1/\left(\dot{k}_{CP}^{-1} + j'^{-1}_{EP_C,C_P} + j'^{-1}_{EP_P,C_P} - (j'_{EP_C,C_P} + j'_{EP_P,C_P})^{-1}\right)$	EP$'$- reserve formation *
5.23	$j_{VP,G_P} = y^{-1}_{EP,VP}(j_{EP,C_P} + j_{EP',C_P} - j_{EP,M_P})_+$	Gross growth rate
5.24	$j_{VP}^{M_P} = (j_{EP,M_P} - \min(j_{EP,C_P} + j_{EP',C_P}, j_{EP,M_P}))\, y^{-1}_{EP,VP}$	Maintenance (structure)
5.25	$\dot{r_P} = j_{VP,G_P} - j_{VP}^{M_P}$	Net specific growth rate
5.26	$j_{EP_i,R_P} = j_{EP_i,C_P} - y_{i,EP} j_{EP',C_P} \quad (i = C, N)$	Rejection rate
5.27	$j_{DOi_L,Ex_P} = y_{DOi_L,VP}\; j_{VP,G_P} \quad (i = C, P)$	DOM$_L$ excretion [4]
5.28	$j_{DOC_S,Ex_P} = (1 - \kappa_{EP}) j_{EP_i,R_P} + (1 + m_{EB})\; j_{B,A_P}, \quad (i = C, P)$	DOC$_S$ excretion [5]
5.29	$j_{DON_S,Ex_P} = (1 - \kappa_{EP}) j_{EP_P,R_P} + (n_{P,B} - n_{P,EP}\; y^{-1}_{B,EP}) j_{B,A_P}$	DON$_S$ excretion [6]
5.30	$j_{IC,Ex_P} = (y_{C,EP} - n_{C,EP})(j_{EP,A_P} + j_{EP',C_P}) + j_{IC,M_P}$	IC excretion[7]
5.31	$j_{IP,Ex_P} = j_{IP,M_P}$	IP excretion[8]

Physiological processes: A (assimilation), C (catabolism), M (maintenance), R (rejection), G (growth), Ex (excretion)

*To simplify the notation, the rate at which substrate molecules, say of type A, arrive and bind at the SU is scaled to the number of molecules, $y_{A,P}$, required to produce one molecule of product P, i.e., $j_A^{'} = \rho_A j_A / y_{A,P}$ where ρ_A is the probability that molecules of substrate A bind to the SU and it is taken to be 1 for all substrates.

[1] Eq. (B.3) in Appendix B
[2] Eq. (B.6) in Appendix B with N and F replaced by IP and B, respectively.
[3] j_C^+, j_P^+, j_B^+: Eq. (3.1) with N, F and E replaced by P and B and EP, respectively.
[4] $y_{DOi_L,VP} = y_{EP,VP} n_{i,EP} - n_{i,VP}$ (i = C, P, Chapter 2, Section 2.2.2)
[5,6] Chapter 2, Eq. (2.10) see also text for details
[6] $n_{P,B} = n_{P,EB}\; m_{EB} + n_{P,VB}$
[7,8] $j_{i,M} = n_{*,EP} j_{EP,M_P} + j_{VP}^{M_P}(n_{*,VP} - y_{EP,VP} n_{*,E}), \quad (i = IC, IP), * = C, P$, (Chapter 2, Eq. (2.12))

the DEB model for photosynthetic cells presented in detail in Chapter 2. Here the limiting nutrient is considered to be phosphorus. Thus, PNF biomass is partitioned into structure M_{VP} and reserves masses M_i (here $i = EP$ (generalized reserves), EP_P (P-reserves), EP_C

(C-reserves) and each pool is assumed to have constant chemical composition, according to the "strong homeostasis" assumption. Although structure and each of the reserves masses have constant stoichiometry, the C:P of the total biomass may vary due to fluctuations in the relative amount of reserves and structure. The assimilation rate of inorganic carbon (IC), inorganic phosphorus (IP) and nutrients obtained from bacteria (B) into generalised reserves (j_{EP,A_P}) is described in detail in Chapter 3 (Section 3.2.1). All other physiological processes taking place in PNF are described mathematically in detail in Chapter 2, with the only difference that here phosphorus is the limiting nutrient instead of nitrogen. Table 5.2 summarizes the equations describing the metabolic fluxes in PNF.

PNF are the main producers of dissolved organic matter through two physiological mechanisms, one associated with growth (passive diffusion mechanism) (Eq. 5.27) and the other with the rejection flux during the reserves formation due to stoichiometric constraints (active exudation mechanism) (first term in Eq. 5.28 and 5.29). A detailed description of the DOM production by phytoplankton through these two excretion mechanisms is given in Chapter 2. Moreover, PNF contribute to the semi-labile DOM_S production via the excretion of the unassimilated organic carbon and phosphorus from the consumed bacteria (second term in Eq. 5.28 and 5.29).

Heterotrophic Bacteria

Bacterial biomass is divided into structural (M_{VB}) and generalized reserves mass (M_{EB}), each having a constant stoichiometry. However, the C:P ratio of total bacterial mass may vary due to fluctuations in the relative amount of reserves and structure. Thus, the molecular elemental ratio of biomass C:P is calculated by $n_{C,B}/n_{P,B}$, where $n_{C,B} = n_{C,EB}\, m_{EB} + n_{C,VB}$ is the total C-mol content of the cells per structural mass of bacteria (B) and $n_{P,B} = n_{P,EB}\, m_{EB} + n_{P,VB}$ is the P-mol content per structural mass of bacteria (B); $n_{*_1,*_2}$ denotes the chemical index of element $*_1$ in compound $*_2$. The reserve density is defined as $m_{EB} = M_{EB}/M_{VB}$.

Bacterial metabolism is linked to the dynamics of the three DOM pools. Table 5.3 summarizes the equations describing the metabolic fluxes in bacteria. Bacteria can act both as consumers and as producers of DOM (Ogawa et al., 2001; Jiao et al., 2010). All pools of DOM have a variable stoichiometry which is defined by the ratio $f_x = X_{DOP_x}/X_{DOC_x}$, $(x = L, S, R)$. For the semi-labile (S) and the semi-refractory (R) fraction of DOM we assume that bacteria first transform them into labile fractions and then assimilate them into generalized reserves. Bacterial uptake/transformation of DOC_x is taken proportional to DOC_x concentration, while the uptake rate of DOP_x is determined by the ratio f_i (Eq. 5.32, 5.33). According to the stoichiometry of DOM, bacteria can either mineralize DOP into inorganic phosphorus or consume inorganic phosphorus additionally to DOP to cover their P requirements. The potential uptake rate of inorganic phosphorus is given by Michaelis-Menten kinetics (Eq. 5.34) (Anderson and Williams, 1998).

The assimilation fluxes of DOM_L are obtained by assuming a constant assimilation effi-

Table 5.3: Equations that describe the physiological processes occurring in heterotrophic bacteria.

No	Equation	Explanation
5.32	$j_{DOC_x,U_B} = \alpha_x \; X_{DOC_x}, \quad x = L, S, R$	DOC uptake
5.33	$j_{DOP_x,U_B} = f_i \; j_{DOC_i,U_B}, \quad x = L, S, R$	DOP uptake[1]
5.34	$j_{IP,U_B} = j_{IP,U_{B_m}} \; \frac{X_{IP}}{K_{IP,B}+X_{IP}}$	Potential IP uptake
5.35	$j_{DOi_L,A_B} = y_B \; j_{DOi_L,U_B} \quad i = C, P$	DOM_L assimilation
5.36	$j_{EB,A_B} = min\left((j_{DOP_L,A_B} + j_{IP,U_B})/n_{P,EB}, j_{DOC_L,A_B}\right)$	E-reserve formation
5.37	$j_{IP,A_B} = j_{DOP_L,A_B} - j_{EB,A_B} \; n_{P,EB}$	IP assimilation/ excretion
5.38	$j_{IC,A_B} = j_{DOC_L,A_B} - j_{EB,A_B}$	IC excretion
5.40a	$\dot{r}_B = \frac{m_{EB} \; \dot{k}_{EB} - j_{EB,M_B}}{m_{E_B}+y_{EB,VB}}$	Net growth rate for $m_{EB} \geq \frac{j_{EB,M_B}}{\dot{k}_{EB}}$
5.40b	$\dot{r}_B = \frac{m_{EB} \; \dot{k}_{EB} - j_{EB,M_B}}{m_{EB}+j_{EB,M_B}/j_{VB,MB}}$	Net growth rate for $m_{E_B} < \frac{j_{EB,M_B}}{\dot{k}_{EB}}$
5.41	$j_{DOi_R,Ex_B} = j_{DOi_R,G_B} + j^M_{V_B} \; n_{i,VB}, \quad i = C, P$	DOM_R excretion[2]
5.42	$j_{Ii,Ex_B} = j_{Ii,A_B} + (1 - y_B) \; j_{DOi_L,U_B} + j^{M_B}_{EB} \; n_{i,EB}, \quad i = C, P$	IC, IP excretion[3]

Physiological processes: A (assimilation), C (catabolism), M (maintenance), R (rejection), G (growth), Ex (excretion)

[1] $f_x = X_{DOP_x}/X_{DOC_x}$

[2] The term $j_{DOi_R,G_B} = y_{DOi_R,V_B} \;\; j_{VB,G_B}, \;\; i = C, P$ where $y_{DOi_R,VB} = y_{EB,VB} n_{i,EB} - n_{i,VB}$ (i = C, P) and $j_{VB,G_B} = (\dot{r}_B)_+$ is the excretion flux of DOM_R during the transformation of EB-reserves into structure VB.

[3] For $i = IP$,the term j_{IP,A_B} (Eq. 5.37) can be either positive or negative, meaning that phosphorus is mineralized or taken up, respectively. The term j_{IC,A_B} (Eq. 5.38) quantifies the excess carbon in DOM_L that cannot be assimilated and it is respired. The term $(1 - y_B) \; j_{DOi_L,U_B}, i = C, P$ is the mineralized fraction of the uptake flux. The last term represents the inorganic carbon and phosphorus released due to maintenance ($j^{M_B}_{EB} = j_{EB,M_B}$ (constant) for $m_{EB} \geq \frac{j_{EB,M_B}}{\dot{k}_{EB}}$ and $j^{M_B}_{EB} = m_{EB} \; (\dot{k}_B - \dot{r}_B)$ for $m_{E_B} < \frac{j_{EB,M_B}}{\dot{k}_{EB}}$ (Eichinger et al., 2009))

ciency y_B, thus Eq. (5.35) gives the assimilation rate of DOM. Thus, the total available flux of phosphate is $j_{DOP_L,A_B} + j_{IP,U_B}$ (Eq. 5.34 and Eq. 5.35). Generalized reserves are formed at a rate j_{EB,A_B}, which depends on the limiting element for reserves formation being P or C (Eq. 5.36). The j_{IP,A_B} flux (Eq. 5.37) can be positive or negative meaning that phosphate is either mineralized or taken up, depending on the difference between DOM and bacteria C:P stoichiometry. Moreover, in the case where the total available flux of phosphate is not enough to allow the assimilation of the labile DOC consumed by bacteria into E-reserves, bacteria respire the excess carbon producing inorganic carbon (Eq. 5.38).

Bacteria are modelled as V1-morphs, according to Kooijman (2010) and Eichinger et al. (2009). The net specific growth rate, $\dot{r}_B$, is given by Eq. 5.40, where $m_{EB} = M_{EB}/M_{VB}$ is the reserve density, $\dot{k}_{EB}$ is the reserve turnover rate, j_{EB,M_B} is the maintenance rate which is paid from the reserves. When the mobilized reserves are not enough to cover the maintenance requirements (Eq. 5.40b), $\dot{r}_B$ will be negative and structure will be used at a rate $j^{M_B}_{VB} = |\dot{r}_B|$

to cover the remaining maintenance costs. The negative growth rate implies the shrinking of the organisms (Eichinger et al., 2009). In the present model, bacteria may produce DOM during growth as a result of the transformation of reserves into structure, which is directed to the semi-refractory DOM pool. This formulation is in line with experimental evidence showing that bacteria rapidly consume labile DOM as they grow and produce refractory DOM (Ogawa et al., 2001; Kawasaki and Benner, 2006; Jiao et al., 2010). Thus, the growth flux contributes to DOM_R production at a specific rate given by the first term of Eq. (5.41). Moreover, according to Eichinger et al. (2009) the use of structure to cover the maintenance costs results in the production of DOM_R, quantified by the last term of Eq. (5.41). The total excretion rate of inorganic carbon and phosphorus produced during assimilation of DOM and maintenance is given by Eq. (5.42). Finally, Bacterial Growth Efficiency (BGE) is calculated as the ratio between the growth rate ($\dot{r}_B$, Eq. 5.40) and the total labile organic carbon uptake rate (Eq. 5.32), while Bacterial Production (BP) is calculated by multiplying the growth rate ($\dot{r}_B$, Eq. 5.40) with the bacterial structural mass (X_{VB}).

Heterotrophic nanoflagellates

Table 5.4: Equations that describe the physiological processes* occurring in heterotrophic nanoflagellates.

No	Equation	Explanation
5.43	$j_{B,U_H} = j_{B,U_{H_m}} \frac{X_{VB}}{X_{VB}+KH_B}$	Uptake of B
5.44	$j_{B,A_H} = y_H \; y_{B,H} \; n_{C,B} \; j_{B,U_H}$	Carbon assimilation[1]
5.45	$\dot{r}_H = j_{B,A_H} - j_{VH,M_H}$	Net growth rate
5.46	$j_{DOi_L,Ex_H} = (1 - y_{B,H}) \; n_{i,B} \; j_{B,U_H}, \quad i = C, P$	DOM_L excretion[2]
5.47	$j_{IC,Ex_H} = (1 - y_H) \; y_{B,H} \; n_{C,B} \; j_{B,U_H} + j_{VH,M_H}$	IC excretion
5.48	$j_{IP,Ex_H} = (n_{P,B} - n_{P,H} \; n_{C,B} \; y_H) \; y_{B,H} \; j_{B,U_H} + n_{P,VH} \; j_{VH,M_H}$	IP excretion

Physiological processes: U (uptake), A (assimilation), M (maintenance), Ex (excretion)

[1] (1-y_H) is the respired fraction of the assimilated carbon (i.e., costs of phagotrophy).
[2] $n_{i,B} = n_{i,EB} \; m_{EB} + n_{i,VB}$

Heterotrophic nanoflagellates are modelled as V1-morphs using a simplified version of the DEB model, where the reserves are omitted, assuming a large turnover rate, which results in zero reserve capacity (Kooijman et al., 2002). Consequently, the proposed model has only one state variable for heterotrophic nanoflagelates (HNF), the structural biomass VH which implies that HNF have a fixed, Redfield C:P ratio as in (Thingstad, 2005). This assumption is an approximation which is justified from the fact that departures from strict homeostasis and, thus, the variability in the C:P ratio are relatively weak in HNF (Grover and Chrzanowski, 2006). Table 5.4 summarizes the equations describing the metabolic fluxes in heterotrophic nanoflagellates.

Bacteria consumption rate by HNF follows Michaelis-Menten kinetics (Eq. 5.43). The assimilation fluxes of bacterial biomass are obtained by assuming a constant assimilation efficiency of bacterial biomass $y_{B,H}$ (Eq. 5.44). The unassimilated carbon and phosphorus are excreted as DOM_L (Eq. 5.46). The mineralization fluxes for IC and IP are given by Eq. (5.47) and Eq. (5.48), respectively. The first term in Eq. (5.47) corresponds to the respired fraction of bacterial carbon due to assimilation costs, and the second term corresponds to the carbon used for maintenance requirements. In case of stoichiometric imbalance between the requirements of HNF and their prey, HNF mineralize the extra phosphorus obtained from bacterial cells at a rate given by the first term of Eq. (5.48).

Mortality

The present conceptual model focuses on the interactions between nanoflagellates and bacteria, whereas consumers of nanoflagellates are not modelled explicitly. Therefore, the effects of predation on HNF and PNF have to be parameterized. This is done assuming that both groups experience a constant non-grazing mortality rate, which is proportional to structural mass concentration. A second rate which is density-dependent also contributes to total mortality experienced by the nanoflagellates and it is used to implicitly model predation effects of higher trophic levels on nanoflagellates. Consequently, predation-related mortality increases with nanoflagellates structural mass concentration (Guyennon et al., 2015; Kreus et al., 2014; Hasumi and Nagata, 2014). Heterotrophic bacteria can also experience non-predatory mortality. The mortality rates of HNF, PNF, and heterotrophic bacteria are given, respectively, by

$$
\begin{aligned}
j_{VH,D_H} &= h_{H_{di}} + h_{H_{dd}}\, X_{VH} \\
j_{VP,D_P} &= h_{P_{di}} + h_{P_{dd}}\, X_{VP} \\
j_{VB,D_B} &= h_B
\end{aligned}
$$

Organic matter resulting from mortality contributes to dissolved organic matter pools. It is assumed that the reserves of dead PNF and HB cells contribute to the DOM_L, while its structure is added to the DOM_R compartment. For HNF, since there is no distinction between reserves and structure it is assumed that half of the biomass is directed to the DOM_L pool and half to the DOM_R compartment.

5.2.2 Model set-up

The simplified microbial food web was simulated by a zero-dimensional (i.e., homogeneous in space) system which is closed in terms of mass. Light is supplied as an external force and it is supposed to be constant and non-limiting for growth ($I = 100$ µmol phot. m^{-2} s^{-1} for all simulations). This set-up represents the stratified, nutrient-depleted upper layer, which typically occurs during summer-early autumn in the EMS. An initial simulation period of

two years was necessary in order to achieve steady-state conditions. Parameters were chosen so as the steady state community, in terms of biomass concentration, would resemble the one found in the ultra-oligotrophic EMS during stratified conditions. In EMS, depth integrated heterotrophic bacterial biomass has been shown to dominate the microbial biomass, being higher than the biomass of pigmented and heterotrophic nanoflagellates (Christaki et al., 2001), whereas during the stratified season PNF biomass may be higher than HNF biomass (e.g., Christaki et al., 1999). Parameter values are given in Table D1 of Appendix D, in which justification on parameter choices is also provided. It should be emphasized that the model presented here is used to examine in a qualitative way the pathways of carbon and phosphorus transfer through the microbial food web components during P-replete and P-limited conditions. It is beyond the scope of the present study to use the model for a quantitative description of the pathways of carbon and phosphorus in the microbial food web of the EMS, since experimental data sets measuring simultaneously specific physiological rates and variables as well as a full representation of all the components of the microbial food web would be necessary. In order to investigate how the P starved microbial community respond to a P "fertilization event", a 50-fold increase of the steady state concentration of inorganic phosphorus was forced (X_{IP} = 1.7 nM at steady state) and the model run for five more days after this "fertilization event". Model outputs are presented as the average of the last 20 days of the simulation before the P addition (steady-state) and the the average of the 5 days directly after P addition.

5.3 Model simulations

Figure 5.2 shows the biomass concentrations and the carbon to phosphorus (C:P) ratio of PNF, HNF and HB before and after the P addition as well as the C:P ratio of labile DOM (DOM_L). P addition alters both the biomass and the C:P ratio of the modelled organisms, with the most effect on the increase of HB and PNF biomass (Fig. 5.2 a) and the decrease in C:P ratio of PNF; a small decrease in C:P ratio of DOM_L was also observed (Fig. 5.2 b).

In order to investigate how the carbon and phosphate fluxes are altered due to a pulse of inorganic phosphate added to a P-depleted and stratified system Sankey diagrams were used. These diagrams show the fluxes of carbon and phosphorus from the one compartment to the other (state variables of the model) before and after inorganic P addition (Fig. 5.3). In such diagrams, the sources are placed to the left and the sinks are placed to the right, while the width of the line connecting the state variables is proportional to the magnitude of the flux between the two compartments. Accordingly, the width of each line on the left axis shows the relative contribution of each compartment to the C or P fluxes in the system.

Figure 5.3 summarizes the fluxes of matter from one model state variable to the other. Looking at the carbon fluxes (Fig. 5.3 a, b), it is obvious that most of the community respiration (production of IC) is due to bacterial respiration before P addition, whereas, after P addition, PNF contribution to the total community respiration increases. In both

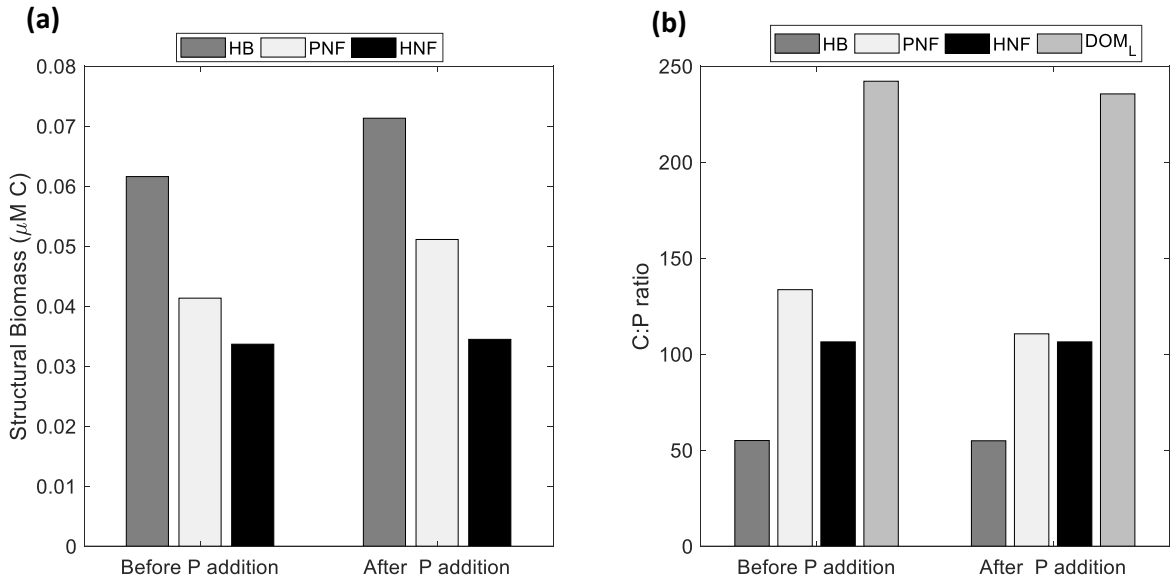

Figure 5.2: (a) Biomass concentrations of heterotrophic bacteria (HB), pigmented nanoflagellates (PNF), heterotrophic nanoflagellates (HNF) and (b) the carbon to phosphorus (C:P) ratio of HB, PNF, HNF and labile DOM (DOM_L) before and after phosphorus (P) addition. Results are presented as the average of the last 20 days of the simulation before P addition (steady-state) and the average of the five days directly after P addition.

conditions, HB and PNF contribute mostly to the total community respiration (production of inorganic carbon (IC)). Regardless of P-availability, PNF and HB mediate most of the C flow through the food web, whereas the role of HNF is limited. Bacterial carbon is equally consumed by HNF and PNF before P addition, whereas, after P addition, HNF are the major consumers of HB carbon. PNF are the major producers of semi-labile DOC (DOC_S) before P addition, however, the allocation of carbon to the semi-labile DOC (DOC_S) compartment by PNF is diminished after P addition and the allocation of carbon to the labile DOC (DOC_L) is slightly enhanced.

In terms of phosphorus fluxes (Fig. 5.3 c, d), HB are responsible for introducing most of the dissolved inorganic phosphorus into the particulate compartment of the microbial food web before P addition and PNF have a minor contribution to the IP uptake flux. After P addition, the role of PNF in the inorganic phosphorus uptake flux is notably enhanced. This is accompanied by a considerable decrease in the bacterial P flux to PNF, as PNF prefer to consume the inorganic P which is now available at high concentrations. Again PNF are the major producers of labile (DOP_L) and semi-labile (DOP_S) DOP, while the allocation of phosphorus to the semi-labile DOP (DOP_S) compartment by PNF is slightly enhanced after P addition. Regardless of P availability, HB are the group mediating most of the P flux through the food web (as shown by the thickness of the corresponding line placed on the left axis), whereas the role of PNF and HNF is comparable. Moreover, HB are mostly

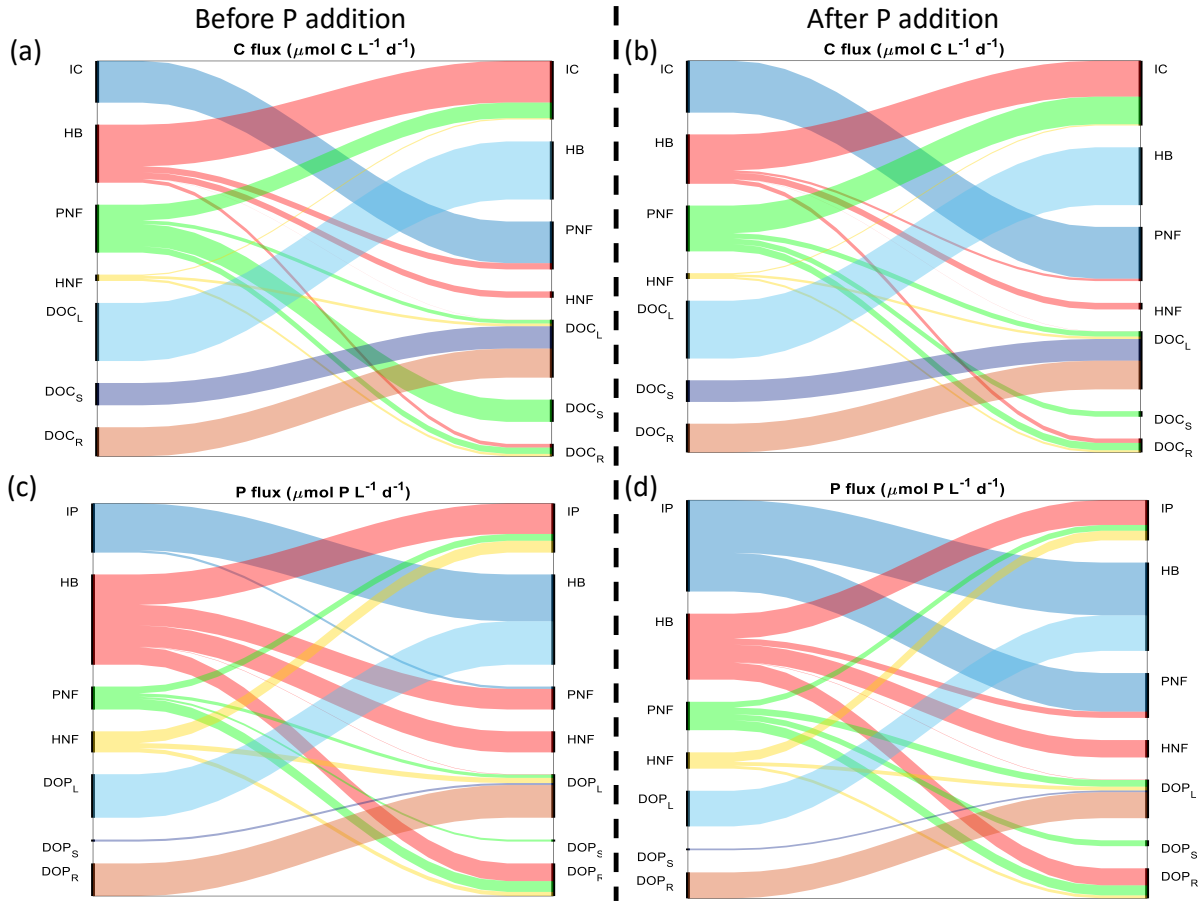

Figure 5.3: Sankey diagrams showing the flow of carbon before (a) and after (b) the simulated phosphorus (P) addition and the flow of phosphorus before (c) and after (d) the simulated P addition, from the one compartment (biotic and abiotic) to the other. Sources are placed to the left and sinks are placed to the right; PNF: pigmented nanoflagellates, HNF: heterotrophic nanoflagellates, HB: heterotrophic bacteria, IC: inorganic carbon, IP: Inorganic phosphorus, DOC_x, DOP_x (x = L (labile), S (semi-labile), R (semi-refractory). Results are presented as the average of the last 20 days of the simulation before P addition (steady-state) and the average of the 5 days directly after P addition.

responsible for P mineralization followed by HNF, whereas the role of PNF as P mineralizers is the less important.

Sankey diagrams were also used to illustrate the effect of P addition in the physiology of the organisms (Fig. 5.4 and 5.6). In these diagrams, inputs are again placed to the left. Metabolic losses due to excretion processes (i.e., respiration/mineralization and exudation) are depicted as arrows with their tip pointing up. The remaining flux available for growth after the metabolic costs have been covered, is depicted with an arrow with its tip pointing to the right. In the following description of model output, the percentage contribution of

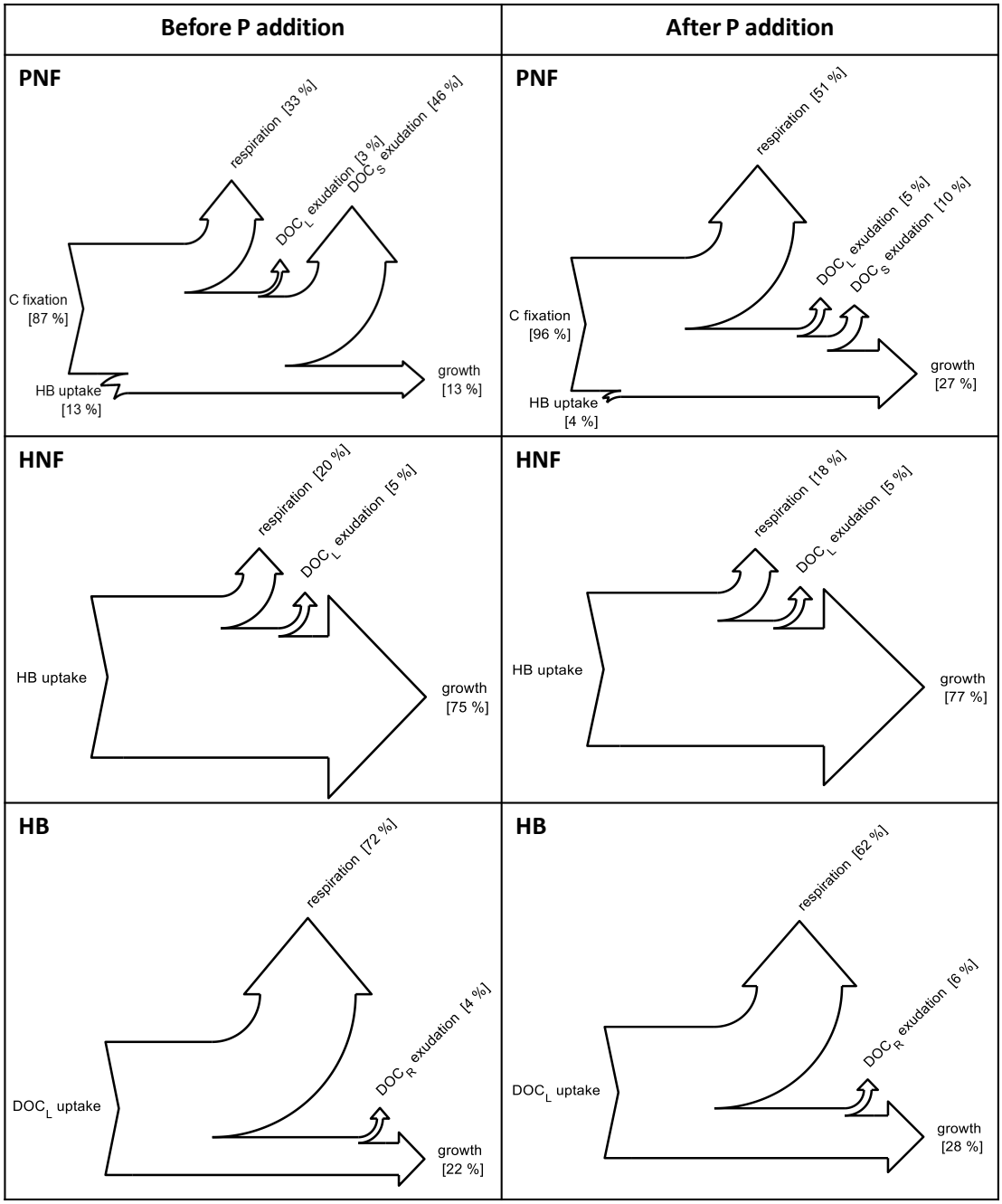

Figure 5.4: Sankey diagrams showing the flow of carbon before and after the simulated phosphorus (P) addition for each group; PNF: pigmented nanoflagellates, HNF: heterotrophic nanoflagellates, HB: heterotrophic bacteria, DOC_i (i = L (Labile), S (Semi-labile), R (Semi-refractory). Results are presented as the average of the last 20 days of the simulation before P addition (steady-state) and the average of the 5 days directly after P addition.

the metabolic processes are reported only to demonstrate the patterns emerged from the simulations. Moreover, it is important to note that the sum of the percentages of loss fluxes do not add up to 100 in PNF and HB. This is due to the presence of reserves in PNF and HB, which means that it is the reserves dynamics and not the assimilation rate that determine the catabolic fluxes that will be used for all the metabolic processes in these organisms.

Fig. 5.4 shows how carbon taken up from the environment is allocated to the different metabolic pathways within the organisms before and after P addition. In PNF (first row in Fig. 5.4), before and after the P-addition, most of the carbon taken up by phytoplankton is through C-fixation during photosynthesis. P addition causes a 3-fold decrease of the relative contribution of bacterial carbon to the total carbon uptake flux in PNF. Before P addition, most of the carbon taken up is exuded as semi-labile DOM, whereas only a small fraction (13% of total C uptake) is allocated to growth in PNF. P addition results in a ca. 2-fold increase in the percentage of assimilated carbon that is allocated to growth. There is also an increase in respiration, which is the result of enhanced growth. Finally, the proportion of carbon that is lost as semi-labile DOC decreases after P-addition. Semi-labile DOC flux is mostly produced due to the active exudation mechanism (Chapter 2, Eq. 2.10). In mixotophic PNF, semi-labile DOC flux has also contributions from the unassimilated bacterial carbon that was consumed by phagotrophy. Therefore, this flux is enhanced when PNF are growing under P-limited conditions, while it is diminished when P-limitation is relaxed.

For HNF (second row in Fig. 5.4), the partitioning of carbon fluxes among the different metabolic processes was not affected importantly by the addition of inorganic P. There was a marginal decrease in the proportion of carbon taken up by HNF that was allocated to respiration and a marginal increase in the proportion of carbon flux allocated to growth. This is due to the fact that maintenance respiration becomes a decreasing fraction of total C utilization as the bacterial carbon uptake flux increases after P addition.

Regarding HB (third row in Fig. 5.4), after P addition, there is a decrease in the proportion of C flux lost through respiration, from 72% to 62%, which is due to the slight decrease in the C:P ratio of labile DOM (DOM_L) (Fig 5.2 b) and mainly due to the increase in the inorganic P that is available for bacterial uptake. This means that the amount of organic carbon that is taken up and has to be respired by HB due to imbalances between the stoichiometry of the substrate (DOM_L) and the requirements of HB, is decreased. This is also obvious by the increase observed in the Bacterial Growth Efficiency (BGE) in the P-replete phase (Fig. 5.5). The relaxation of P-limitation results in an increase in the proportion of C flux allocated to growth (Fig. 5.4) and, subsequently, to an enhanced production of semi-refractory (DOC_R) by HB as a result of enhanced growth.

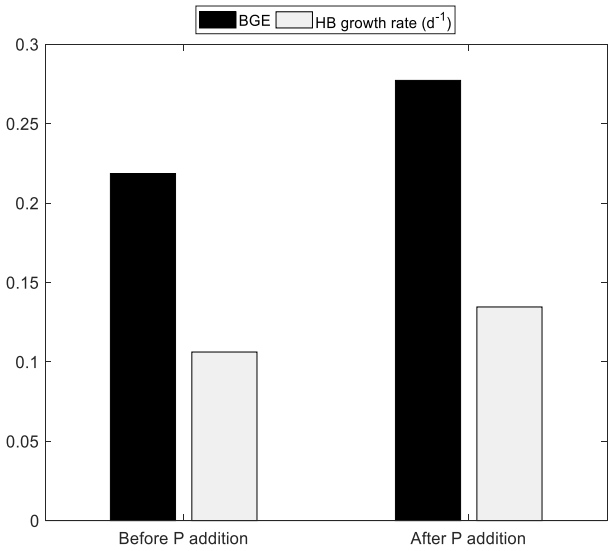

Figure 5.5: Bacterial Growth Efficiency (BGE) and structural mass specific growth rate (r_B (Eq. 5.40)) of heterotrophic bacteria (HB) before and after the simulated phosphorus (P) addition. Results are presented as the average of the last 20 days of the simulation before P addition (steady-state) and the average of the 5 days directly after P addition.

Fig. 5.6 shows how phosphorus taken up from the environment is allocated to the different metabolic pathways within the organisms before and after P addition. During the P-limited phase, PNF (first row in Fig. 5.6) cover most of their phosphorus needs through mixotrophy. The consumption of HB accounts for up to 90% of their total P uptake, whereas only 10% of their P uptake is due to inorganic phosphorus uptake. The opposite is observed during the P-replete phase, where inorganic phosphorus uptake is the dominant pathway of phosphorus acquisition, whereas P uptake due to HB consumption accounts for 14% of the total P uptake flux. In the P-depleted phase most of the P uptake flux is allocated to growth, while maintenance processes consume 30% of P uptake flux. Each of the fluxes of dissolved organic phosphorus release as labile and semi-labile DOM accounts for <10% of the total P uptake flux. During the P-replete phase most of the P taken up is again allocated to growth, however, only 13% of the P taken up is lost through maintenance processes. This is due to the fact that mineralization due to maintenance becomes a decreasing fraction of total P uptake as the P uptake flux is enhanced after P addition. Moreover, there is an increase in the percentage of P lost through exudation of DOP_S. This increase indicates a high catabolic flux from the EP_P-reserve, in surplus of the cell's needs, part of which is excreted in the environment. It should be noted that, in the P-replete phase, the sum of percentages of the consumption fluxes (tips of the arrows on the right side of the figure) deviate from 100. This is the result of luxury consumption of P which is taken up in excess of the immediate cell's needs and it is stored to the E_P-reserves, whereas the catabolic rate determines how much of the P uptake is actually used to cover the metabolic needs of the cell. Luxury consumption is also evident from the decrease in the C:P ratio of PNF after P addition (Fig. 5.2 b).

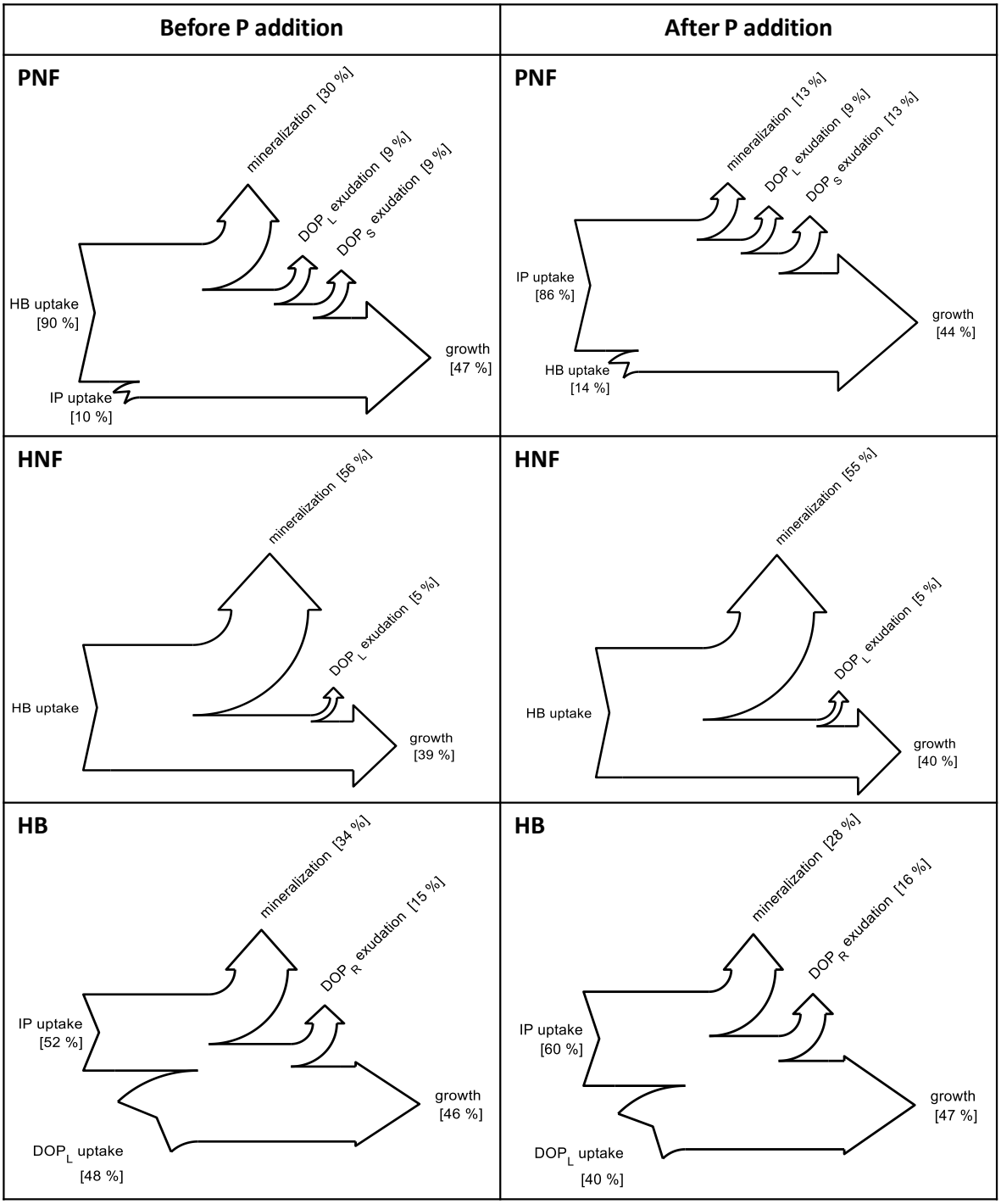

Figure 5.6: Sankey diagrams showing the flow of phosphorus (P) before and after the simulated P addition for each group; PNF: pigmented nanoflagellates, HNF: heterotrophic nanoflagellates, HB: heterotrophic bacteria, DOC_i (i = L (Labile), S (Semi-labile), R (Semi-refractory). Results are presented as the average of the last 20 days of the simulation before P addition (steady-state) and the average of the 5 days directly after P addition.

In HNF (second row in Fig. 5.6), there is no notable change of the partition of P uptake to the different metabolic processes due to P addition. HB (third row in Fig. 5.6) are almost equally depended on the uptake of both labile DOP (DOP_L) and inorganic P to cover their phosphorus needs before P addition. During the P-depleted phase most of the P taken up is allocated to growth (46% of the total P uptake flux), while an important fraction of P (34%) is lost through mineralization. After P addition, most of the P taken up is in the inorganic form, however, labile DOP accounts for a major fraction (40%) of the total P uptake flux. During the P-replete phase, most of P taken up is allocated to growth, whereas there is a decrease in the proportion of P taken up that is lost through mineralization. It should be noted that mineralization of P has inputs from maintenance processes and from the assimilation costs of DOP_L. Both of these processes are not affected by P addition, however, due to the increase in the P uptake rate following P addition (not shown) the proportion of P losses over the total P uptake flux decreases. The mineralization of P as a result of the stoichiometric imbalance between labile DOM taken up and the stoichiometric requirements of HB, which is quantified by the first term of Eq. 5.42, is negative before and after P addition. This means that P is taken up from the environment by HB in order to cover their phosphorus requirements and it is also evident from the C:P ratio in DOM_L, which is always less than the stoichiometric requirements of HB (Fig. 5.2 b). Overall, there are no noteworthy differences due to P addition in the partition of P flux for the different physiological processes of HB. Moreover, an enhanced production of semi-refractory DOP (DOP_R) by HB is observed after P addition, which is the relult of the enhanced HB growth.

In mixotrophic PNF, DOC is released to the environment as a function of C fixation as in all photosynthetic cells (Chapter 2) and also as a function of phagotrophy, since type IIA mixotrophs are unable to use organic carbon from their prey, as they depend on photosynthesis to cover their carbon needs (Chapter 3). This excess carbon is excreted as semi-labile carbon (DOC_S) outside the cells. In that way, PNF redistribute some of the particulate organic C into the labile and semi-labile dissolved organic matter pool, which is again available for bacterial use. Despite the fact that PNF are able to cover some of their P needs through bacterial consumption, this process alone cannot cover their phosphorus requirements because P is scarce in the system. P-limitation is evident by the increased C:P ratio during the P-limited period (Fig. 5.2 b). The increased C:P ratio results in an elevated excretion rate of semi-labile dissolved organic carbon (Fig. 5.7) through the mechanism of active exudation, which is the most important source of dissolved organic carbon for HB in this system (Fig. 5.3a). PNF fuel bacterial production by providing HB with DOC, thus allowing bacteria to acquire inorganic P. During the P-depleted period, PNF are major consumers of bacteria, harvesting almost half of the bacterial production (Fig. 5.8), with bacterial P covering most of the P requirements of PNF (Fig. 5.6). Thus, when P in the system is scarce, bacterial production fuels back primary production. After P addition, the role of PNF as bacterial consumers decreases, while HNF become the dominant bacterial consumers (Fig. 5.8).

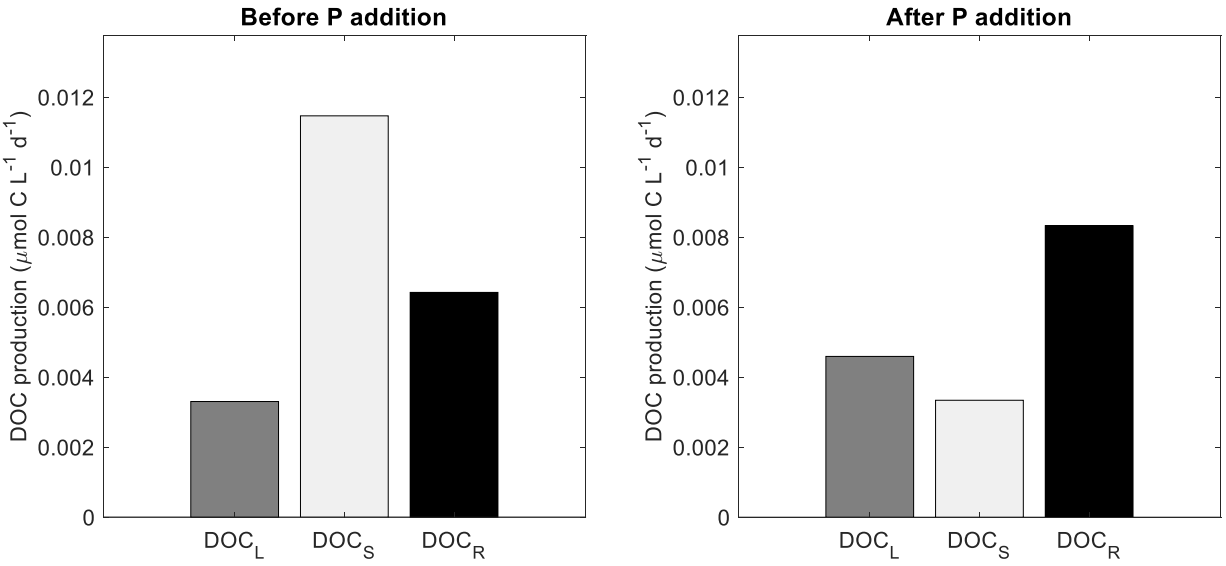

Figure 5.7: Mean rates of labile (DOC_L), semi-labile (DOC_S) and semi-refractory (DOC_R) Dissolved Organic Carbon (DOC) production before and after the simulated phosphorus (P) addition. Results are presented as the average of the last 20 days of the simulation before P addition (steady-state) and the average of the 5 days directly after P addition.

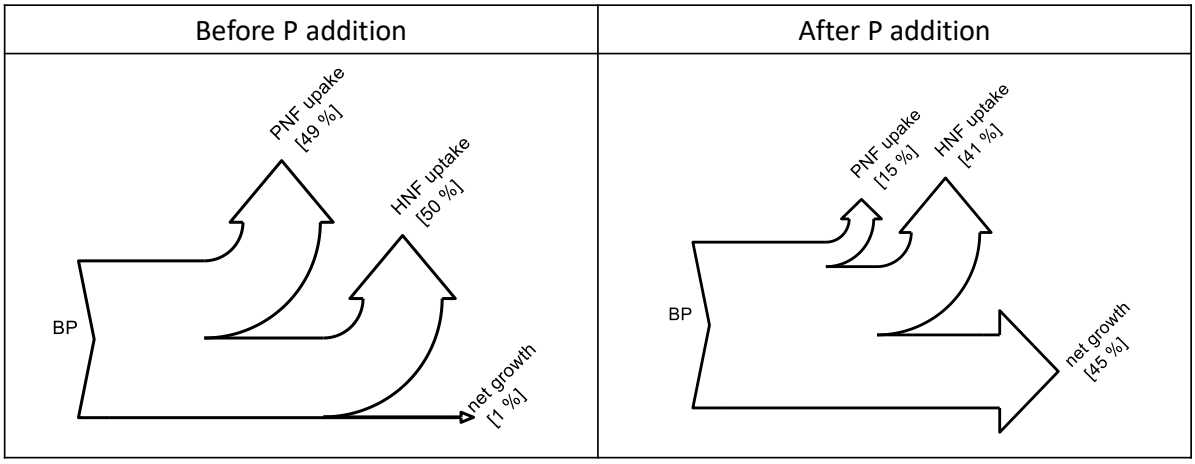

Figure 5.8: Bacterial Production partition between pigmented and heterotrophic nanoflagellates before and after the simulated phosphorus (P) addition. Results are presented as the average of the last 20 days of the simulation before the P addition (steady-state) and the average of the 5 days directly after P addition.

5.4 Discussion and Synthesis

In this chapter, the insights from the theoretical and experimental work presented earlier in this thesis are combined into an idealized, simplified microbial food web model focusing on the bacteria-nanoflagellates interactions. The model is used in a qualitative manner, aiming to demonstrate the effects of two key physiological processes of PNF, these being DOM release (via the passive diffusion and the active exudation mechanism) and mixotrophy, on the pathways of phosphorus and carbon flow through the heterotrophic bacteria-nanoflagellates link of the microbial food web in the EMS. Since the main focus of this theoretical study is the bacteria-nanoflagellates interactions, other groups of the microbial food web such as cyanobacteria (*Synechococcus* and *Prochlorococcus*) and ciliates were not considered. In the following subsections a) the role of pigmented nanoflagellates in controlling bacterial production, b) the role of mixotrophy in supporting primary production of pigmented nanoflagellates, and c) the effect of mixotrophy on phosphorus flux through the microbial food web in the EMS are discussed in a synthesizing context.

5.4.1 The role of pigmented nanoflagellates in controlling bacterial production

In the established microbial loop concept, photosynthetically produced DOM and further released through various processes, such as sloppy feeding, viral lysis and mainly extracellular release by phytoplankton, is fueling bacterial growth. HNF consume bacteria and therefore energy and nutrients are transferred to higher trophic levels via the heterotrophic bacteria - nanoflagellates - microzooplankton link. As a result, the energy and nutrients that could have been lost as dissolved organic matter, are efficiently reintroduced to the microbial food web, supporting the overall productivity of the system. However, it appears paradoxical that in oligotrophic systems where nutrients are scarce, phytoplankton provide organic substrates that fuel bacterial metabolism, while at the same time bacteria compete with phytoplankton for inorganic nutrients (Bratbak and Thingstad, 1985), rather unequally, since bacteria are much more efficient in taking up inorganic nutrients and especially phosphorus (Moutin et al., 2002). It has been suggested that this paradox could be resolved by taking into account the nutrient regeneration by bacterial predators, mainly HNF (Thingstad and Rassoulzadegan, 1995, 1999). These regenerated nutrients are then again available to phytoplankton. However, the presence of mixotrophic PNF in the EMS microbial food web, as it was demonstrated experimentally in Chapter 4, provides a potential answer to this paradox. Simulations of the present model, in accordance with the results from the microcosm experiment reported in Chapter 4, indicate that the significance of PNF as bacterial grazers is nutrient-depended. PNF are major consumers of bacteria under P depleted conditions. However, PNF lower their ingestion rates in response to P enrichment, enhancing the relative importance of bacterial removal by HNF. The results of the present study support the view of PNF "farming" bacteria, as proposed earlier by Thingstad et al. (1996) and Mitra

et al. (2014). In this situation, PNF support bacterial production by providing their surplass of dissolved organic carbon and thus promote the uptake of inorganic phosphorus by HB. At the same time, PNF consume the P-rich bacteria, thus, accessing the scarce inorganic nutrients in a pelleted form (Thingstad et al., 1996; Mitra et al., 2014).

DOM release by PNF, similarly to bacterial consumption, is a nutrient depended physiological process. As shown by the model simulations in the present work, most of the carbon fixed by PNF during periods of low P availability is excreted as semi-labile DOC (DOC_S), mainly through the active exudation mechanism of DOM release. The unassimilated carbon from consumed bacteria is also excreted as semi-labile DOM. This DOC_S released by PNF is the primary source of carbon for bacteria during the P depleted phase, as shown by the food web simulation of the present study (Fig. 5.4 and 5.7). This excreted DOC consists of High Molecular Weight (HMW, >10 kDa) and of complex heteropolyssacharides. Due to its large size, DOC_S produced via the active exudation mechanism by PNF, should be first hydrolyzed to Low Molecular Weigh (LMW) monomers by extracellular enzymes prior to utilization by bacteria (Arnosti, 2011). In the present model, this time-consuming hydrolysis processes is manifested in the arrival rate of DOM_S, which is an order of magnitude lower than the maximum uptake rate of DOM_L (Table D1). As soon as bacteria transform semi-labile DOC_S into labile DOC_L, they have to take up inorganic P in order to use this labile DOC_L, since the C:P ratio in the DOM_L compartment does not match the requirements of heterotrophic bacteria (Fig. 5.2). However, due to the low P availability in the system, bacteria cannot consume efficiently the available DOC_L during the P-depleted phase. Thus, PNF, and phytoplankton in general, use the uncoupling between carbon assimilation and biomass production to their strategic advantage (Berman-Frank and Dubinsky, 1999). PNF are able to maintain their cell homeostasis through regulated excretion under nutrient limited conditions. Regulated excretion by PNF involves complex physiological processes related to the transformation, transport and release of the excreted compounds through the cell membrane (Chin et al., 2004; Borchard and Engel, 2015). It seems that the mechanism of regulated excretion allows photosynthetic cells to alter the chemical properties of the produced DOM, making it less accessible to heterotrophic bacteria (Puddu et al., 2003; Borchard and Engel, 2015). In the end, the excreted molecules of HMW semi-labile DOC, due to their large size and, consequently, their lower diffusion rates, can have a higher residence time in the phycosphere, which is defined as the phytoplanktonic cell surface and the directly surrounding space (Mühlenbruch et al., 2018). This, along with the fact that bacteria have to hydrolyse the HMW compounds before assimilating them, may increase the time that bacteria are staying close to the phycosphere, which allows the phytoplankton cell to benefit from the mineralization of nutrients by bacteria when nutrients are scarce in the system (Seymour et al., 2017; Mühlenbruch et al., 2018). In light of the mixotrophic potential of PNF, another hypothesis is that through regulated excretion of DOM under nutrient limited condition, PNF attract and sustain bacterial cells to their phycosphere, thus, facilitating subsequent consumption of bacteria during mixotrophy. These could be alternative resolutions to the paradoxical situation of nutrient limited PNF, but also of non mixotrophic phytopankton, releasing DOM that supports their competitors' growth.

During the P replete phase, the increase in P availability results in a decrease in the production rate of semi-labile (DOC_S) by PNF and to an increased production of labile DOC (DOC_L). The main source of DOC_L is PNF, through the passive diffusion mechanism of DOM release (Fig. 5.4). As discussed in Chapter 2, this excreted DOM consists of small-sized carbohydrates (<10 kDa) with a molecular composition similar to the cellular material, often with high mole percentages of glucose (Biersmith and Benner, 1998; Borchard and Engel, 2015). Additionally, the simulations of the present model show a slight decrease in the C:P ratio of DOM_L. This DOM is efficiently utilized by bacteria (Hama and Yanagi, 2001; Puddu et al., 2003; Pete et al., 2010; Wear et al., 2015a).

A comparison of the mean Bacterial Growth Efficiency (BGE) and the bacterial growth rate, before and after the P addition shows that BGE and growth rate increase during the P replete phase. These model results support the view that the combination of low biodegradability of semi-labile organic carbon and the low availability of phosphate limits bacterial growth, while the increased production of DOM_L along with the increased availability of inorganic P stimulates bacterial growth as initially proposed by Amon and Benner (1996). These results pinpoint the importance of distinguishing between the fractions of DOM and of accounting for the different mechanisms of DOM release by phytoplankton because these mechanisms have implications for the uptake and use of the produced organic matter by bacteria.

5.4.2 The effect of mixotrophy on the flow of phosphorus through the microbial food web

Up to date, studies trying to resolve the pathways of phosphorus flux through the microbial food web in the P-limited EMS, describe bacteria and phytoplankton as osmotrophs and heterotrophic flagellates and ciliates as phagotrophs, while the role of mixotrophy among PNF has been overlooked (e.g., Thingstad et al., 2005). The results of the present work, however, highlight the role of PNF as a key component of the microbial food web mediating P transfer in the stratified P-depleted surface waters in the EMS.

In an experimental attempt to resolve the pathways of phosphorus flux through the microbial food web, phosphate was added to P-depleted surface waters of the EMS (Krom et al., 2005, CYCLOPS experiment). The results suggested the existence of two, non-mutually exclusive mechanisms that mediate the rapid transfer of P through the microbial food web to copepods. These are the trophic "by-pass" mechanism and the "tunneling" mechanism. As described in Thingstad et al. (2005), in the trophic "by-pass" mechanism, the added phosphate is taken up by heterotrophic bacteria and phytoplankton. However, as heterotrophic bacteria access dissolved organic nitrogen (DON) more efficiently, their production is elevated compared to phytoplankton. Therefore, phosphate stimulated bacterial production is channeled to the food web through an efficient predatory food chain consisting of bacteria-heterotrophic nanoflagellates-ciliates-copepods, by-passing the phytoplankton link. In the "tunneling" mechanism, both bacteria and phytoplankton take up the added phosphate, in

excess of their immediate needs for growth (i.e., luxury consumption) changing their stoichiometry and becoming P-rich food for P-starved grazers, thus stimulating the growth of microzooplankton (Thingstad et al., 2005). Both mechanisms indicate tight predator-prey relationships between the microbial heterotrophs that transfer the limiting element to higher trophic levels efficiently, without obvious biomass oscillations (Tanaka et al., 2007). Indeed, in the EMS, log-log linear regression between bacterial biomass and production suggests that bacteria are top down controlled in the EMS (Siokou-Frangou et al., 2010). Previous studies have shown that HNF grazing is an important source of bacterial mortality, accounting from 45 – 87% of daily bacterial production in an East-West Mediterranean transect (Christaki et al., 2001).

The two proposed mechanisms of P transfer in the EMS, trophic "by-pass" and "tunneling", were inferred based on a strict description of osmotrophs and phagotrophs, which however, could mask the possible effect of mixotrophic pigmented nanoflagellates. The results from both the experiments and the model simulations of the present study, show that, PNF are a relevant and major source of bacterial mortality exerting top-down control on bacteria during periods of low P availability. Thus, under P-limited conditions, PNF contribute to the trophic "by-pass" pathway. The addition of phosphate alters the functioning of the food web and leads to an immediate response of PNF by lowering their ingestion rates and, thus, enhancing the relative contribution of HNF to the trophic "by-pass" pathway. However, the trophic "by-pass" performed by PNF under P-limited conditions would not induce elevated microzooplankton and, consequently, copepod growth as is the case in P replete conditions when the trophic by-pass is mediated by HNF. This is expected because the C:P ratio of PNF remains elevated during the P-depleted phase (Fig. 5.2), since P in the system is limiting. Thus, PNF growing under P-depleted conditions do not, eventually, match the stoichiometric requirements of microzooplankton (Mitra et al., 2014).

5.4.3 The role of mixotrophy in supporting primary production of pigmented nanoflagellates

The 2–5 µm size fraction, mostly comprising PNF, contributes significantly to primary production in the EMS (Ignatiades et al., 2002; Psarra et al., 2005; Varkitzi et al., 2020). However, there seems to be a discrepancy between the contribution of PNF to primary production and their respective inorganic P uptake. For example, PNF were responsible for 45% of total primary production but only for 4% of inorganic P uptake during the CYCLOPS experiment (Flaten et al., 2005). The discrepancy between inorganic C uptake (primary production) rates and inorganic P uptake rates may be better understood considering the importance of P-dependent mixotrophy for the growth of PNF in the EMS, as it was experimentally demonstrated in the present study (Chapter 4).

According to the present model simulations and for the current set of parameter values, during the P-depleted period, 41% of primary production (excluding carbon taken up from bacteria and excreted, data not shown) is released as labile and mostly semi-labile DOC by

PNF mainly via the active exudation mechanism, supporting bacterial production. In turn, almost half of the bacterial production (Fig. 5.8) fuels primary production of PNF in terms of P. These processes can be conceptually described as an alternative microbial loop, in respect to the established paradigm involving heterotrophic bacteria and HNF, where HNF and PNF share the role of bacterial consumers. Such an alternative microbial loop appears as a self-sustaining system which is consistent with the hypothesis of little energy transfer to the higher trophic levels (Turley et al., 2000; Siokou-Frangou et al., 2010) and an efficient internal recycling of organic matter in the EMS (Moutin and Raimbault, 2002). The existence of this "shortcut in the microbial loop" in the EMS, whereby PNF are important consumers of bacteria, has been previously suggested by Ptacnik et al. (2016) who demonstrated that the impact of PNF is light dependent. The present study convincingly demonstrates the existence of the aforementioned shortcut in the microbial loop and provides novel evidence that the impact of PNF on bacteria in the EMS is also P-dependent.

Interestingly, the true importance of mixotrophy would be masked if one looks only at the carbon budget of PNF. According to the results of the field experiments (Chapter 4, Section 4.3), PNF consumed bacterial carbon equivalent to 3.5 – 14.2% of their own carbon content daily. Additionally, model simulations presented in this chapter showed that the contribution of bacterial carbon constitutes only a small fraction of the total C uptake by PNF (13% before P addition and 4% after P addition). The importance of mixotrophic nutrition for PNF in the EMS is evident when looking at the P budget of PNF during the P-depleted period (Fig. 5.6). During this period, according to the present model simulations, most of phosphorus needs of PNF are covered by HB uptake. As soon as P is added to the system, most of the P uptake by PNF is due to inorganic P acquisition rather than HB consumption. This switch, however, is not observed in the C uptake pathways as photosynthesis is the main source of organic carbon acquisition regardless of P availability. This pattern of alternating P acquisition pathways but constant dependence on photosynthetically produced C shown by the present model simulations, may complement the experimental observations of the "NUTRITUNNEL" P-enrichment experiment in the EMS (Pitta et al., 2016). In this experiment nanophytoplankton was found responsible for a significant fraction of total primary production regardless of P availability (65% of the total primary production in the P amended mesocosms and 54% in the control treatment). However, the authors report a significant contribution by nanophytoplankton (>2 μm) to the inorganic P uptake in the P amended treatment, ranging between 33% and 80% of the total inorganic P uptake by osmotrophs. On the other hand, nanophytoplankton contribution in the P uptake in the unperturbed, control treatment was <13%. Thus, in light of the findings of the present study regarding the mixotrophic potential of PNF, the observed patterns may be better understood. Similar discrepancies in the contribution to CO_2 and PO_4 assimilation rates by PNF when compared to photosynthetic prokaryotes, have been reported also in the P-depleted western and central subtropical North Atlantic, where PNF seem to cover most their P requirements through mixotrophy (Hartmann et al., 2012; Duhamel et al., 2019). These observations suggest that the results of the present thesis may be relevant for larger oceanic areas characterized by P-deficiency as in the EMS.

It is worth mentioning that the present model was able to bring out these patterns of photosynthesis depended carbon acquisition and alternating P acquisition pathways due to the mechanistic modelling approach, which was based on SU kinetics and the rules of the sequential - complementary transformation in type IIA mixotrophs (see Chapter 3 and references therein). This pinpoints the importance of differentiating among the various types among PNF since their ecosystem impact, in terms of carbon and phosphorus fluxes, depends on their nutritional strategy, as demonstrated theoretically in Chapter 3. It is suggested that, when possible, the representation of mixotrophy among PNF in the biogeochemical models should be informed by the experimental evidence, as was done in the present study. Finally, it should be noted that the model presented in this chapter accounts only for one limiting nutrient that is phosphorus. This formulation was based on the findings of the field and microcosm experiments presented in Chapter 4, where PNF ingestion rates were correlated with phosphate availability but not with nitrogen availability. Thus, the experimental observations, along with the theoretical simulations of the present study, demonstrate the different fates of bacterial C and P and the importance of multi-element based models for describing the mixotrophic nutrition. It should be noted that when bacteria and protists are co-limited by more than one nutrients, a case that can be frequently observed in the EMS (e.g., Tanaka et al., 2011), mixotrophic nutrition could be more accurately described by multi-element based models, which, however, entail costs in terms of model complexity and computational power.

5.4.4 Future outlook

Disentangling the role of mixotrophic PNF in food web dynamics requires a combination of experimental work, field investigation and theoretical analysis (Thingstad et al., 1996). In this respect, the present study comprises an initial, integrated effort that offers a conceptual framework for the flows of carbon and phosphorus through the heterotrophic bacteria - nanoflagellates link in the EMS. The insights emerged from the theoretical simulations, presented in this chapter, are directly applicable to microcosm experiments. These experiments should be designed in a way that allows to determine which microbial group is doing what and should provide accurate descriptions of the physiological rates (e.g., primary production, grazing, nutrient uptake, growth) of the key components of the microbial food web, these being PNF, HNF and heterotrophic bacteria but also ciliates and cynaobacteria, that were not considered in the present study. Recent advances in flow cytometry cell sorting of samples incubated with stable or radioactive molecules are an appropriate tool for this purpose that have already provided a deeper understanding of physiological rates and processes of the distinct microbial groups (e.g., Zubkov and Tarran, 2008; Lomas et al., 2011; Duhamel et al., 2019). The application of omics tools to elucidate the functional diversity of marine microbes is also a promising approach (Caron et al., 2017). Additionally, the present study demonstrated the implications of the two mechanisms of DOM release for the quality of the produced DOM and its consumption by bacteria. In light of these findings experimental studies should focus on measuring the DOM production rates by the distinct

photosynthetic microbes assemblages (PNF, cyanobacteria) as well as on the molecular and elemental characterization of the produced DOM and its effect on bacterial growth.

The experimental evidence of the present study suggest that PNF in the EMS can be conceptually integrated in biogeochemical models as type IIA mixotrophs, where feeding is initiated in response to nutrient limitation in order to obtain the limiting nutrient. Nevertheless, PNF assemblage in the EMS harbors great functional diversity (Man-Aharonovich et al., 2010) and possibly other mixotrophic types (i.e., type IIB, IIC, IIIA) may be present in the nanoflagellate assemblage of this environment. However, the combined effect of other mixotrophic types in the EMS could be masked by the most abundant type IIA mixotrophs, or the relative abundances of different types of mixotrophs could follow a seasonal pattern, both of which are worthy of further investigation. A promising method to identify the distinct phylogenetic groups of small PNF and their grazing effect on bacteria is the Tyramide Signal Amplification Fluorescence In Situ Hybridization (TSA-FISH) method (Jardillier et al., 2010; Unrein et al., 2014). Combining this technique with FLB grazing experiments is a promising tool for the quantification of the ingestion rates of specific phylogenetic groups among PNF and the identification of environmental factors (i.e., light, prey availability, micro- and macro- nutrients) that potentially regulate the grazing activity of these distinct phylogenetic groups.

It is expected that such a concerted effort, which focuses on the underlying physiological mechanisms, combining various tools and experimental approaches, will generate crucial information on microbial community function and will allow for understanding and predicting the impacts of global environmental change on marine ecosystems.

Chapter 6

Conclusions

Oligotrophic systems comprise 40% of the earth's surface with their area currently expanding (Polovina et al., 2008; Capotondi et al., 2012). Their vast area coverage counterbalances the low primary production of these waters and pinpoints their significant contribution to global primary production and biogeochemical cycles. Most of the energy and nutrient fluxes in these systems are mediated by the microbial food web which comprises a diverse assemblage of photosynthetic organisms and heterotrophs. In order to cope with severe nutrient limitation photosynthetic organisms have developed a series of physiological and ecological adaptations to sustain growth. In the present thesis two aspects of phytoplankton ecophysiology, which are particularly important in oligotrophic aquatic ecosystems, were examined: a) the ability of photosynthetic cells to produce dissolved organic matter of variable quality which may affect bacterial growth and b) the ability of pigmented nanoflagellates to consume bacteria, through mixotrophy. The combination of theoretical and experimental approaches, by using mathematical models as well as field and laboratory experiments, provided in-depth insights on phytoplankton ecophysiology in the ultra-oligotrophic Eastern Mediterranean Sea (EMS).

Two non-mutually exclusive conceptual mechanisms of DOM release by phytoplankton have been proposed, that is passive diffusion and active exudation. In this thesis, a model based on Dynamic Energy Budget (DEB) theory was presented which mechanistically describes the two physiological processes of DOM release under varying inorganic nutrients availability. The two alternative mechanisms of DOM release emerge from the theory; passive diffusion is related to the process of phytoplankton growth and lysis of the cells and active exudation is related to the excretion of the non-limiting compound. According to the model output, their relative importance depends on the nutrient-status of the cells. The presented model for photosynthetic growth links phytoplankton physiology to the composition and subsequent bacterial utilization of photosynthetically-derived DOM. Thus, the present study contributes towards understanding the patterns of DOM fluxes in marine oligotrophic ecosystems and the interlinked relationship between phytoplankton as producers of DOM and bacteria as consumers of DOM.

Pigmented nanoflagellates (PNF) comprise a diverse assemblage with a whole range of photosynthetic and feeding potential and with various metabolic responses to environmental drivers, such as light, nutrients and prey availability. In the present study, a mathematical framework was developed for the distinct functional responses of four types of PNF, taking into account the dynamic interaction of phototrophy and phagotrophy. This study highlights the dependence of the net ecosystem role of PNF, as producers or consumers, on the mixotrophic strategy and also on the prevailing environmental conditions. From the results presented in this work, it is obvious that the response of food web dynamics and flow of elements to changing environmental conditions will depend, among others, on the prevailing mixotrophic assemblage. However, spatiotemporal variations of mixotrophic strategies remain largely unresolved to date (Leles et al., 2019; Wilken et al., 2019). Thus, the present work highlights the importance of differentiating among the four nutritional strategies observed in PNF in field and modelling studies in order to adequately describe carbon and nutrient fluxes in aquatic systems. The general mathematical framework offered by this study can be used to integrate the functional diversity of PNF in aquatic ecosystems models.

The experimental work conducted in this study combined both field and laboratory grazing experiments aiming to quantify the importance of PNF among the nanoflagellates assemblage as consumers of bacteria in the EMS. During the field experiments PNF were found to be the dominant grazers of prokaryotic picoplankton in the vicinity of the deep chlorophyll maximum layer, along a longitudinal transect in the NW Levantine (EMS). A negative relationship between phosphate concentration and ingestion rate of PNF on prokaryotic picoplankton was observed suggesting that phosphorus availability regulates the ingestion rates of PNF in the EMS. Subsequent microcosm experiments with nutrient depleted water from the Cretan Sea (EMS), during the late stratified season, confirmed the observation from field experiments. The results showed that PNF responded immediately to P addition by lowering their ingestion rate, whereas P availability had no regulating effect upon the ingestion rates of HNF. On the other hand, PNF dominated bacterivory in the unperturbed, P-depleted bottles (control), whereas, in the P amended treatment HNF and PNF contributed equally to total bacterivory. The results obtained through the series of nanoflagellates grazing experiments pinpoint the importance of mixotrophy as a trophic mode for PNF in the ultra-oligotrophic P-limited EMS. This study emphasizes the major role of PNF as consumers of bacteria under P-depleted conditions and reveals that the functional role of PNF as bacteria consumers in the EMS is not fixed, but it depends on P availability. Thus, in response to phosphorus enrichment PNF lower their ingestion rates, enhancing the relative importance of bacterial removal by HNF.

The combination of theoretical simulations and experimental observations suggest complex interactions between PNF and bacteria in the oligotrophic EMS. Under P-limited conditions, PNF support bacterial production as they provide their surplus of energy as dissolved organic carbon to heterotrophic bacteria and, thus, promoting the uptake of inorganic phosphorus by heterotrophic bacteria. At the same time, PNF consume the P-rich bacteria, thus, accessing the scarce inorganic nutrients in a pelleted form which resembles a situation where

PNF are "farming" the bacteria (Thingstad et al., 1996; Mitra et al., 2014). Moreover, the DOM that PNF produce under P-limited conditions originates from the active exudation mechanism. The DOM produced by this mechanism is less efficiently utilized by bacteria, due to its chemical properties and its stoichiometry. The aforementioned interactions change as soon as P is added to the system. PNF respond to the increase in phosphate concentration by lowering their ingestion rates, while most of the DOM produced is labile, since the passive diffusion mechanism mediates most of DOM release. This DOM supports higher rates of bacterial production. The results of the present study further suggest alternating pathways of P transfer through the microbial food web components during P-replete and P-limited conditions. Pigmented nanoflagellates hold a key role in the trophic "by-pass" *sensu* Thingstad et al. (2005) under P-limited conditions, whereas the role of heterotrophic nanoflagellates in this pathway becomes more prominent under P-replete conditions.

In conclusion, the phosphorus driven trophic and physiological shifts of resource uptake pathways, through osmotrophy or phagotrophy, as well as in excretion processes of dissolved organic matter, cause significant alterations on the flow of carbon and nutrients through the microbial food web. Particularly, in the EMS with its pulsed nutrient inputs either from the Saharan dust storms or from the vertical exchange of water masses at mesoscale structures comprising numerous semi-permanent eddies of the EMS, such shifts may have important implications for food web dynamics and ecosystem functioning. The present study supports the existence of a self-sustaining system during P-depleted periods in the EMS, which consists of heterotrophic bacteria and PNF. This system can be conceptually described as an alternative microbial loop, in respect to the established paradigm involving HNF as the consumers of heterotrophic bacteria. In this alternative microbial loop, PNF have the functional role of primary producers of DOM and, at the same time, share with HNF the functional role of bacterial consumers. The present thesis demonstrates that this "shortcut in the microbial loop", and accordingly, the impact of PNF on bacteria in the EMS is phosphorus-dependent in addition to being light-dependent, as suggested by Ptacnik et al. (2016). The conceptual framework presented here may be of use for the configuration of the pigmented nanoflagellates-bacteria interactions in the existing biogeochemical model for the EMS (Petihakis et al., 2009; Tsiaras et al., 2017; Petihakis et al., 2018). Moreover, the findings of the present study may be also relevant for the functioning of other oligotrophic systems with similar characteristics such as the P-depleted western subtropical North Atlantic (Duhamel et al., 2019). Finally, the present study pinpoints the importance of accounting for the highly flexible and adaptive physiology of photosynthetic protists in biogeochemical models in order to understand the functioning of oligotrophic systems and to predict their response to global environmental changes.

Appendices

Appendix A

Supplementary information for Chapter 2

The parameter ρ_L

This section gives some background to the approach taken to model the effects of cellular nitrogen content on photosynthesis. The parameter ρ_L is the binding probability of photons that will serve the linear electron flow (LEF) and provide reductant for inorganic carbon fixation. ρ_L can be described by the relationship: $\rho_L = \alpha F_v/F_m$, where F_v/F_m is the maximum quantum yield of PSII and α is the allocation coefficient of excitation energy to LEF (Papadakis et al., 2012). F_v/F_m is reduced under nitrogen starvation (Kamalanathan et al., 2016; Parkhill et al., 2001) as the machinery of light reactions (chloroplasts) is protein-based and therefore nitrogen-rich (Bonachela et al., 2013). In addition, in response to nitrogen starvation, part of the energy from PSII, maybe allocated to other energy quenching processes such as the cyclic electron flow (CEF) that do not involve carbon fixation (Berges et al., 1996). However, experimental evidence suggests that under nitrogen-limiting conditions photosynthesis, although reduced, is sustained at positive values (Granum et al., 2002; Kamalanathan et al., 2016). Thus, a sigmoid function can be used to describe a smooth decrease from a maximum to minimum value in relation to the N-status of the cells. One way to mathematically describe ρ_L as a function of the N-status of the cells, q_N, via a sigmoid function is

$$\rho_L = \rho_{L_{max}} - (\rho_{L_{max}} - \rho_{L_{min}})e^{-bq_N^2} \tag{A.1}$$

where $q_N = \frac{n_{N,E}M_E + M_{E_N}}{n_{N,V}M_V}$ is the nitrogen content in the reserves relative to structure. The maximum value $\rho_{L_{max}}$ can be approximated by the maximum quantum yield of PSII (F_v/F_m) assuming photoinhibition is minimum and all the excitation energy is allocated to LEF (i.e., $\alpha = 1$). Thus, the value for $\rho_{L_{max}}$ was taken from Parkhill et al. (2001), who found that nitrogen-replete cultures of *Thalassiosira pseudonana* had consistently F_v/F_m of 0.65. The

minimum value, $\rho_{L_{min}}$, was inferred by fitting the model to the experimental data. The parameter b is a dimensionless nonnegative constant that controls the shape of the function.

Calculation of $y_{L,C}$

The stoichiometric coefficient $y_{L,C}$ that denotes the moles of photons required per mole of organic carbon produced was calculated as follows: 0.2 mol NADPH are evolved per mol photons absorbed (Lika and Papadakis, 2009), thus 5 photons are required per mol of NADPH. From the Calvin-Benson cycle stoichiometry 2 moles of NADPH are required per mole of inorganic carbon fixed, thus $y_{L,C} = 10$ mol photons (mol C)$^{-1}$.

Calculation of n_{NV}

The stoichiometric coefficient of biomass was calculated from biomass parameter values taken from Gallager and Mann (1981), assuming that under low light and nutrient conditions the reserves should be at minimum and thus elemental composition of cells should be representative of structural mass. Therefore the minimum values of 5.1 pg C cell^{-1} and 0.47 pg N cell^{-1} (Table 1 in (Gallager and Mann, 1981)) where used to calculate n_{NV}. The stoichiometric coefficient of generalized reserves, n_{NE}, was also assumed to be equal to n_{NV}.

Reserve formation for two limiting inorganic nutrients

In this transformation, using SU dynamics, nitrogen (N), phosphorus (P) and Carbon, (C) are complementary substrates and their binding to the SU is parallel. According to (Kooijman, 2010), the specific assimilation flux of generalized reserves, E and E' is

$$j_{E,A} = \Big((j_{E,A_m})^{-1} + j_{C,A}^{'-1} + j_{N,A}^{'-1} + j_{P,A}^{'-1} - (j_{C,A}^{'} + j_{N,A}^{'})^{-1} - (j_{C,A}^{'} + j_{P,A}^{'})^{-1} - (j_{P,A}^{'} + j_{N,A}^{'})^{-1} + (j_{C,A}^{'} + j_{N,A}^{'} + j_{P,A}^{'})^{-1} \Big)^{-1} \tag{A.2}$$

where $j_{i,A}^{'} = \rho_i j_{i,A}/y_{i,E}$ denotes the specific arrival rate of substrate i (C, N, P), ρ_i its binding probability to the SU, and $y_{i,E}$ the yield coefficient that represents the mole of the compound i required to form one mole of the generalized reserves, E. j_{E,A_m} denotes the structure-specific maximum assimilation rate of generalized reserves.

Table A1: Table of parameter values.

Symbol	Value	Units	Source
L	100	μmol photons m^{-2} s^{-1}	Assumed
$\rho_{L_{max}}$	0.650	–	Parkhill et al. (2001)
$\rho_{L_{min}}$	0.024	–	Estimated
b	2.84	–	Estimated
α_L	6×10^{-6}	m^2 (μmol C)$^{-1}$	Lika and Papadakis (2009)
$\dot{h}$	0.01	d^{-1}	Assumed
K_{IC}	233	μ M	Clark and Flynn (2000)
K_N	0.4	μ M	Eppley et al. (1969)
$j_{IC,A_m} = j_{C,A_m} = j_{E,A_m}$	5.1	mol C (mol C)$^{-1}$ d^{-1}	Geider et al. (1998)
j_{N,A_m}	0.14	mol N (mol C)$^{-1}$ d^{-1}	Estimated
$k_E = k_{E_C} = k_{E_N}$	1.96	d^{-1}	Estimated
$j_{E,M}$	0.01	d^{-1}	Geider and Osborne (1989)
$y_{L,C}$	10	mol photons (mol C)$^{-1}$)	Calculated*
$y_{IC,C}$	1	mol IC (mol C)$^{-1}$	
$y_{C,E}$	1.32	mol C (mol C)$^{-1}$	Geider and Osborne (1989)
$n_{C,V} = n_{C,E}$	1	mol C (mol C)$^{-1}$	
$y_{N,E} = n_{N,E} = n_{N,V}$	0.079	mol N (mol C)$^{-1}$	Gallager and Mann (1981)
$y_{E,V}$	1.20	mol C (mol C)$^{-1}$	Estimated
κ_{E_C}	0.95	d^{-1}	Assumed
κ_{E_N}	0.95	d^{-1}	Assumed

Appendix B

Supplementary information for Chapter 3

Derivation of the four models of mixotrophy

This appendix provides the derivation of the mathematical models for the four different types of mixotrophic nutrition of PNF. The uptake rates of inorganic carbon, inorganic nutrients, N, and prey, F, follow classic Michaelis-Menten kinetics given by

$$j_i = j_{i,A_m} \frac{X_i}{X_i + K_i}, \quad (i = IC, N, F) \tag{B.1}$$

where j_{i,A_m} is the maximum uptake rate of substrate i, X_i denotes the concentration of substrate i and K_i is the half-saturation constant. PNF have a photosynthetic system with which they stepwise convert light (L) and inorganic carbon (IC) into organic carbon (C). Photons arrive at photosynthetic units (PSUs) at a rate proportional to incident light intensity and bind to PSUs with a probability ρ_L. The specific photons' arrival rate is

$$j_L = \alpha_L L \tag{B.2}$$

with α_L the specific photons arrival cross section. All fluxes of substrates are expressed as specific fluxes (i.e., per unit of structural mass) and denoted as j_*.

Next we focus on the formalism for the mechanisms of SUs processing resources acquired via phototrophy and phagotrophy. To simplify the notation, the rate at which substrate molecules, say of type A, arrive and bind to the SU is scaled to the number of molecules, y_{AP}, required to produce one molecule of product P, i.e., $j'_A = \rho_A j_A / y_{AP}$ where ρ_A is the probability that molecules of substrate A bind to the SU.

Type IIA

Type IIA PNF are primary phototrophic but consume prey to obtain limiting inorganic nutrients. In these PNF, first light and inorganic carbon, are processed by the SU_C (Fig. 3.1) to produce organic carbon in a complementary and parallel transformation meaning that both substrates are required to form the product and that the binding of one substrate to the SU is independent from the binding of the other (see for example Lika and Papadakis (2009) and Chapter 2). Thus, the specific organic carbon production rate is given by

$$j_C = \left(\dot{k}_C^{-1} + j_{IC}'^{-1} + j_L'^{-1} - (j_{IC}' + j_L')^{-1}\right)^{-1} \tag{B.3}$$

In type IIA transformation (Fig. 3.2a), the possible states of the SUs are five: $\theta_{..}$, $\theta_{C.}$, $\theta_{.N}$, θ_{CN}, and θ_{CF}. A free SU ($\theta_{..}$) may bind the organic carbon from photosynthesis, C, or inorganic nutrient, N, giving the states $\theta_{C.}$ or $\theta_{.N}$, respectively; the dot means absence of substrate. These SUs may bind the absent substrate, giving the state θ_{CN}, to form reserves and then return to the state $\theta_{..}$. An SU at the state $\theta_{C.}$ may also bind nutrients obtained from phagotrophy, giving the state θ_{CF} which either return to the state $\theta_{..}$ by forming the product E or may reject the substrate from phagotrophy if an inorganic nutrient molecule arrives resulting to the state θ_{CN}. The dynamics of the SU fractions are given by the following system of differential equations

$$\begin{aligned}
&\frac{d}{dt}\theta_{..} = -(j_N' + j_C')\theta_{..} + \dot{k}_{CN}\theta_{CN} + \dot{k}_{CF}\theta_{CF}\\
&\frac{d}{dt}\theta_{.N} = j_N'\theta_{..} - j_C'\theta_{.N}\\
&\frac{d}{dt}\theta_{C.} = j_C'\theta_{..} - (j_N' + j_F')\theta_{C.}\\
&\frac{d}{dt}\theta_{CN} = j_C'\theta_{.N} + j_N'(\theta_{C.} + \theta_{CF}) - \dot{k}_{CN}\theta_{CN}\\
&\frac{d}{dt}\theta_{CF} = j_F'\theta_{C.} - (j_N' + \dot{k}_{CF})\theta_{CF}\\
&\theta_{..} + \theta_{C.} + \theta_{.N} + \theta_{CN} + \theta_{CF} = 1
\end{aligned} \tag{B.4}$$

where $\dot{k}_{CN}$ and $\dot{k}_{CF}$ are the handling rates of the substrates and j_C', j_N' and j_F' are the scaled specific arrival fluxes of photosynthetically produced organic carbon, inorganic nutrients and prey ($j_\star' = \rho_\star j_\star / y_\star$). j_N and j_F are given by Eq. (B.1).

If we assume quasi steady-state, we can solve the system (B.4) to obtain the quasi steady-

state solution of the fraction of SUs at different states

$$\begin{aligned}
\hat{\theta}_{..} &= \left(\frac{j'_N}{j'_C} + \left(1 + \frac{j'_N}{\dot{k}_{CN}}\right)\left(1 + \frac{j'_C}{j'_N + j'_F}(1 + \frac{j'_F}{j'_N + \dot{k}_{CF}})\right)\right)^{-1} \\
\hat{\theta}_{.N} &= \frac{j'_N}{j'_C}\hat{\theta}_{..} \\
\hat{\theta}_{C.} &= \frac{j'_C}{j'_N + j'_F}\hat{\theta}_{..} \\
\hat{\theta}_{CN} &= \frac{j'_N}{\dot{k}_{CN}}\left(1 + \frac{j'_C}{j'_N + j'_F}(1 + \frac{j'_F}{j'_N + \dot{k}_{CF}})\right)\hat{\theta}_{..} \\
\hat{\theta}_{CF} &= \frac{j'_F}{j'_N + \dot{k}_{CF}}\frac{j'_C}{j'_N + j'_F}\theta_{..}
\end{aligned} \tag{B.5}$$

The rate of reserve assimilation $j_{E,A}$ consists of two terms representing the two routes of reserve formation

$$j_{E,A} = \dot{k}_{CN}\hat{\theta}_{CN} + \dot{k}_{CF}\hat{\theta}_{CF} \tag{B.6}$$

The organic carbon from photosynthesis and the nutrients obtained from prey are processed sequentially (Brandt et al., 2003), meaning that phagotrophy cannot proceed without photosynthesis.

In the absence of prey (i.e., $j'_F = 0$), Eq. (B.6) takes the form

$$j_{E,A} = \left(\dot{k}_{CN}^{-1} + j_C'^{-1} + j_N'^{-1} - (j'_C + j'_N)^{-1}\right)^{-1}$$

which is equivalent to reserve formation of a phototroph (see Chapter 2, Eq. 2.6). This corresponds to a complementary and parallel transformation (Brandt et al., 2003) of the two substrates, the photosynthetically produced organic carbon and the inorganic nutrient. On the other extreme, in the absence of inorganic nutrient (i.e., $j'_N = 0$), the rate of reserve assimilation Eq. (B.6) reduces to

$$j_{E,A} = \left(\dot{k}_{CF}^{-1} + j_C'^{-1} + j_F'^{-1}\right)^{-1}$$

Type IIB

In type IIB mixotrophy, phagotrophy complements required organic compounds necessary for growth. In this type of transformation both phototrophy and phagotrophy are required to form organic carbon (Fig. 3.2b, left). The possible states of the SUs are: $\theta_{..}$, $\theta_{C_s.}$ and θ_{C_sF}. A free SU ($\theta_{..}$) binds arriving molecules from an intermediate product, C_s, formed during photosynthesis, combining light and inorganic carbon, arriving at the state $\theta_{C_s.}$. Subsequently, it binds the complementary growth factor from phagotrophy arriving at state

θ_{C_sF}. An SU at the state θ_{C_sF} returns to the state $\theta_{..}$ by forming organic carbon C. The dynamics of the fraction of the SUs at the different states are given by

$$\begin{aligned}
\frac{d}{dt}\theta_{..} &= -j'_{C_s}\theta_{..} + \dot{k}_{C_sF}\theta_{C_sF} \\
\frac{d}{dt}\theta_{C_s.} &= j'_{C_s}\theta_{..} - j'_F\theta_{C_s.} \\
\frac{d}{dt}\theta_{C_sF} &= j'_F\theta_{C_s.} - \dot{k}_{C_sF}\theta_{C_sF} \\
\theta_{..} + \theta_{C_s.} + \theta_{C_sF} &= 1
\end{aligned} \tag{B.7}$$

where $j'_\star = \rho_\star j_\star / y_\star$ are the scaled specific arrival fluxes (j_{C_s} is given by Eq. (B.3) with $\dot{k}_C = 0$ and j_F is given by Eq. (B.1)) and $\dot{k}_{C_sF}$ is the handling rate of the substrates.

As in type IIA, we assume quasi steady-state to obtain the quasi steady-state solution of the fraction of SUs at different states

$$\begin{aligned}
\hat{\theta}_{..} &= j'^{-1}_{C_s}\left(\dot{k}^{-1}_{C_sF} + j'^{-1}_{C_s} + j'^{-1}_F\right)^{-1} \\
\hat{\theta}_{C_s.} &= j'^{-1}_F\left(\dot{k}^{-1}_{C_sF} + j'^{-1}_{C_s} + j'^{-1}_F\right)^{-1} \\
\hat{\theta}_{C_sF} &= \dot{k}^{-1}_{C_sF}\left(\dot{k}^{-1}_{C_sF} + j'^{-1}_{C_s} + j'^{-1}_F\right)^{-1}
\end{aligned} \tag{B.8}$$

The rate of organic carbon assimilation is $j_C = \dot{k}_{C_sF}\hat{\theta}_{C_sF}$, i.e.,

$$j_C = \left(\dot{k}^{-1}_{C_sF} + j'^{-1}_{C_s} + j'^{-1}_F\right)^{-1} \tag{B.9}$$

Consequently, the organic carbon (C) in combination with both inorganic nutrients and nutrients obtained from prey (N) will form the generalized reserves (E), in a complementary and parallel transformation (Fig. 3.2b, right). For this transformation the possible states of the SUs are: $\theta_{..}$, $\theta_{C.}$, $\theta_{.N}$ and θ_{CN}. Following the same steps as above (see Lika and Papadakis (2009) for details), we derive the rate of E-reserves formation given by

$$j_{E,A} = \left(\dot{k}^{-1}_{CN} + j'^{-1}_C + j'^{-1}_N - (j'_C + j'_N)^{-1}\right)^{-1} \tag{B.10}$$

The nutrient flux j_N is given by

$$j_N = j_{N,A_m}\frac{X_N}{X_N + K_N} + n_{NF}y_{FC}j_C \tag{B.11}$$

where the first term corresponds to the inorganic nutrients flux taken up from the environment (as in Eq.(B.1)) and the second term corresponds to the nutrients assimilated from the consumed prey with j_C given by Eq. (B.9).

Type IIC

In type IIC mixotrophy, phototrophy is the dominant mode of nutrition, while phagotrophy is initiated in response to light limitation as a strategy to obtain energy and carbon (Fig. 3.1c). In this type of transformation the possible states of the SUs are: $\theta_{..}$, $\theta_{C_s.}$ and $\theta_{.F}$. A free SU ($\theta_{..}$) may bind the intermediate substance C_s or the substrate F giving the states $\theta_{C_s.}$ or $\theta_{.F}$, respectively. A SU at the state $\theta_{.F}$ may either return to the state $\theta_{..}$ by forming the product E or may reject the substrate from phagotrophy in favor of C_s and return to the state $\theta_{C_s.}$. A SU at the state $\theta_{C_s.}$ returns to the state $\theta_{..}$ by handling the substrate C_s and producing organic carbon C. The dynamics of the fraction of the SUs at the different states are given by

$$\begin{aligned}
&\frac{d}{dt}\theta_{..} = -(j'_{C_s} + j'_F)\theta_{..} + \dot{k}_C\theta_{C_s.} + \dot{k}_F\theta_{.F} \\
&\frac{d}{dt}\theta_{C_s.} = j'_{C_s}\theta_{..} - \dot{k}_C\theta_{C_s.} + j'_{C_s}\theta_{.F} \\
&\frac{d}{dt}\theta_{.F} = j'_F\theta_{..} - (\dot{k}_F + j'_{C_s})\theta_{.F} \\
&\theta_{..} + \theta_{C_s.} + \theta_{.F} = 1
\end{aligned} \tag{B.12}$$

where $j'_\star = \rho_\star j_\star / y_\star$ are the scaled arrival fluxes: j_{C_s} is given by Eq. (B.3) with $\dot{k}_C = 0$ and j_F by Eq. (B.1). $\dot{k}_C$, $\dot{k}_F$ are the handling rates of the substrates.

Consequently, the quasi steady-state solution of the fraction of SUs at different states are

$$\begin{aligned}
&\hat{\theta}_{..} = \dot{k}_C(\dot{k}_F + j'_{C_s}) \left((\dot{k}_F + j'_{C_s} + j'_F)(\dot{k}_C + j'_{C_s})\right)^{-1} \\
&\hat{\theta}_{C_s.} = j'_{C_s} \left(\dot{k}_C + j'_{C_s}\right)^{-1} \\
&\hat{\theta}_{.F} = \dot{k}_C j'_F \left(\dot{k}_C + j'_{C_s}\right)^{-1} \left(\dot{k}_F + j'_{C_s} + j'_F\right)^{-1}
\end{aligned} \tag{B.13}$$

The rate of E-reserve formation via the phagotrophic pathway is $j_{EA}^{phago} = \dot{k}_F\hat{\theta}_{.F}$, i.e.,

$$j_{E,A}^{phago} = (\dot{k}_F\dot{k}_C j'_F) \left((\dot{k}_F + j'_{C_s} + j'_F)(\dot{k}_C + j'_{C_s})\right)^{-1} \tag{B.14}$$

The rate of organic carbon assimilation is

$$j_C = \dot{k}_C\hat{\theta}_{C_s.} = (\dot{k}_C^{-1} + j'^{-1}_{C_s})^{-1} = \left(\dot{k}_C^{-1} + j'^{-1}_{IC} + j'^{-1}_L - (j'_{IC} + j'_L)^{-1}\right)^{-1} \tag{B.15}$$

(as in Eq. (B.3)). In the next step, the organic carbon in combination with inorganic nutrients will form the generalized reserves E, in a complementary and parallel transformation

(Fig. 3.2c, right). As in type IIB, the rate of E-reserves formation via the phototrophic pathway is

$$j_{E,A}^{photo} = \left(\dot{k}_{CN}^{-1} + j_C'^{-1} + j_N'^{-1} - (j_C' + j_N')^{-1}\right)^{-1} \tag{B.16}$$

with j_N given by Eq. (B.1). Finally, the two pathways combined produce E-reserves at a rate

$$j_{E,A} = j_{EA}^{photo} + j_{E,A}^{phago} \tag{B.17}$$

Type IIIA

In type IIIA mixotrophy, phototrophy is initiated when prey is limiting (Fig. 3.1d). In this type of transformation the possible states of the SUs are: $\theta_{\cdot}$, θ_{C_s} and θ_F. Thus, a free SU ($\theta_{\cdot}$) may bind the intermediate substance C_s or the substrate F giving the states θ_{C_s} or θ_F, respectively. A SU at the state θ_{C_s} may either return to the state $\theta_{\cdot}$ by handling the intermediate product C_s and producing organic carbon C or may reject the substrate C_s in favor of the substrate F and go to the state θ_F. A SU at the state θ_F returns to the state $\theta_{\cdot}$ by forming the product E. The dynamics of the fraction of the SUs at the different states are given by

$$\begin{aligned}
&\frac{d}{dt}\theta_{\cdot\cdot} = -(j_{C_s}' + j_F')\theta_{\cdot\cdot} + \dot{k}_C\theta_{C_s\cdot} + \dot{k}_F\theta_{\cdot F} \\
&\frac{d}{dt}\theta_{C_s\cdot} = j_{C_s}'\theta_{\cdot\cdot} - (\dot{k}_C + j_F')\theta_{C_s\cdot} \\
&\frac{d}{dt}\theta_{\cdot F} = j_F'\theta_{\cdot\cdot} - \dot{k}_F\theta_{\cdot F} + j_F'\theta_{C_s\cdot} \\
&\theta_{\cdot\cdot} + \theta_{C_s\cdot} + \theta_{F\cdot} = 1
\end{aligned} \tag{B.18}$$

where $j_\star' = \rho_\star j_\star / y_\star$ are the scaled arrival fluxes: j_{C_s} is given by Eq. (B.3) with $\dot{k}_C = 0$ and j_F by Eq. (B.1). $\dot{k}_C$, $\dot{k}_F$ are the handling rates of the substrates.

Consequently, the quasi steady-state solution of the fraction of SUs at different states are

$$\begin{aligned}
&\hat{\theta}_{\cdot\cdot} = \dot{k}_F(\dot{k}_C + j_F')\left((\dot{k}_C + j_{C_s}' + j_F')(\dot{k}_F + j_F')\right)^{-1} \\
&\hat{\theta}_{C_s\cdot} = \dot{k}_F j_{C_s}'\left(\dot{k}_F + j_F'\right)^{-1}\left(\dot{k}_C + j_{C_s}' + j_F'\right)^{-1} \\
&\hat{\theta}_{\cdot F} = j_F'\left(\dot{k}_F + j_F'\right)^{-1}
\end{aligned} \tag{B.19}$$

The rate of E-reserve formation via the phagotrophic pathway is $j_{E,A}^{phago} = \dot{k}_F \hat{\theta}_{.F}$, i.e.,

$$j_{E,A}^{phago} = \left(\dot{k}_F^{-1} + j_F'^{-1}\right)^{-1} \tag{B.20}$$

The rate of organic carbon assimilation is $j_C = \dot{k}_C \hat{\theta}_{C_s.}$, i.e.,

$$j_C = (\dot{k}_C \dot{k}_F j'_{C_s}) \left((\dot{k}_C + j'_F + j'_{C_s})(\dot{k}_F + j_F)\right)^{-1} \tag{B.21}$$

The organic carbon in combination with inorganic nutrients will form the generalized reserves E, in a complementary and sequential transformation (Fig. 3.2d, right). For this transformation the possible states of the SUs are: $\theta_{..}$, $\theta_{C.}$ and θ_{CN}. Following the same steps that gave Eq. (B.9), the rate of E-reserves formation via the phototrophic pathway is

$$j_{E,A}^{photo} = (\dot{k}_{CN}^{-1} + j_C'^{-1} + j_N'^{-1})^{-1} \tag{B.22}$$

with j_N given by Eq. (B.1). Finally, the two pathways combined produce E-reserves at a rate

$$j_{E,A} = j_{E,A}^{photo} + j_{E,A}^{phago} \tag{B.23}$$

DEB model for algal growth

This appendix provides a brief description of the DEB model for photosynthetic cells, presented in Chapter 2, as it was adapted to model the growth dynamics of the four types of PNF in Chapter 3. The assimilation (A) of generalized reserves for the four types of PNF, described in section 3.2, is based on SU kinetics, which imply rejection fluxes due to stoichiometric constraints. The assimilation fluxes $j_{E_C,A}$ and $j_{E_N,A}$, quantified by Eq. (B1.2) for types IIA, IIB and IIC, are directed to the E_C and E_N reserves, respectively, whereas type IIIA mixotrophs, being primarily heterotrophic, do not have the E_C and E_N reserves and any excess fluxes are excreted to the environment. During catabolism (C), reserves are mobilized to allow the growth (G) and maintenance (M) of the organisms. Reserve densities $m_E = M_E/M_V$, $m_{E_i} = M_{E_i}/M_V$ with $i = C, N$, where M_* denotes the masses of structure ($* = V$) and reserves ($* = E, E_C, E_N$), follow first-order kinetics and the resulting catabolic fluxes $j_{E,C}$ and $j_{E_i,C}$, given by Eq. (B1.3), are used by the organism for maintenance and growth. The reserve turnover rate, $\dot{k}$, is constant and is taken to be the same for all reserves (Kooijman, 2010; Lorena et al., 2010). The specific catabolic fluxes, $j_{Ei,C}$ from E_i–reserves ($i = C, N$) are combined by a synthesizing unit to form a compound E' identical to the generalized reserve E according to Eq. (B1.4), while the catabolic fluxes from E_C and E_N reserves that cannot be used for E' production are rejected at a rate given by Eq. (B1.5). A fraction of this flux κ_{E_i}, with $i = C, N$, is fed back to the respective reserves (E_C, E_N) and

the rest $(1 - \kappa_{E_i})$ is excreted outside the cell. The two catabolic fluxes, $j_{E,C}$ and $j_{E',C}$ are combined together by the growth SU, which is assumed to be fast enough to avoid spoiling of reserves, to form the flux $j_{V,G}$ (Eq. B1.6) which will be used for growth after covering the maintenance costs of the cell, $j_{E,M}$. In case that the catabolic fluxes are not enough to pay the maintenance costs the flux $j_{V,G}$ is zero and the remainder is covered from structure at a rate j_V^M (Eq. B1.7). The net specific growth rate, $\dot{r}$ (Eq. B1.8), is calculated numerically and it can take negative values when $j_V^M > 0$.

Table B1: Equations that describe the physiological processes occurring in the mixotroph after the assimilation of generalized reserves, E.

No	Equation	Explanation
B1.1	$j_{E,A}$	E- reserve formation [1]
B1.2	$j_{E_i,A} = j_i - j_i^+ \quad (i = C, N)$	E_C- and E_N- reserve formation [2–5]
B1.3	$j_{E_i,C} = m_{E_i}(\dot{k} - \dot{r}) \quad (i = -, C, N)$	E, E_C, E_N catabolic rate
B1.4	$j_{E',C} = \left(\dot{k}_{CN}^{-1} + j'^{-1}_{E_C,C} + j'^{-1}_{E_N,C} - (j'_{E_C,C} + j'_{E_N,N})^{-1}\right)^{-1}$	E$'$-formation rate
B1.5	$j_{E_i,R} = j_{E_i,C} - y_{i,E'} j_{E',C} \quad (i = C, N)$	Rejection rate
B1.6	$j_{V,G} = y_{E,V}^{-1}(j_{E,C} + j_{E',C} - j_{E,M})_+$	Gross growth rate
B1.7	$j_V^M = (j_{E,M} - \min(j_{E,C} + j_{E',C}, j_{E,M}))\, y_{E,V}^{-1}$	Maintenance rate paid by structure
B1.8	$\dot{r} = j_{V,G} - j_V^M$	Net specific growth rate

Physiological processes: A (assimilation), C (catabolism), M (maintenance), R (rejection), G (growth)
[1] IIA: Eq. (B.6), IIB: Eq. (B.10), IIC: Eq. (B.17), IIIA: Eq. (B.23)
[2] IIA: j_C (Eq. B.3), j_N (Eq. B.1), j_C^+, j_N^+, (Eq. 3.1)
[3] IIB: j_C (Eq. B.9), j_N (Eq. B.11), j_C^+, j_N^+, (Eq. 3.2)
[4] IIC: j_C (Eq. B.15), j_N (Eq. B.1), j_C^+, j_N^+, (Eq. 3.3)
[5] IIIA: has only E-reserves, thus $j_{E_i,A} = 0$ and, consequently, $j_{E_i,C} = 0$ and $j_{E',C} = 0$.

Parameter values

Parameters that are specific to mixotrophic nanoflagellates have been poorly characterised to date, which means that in most cases our parameter choices are, necessarily, arbitrary. Nevertheless, this approach is reasonable, since our aim in this work was to evaluate the qualitative behaviour of the models developed here for the four type of mixotrophic nanoflagellates and compare them with experimentally derived patterns and observations. As such, following the approach of Crane and Grover (2010), most of the phototrophy related parameters were assumed to be similar to those of pure phototrophs, and the phagotrophy related parameters were assumed to be similar to pure phagotrophs. The latter assumption finds support in some experimental evidence suggesting that the grazing rates of pure phagotrophs and

phototrophs can be similar (e.g., Porter, 1988; Tsai et al., 2011, Chapter 4 of the present thesis).

The binding probability of photons, ρ_L, (Eq. B.2) is a compound parameter calculated by Eq. A.1. Parameters ρ_{Lmin} and ρ_{Lmax} correspond to the minimum and maximum binding probabilities to the SU, respectively therefore they are constrained in the interval (0, 1]. ρ_{Lmin} and b was taken from Chapter 2 (Appendix A, Table A1), whereas for ρ_{Lmax} we assumed a maximum value of 1. α_L was taken from (Lika and Papadakis, 2009). K_{IC} was taken from Clark and Flynn (2000). K_N was taken from Eppley et al. (1969), while j_{N,A_m} had to be assumed. Note however, that key parameters of nutrient uptake, such as the maximum uptake rate and the half saturation constant, often depend on growth conditions, and thus can vary greatly (Litchman et al., 2007). The handling rate $\dot{k}_C$ corresponds to the maximum rate of carbohydrates formation (i.e. maximum rate of photosynthesis) and it was taken from (Crane and Grover, 2010). In the absence of available data all handling rates for the rest of the substrates were assumed to be equal to $\dot{k}_C$. j_{IC,A_m} was taken from Chapter 2 (Appendix A, Table A1). The specific respiration rate (maintenance rate $j_{E,M}$ in our model) was taken from (Geider and Osborne, 1989). In order to obtain a value for the half saturation constant for prey uptake K_F, we transformed the values reported in Mohapatra and Fukami (2004) for two marine heterotrophic nanoflagellates preying on bacteria from [number of bacteria mL^{-1}] to [µM] using a conversion factor of 20 fg C (bacterial cell)$^{-1}$ (Lee and Fuhrman, 1987). This gave a range for K_F from 2.3 μM – 15.8 μ M and our choice was based on this range, whereas, the maximum prey ingestion rate j_F had to be assumed.

The reserve turnover rate $\dot{k}$ was adjusted from (Lorena et al., 2010). The stoichiometric coefficient y_{LC} was taken from Chapter 2 (Appendix A, Table A1). The elemental composition for nanoflagellates structure, generalized reserve and prey (n_{*1*2}) was derived assuming Redfield molar ratio (C:N = 106:16). The stoichiometric coefficient y_{NE} was assumed to be the same as n_{NE}. The stoichiometric coefficient y_{EV}, which quantifies the cost of transformation was taken from Chapter 2 (Appendix A, Table A1) and we assumed the same value for y_{CE}, which quantifies the cost of reserve formation. The stoichiometric coefficient y_{ICC} that couples inorganic carbon to organic carbon formation results from the stoichiometry of dark reactions. The stoichiometric coefficient y_{C_sC} was based on Caron et al. (1993) who found that in *Dinobryon cylindricum* most of the organic carbon of this mixotroph ($\geqslant 75\%$) was produced via photosynthesis. The phagotrophy yield coefficient had to be assumed, while the stoichiometric coefficient y_{FC} that stoichiometrically couples phagotrophy rate with the organic carbon formation rate for type IIB is calculated from y and y_{C_sC}. For types IIA, IIC, IIA phagotrophy rate is coupled to the generalized reserves formation rate with the stoichiometric coefficient y_{FC} which is calculated from the phagotrophy yield (y).

Table B2: Table of parameter values. IC: inorganic carbon, N: nutrients, F: bacterial prey, C: organic carbon, C_s: intermediate product during photosynhtesis, E: generalised reserves, E_C: carbon reserves, E_N: nutrients reserves, V: structure

Symbol	Value	Name (Units)
ρ_{Lmin}; ρ_{Lmax}; b	0.2; 1; 2.84	For ρ_L^*: photons' binding probability (–)
α_L	6×10^{-6}	Photons' arrival cross section (m^2 (µmol C)$^{-1}$)
K_{IC}	663	Half-saturation constant for IC (μM)
K_N	0.5	Half-saturation constant for N (μM)
K_F	2.5	Half-saturation constant for F (μM)
j_{IC,A_m}	5.1	Max. uptake rate of IC (d^{-1})
j_{F,A_m}	2.5	Max. uptake rate of F (d^{-1})
j_{N,A_m}	0.5	Max. uptake rate of N (d^{-1})
$\dot{k}_C = \dot{k}_{CN} = \dot{k}_{CF}$	1	Handling rates (d^{-1})
$\dot{k}_F = \dot{k}_{C_sF}$	1	Handling rates (d^{-1})
$\dot{k}$	2.7	Reserves turnover rate (d^{-1})
$j_{E,M}$	0.01	Maintenance rate (d^{-1})
y_{LC}	10	Stoichiometric coefficient (mol phot. (mol C)$^{-1}$)
y_{ICC}	1	Stoichiometric coefficient (mol IC (mol C)$^{-1}$)
y_{C_sC} (IIB; IIC; IIIA)	0.75; 1; 1	Stoichiometric coefficient (mol C (mol C)$^{-1}$)
y	0.9	phagotrophy yield (–)
y_{FC} (IIB)	$(1 - y_{C_sC})\ y^{-1}$	Stoichiometric coefficient (mol C (mol C)$^{-1}$)
y_{FE} (IIC; IIIA)	y^{-1}	Stoichiometric coefficient (mol C (mol C)$^{-1}$)
y_{FE} (IIA)	$n_{NE}\ (n_{NF}\ y)^{-1}$	Stoichiometric coefficient (mol C (mol C)$^{-1}$)
y_{CE}	1.2	Stoichiometric coefficient (mol C (mol C)$^{-1}$)
y_{NE}	0.15	Stoichiometric coefficient (mol N (mol C)$^{-1}$)
y_{EV}	1.2	Stoichiometric coefficient (mol C (mol C)$^{-1}$)
$n_{CE} = n_{CV} = n_{CF}$	1	Chemical index of C in E, V, F (mol C (mol C)$^{-1}$)
$n_{NE} = n_{NV} = n_{NF}$	0.15	Chemical index of N in E, V, F (mol N (mol C)$^{-1}$)
κ_{E_C}	0.95	Fraction of rejected flux of E_C returning to E_C (d^{-1})
κ_{E_N}	0.95	Fraction of rejected flux of E_N returning to E_N (d^{-1})

*ρ_L is calculated according to Eq. A.1

Appendix C

Supplementary information for Chapter 4

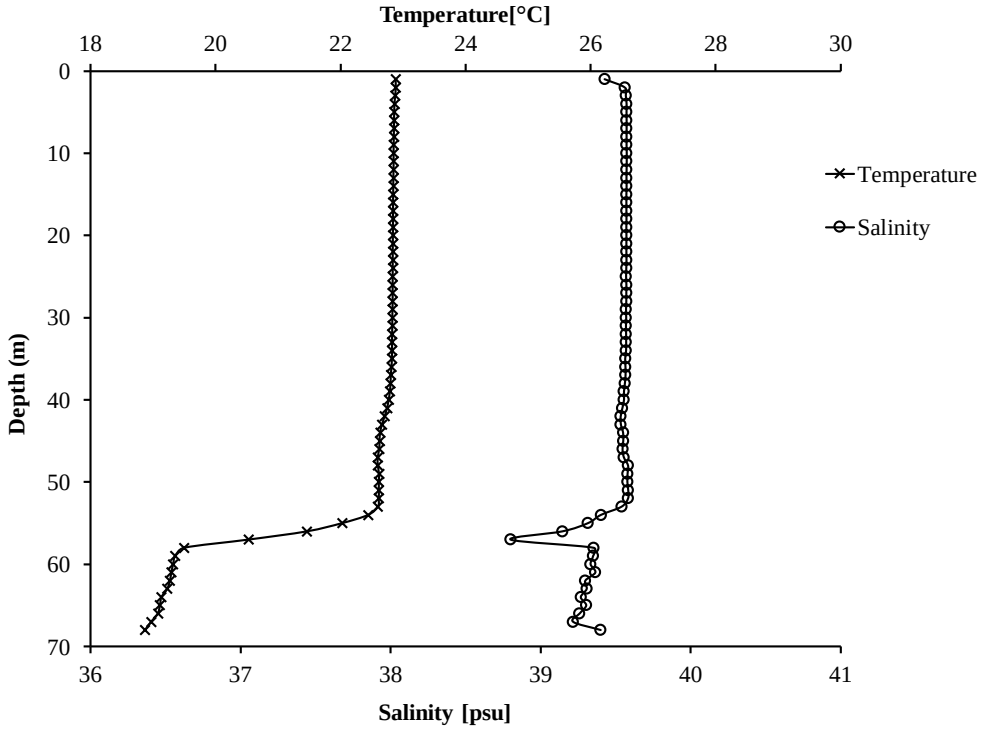

Figure C.1: Vertical profiles of temperature (°C) and salinity (psu) at the sampling site at the date of sampling (18 October 2018).

Appendix D

Supplementary information for Chapter 5

Parameter values

Parameter values are presented in Table D1. Some parameter values were taken from published literature. However, in the absence of an appropriate data set that would simultaneously cover all physiological processes of the specific groups of organisms studied here (e.g., nutrient acquisition, ingestion rates, photosynthesis rate, growth rates, respiration rates etc.) some other parameter values had to be assumed. When it was possible, a qualitative approach in parameter choice was taken. For example, the maximum uptake rate of inorganic phosphorus for HB ($j_{IP,U_{B_m}}$) was assumed to be 3 times that of PNF as it was shown in Moutin et al. (2002). The half-saturation constant for inorganic phosphorus of bacteria KB_{IP} was also assumed to be lower than that of PNF. This assumption reflects the fact that bacteria are better competitors for P uptake than PNF at low P concentrations (Moutin et al., 2002). The $y_{C,EP}$ is the stoichiometric coefficient that quantifies the amount of carbon used per mol of EP reserve formed in PNF. This coefficient entails the metabolic costs of mixotrophy, as discussed in Chapter 3, and corresponds to the carbon assimilation efficiency ($1/y_{C,EP}$). Since mixotrophs are assumed to have higher costs than pure autotrophs and heterotrophs (Raven, 1997), the carbon assimilation efficiency of PNF ($1/y_{C,EP}$) is taken to be lower than the carbon assimilation efficiency of HNF quantified by y_H. The maximum uptake rates of bacteria for HNF and PNF $j_{B,U_{P_m}}$ and $j_{B,U_{H_m}}$, respectively, were taken to be the same. This assumption finds support in some experimental evidence suggesting that the grazing rates of pure phagotrophs and phototrophs can be similar (e.g., Porter, 1988; Tsai et al., 2011, Chapter 4 of the present thesis). On the other hand, it has been been suggested that in low prey availability HNF cannot compete efficiently with PNF (Fischer et al., 2017). This is taken into account in the present model assuming a higher half-saturation constant for HNF in comparison to that of PNF.

Despite the aforementioned assumptions, the approach taken here regarding the param-

eters choice is reasonable, since the aim of the theoretical study presented in Chapter 5 was to qualitatively demonstrate the effect of phosphorus availability on key trophic interactions and on physiological processes of heterotrophic bacteria and heterotrophic and pigmented nanoflagellates in the oligotrophic EMS. Nevertheless, in order to obtain quantitative representations of the modelled organisms, detailed studies on their cellular physiology and metabolism are urgently needed.

Table D1: Table of parameter values. Subscripts: IC: Inorganic Carbon, IP: Inorganic Phosphorus, C: Carbon P: Phosphorus, $V*$: structural mass of organism $*$, $E*$ generalized reserve of organism $*$, EP_C: Carbon-reserves of PNF , EP_P: Phosphorus reserves of PNF. Organism $*$ are symbolized as ($* = P$: PNF, $* = B$: Bacteria, $* = H$: HNF.

Symbol	Value	Name (Units)
Pigmented Nanoflagellates		
ρ_{Lmin}; ρ_{Lmax}; b	0.2; 1; 2.84	For ρ_L: photons' binding probability (–) [1]
α_L	6×10^{-6}	Photons' arrival cross section (m^2 (µmol C)$^{-1}$) [1]
KP_{IC}	663	Half-saturation constant for IC (μM) [1]
KP_{IP}	0.05	Half-saturation constant for IP (μM)
KP_B	0.2	Half-saturation constant for B (μM)
$j_{IC,U_{P_m}}$	5.1	Max. uptake rate of IC (d^{-1}) [1]
$j_{B,U_{P_m}}$	1.1	Max. uptake rate of B (d^{-1})
$j_{IP,U_{P_m}}$	0.005	Max. uptake rate of IP (d^{-1})
$\dot{k}_C = \dot{k}_{C,P} = \dot{k}_{C,B}$	1	Handling rates (d^{-1}) [1]
$\dot{k}_{EP}$	1.5	Reserves turnover rate (d^{-1})
j_{EP,M_P}	0.05	Maintenance rate (d^{-1}) [2]
$y_{L,C}$	10	Stoichiometric coefficient (mol phot. (mol C)$^{-1}$) [1]
$y_{IC,C}$	1	Stoichiometric coefficient (mol IC (mol C)$^{-1}$)
$y_{B,EP}$	$n_{P,EP}\ (n_{P,B}\ y_{B,P})^{-1}$	Stoichiometric coefficient* (mol C (mol C)$^{-1}$) [1]
$y_{B,P}$	0.9	Assimilated fraction of B [1]
$y_{C,EP}$	1.95	Stoichiometric coefficient (mol C (mol C)$^{-1}$)
$y_{P,EP}$	0.0094	Stoichiometric coefficient (mol P (mol C)$^{-1}$)
$y_{EP,VP}$	1.2	Stoichiometric coefficient (mol C (mol C)$^{-1}$) [1]
$n_{C,EP} = n_{C,VP}$	1	Chemical index of C in EP, VP (mol C (mol C)$^{-1}$)
$n_{P,EP} = n_{P,VP}$	0.0094	Chemical index of P in EP, VP (mol P (mol C)$^{-1}$) [3]
$\kappa_{EP_C} = \kappa_{EP_P}$	0.5	Fraction of rejected flux returning to EP_C/EP_P (d^{-1})
$h_{P_{dd}}$	0.7	Density dependent mortality rate (d^{-1} µM $^{-1}$)
$h_{P_{di}}$	0.05	Mortality rate (d^{-1}) [2]
Heterotrophic Bacteria		
α_L	2	Arrival rate of DOM$_L$ (L (µmol VB d)$^{-1}$) [4]
α_S	0.2	Arrival rate of DOM$_S$ (L (µmol VB d)$^{-1}$) [4]
α_R	0.02	Arrival rate of DOM$_R$ (L (µmol VB d)$^{-1}$) [4]
y_B	0.4	Assimilated fraction of DOM (–) [4]
$j_{IP,U_{B_m}}$	$3 * j_{IP,U_{P_m}}$	Max. uptake rate of IP (d^{-1})
KB_{IP}	0.01	Half-saturation constant for IP (μM)
$\dot{k}_{EB}$	1.5	Reserves turnover rate (d^{-1})
j_{EB,M_B}	0.01	Maintenance rate (d^{-1}) [2]
j_{VB,M_B}	0.008	Turnover rate of structure (d^{-1}) [5]

$n_{C,EB} = n_{C,VB}$	1	Chemical index of C in EB, VB (mol C (mol C)$^{-1}$)
$n_{P,EB}$	0.02	Chemical index of P in EB (mol C (mol C)$^{-1}$) [6]
$n_{P,VB}$	0.018	Chemical index of P in VB (mol C (mol C)$^{-1}$) [6]
$y_{EB,VB}$	1.2	Stoichiometric coefficient (mol C (mol C)$^{-1}$)
h_B	0.01	Mortality rate (d^{-1})

Heterotrophic Nanoflagellates

KH_B	0.7	Half-saturation constant for B (μM)
$j_{B,U_{H_m}}$	1.1	Max. uptake rate of B (d^{-1})
$y_{B,H}$	0.95	Assimilated fraction of B (–)
y_H	0.9	Assimilation efficiency of carbon in B (–)
j_{VH,M_H}	0.01	Maintenance rate (d^{-1})
$n_{C,VH}$	1	Chemical index of C in VH (mol C (mol C)$^{-1}$)
$n_{P,VH}$	0.0094	Chemical index of P in VH (mol P (mol C)$^{-1}$) [3]
$h_{H_{dd}}$	0.7	Density dependent mortality rate (d^{-1} µM^{-1})
h_{H_di}	0.05	Mortality rate (d^{-1}) [2]

---

* $n_{P,B} = n_{P,EB}\ m_{EB} + n_{P,VB}$ is the P-mol content per structural mass of bacteria (B).

[1] see Appendix B for details
[2] Tsiaras et al. (2017)
[3] On the basis of Redfield ratio (Redfield, 1958)
[4] Polimene et al. (2006)
[5] Eichinger et al. (2009)
[6] Fagerbakke et al. (1996)

Bibliography

Alcoverro, T., Conte, E., Mazzella, L., 2000. Production of Mucilage By the Adriatic Epipelic Diatom *Cylindrotheca closterium* (Bacillariophyceae) Under Nutrient Limitation. Journal of Phycology 36, 1087–1095.

Allen, J. I., Polimene, L., 2011. Linking physiology to ecology: Towards a new generation of plankton models. Journal of Plankton Research 33, 898–997.

Aluwihare, L. I., Repeta, D. J., 1999. A comparison of the chemical characteristics of oceanic DOM and extracellular DOM produced by marine algae. Marine Ecology Progress Series 186, 105–117.

Amon, R. M., Benner, R., 1996. Bacterial utilization of different size classes of dissolved organic matter. Limnology and Oceanography 41, 41–51.

Anderson, R., Charvet, S., Hansen, P. J., 2018. Mixotrophy in Chlorophytes and Haptophytes – Effect of Irradiance, Macronutrient, Micronutrient and Vitamin Limitation. Frontiers in Microbiology 9, 1704.

Anderson, R., Jürgens, K., Hansen, P. J., 2017. Mixotrophic Phytoflagellate Bacterivory Field Measurements Strongly Biased by Standard Approaches: A Case Study. Frontiers in Microbiology 8, 1398.

Anderson, T. R., Pondaven, P., 2003. Non-Redfield carbon and nitrogen cycling in the Sargasso Sea: pelagic imbalances and export flux. Deep Sea Research Part I: Oceanographic Research Papers 50, 573–591.

Anderson, T. R., Williams, P. J. L., 1998. Modelling the seasonal cycle of dissolved organic carbon at station E-1 in the English Channel. Estuarine, Coastal and Shelf Science 46, 93–109.

Antoine, D., Andrè, J. M., Morel, A., 1996. Oceanic primary production 2. Estimation at global scale from satellite (Coastal Zone Color Scanner) chlorophyll. Global Biogeochemical Cycles 10, 57–69.

Arenovski, A. L., Lim, E. L., Caron, D. A., 1995. Mixotrophic nanoplankton in oligotrophic surface waters of the Sargasso Sea may employ phagotrophy to obtain major nutrients. Journal of Plankton Research 17, 801–820.

Arnosti, C., 2011. Microbial Extracellular Enzymes and the Marine Carbon Cycle. Annual

Review of Marine Science 3, 401–425.

Azam, F., Fenchel, T., Field, J., Gray, J., Meyer-Reil, L., Thingstad, T. F., 1983. The Ecological Role of Water-Column Microbes in the Sea. Marine Ecology Progress Series 10, 257–263.

Baird, M. E., Suthers, I. M., 2007. A size-resolved pelagic ecosystem model. Ecological Modelling 203, 185–203.

Baklouti, M., Diaz, F., Pinazo, C., Faure, V., Quéguiner, B., 2006. Investigation of mechanistic formulations depicting phytoplankton dynamics for models of marine pelagic ecosystems and description of a new model. Progress in Oceanography 71, 1–33.

Baretta-Bekker, J., Baretta, J., Ebenhöh, W., 1997. Microbial dynamics in the marine ecosystem model ERSEM II with decoupled carbon assimilation and nutrient uptake. Journal of Sea Research 38, 195–211.

Benner, R., Amon, R. M., 2015. The Size-Reactivity Continuum of Major Bioelements in the Ocean. Annual Review of Marine Science 7, 185–205.

Berge, T., Chakraborty, S., Hansen, P. J., Andersen, K. H., 2016. Modeling succession of key resource-harvesting traits of mixotrophic plankton. The ISME Journal 11, 212–223.

Berges, J. A., Charlebois, D. O., Mauzerall, D. C., Falkowski, P. G., 1996. Differential Effects of Nitrogen Limitation on Photosynthetic Efficiency of Photosystems I and II in Microalgae. Plant Physiology 110, 689–696.

Berman-Frank, I., Dubinsky, Z., 1999. Balanced Growth in Aquatic Plants: Myth or Reality? Phytoplankton use the imbalance between carbon assimilation and biomass production to their strategic advantage. BioScience 49, 29–37.

Bernard, I., de Kermoysan, G., Pouvreau, S., 2011. Effect of phytoplankton and temperature on the reproduction of the Pacific oyster *Crassostrea gigas*: Investigation through DEB theory. Journal of Sea Research 66, 349–360.

Bertilsson, S., Berglund, O., Karl, D., Chisholm, S., 2003. Elemental composition of marine Prochlorococcus and *Synechococcus*: implications for the ecological stoichiometry of the sea. Limnology and Oceanography 48, 1721–1731.

Biddanda, B., Benner, R., 1997. Carbon, nitrogen, and carbohydrate fluxes during the production of particulate and dissolved organic matter by marine phytoplankton. Limnology and Oceanography 42, 506–518.

Biersmith, A., Benner, R., 1998. Carbohydrates in phytoplankton and freshly produced dissolved organic matter. Marine Chemistry 63, 131–144.

Bird, D. F., Kalff, J., 1987. Algal phagotrophy: Regulating factors and importance relative to photosynthesis in *Dinobryon* (Chrysophyceae). Limnology and Oceanography 32, 277–284.

Bissett, W. P., Walsh, J. J., Dieterle, D. A., Carder, K. L., 1999. Carbon cycling in the upper waters of the Sargasso Sea: I. Numerical simulation of differential carbon and nitrogen fluxes. Deep-Sea Research Part I: Oceanographic Research Papers 46, 205–269.

Bjørnsen, P. K., 1988. Phytoplankton exudation of organic matter: Why do healthy cells do it? Limnology and Oceanography 33, 151–154.

Bonachela, J. A., Allison, S. D., Martiny, A. C., Levin, S. A., 2013. A model for variable phytoplankton stoichiometry based on cell protein regulation. Biogeosciences 10, 4341–4356.

Borchard, C., Engel, A., 2012. Organic matter exudation by *Emiliania huxleyi* under simulated future ocean conditions. Biogeosciences 9, 3405–3423.

Borchard, C., Engel, A., 2015. Size-fractionated dissolved primary production and carbohydrate composition of the coccolithophore *Emiliania huxleyi*. Biogeosciences 12, 1271–1284.

Brandt, B. W., Van Leeuwen, I. M., Kooijman, S. A.L.M, 2003. A general model for multiple substrate biodegradation. Application to co-metabolism of structurally non-analogous compounds. Water Research 37, 4843–4854.

Bratbak, G., Thingstad, T. F., 1985. Phytoplankton-bacteria interactions: an apparent paradox? Analysis of a model system with both competition and commensalism. Marine Ecology Progress Series 25, 23–30.

Brutemark, A., Granéli, E., 2011. Role of mixotrophy and light for growth and survival of the toxic haptophyte *Prymnesium parvum*. Harmful Algae 10, 388–394.

Callieri, C., Karjalainen, M., Passoni, S., 2002. Grazing by ciliates and heterotrophic nanoflagellates on picocyanobacteria in Lago Maggiore, Italy. Journal of Plankton Research 24, 785–796.

Capotondi, A., Alexander, M. A., Bond, N. A., Curchitser, E. N., Scott, J. D., 2012. Enhanced upper ocean stratification with climate change in the CMIP3 models. Journal of Geophysical Research 117, C04031.

Carlson, C. A., Hansell, D. A., 2015. DOM Sources, Sinks, Reactivity, and Budgets. In: Hansell, D., Carlson, C. (Eds.), *Biogeochemistry of Marine Dissolved Organic Matter: Second Edition*. Elsevier.

Caron, D. A., Sanders, R. W., Lim, E. L., Marrasé, C., Amaral, L. A., Whitney, S., Aoki, R. B., Porter, K. G., 1993. Light-dependent phagotrophy in the freshwater mixotrophic chrysophyte *Dinobryon cylindricum*. Microbial Ecology 25, 93–111.

Caron, D. A., Dam, H. G., Kremer, P., Lessard, E. J., Madin, L. P., Malone, T. C., Napp, J. M., Peele, E. R., Roman, M. R., Youngbluth, M. J., 1995. The contribution of microorganisms to particulate carbon and nitrogen in surface waters of the Sargasso Sea near Bermuda. Deep-Sea Research Part I 42, 943–972.

Caron, D. A., Peele, E. R., Lim, E. L., Dennett, M. R., 1999. Picoplankton and nanoplankton and their trophic coupling in surface waters of the Sargasso Sea south of Bermuda. Limnology and Oceanography 44, 259–272.

Caron, D.A., Alexander, H., Allen, A.E., Archibald, J.M., Armbrust, E.V., Bachy, C., Bell, C.J., Bharti, A., Dyhrman, S.T., Guida, S.M., Heidelberg, K.B., Kaye, J.Z., Metzner, J.,

Smith, S.R., Worden, A.Z., 2017. Probing the evolution, ecology and physiology of marine protists using transcriptomics. Nature Reviews Microbiology 15, 6–20.

Carpenter, K. J., Bose, M., Polerecky, L., Lie, A. A. Y., Heidelberg, K.B, Caron, D,A, 2018. Single-Cell View of Carbon and Nitrogen Acquisition in the Mixotrophic Alga *Prymnesium parvum* (Haptophyta) Inferred From Stable Isotope Tracers and NanoSIMS. Fronitiers in Marine Science 5, 157.

Carvalho, W. F., Granéli, E., 2010. Contribution of phagotrophy versus autotrophy to Prymnesium parvum growth under nitrogen and phosphorus sufficiency and deficiency. Harmful Algae 9, 105–115.

Chan, Y.-f., Tsai, A.-y., Chiang, K.-p., Hsieh, C.-h., 2009. Pigmented Nanoflagellates Grazing on *Synechococcus*: Seasonal Variations and Effect of Flagellate Size in the Coastal Ecosystem of Subtropical Western Pacific. Microbial Ecology 58, 548–557.

Chin, W. C., Orellana, M. V., Quesada, I., Verdugo, P., 2004. Secretion in unicellular marine phytoplankton: Demonstration of regulated exocytosis in *Phaeocystis globosa*. Plant and Cell Physiology 45, 535–542.

Cho, B., Azam, F., 1990. Biogeochemical significance of bacterial biomass in the ocean's euphotic zone. Marine Ecology Progress Series 63, 253–259.

Christaki, U., Giannakourou, A., Van Wambeke, F., Grégori, G., 2001. Nanoflagellate predation on auto- and heterotrophic picoplankton in the oligotrophic Mediterranean Sea. Journal of Plankton Research 23, 1297–1310.

Christaki, U., Van Wambeke, F., Dolan, J. R., 1999. Nanoflagellates (mixotrophs, heterotrophs and autotrophs) in the oligotrophic eastern Mediterranean: standing stocks, bacterivory and relationships with bacterial production. Marine Ecology Progress Series 181, 297–307.

Claquin, P., Martin-Jézéquel, V., Kromkamp, J. C., Veldhuis, M. J., Kraay, G. W., 2002. Uncoupling of silicon compared with carbon and nitrogen metabolisms and the role of the cell cycle in continuous cultures of *Thalassiosira pseudonana* (Bacillariophyceae) under light, nitrogen and phosphorus control. Journal of Phycology 38, 922–930.

Clark, D. R., 1999. Carbon-nitrogen stress, and the growth of marine phytoplankton. Ph.D. thesis, University of Wales Swansea.

Clark, D. R., Flynn, K. J., 2000. The relationship between the dissolved inorganic carbon concentration and growth rate in marine phytoplankton. Proceedings of the Royal Society B: Biological Sciences 267, 953–959.

Conan, P., Søndergaard, M., Kragh, T., Thingstad, F., Pujo-Pay, M., Williams, P. J. l. B., Markager, S., Cauwet, G., Borch, N. H., Evans, D., Riemann, B., 2007. Partitioning of organic production in marine plankton communities: The effects of inorganic nutrient ratios and community composition on new dissolved organic matter. Limnology and Oceanography 52, 753–765.

Crane, K. W., Grover, J. P., 2010. Coexistence of mixotrophs, autotrophs, and heterotrophs in planktonic microbial communities. Journal of Theoretical Biology 262, 517–527.

Cullen, J. J., Geider, R. J., Ishizaka, J., Kiefer, D. A., 1993. Towards a General Description of Phytoplankton Growth for Biogeochemical Models. In: Evans G.T., Fasham M.J.R. (Eds.) *Towards a Model of Ocean Biogeochemical Processes. NATO ASI Series (Series I: Global Environmental Change), vol 10*. Springer.

De Philippis, R., Sili, C., Vincenzini, M., 1996. Response of an exopolysaccharide-producing heterocystous cyanobacterium to changes in metabolic carbon flux. Journal of Applied Phycology 8, 275–281.

Delwiche, C.F., 1999. Tracing the thread of plastid diversity through the tapestry of life. The American Naturalist 154, S164–S177.

Denis, M., Thyssen, M., Martin, V., Manca, B., Viducci, F., 2010. Ultraphytoplankton basin-scale distribution in the eastern Mediterranean Sea in winter: link to hydrodynamism and nutrients. Biogeosciences 7, 2227–2244.

Dolan, J. R., Šimek, K., 1998. Ingestion and digestion of an autotrophic, picoplankter, Synechococcus, by a heterotrophic nonoflagellate, *Bodo saltans*. Limnology and Oceanography 43, 1740–1746.

Dolan, J. R., Šimek, K., 1999. Diel periodicity in *Synechococcus* populations and grazing by heterotrophic nanoflagellates: Analysis of food vacuole contents. Limnology and Oceanography 44, 1565–1570.

Doney, S. C., Lima, I., Lindsay, K., Moore, K. J., Dutkiewicz, S., Friedrichs, M. A., Matear, R. J., 2001. Marine biogeochemical modeling: Recent advances and future challenges. Oceanography 14, 93–107.

Droop, M. R., 1968. Vitamin B12 and Marine Ecology. IV. The Kinetics of Uptake, Growth and Inhibition in *Monochrysis lutheri*. Journal of the Marine Biological Association of the United Kingdom 48, 689–733.

Druon, J. N., Mannino, A., Signorini, S., McClain, C., Friedrichs, M., Wilkin, J., Fennel, K., 2010. Modeling the dynamics and export of dissolved organic matter in the Northeastern U.S. continental shelf. Estuarine, Coastal and Shelf Science 88, 488–507.

Ducklow, H. W., Purdie, D. A., Williams, P. J. L., Davies, J. M., 1986. Bacterioplankton: A Sink for Carbon in a Coastal Marine Plankton Community. Science 232, 865–867.

Duhamel, S., Kim, E., Sprung, B., Anderson, O. R., 2019. Small pigmented eukaryotes play a major role in carbon cycling in the P-depleted western subtropical North Atlantic, which may be supported by mixotrophy. Limnology and Oceanography 64, 2424-2440.

Eichinger, M., Kooijman, S., Sempéré, R., Lefèvre, D., Grégori, G., Charrière, B., Poggiale, J., 2009. Consumption and release of dissolved organic carbon by marine bacteria in a pulsed-substrate environment: from experiments to modelling. Aquatic Microbial Ecology 56, 41–54.

Engel, A., Delille, B., Jacquet, S., Riebesell, U., Rochelle-Newall, E., Terbrüggen, A., Zondervan, I., 2004. Transparent exopolymer particles and dissolved organic carbon production by Emiliania huxleyi exposed to different CO_2 concentrations: A mesocosm experiment. Aquatic Microbial Ecology 34, 93–104.

Eppley, R. W., Rogers, J. N., Mccarthy, J. J., 1969. Half-saturation constants for uptake of nitrate and ammonium by marine phytoplankton. Limnology and Oceanogrophy 14, 912–920.

Epstein, S. S., Shiaris, M. P., 1992. Size-selective grazing of coastal bacterioplankton by natural assemblages of pigmented flagellates, colorless flagellates, and ciliates. Microbial Ecology 23, 211–225.

Falkowski, P. G., Fenchel, T., Delong, E. F., 2008. The microbial engines that drive earth's biogeochemical cycles. Science 320, 1034–1039.

Falkowski, P. G., Raven, J. A., 2007. Aquatic Photosynthesis, 2nd Edition. Princeton University Press.

Fennel, K., Gehlen, M., Brasseur, P., Brown, C. W., Ciavatta, S., Cossarini, G., Crise, A., Edwards, C. A., Ford, D., Friedrichs, M. A., Gregoire, M., Jones, E., Kim, H. C., Lamouroux, J., Murtugudde, R., Perruche, C., GODAE OceanView Marine Ecosystem Analysis and Prediction Task Team, 2019. Advancing marine biogeochemical and ecosystem reanalyses and forecasts as tools for monitoring and managing ecosystem health. Frontiers in Marine Science 6, 89.

Fagerbakke, K. M., Heldal,M., Norland., S., 1996. Content of carbon, nitrogen, oxygen, sulfur and phosphorus in native aquatic and cultured bacteria. Aquatic Microbial Ecology 10, 15–27.

Field, C. M., Behrenfeld, M. J., Randerson, J., Falkowski, P. G., 1998. Primary Production of the Biosphere. Science 281, 237–240.

Fischer, R., Giebel, H.A., Hillebrand, H., Ptacnik, R., 2017. Importance of mixotrophic bacterivory can be predicted by light and loss rates. Oikos 126, 713–722.

Flynn, K., 2008. Use, abuse, misconceptions and insights from quota models – The Droop cell quota model 40 years on. Oceanography and Marine Biology: An Annual Review 46, 1–23.

Flynn, K. J., 2010. Ecological modelling in a sea of variable stoichiometry: Dysfunctionality and the legacy of Redfield and Monod. Progress in Oceanography 84, 52–65.

Flynn, K. J., Berry, L. S., 1999. The loss of organic nitrogen during marine primary production may be significantly overestimated when using ^{15}N substrates. Proceedings of the Royal Society B: Biological Sciences 266, 641–647.

Flynn, K. J., Clark, D. R., Xue, Y., 2008. Modeling the release of dissolved organic matter by phytoplankton. Journal of Phycology 44, 1171–1187.

Flynn, K. J., Mitra, A., 2009. Building the "perfect beast": Modelling mixotrophic plankton.

Journal of Plankton Research 31, 965–992.

Flynn, K. J., Stoecker, D. K., Mitra, A., Raven, J. A., Glibert, P. M., Hansen, P. J., Granéli, E., Burkholder, J. M., 2013. Misuse of the phytoplankton-zooplankton dichotomy: The need to assign organisms as mixotrophs within plankton functional types. Journal of Plankton Research 35, 3–11.

Fogg, G. E., 1983. The Ecological Significance of Extracellular Products of Phytoplankton Photosynthesis. Botanica Marina XXVI, 3–14.

Flaten, F. G. A., Skjoldal, E. F., Krom, M. D., Law, C. S., Mantoura, R. F. C., Pitta, P., Psarra, S., Tanaka, T., Tselepides, A., Woodward, E. M. S., Zohary, T., Thingstad, T. F., 2005. Studies of the microbial P-cycle during a Lagrangian phosphate-addition experiment in the Eastern Mediterranean. Deep-Sea Research Part II: Topical Studies in Oceanography 52, 2928–2943.

Fouilland, E., Tolosa, I., Bonnet, D., Bouvier, C., Bouvier, T., Bouvy, M., Got, P., Le Floc'h, E., Mostajir, B., Roques, C., Sempéré, R., Sime-Ngando, T., Vidussi, F., 2014. Bacterial carbon dependence on freshly produced phytoplankton exudates under different nutrient availability and grazing pressure conditions in coastal marine waters. FEMS Microbiology Ecology 87, 757–769.

Franks, P. J., 2009. Planktonic ecosystem models: Perplexing parameterizations and a failure to fail. Journal of Plankton Research 31, 1299–1306.

Frias-Lopez, J., Thompson, A., Waldbauer, J., Chisholm, S. W., 2009. Use of stable isotope-labelled cells to identify active grazers of picocyanobacteria in ocean surface waters. Environmental microbiology 11, 512–525.

Fuhrman, J. A., 1999. Marine viruses and their biogeochemical and ecological effects. Nature 339, 541–548.

Gallager, S. M., Mann, R., 1981. The effect of varying carbon/nitrogen ratio in the phytoplankter *Thalassiosira pseudonana* (3H) on its food value to the bivalve *Tapes japonica*. Aquaculture 26, 95–105.

Gasol, J. M., Del Giorgio, P. A., 2000. Using flow cytometry for counting natural planktonic bacteria and understanding the structure of planktonic bacterial communities. Scientia Marina 64, 197–224.

Gehlen, M., Barciela, R., Bertino, L., Brasseur, P., Butenschön, M., Chai, F., Crise, A., Drillet, Y., Ford, D., Lavoie, D., Lehodey, P., Perruche, C., Samuelsen, A., Simon, E., 2015. Building the capacity for forecasting marine biogeochemistry and ecosystems: Recent advances and future developments. Journal of Operational Oceanography 8, s168–s187.

Geider, R., La Roche, J., 2002. Redfield revisited: variability of C:N:P in marine microalgae and its biochemical basis Redfield revisited: variability of C:N:P in marine microalgae and its biochemical basis. European Journal of Phycology 37, 37–41.

Geider, R. J., MacIntyre, H. L., Kana, T. M., 1998. A dynamic regulatory model of phyto-

planktonic acclimation to light, nutrients, and temperature. Limnology and Oceanography 43, 679–694.

Geider, R. J., MacIntyre, H. L., Kana, T. M., 1996. A dynamic model of photoadaptation. Limnology and Oceanography 41, 1–15.

Geider, R. J., Osborne, B. A., 1989. Respiration and microalgal growth: a review of the quantitative relationship between dark respiration and growth. New Phytologist 112, 327–341.

Gerea, M., Queimalinos, C., Unrein, F., 2018. Grazing impact and prey selectivity of picoplanktonic cells by mixotrophic flagellates in oligotrophic lakes. Hydrobiologia 831, 5–21

Ghyoot, C., Flynn, K. J., Mitra, A., Lancelot, C., Gypens, N., 2017. Modeling Plankton Mixotrophy: A Mechanistic Model Consistent with the Shuter-Type Biochemical Approach. Frontiers in Ecology and Evolution 5, 78.

Glibert, P. M., Kana, T. M., Brown, K., 2013. From limitation to excess: The consequences of substrate excess and stoichiometry for phytoplankton physiology, trophodynamics and biogeochemistry, and the implications for modeling. Journal of Marine Systems 125, 14–28.

Goldman, J. C., Mccarthyt, J. J., Peavy, D. G., 1979. Growth rate influence on the chemical composition of phytoplankton in oceanic waters. Nature 279, 1.

Granum, E., Kirkvold, S., Myklestad, S. M., 2002. Cellular and extracellular production of carbohydrates and amino acids by the marine diatom *Skeletonema costatum*: Diel variations and effects of N depletion. Marine Ecology Progress Series 242, 83–94.

Grossowicz, M., Marques, G. M., van Voorn, G. A., 2017a. A dynamic energy budget (DEB) model to describe population dynamics of the marine cyanobacterium *Prochlorococcus marinus*. Ecological Modelling 359, 320–332.

Grossowicz, M., Roth-Rosenberg, D., Aharonovich, D., Silverman, J., Follows, M. J., Sher, D., 2017b. *Prochlorococcus* in the lab and *in silico*: The importance of representing exudation. Limnology and Oceanography.

Grover, J.P., Chrzanowski, T.H., 2006. Stoichiometry and growth kinetics in the "smallest zooplankton" - Phagotrophic flagellates. Archiv fur Hydrobiologie 167, 467–487.

Guieu, C., Aumont, O., Paytan, A., Bopp, L., Law, C. S., Mahowald, N., Achterberg, E. P., Marañón, E., Salihoglu, B., Crise, A., Wagener, T., Herut, B., Desboeufs, K., Kanakidou, M., Olgun, N., Peters, F., Völker, C., , 2014. The significance of the episodic nature of atmospheric deposition to Low Nutrient Low Chlorophyll regions. Global Biogeochemical Cycles 28, 1179–1198.

Guyennon, A., Baklouti, M., Diaz, F., Palmieri, J., Beuvier, J., Lebaupin-Brossier, C., Arsouze, T., Beranger, K., Dutay, J. C., Moutin, T., 2015. New insights into the organic carbon export in the Mediterranean Sea from 3-D modeling. Biogeosciences 12, 7025–7046.

Hall, J. A., Barrett, D. P., James, M. R., 1993. The importance of phytoflagellate, heterotrophic flagellate and ciliate grazing on bacteria and picophytoplankton sized prey in

a coastal marine environment. Journal of Plankton Research 15, 1075–1086.

Hama, T., Yanagi, K., 2001. Production and neutral aldose composition of dissolved carbohydrates excreted by natural marine phytoplankton populations. Limnology and Oceanography 46, 1945–1955.

Hammer, A. C., Pitchford, J. W., 2005. The role of mixotrophy in plankton bloom dynamics, and the consequences for productivity. ICES Journal of Marine Science 62, 833–840.

Hansell, D., Carlson, C., Repeta, D., Schlitzer, R., 2009. Dissolved Organic Matter in the Ocean: A Controversy Stimulates New Insights. Oceanography 22, 202–211.

Hansell, D. A., 2013. Recalcitrant Dissolved Organic Carbon Fractions. Annual Review of Marine Science 5, 421–445.

Hansen, P. J., Hjorth, M., 2002. Growth and grazing responses of *Chrysochromulina ericina* (Prymnesiophyceae): The role of irradiance, prey concentration and pH. Marine Biology 141, 975–983.

Hartmann, M., Grob, C., Tarran, G. A., Martin, A. P., Burkill, P. H., Scanlan, D. J., Zubkov, M. V., 2012. Mixotrophic basis of Atlantic oligotrophic ecosystems. Proceedings of the National Academy of Science 109, 5756–5760.

Hartmann, M., Zubkov, M. V., Scanlan, D. J., Lepère, C., 2013. *In situ* interactions between photosynthetic picoeukaryotes and bacterioplankton in the Atlantic Ocean: evidence for mixotrophy. Environmental Microbiology Reports 5, 835–840.

Hasumi, H., Nagata, T., 2014. Modeling the global cycle of marine dissolved organic matter and its influence on marine productivity. Ecological Modelling 288, 9–24.

Havskum, H., Riemann, B., 1996. Ecological importance of bacterivorous, pigmented flagellates (mixotrophs) in the Bay of Aarhus, Denmark. Marine Ecology Progress Series 137, 251–263.

Hopkinson, C. S., Vallino, J. J., 2005. Efficient export of carbon to the deep ocean through dissolved organic matter. Nature 433, 142–145.

Ignatiades, L., Gotsis-Skretas, O., Pagou, K., Krasakopoulou, E., 2009. Diversification of phytoplankton community structure and related parameters along a large-scale longitudinal east – west transect of the Mediterranean Sea. Journal of Plankton Research 31, 411–428.

Ignatiades, L., Psarra, S., Zervakis, V., Pagou, K., Souvermezoglou, E., Assimakopoulou, G., Gotsis-Skretas, O., 2002. Phytoplankton size-based dynamics in the Aegean Sea (Eastern Mediterranean). Journal of Marine Systems 36, 11–28.

Jardillier, L., Zubkov, M. V., Pearman, J., Scanlan, D. J., 2010. Significant CO2 fixation by small prymnesiophytes in the subtropical and tropical northeast Atlantic Ocean. The ISME journal 4, 1180–1192.

Jiao, N., Herndl, G. J., Hansell, D. A., Benner, R., Kattner, G., Wilhelm, S. W., Kirchman, D. L., Weinbauer, M. G., Luo, T., Chen, F., Azam, F., 2010. Microbial production of

recalcitrant dissolved organic matter: long-term carbon storage in the global ocean. Nature Reviews Microbiology 8, 593–599.

Jiao, N., Robinson, C., Azam, F., Thomas, H., Baltar, F., Dang, H., Hardman-Mountford, N. J., Johnson, M., Kirchman, D. L., Koch, B. P., Legendre, L., Li, C., Liu, J., Luo, T., Luo, Y. W., Mitra, A., Romanou, A., Tang, K., Wang, X., Zhang, C., Zhang, R., 2014. Mechanisms of microbial carbon sequestration in the ocean – Future research directions. Biogeosciences 11, 5285–5306.

Jones, H. L. J., 1997. A classification of mixotrophic protists based on their behaviour. Freshwater Biology 37, 35–43.

Kamalanathan, M., Pierangelini, M., Shearman, L. A., Gleadow, R., Beardall, J., 2016. Impacts of nitrogen and phosphorus starvation on the physiology of *Chlamydomonas reinhardtii*. Journal of Applied Phycology 28, 1509–1520.

Karayanni, H., Christaki, U., Van Wambeke, F., Thyssen, M., Denis, M., 2008. Heterotrophic nanoflagellate and ciliate bacterivorous activity and growth in the northeast Atlantic Ocean: a seasonal mesoscale study. Aquatic Microbial Ecology 51, 169–181.

Kassambara, A., Mundt, F., 2017. Factoextra: extract and visualize the results of multivariate data analyses.

Kawasaki, N., Benner, R., 2006. Bacterial release of dissolved organic matter during cell growth and decline: Molecular origin and composition. Limnology and Oceanography 51, 2170–2180.

Keeling, P. J., 2013. The Number, Speed, and Impact of Plastid Endosymbioses in Eukaryotic Evolution. Annual Review of Plant Biology 64, 583–607.

Keller, D. P., Hood, R. R., 2011. Modeling the seasonal autochthonous sources of dissolved organic carbon and nitrogen in the upper Chesapeake Bay. Ecological Modelling 222, 1139–1162.

Kirk, J. T., 2011. Light and Photosynthesis in Aquatic Ecosystems, 3rd Edition. Cambridge University Press.

Kirkham, A. R., Lepère, C., Jardillier, L. E., Not, F., Bouman, H., Mead, A., Scanlan, D. J., 2013. A global perspective on marine photosynthetic picoeukaryote community structure. The ISME journal, 1–15.

Kooijman, S., 1998. The Synthesizing Unit as model for the stoichiometric fusion and branching of metabolic fluxes. Biophysical Chemistry 73, 179–188.

Kooijman, S., Dijkstra, H., Kooi, B., 2002. Light-induced Mass Turnover in a Mono-species Community of Mixotrophs. Journal of Theoretical Biology 214, 233–254.

Kooijman, S. A. L. M., 2010. Dynamic Energy Budget theory for metabolic organisation, 3rd Edition. Cambridge University Press.

Koroleff, F., 1970. Direct determination of ammonia in natural waters as indophenol blue. Cons. Int. Explor. Mer., Information on techniques and methods for sea water analysis

(and laboratory report) 3, 19–22.

Kreus, M., Schartau, M., Engel, A., Nausch, M., Voss, M., 2014. Variations in the elemental ratio of organic matter in the central Baltic Sea: Part I-Linking primary production to remineralization. Continental Shelf Research 100, 25–45.

Kriest, I., Oschlies, A., 2007. Modelling the effect of cell-size-dependent nutrient uptake and exudation on phytoplankton size spectra. Deep-Sea Research Part I: Oceanographic Research Papers 54, 1593–1618.

Krom, M., Groom, S., Zohary, T., 2003. The Eastern Mediterranean. In: Black, K., Shimmield, G. (Eds.), *Biogeochemistry of Marine Systems*. Blackwell Publishing Ltd.

Krom, M. D., Kress, N., Brenner, S., Gordon, L. I., 1991. Phosphorus limitation of primary productivity in the eastern Mediterranean Sea. Limnology and Oceanography 36, 424–432.

Krom, M. D., Woodward, E. M., Herut, B., Kress, N., Carbo, P., Mantoura, R. F., Spyres, G., Thingsted, T. F., Wassmann, P., Wexels-Riser, C., Kitidis, V., Law, C., Zodiatis, G., 2005. Nutrient cycling in the south east Levantine basin of the eastern Mediterranean: Results from a phosphorus starved system. Deep-Sea Research Part II: Topical Studies in Oceanography 52, 2879–2896.

Lagaria, A., Mandalakis, M., Mara, P., Frangoulis, C., Karatsolis, B. T., Pitta, P., Triantaphyllou, M., Tsiola, A., Psarra, S., 2017a. Phytoplankton variability and community structure in relation to hydrographic features in the NE Aegean frontal area (NE Mediterranean Sea). Continental Shelf Research 149, 124–137.

Lagaria, A., Mandalakis, M., Mara, P., Papageorgiou, N., Pitta, P., Tsiola, A., Kagiorgi, M., Psarra, S., 2017b. Phytoplankton Response to Saharan Dust Depositions in the Eastern Mediterranean Sea: A Mesocosm Study. Frontiers in Marine Science 3, 287.

Lagaria, A., Psarra, S., Gogou, A., Tuğrul, S., Christaki, U., 2013. Particulate and dissolved primary production along a pronounced hydrographic and trophic gradient (Turkish Straits System-NE Aegean Sea). Journal of Marine Systems 119–120, 1–10.

Lagaria, A., Psarra, S., Lefèvre, D., Van Wambeke, F., Courties, C., Pujo-Pay, M., Oriol, L., Tanaka, T., Christaki, U., 2011. The effects of nutrient additions on particulate and dissolved primary production and metabolic state in surface waters of three Mediterranean eddies. Biogeosciences 8, 2595–2607.

Lalli, C. M., Parsons, T. R., 1997. Biological Oceanography: An Introduction, 2nd Edition. Elsevier.

Landry, M. R., Lehner-Fournier, J. M., Sundstrom, J. A., Fagerness, V. L., Selph, K. E., 1991. Discrimination between living and heat-killed prey by a marine zooflagellate, *Paraphysomonas vestita* (Stokes). Journal of Experimental Marine Biology and Ecology 146, 139–151.

Lee S., Fuhrman, J. A., 1987. Relationships between biovolume and biomass of naturally derived marine bacterioplanktonton. Applied and Environmental Microbiology 5, 1298–

1303.

Legendre, L., Rassoulzadegan, F., 1996. Food-web mediated export of biogenic carbon in oceans: Hydrodynamic control. Marine Ecology Progress Series 145, 179–193.

Leles, S. G., Mitra, A., Flynn, K. J., Tillmann, U., Stoecker, D., Jeong, H. J., Burkholder, J. A., Hansen, P. J., Caron, D. A., Glibert, P. M. Hallegraeff, G., Raven, J. A., Sanders, R. W., Zubkov, M., 2019. Sampling bias misrepresents the biogeographical significance of constitutive mixotrophs across global oceans. Global Ecology and Biogeography 28, 418–428.

Leles, S. G., Polimene, L., Bruggeman, J., Blackford, J., Ciavatta, S., Mitra, A., Flynn, K. J., 2018. Modelling mixotrophic functional diversity and implications for ecosystem function. Journal of Plankton Research 40, 627–642.

Li, W., 1994. Primary production of prochlorophytes , cyanobacteria , and eucaryotic ultraphytoplankton : Measurements from flow cytometric sorting. Limnology and Oceanography 39, 169–175.

Lie, A. A. Y., Liu, Z., Terrado, R., Tatters, A. O., Heidelberg, K. B., Caron, D. A., 2017. Effect of light and prey availability on gene expression of the mixotrophic chrysophyte, *Ochromonas* sp. BMC Genomics 18, 163.

Lie, A. A., Liu, Z., Terrado, R., Tatters, A. O., Heidelberg, K. B., Caron, D. A., 2018. A tale of two mixotrophic chrysophytes: Insights into the metabolisms of two *Ochromonas* species (Chrysophyceae) through a comparison of gene expression. PLoS ONE 13, e0192439.

Lika, K., Nisbet, R. M., 2000. A dynamic energy budget model based on partitioning of net production. Journal of mathematical biology 41, 361–386.

Lika, K., Papadakis, I. A., 2009. Modeling the biodegradation of phenolic compounds by microalgae. Journal of Sea Research 62, 135–146.

Litchman, E., Klausmeier, C. A., Schofield, O. M., Falkowski, P. G., 2007. The role of functional traits and trade-offs in structuring phytoplankton communities: Scaling from cellular to ecosystem level. Ecology Letters 10, 1170–1181.

Liu, Z., Jones, A. C., Campbell, V., Hambright, K. D., Heidelberg, K. B., Caron, D. a., 2015a. Gene expression in the mixotrophic prymnesiophyte, *Prymnesium parvum*, responds to prey availability. Frontiers in Microbiology 6, 1–12.

Liu, Z., Koid, A. E., Terrado, R., Campbell, V., Caron, D. a., Heidelberg, K. B., 2015b. Changes in gene expression of *Prymnesium parvum* induced by nitrogen and phosphorus limitation. Frontiers in Microbiology 6, 319.

Liu, Z., Campbell, V., Heidelberg, K. B., Caron, D. A., 2016. Gene expression characterizes different nutritional strategies among three mixotrophic protists. FEMS Microbiology Ecology 92, fiw106.

Lomas, M. W., Rumbley, C. J., Glibert, P. M., 2000. Ammonium release by nitrogen sufficient diatoms in response to rapid increases in irradiance. Journal of Plankton Research 22,

2351–2366.

Lomas, M.W., Bronk, D.A., van den Engh, G., 2011. Use of Flow Cytometry to Measure Biogeochemical Rates and Processes in the Ocean. Annual Review of Marine Science 3, 537–566.

Longhurst, A., Sathyendranath, S., Platt, T., Caverhill, C., 1995. An estimate of global primary production in the ocean from satellite radiometer data. Journal of Plankton Research 17, 1245–1271.

López-Sandoval, D. C., Fernández, A., Marañón, E., 2011. Dissolved and particulate primary production along a longitudinal gradient in the Mediterranean Sea. Biogeosciences 8, 815–825.

Lorena, A., Marques, G. M., Kooijman, S. A. L. M., Sousa, T., 2010. Stylized facts in microalgal growth: interpretation in a dynamic energy budget context. Philosophical Transactions of the Royal Society of London, Series B, Biological sciences 36, 3509-3521.

Mackey, M. D., Mackey, D. J., Higgins, H. W., Wright, S. W., 1996. CHEMTAX - A program for estimating class abundances from chemical markers: Application to HPLC measurements of phytoplankton. Marine Ecology Progress Series 144, 265–283.

Mague, T. H., Friberg, E., Hughes, D. J., Morris, I., 1980. Extracellular release of carbon by marine phytoplankton; a physiological approach. Limnology and Oceanography 25, 262–279.

Man-Aharonovich, D., Philosof, A., Kirkup, B. C., Le Gall, F., Yogev, T., Berman-Frank, I., Polz, M. F., Vaulot, D., Béjà, O., 2010. Diversity of active marine picoeukaryotes in the Eastern Mediterranean Sea unveiled using photosystem-II psbA transcripts. The ISME Journal 4, 1044–1052.

Marañón, E., Cermeño, P., Fernández, E., Rodríguez, J., Zabala, L., 2004. Significance and mechanisms of photosynthetic production of dissolved organic carbon in a coastal eutrophic ecosystem. Limnology and Oceanography 49, 1652–1666.

Marañón, E., Cermeño, P., López-Sandoval, D. C., Rodríguez-Ramos, T., Sobrino, C., Huete-Ortega, M., Blanco, J. M., Rodríguez, J., 2013. Unimodal size scaling of phytoplankton growth and the size dependence of nutrient uptake and use. Ecology Letters 16, 371–379.

Marañón, E., Pérez, V., Fernández, E., Anadón, R., Bode, A., González, N., Huskin, I., Isla, A., Morán, X. A. G., Mouriño, B., Quevedo, M., Robinson, C., Serret, P., Teira, E., Varela, M. M., Woodward, E. M. S., Zubkov, M. V., 2007. Planktonic carbon budget in the eastern subtropical North Atlantic. Aquatic Microbial Ecology 48, 261–275.

Marques, G. M., Augustine, S., Lika, K., Pecquerie, L., Domingos, T., Kooijman, S. A. L. M., 2018. The AmP project: Comparing species on the basis of dynamic energy budget parameters. PLoS Comput Biol 14, e1006100.

Marques, G. M., Lika, K., Pecquerie, L., Kooijman, S. A., jan 2019. Fitting multiple models to multiple data sets. Journal of Sea Research 143, 48–56.

Marques, G. M., Mateus, M., Domingos, T., sep 2014. Can we reach consensus between marine ecological models and DEB theory? A look at primary producers. Journal of Sea Research 94, 92–104.

McKie-Krisberg, Z. M., Gast, R. J., Sanders, R. W., 2015. Physiological Responses of Three Species of Antarctic Mixotrophic Phytoflagellates to Changes in Light and Dissolved Nutrients. Microbial Ecology 70, 21–29.

Mckie-Krisberg, Z. M., Sanders, R. W., 2014. Phagotrophy by the picoeukaryotic green alga Micromonas : implications for Arctic Oceans. The ISME journal 8, 1953–1961.

Mitra, A., Flynn, K. J., Burkholder, J. M., Berge, T., Calbet, A., Raven, J. A., Granéli, E., Glibert, P. M., 2014. The role of mixotrophic protists in the biological carbon pump. Biogeosciences 11, 995–1005.

Mitra, A., Flynn, K. J., Tillmann, U., Raven, J. A., Caron, D., Stoecker, D. K., Not, F., Hansen, P. J., Hallegraeff, G., Sanders, R., Wilken, S., McManus, G., Johnson, M., Pitta, P., Våge, S., Berge, T., Calbet, A., Thingstad, T. F., Jeong, H. J., Burkholder, J., Glibert, P. M., Granéli, E., Lundgren, V., 2016. Defining Planktonic Protist Functional Groups on Mechanisms for Energy and Nutrient Acquisition; Incorporation of Diverse Mixotrophic Strategies. Protist 167, 106–120.

Mohapatra, B. R., Fukami, K., 2004. Comparison of the numerical grazing response of two marine heterotrophic nanoflagellates fed with different bacteria. Journal of Sea Research 52, 99–107.

Møller, E. F., 2007. Production of dissolved organic carbon by sloppy feeding in the copepods *Acartia tonsa* , C*entropages typicus*, and *Temora longicornis*. Limnologica 52, 79–84.

Mongin, M., Nelson, D. M., Pondaven, P., Tréguer, P., 2003. Simulation of upper-ocean biogeochemistry with a flexible-composition phytoplankton model: C, N and Si cycling and Fe limitation in the Southern Ocean. Deep-Sea Research Part II: Topical Studies in Oceanography 53, 601–619.

Morán, X. A. G., Estrada, M., Gasol, J. M., Pedrós-Alió, C.,2002. Dissolved primary production and the strength of phytoplankton-bacterioplankton coupling in contrasting marine regions. Microbial Ecology 44, 217–223.

Moutin, T., Raimbault, P., 2002. Primary production, carbon export and nutrients availability in western and eastern Mediterranean Sea in early summer 1996 (MINOS cruise). Journal of Marine Systems 33-34, 273–288.

Moutin, T., Thingstad, T. F., Van Wambeke, F., Marie, D., Slawyk, G.,Raimbault, P., Claustre, H., 2002. Does competition for nanomolar phosphate supply explain the predominance of the cyanobacterium Synechococcus?nLimnology and Oceanography 47, 1562–1567.

Moutin, T., Prieur, L., 2012. Influence of anticyclonic eddies on the Biogeochemistry from the Oligotrophic to the Ultraoligotrophic Mediterranean (BOUM cruise). Biogeosciences 9, 3827–3855.

Mueller, B., den Haan, J., Visser, P. M., Vermeij, M. J. A., van Duyl, F. C., 2016. Effect of light and nutrient availability on the release of dissolved organic carbon (DOC) by Caribbean turf algae. Scientific reports 6, 23248.

Mühlenbruch, M., Grossart, H. P., Eigemann, F., Voss, M., 2018. Mini-review: Phytoplankton-derived polysaccharides in the marine environment and their interactions with heterotrophic bacteria. Environmental Microbiology 20, 2671–2685.

Muller, E., Ananthasubramaniam, B., Klanjšček, T., Nisbet, R. M., 2011. Entrainment of cell division in phytoplankton with dynamic energy budgets. Journal of Sea Research 66, 447–455.

Muller, E., 2019. Synthesizing units as modeling tool for photosynthesizing organisms with photoinhibition and nutrient limitation. Ecological Modelling 222, 637–644.

Myklestad, S., 2000. Dissolved Organic Carbon from Phytoplankton. In: Wangersky, P. (Ed.), Marine Chemistry. The Handbook of Environmental Chemistry. Vol. 5D. Springer Berlin Heidelberg.

Myklestad, S., Holmhansen, O., Varum, K. M., Volcani, B. E., 1989. Rate of release of extracellular amino-acids and carbohydrates from the marine diatom *Chaetoceros affinis*. Journal of Plankton Research 11, 763–773.

Myklestad, S. M., 1995. Release of extracellular products by phytoplankton with special emphasis on polysaccharides. Science of the Total Environment 165, 155–164.

Nagao, F., Miyazaki, T., 2002. Release of dissolved organic nitrogen from *Scenedesmus quadricauda* (Chlorophyta) and *Microcystis novacekii* (Cyanobacteria). Aquatic Microbial Ecology 2, 275–284.

Ng, W. H. A., Liu, H., 2016. Diel periodicity of grazing by heterotrophic nanoflagellates influenced by prey cell properties and intrinsic grazing rhythm. Journal of Plankton Research 38, 636–651.

Nygaard, K., Tobiesen, A., 1993. Bacteriovory in algae: A survival strategy during nutrient limitation. Limnology and Oceanography 38, 273–279.

Obernosterer, I., Herndl, G. J., 1995. Phytoplankton extracellular release and bacterial growth: Dependence on the inorganic N:P ratio. Marine Ecology Progress Series 116, 247–258.

Ogawa, H., Amagai, Y., Koike, I., Kaiser, K., Benner, R., 2001. Production of refractory dissolved organic matter by bacteria. Science 292, 917–920.

Orellana, M. V., Pang, W. L., Durand, P. M., Whitehead, K., Baliga, N. S., 2013. A Role for Programmed Cell Death in the Microbial Loop. PLoS ONE 8, e62595.

Pachiadaki, M. G., Taylor, C., Oikonomou, A., Yakimov, M. M., Stoeck, T., Edgcomb, V., 2016. In situ grazing experiments apply new technology to gain insights into deep-sea microbial food webs. Deep-Sea Research Part II: Topical Studies in Oceanography 129, 223–231.

Pahlow, M., Vézina, A. F., Casault, B., Maass, H., Malloch, L., Wright, D. G., Lu, Y., 2008. Adaptive model of plankton dynamics for the North Atlantic. Progress in Oceanography 76, 151–191.

Pålsson, C., Granéli, W., 2003. Diurnal and seasonal variations in grazing by bacterivorous mixotrophs in an oligotrophic clearwater lake. Archiv fur Hydrobiologie 157, 289–307.

Papadakis, I. A., Kotzabasis, K., Lika, K., 2005. A cell-based model for the photoacclimation and CO2-acclimation of the photosynthetic apparatus. Biochimica et Biophysica Acta 1708, 250–261.

Papadakis, I. A., Kotzabasis, K., Lika, K., 2012. Modeling the dynamic modulation of light energy in photosynthetic algae. Journal of Theoretical Biology 300, 254–264.

Parkhill, J. P., Maillet, G., Cullen, J. J., 2001. Fluorescence-based maximal quantum yield for PSII as a diagnostic of nutrient stress. Journal of Phycology 37, 517–529.

Pecquerie, L., Johnson, L. R., Kooijman, S. A. L. M., Nisbet, R. M., 2011. Analyzing variations in life-history traits of Pacific salmon in the context of Dynamic Energy Budget (DEB) theory. Journal of Sea Research 66, 424–433.

Pecquerie, L., Petitgas, P., Kooijman, S. a. L. M., 2009. Modeling fish growth and reproduction in the context of the Dynamic Energy Budget theory to predict environmental impact on anchovy spawning duration. Journal of Sea Research 62, 93–105.

Pereira, S., Zille, A., Micheletti, E., Moradas-Ferreira, P., De Philippis, R., Tamagnini, P., 2009. Complexity of cyanobacterial exopolysaccharides: Composition, structures, inducing factors and putative genes involved in their biosynthesis and assembly. FEMS Microbiology Reviews 33, 917–941.

Pernthaler, J., Šimek, K., Sattler, B., Schwarzenbacher, A., Bobkova, J., Psenner, R., 1996. Short-term changes of protozoan control on autotrophic picoplankton in an oligo-mesotrophic lake. Journal of Plankton Research 18, 443–462.

Perry, M. J., 1976. Phosphate utilization by an oceanic diatom in phosphorus-limited chemostat culture and in the oligotrophic waters of the central North Pacific. Limnology and Oceanography 21, 88–107.

Pete, R., Davidson, K., Hart, M. C., Gutierrez, T., Miller, A. E., 2010. Diatom derived dissolved organic matter as a driver of bacterial productivity: The role of nutrient limitation. Journal of Experimental Marine Biology and Ecology 391, 20–26.

Petihakis, G., Perivoliotis, L., Korres, G., Ballas, D., Frangoulis, C., Pagonis, P., Ntoumas, M., Pettas, M., Chalkiopoulos, A., Sotiropoulou, M., Bekiari, M., Kalampokis, A., Ravdas, M., Bourma, E., Christodoulaki, S., Zacharioudaki, A., Kassis, D., Potiris, E., Triantafyllou, G., Tsiaras, K., Krasakopoulou, E., Velanas, S., Zisis, N., 2018. An integrated open-coastal biogeochemistry, ecosystem and biodiversity observatory of the eastern Mediterranean - The Cretan Sea component of the POSEIDON system. Ocean Science 14, 1223–1245.

Petihakis, G., Triantafyllou, G., Tsiaras, K., Korres, G., Pollani, A., Hoteit, I., 2009. Eastern Mediterranean biogeochemical flux model - Simulations of the pelagic ecosystem. Ocean Science 5, 29–46.

Pitta, P., Giannakourou, A., Christaki, U., 2001. Planktonic ciliates in the oligotrophic Mediterranean Sea: Longitudinal trends of standing stocks, distributions and analysis of food vacuole contents. Aquatic Microbial Ecology 24, 297–311.

Pitta, P., Kanakidou, M., Mihalopoulos, N., Christodoulaki, S., Dimitriou, P., Frangoulis P., Giannakourou, G., Kagiorgi, M., Lagaria, A., Nikolaou, P., Papageorgiou, N., Psarra, S., Santi, I., Tsapakis, M., Tsiola, A., Violaki, K., Petihakis, G., 2017. Saharan Dust Deposition Effects on the Microbial Food Web in the Eastern Mediterranean: A Study Based on a Mesocosm Experiment. Frontiers in Marine Science 4, 117.

Pitta, P., Nejstgaard, J. C., Tsagaraki, T. M., Zervoudaki, S., Egge, J. K., Frangoulis, C., Lagaria, A., Magiopoulos, I., Psarra, S., Sandaa, R. A., Skjoldal, E. F., Tanaka, T., Thyrhaug, R., Thingstad, T. F., 2016. Confirming the "rapid phosphorus transfer from microorganisms to mesozooplankton in the Eastern Mediterranean Sea" scenario through a mesocosm experiment. Journal of Plankton Research 38, 502–521.

Pitta, P., Stambler, N., Tanaka, T., Zohary, T., Tselepides, A., Rassoulzadegan, F., 2005. Biological response to P addition in the Eastern Mediterranean Sea. The microbial race against time. Deep-Sea Research Part II: Topical Studies in Oceanography 52, 2961–2974.

Polimene, L., Allen, J. I., Zavatarelli, M., 2006. Model of interactions between dissolved organic carbon and bacteria in marine systems. Aquatic Microbial Ecology 43, 127–138.

Polovina, J. J., Howell, E. A., Abecassis, M., 2008. Ocean's least productive waters are expanding. Geophysical Research Letters 35, L03618.

Porter, K. G., 1988. Phagotrophic phytoflagellates in microbial food webs. Hydrobiologia 159, 89–97.

Psarra, S., Tselepides, A., Ignatiades, L., 2000. Primary productivity in the oligotrophic Cretan Sea (NE Mediterranean): seasonal and interannual variability. Progress in Oceanography 46, 187–204.

Psarra, S., Zohary, T., Krom, M. D., Mantoura, R. F. C., Polychronaki, T., Stambler, N., Tanaka, T., Tselepides, A.,Thingstad, T. F., 2005. Phytoplankton response to a Lagrangian phosphate addition in the Levantine Sea (Eastern Mediterranean). Deep-Sea Research Part II: Topical Studies in Oceanography 52, 2944–2960.

Ptacnik, R., Gomes, A., Royer, S.-j., Berger, S. A., Calbet, A., Nejstgaard, J. C., Gasol, J. M., Isari, S., Moorthi, S. D., Ptacnikova, R., Striebel, M., Sazhin, A. F., Tsagaraki, T. M., Zervoudaki, S., Altoja, K., Dimitriou, P., Lass, P., Gazihan, A., Martinez, A. R., Schabhüttl, S., Santi, I., Sousoni, D., Pitta, P., 2016. A light-induced shortcut in the planktonic microbial loop. Scientific Reports 6, 29286.

Puddu, A., Zoppini, A., Fazi, S., Rosati, M., Amalfitano, S., Magaletti, E., 2003. Bacterial uptake of DOM released from P-limited phytoplankton. FEMS Microbiology Ecology 46,

257–268.

Pujo-Pay, M., Conan, P., Raimbault, P., 1997. Excretion of dissolved organic nitrogen by phytoplankton assessed by wet oxidation and ^{15}N tracer procedures. Marine Ecology Progress Series 153, 99–111.

R Core Team, 2019. R: A Language and Environment for Statistical Computing. http://www.r-project.org/index.html

Rahav, E., Belkin, N., Paytan, A., Herut, B., 2018. Phytoplankton and bacterial response to desert dust deposition in the coastal waters of the southeastern Mediterranean Sea: A four-year in situ survey. Atmosphere 9, 305.

Raven, J. A., 1997. Phagotrophy in phototrophs. Limnology and Oceanography 42, 198–205.

Redfield, A. C., 1958. The biological control of chemical factors in the environment. American Scientist 46, 230A, 205–221.

Repeta, D. J., 2015. Chemical Characterization and Cycling of Dissolved Organic Matter. In Hansell, D., A. and Carlson, C., A. (Eds.), *Biogeochemistry of Marine Dissolved Organic Matter (second edition)*. Elsevier.

Riebesell, U., Wolf-Gladrow, D., 2002. Supply and Uptake of Inorganic Nutrients. In: Williams, P. J. l. B., Thomas, D. N., Colin, S. R. (Eds.), *Phytoplankton productivity : Carbon Assimilation in Marine and Freshwater Ecosystems*. Wiley-Blackwell.

Rimellin, P., Moutin, T., 2005. Re-examination of the Magic method to determine low orthophosphate concnetration in seawater. Analytica Chimica Acta, 548, 174–182.

Robarts, R. D., Zohary, T., Waiser, M. J., Yacobi, Z., 1996. Bacterial abundance, biomass and production in relation to phytoplankton biomass in the Levantine Basin of the southeastern Mediterranean Sea. Marine Ecology Progress Series 137, 273–281.

Rocha, C., Edwards, C. A., Roughan, M., Cetina-Heredia, P., Kerry, C., 2019. A high-resolution biogeochemical model (ROMS 3.4+bio-Fennel) of the East Australian current system. Geoscientific Model Development 12, 441–456.

Rohatgi, A., 2017. WebPlotDigitizer. http://arohatgi.info/WebPlotDigitizer.

Rosland, R., Strand, Alunno-Bruscia, M., Bacher, C., Strohmeier, T., 2009. Applying Dynamic Energy Budget (DEB) theory to simulate growth and bio-energetics of blue mussels under low seston conditions. Journal of Sea Research 62, 49–61.

Ross, O. N., Geider, R. J., 2009. New cell-based model of photosynthesis and photoacclimation: accumulation and mobilisation of energy reserves in phytoplankton. Marine Ecology Progress Series 383, 53–71.

Rothhaupt, K. O., 1996a. Laboratorary experiments with a mixotrophic chrysophyte and obligately phagotrophic and photographic competitors. Ecology 77, 716–724.

Rothhaupt, K. O., 1996b. Utilization of substitutable carbon and phosphorus sources by the mixotrophic chrysophyte Ochromonas SP. Ecology 77, 706–715.

Rothhaupt, K. O., 1997. Nutrient turnover by freshwater bacterivorous flagellates: Differences between a heterotrophic and a mixotrophic chrysophyte. Aquatic Microbial Ecology 12, 65–70.

Saad, E. M., Longo, A. F., Chambers, L. R., Huang, R., Benitez-Nelson, C., Dyhrman, S. T., Diaz, J. M., Tang, Y., Ingall, E. D., 2016. Understanding marine dissolved organic matter production: Compositional insights from axenic cultures of *Thalassiosira pseudonana*. Limnology and Oceanography 61, 2222–2233.

Safi, K. A., Hall, J. A., 1999. Mixotrophic and heterotrophic nanoflagellate grazing in the convergence zone east of New Zealand. Aquatic Microbial Ecology 20, 83–93.

Sanders, R. W., 1991. Mixotrophic Protists In Marine and Freshwater Ecosystems. The Journal of Protozoology 38, 76–81.

Sanders, R. W., Caron, D. A., Davidson, J. M., Dennett, M. R., Moran, D. M., 2001. Nutrient acquisition and population growth of a mixotrophic alga in axenic and bacterized cultures. Microbial Ecology 42, 513–523.

Sanders, R. W., Gast, R. J., 2012. Bacterivory by phototrophic picoplankton and nanoplankton in Arctic waters. FEMS Microbiology Ecology 82, 242–253.

Sato, M., Shiozaki, T., Hashihama, F., 2017. Distribution of mixotrophic nanoflagellates along the latitudinal transect of the central North Pacific. Journal of Oceanography 73, 159–168.

Schartau, M., Engel, A., Schröter, J., Thoms, S., Völker, C., Wolf-Gladrow, D., 2007. Modelling carbon overconsumption and the formation of extracellular particulate organic carbon. Biogeosciences 4, 13–67.

Selosse, M. A., Charpin, M., Not, F., 2017. Mixotrophy everywhere on land and in water: the grand écart hypothesis. Ecology Letters 20, 246–263.

Seymour, J. R., Amin, S. A., Raina, J. B., Stocker, R., 2017. Zooming in on the phycosphere: The ecological interface for phytoplankton-bacteria relationships. Nature Microbiology 2, 17065.

Sharma, S., Steuer, R., 2019. Modelling microbial communities using biochemical resource allocation analysis. Journal of the Royal Society, Interface 16, 20190474.

Sherr, B. F., Sherr, E. B., Fallon, R. D., 1987. Use of monodispersed, fluorescently labeled bacteria to estimate in situ protozoan bacterivory. Applied and environmental microbiology 53, 958–965.

Sherr, E. B., Sherr, B. F., 1994. Bacterivory and Herbivory: Key Roles of Phagotrophic Protists in Pelagic Food Webs. Microbial Ecology 28, 223–235.

Shuter, B., 1979. A model of physiological adaption in unicellular algae. Journal of Theoretical Biology 78, 519–552.

Sieburth, J. M., Smetacek, V., Lenz, J., 1978. Pelagic ecosystem structure: Heterotrophic compartments of the plankton and their relationship to plankton size fractions. Limnology

and Oceanography 23, 1256–1263.

Šimek, K., Hartman, P., Nedoma, J., Pernthaler, J., Springmann, D., Vrba, J., Psenner, R., 1997. Community structure, picoplankton grazing and zooplankton control of heterotrophic nanoflagellates in a eutrophic reservoir during the summer phytoplankton maximum. Aquatic Microbial Ecology 12, 49–63.

Siokou-Frangou, I., Bianchi, M., Christaki, U., Christou, E. D., Giannakourou, A., Gotsis, O., Ignatiades, L., Pagou, K., Pitta, P., Psarra, S., Souvermezoglou, E., Van Wambeke, F., Zervakis, V., 2002. Carbon flow in the planktonic food web along a gradient of oligotrophy in the Aegean Sea (Mediterranean Sea). Journal of Marine Systems 33-34, 335–353.

Siokou-Frangou, I., Christaki, U., Mazzocchi, M. G., Montresor, M., Ribera d' Alcalá, M., Vaqué, D., Zingone, A., 2010. Plankton in the open Mediterranean Sea : a review. Biogeosciences 7, 1543–1586.

Sousa, T., Domingos, T., Kooijman, S. a. L. M., 2008. From empirical patterns to theory: a formal metabolic theory of life. Philosophical Transactions of the Royal Society of London. Series B, Biological sciences 363, 2453–2464.

Sousa, T., Domingos, T., Poggiale, J.-C., Kooijman, S. a. L. M., 2010. Dynamic energy budget theory restores coherence in biology. Philosophical Transactions of the Royal Society of London. Series B, Biological sciences 365, 3413–3428.

Spitz, Y., Moisan, J., Abbott, M., 2001. Configuring an ecosystem model using data from the Bermuda Atlantic Time Series (BATS). Deep Sea Research II 48, 1733–1768.

Steemann-Nielsen, E., 1952. The use of radioactive carbon (14C) for measuring organic production in the sea. J. Cons. Int. Explor. Mer 18, 117–140.

Stickney, H. L., Hood, R. R., Stoecker, D. K., 2000. The impact of mixotrophy on planktonic marine ecosystems. Ecological Modelling 125, 203–230.

Stoecker, D. K., 1998. Conceptual Models of Mixotrophy in Planktonic Protists and some Ecological and Evolutionary Implications. European Journal of Protistology 34, 281–290.

Stoecker, D. K., Hansen, P. J., Caron, D. A., Mitra, A., 2017. Mixotrophy in the Marine Plankton. Annual Review of Marine Science 9, 311-335.

Strickland, J. D. H., Parsons, T. R., 1977. A practical handbook of sea water analysis. Fisheries Research Board of Canada 167, 71–76.

Talmy, D., Blackford, J., Hardman-Mountford, N., Polimene, L., Follows, M., Geider, R., 2014. Flexible C:N ratio enhances metabolism of large phytoplankton when resource supply is intermittent. Biogeosciences 11, 5179–5214.

Tanaka, T., Thingstad, T. F., Christaki, U., Colombet, J., Courties, C., Grattepanche, J., 2011. Lack of P-limitation of phytoplankton and heterotrophic prokaryotes in surface waters of three anticyclonic eddies in the stratified Mediterranean Sea. Biogeosciences 8, 525–538.

Tanaka, T., Zohary, T., Krom, M. D., Law, C. S., Pitta, P., Psarra, S., Rassoulzadegan, F.,

Thingstad, T. F., Tselepides, A., Woodward, E. M. S., Flaten, G. A. F., Skjoldal, E. F., Zodiatis, G., 2007. Microbial community structure and function in the Levantine Basin of the eastern Mediterranean. Deep-Sea Research Part I: Oceanographic Research Papers 54, 1721–1743.

Teira, E., Hernando-Morales, V., Fernández, A., Martínez-García, S., Álvarez-Salgado, X. A., Bode, A., Varela, M. M., 2015. Local differences in phytoplankton-bacterioplankton coupling in the coastal upwelling off Galicia (NW Spain). Marine Ecology Progress Series 528, 53–69.

Teira, E., Pazo, M. J., Serret, P., Fernandez, E., 2001a. Dissolved organic carbon production by microbial populations in the Atlantic Ocean. Limnology and Oceanography 46, 1370–1377.

Teira, E., Serret, P., Fernández, E., 2001b. Phytoplankton size-structure, particulate and dissolved organic carbon production and oxygen fluxes through microbial communities in the NW Iberian coastal transition zone. Marine Ecology Progress Series 219, 65–83.

Teixeira, C. M., Sousa, T., Marques, G. M., Domingos, T., Kooijman, S. A., 2014. A new perspective on the growth pattern of the Wandering Albatross (Diomedea exulans) through DEB theory. Journal of Sea Research 94, 117–127.

Terrado, R., Pasulka, A., Lie, A. A., Orphan, V. J., Heidelberg, K. B., Caron, D. A., 2017. Autotrophic and heterotrophic acquisition of carbon and nitrogen by a mixotrophic chrysophyte. The ISME journal 11, 2022–2034.

Thingstad, T. F., Rassoulzadegan, F., 1995. Nutrient limitations, microbial food webs, and biological C-pumps: Suggested interactions in a P-limited Mediterranean. Marine Ecology Progress Series 117, 299–306.

Thingstad, T.F., Rassoulzadegan, F., 1999. Conceptual models for the biogeochemical role of the photic zone microbial food web, with particular reference to the Mediterranean Sea. Progress in Oceanography 44, 271–286.

Thingstad, T. F., Havskum, H., Garde, K., Riemann, B., 1996. On the Strategy of "Eating Your Competitor": A Mathematical Analysis of Algal Mixotrophy. Ecology 77, 2108–2118.

Thingstad, T. F., Hagström, Å., Rassoulzadegan, F., 1997. Accumulation of degradable DOC in surface waters: Is it caused by a malfunctioning microbial loop? Limnology and Oceanography 42, 398–404.

Thingstad, T. F, Krom, M. D, Mantoura, R. F. C., Flaten, G. A. F, Groom, S., Herut, B., Kress, N., Law, C. S., Pasternak, A., Pitta, P., Psarra, S., Rassoulzadegan, F., Tanaka, T., Tselepides, A., Wassmann, P., Woodward, E. M. S., Wexels Riser, C., Zodiatis, G., Zohary, T., 2005. Nature of P limitation in the ultraoligotrophic Eastern Mediterranean. Science 309, 1068–1071.

Thingstad, T., 2005. Simulating the response to phosphate additions in the oligotrophic eastern Mediterranean using an idealized four-member microbial food web model. Deep-Sea Research Part II: Topical Studies in Oceanography 52, 3074–3089.

Thornton, D. C. O., 2014. Dissolved organic matter (DOM) release by phytoplankton in the contemporary and future ocean . European Journal of Phycology 49, 20–46.

Tittel, J., Bissinger, V., Zippel, B., Gaedke, U., Bell, E., Lorke, A., Kamjunke, N., 2003. Mixotrophs combine resource use to outcompete specialists: implications for aquatic food webs. PNAS 100, 12776–12781.

Troost, T., Kooi, B., Kooijman, S., 2005a. Ecological Specialization of Mixotrophic Plankton in a Mixed Water Column. The American Naturalist 166, E45–E61.

Troost, T. A., Kooi, B. W., Kooijman, S. A. L. M., 2005b. When do mixotrophs specialize? Adaptive dynamics theory applied to a dynamic energy budget model. Mathematical Biosciences 193, 159–182.

Tsai, A. Y., Chiang, K. P., Chan, Y. F., Lin, Y. C., Chang, J., 2007. Pigmented nanoflagellates in the coastal western subtropical Pacific are important grazers on Synechococcus populations. Journal of Plankton Research 29, 71–77.

Tsai, A. Y., Gong, G. C., Sanders, R. W., Chen, W. H., Chao, C. F., Chiang, K. P., 2011. Importance of bacterivory by pigmented and heterotrophic nanoflagellates during the warm season in a subtropical western Pacific coastal ecosystem. Aquatic Microbial Ecology 63, 9–18.

Tsiaras, K. P., Christodoulaki, S., Petihakis, G., Frangoulis, C., Triantafyllou, G., 2017. Model simulations of a mesocosm experiment investigating the response of a Low Nutrient Low Chlorophyll (LNLC) marine ecosystem to atmospheric deposition events. Frontiers in Marine Science 4, 120.

Turley, C. M., Bianchi, M., Christaki, U., Conan, P., Harris, J. R. W., Psarra, S., Ruddy, G., Stutt, E. D., Tselepides, A., Van Wambeke, F., 2000. Relationship between primary producers and bacteria in an oligotrophic sea - The Mediterranean and biogeochemical implications. Marine Ecology Progress Series 193, 11–18.

Uitz, J., Claustre, H., Gentili, B., Stramski, D., 2010. Phytoplankton class-specific primary production in the world's oceans: Seasonal and interannual variability from satellite observations. Global Biogeochemical Cycles 24, GB3016.

Underwood, G. J. C., Boulcott, M., Raines, C., 2004. Environmental effects on exopolymer production by marine benthic diatoms: dynamics, changes in composition, and pathways of production. Journal of Phycology 40, 293–304.

Unrein, F., Massana, R., Alonso-Sáez, L., Gasol, J. M., 2007. Significant year-round effect of small mixotrophic flagellates on bacterioplankton in an oligotrophic coastal system. Limnology and Oceanography 52, 456–469.

Unrein, F., Gasol, J. M., Not, F., Forn, I., Massana, R., 2014. Mixotrophic haptophytes are key bacterial grazers in oligotrophic coastal waters. The ISME Journal 8, 164–176.

Urbani, R., Magaletti, E., Sist, P., Cicero, A. M., 2005. Extracellular carbohydrates released by the marine diatoms *Cylindrotheca closterium*, *Thalassiosira pseudonana* and

Skeletonema costatum: Effect of P-depletion and growth status. Science of the Total Environment 353, 300–306.

Våge, S., Castellani, M., Giske, J., Thingstad, T. F., 2013. Successful strategies in size structured mixotrophic food webs. Aquatic Ecology 47, 329–347.

Vallino, J., 2000. Improving marine ecosystem models: use of data assimilation and mesocosm experiments. Journal of Marine Research 58, 117–164.

Van Den Meersche, K., Middelburg, J. J., Soetaert, K., van Rijswijk, P., Boschker, H. T. S., Heip, C. H. R., 2004. Carbon-nitrogen coupling and algal-bacterial interactions during an experimental bloom: Modeling a 13 C tracer experiment. Limnology and Oceanography 49, 862–878.

Wambeke, F., Christaki, U., Bianchi, M., Psarra, S., Tselepides, A., 2000. Heterotrophic bacterial production in the Cretan Sea (NE Mediterranean). Progress in Oceanography 46, 205–216.

Van Wambeke, F., Christaki, U., Giannakourou, A., Moutin, T., Souvemerzoglou, K., 2002. Longitudinal and vertical trends of bacterial limitation by phosphorus and carbon in the Mediterranean Sea. Microbial Ecology 43, 119–133.

Vaqué, D., Boras, J. A., Torrent-Llagostera, F., Agustí, S., Arrieta, J. M., Lara, E., Castillo, Y. M., Duarte, C. M., Sala, M. M., 2017. Viruses and Protists Induced-mortality of Prokaryotes around the Antarctic Peninsula during the Austral Summer Frontiers in Microbiology 8, 241.

Vaqué, D., Calderón-Paz, J. I., Guixa-Boixereu, N., Pedrós-Alió, C., 2002. Spatial distribution of microbial biomass and activity (bacterivory and bacterial production) in the northern Weddell Sea during the austral summer (January 1994). Aquatic Microbial Ecology 29, 107–121.

Varkitzi, I., Psarra, S., Assimakopoulou, G., Pavlidou, A., Krasakopoulou, E., Velaoras, D., Papathanassiou, E., Pagou, K., 2020. Phytoplankton dynamics and bloom formation in the oligotrophic Eastern Mediterranean: Field studies in the Aegean, Levantine and Ionian seas. Deep-Sea Research Part II: Topical Studies in Oceanography 171, 104662.

Vaulot, D., LeBot, N., Marie, D., Fukai, E., 1996. Effect of phosphorus on the *Synechococcus* cell cycle in surface Mediterranean waters during summer. Applied and Environmental Microbiology 62, 2527–2533.

Vázquez-Domínguez, E., Peters, F., Gasol, J. M., Vaqué, D., 1999. Measuring the grazing losses of picoplankton: Methodological improvements in the use of fluorescently labeled tracers combined with flow cytometry. Aquatic Microbial Ecology 20, 119–128.

Velaoras, D., Papadopoulos, V. P., Kontoyiannis, H., Cardin, V., Civitarese, G., 2018. Water masses and hydrography during April and June 2016 in the Cretan Sea and Cretan Passage (Eastern Mediterranean Sea). Deep Sea Research Part II: Topical Studies in Oceanography 164, 25–40.

Vichi, M., Pinardi, N., Masina, S., 2007. A generalized model of pelagic biogeochemistry.for the global ocean ecosystem. Part I: Theory. Journal of Marine Systems 64, 89–109.

Vidussi, F., Claustre, H., Manca, B. B., Luchetta, A., Jean-Claude, M., 2001. P Phytoplankton pigment distribution in relation to upper thermocline circulation in the eastern Mediterranean Sea during winter. Journal of Geophysical Research 106, 939–956.

Ward, B. A., Dutkiewicz, S., Barton, A. D., Follows, M. J., 2011. Biophysical aspects of resource acquisition and competition in algal mixotrophs. The American naturalist 178, 98–112.

Ward, B. A., Follows, M. J., 2016. Marine mixotrophy increases trophic transfer efficiency, mean organism size, and vertical carbon flux. Proceedings of the National Academy of Sciences 113, 2958–63

Wear, E. K., Carlson, C. A., James, A. K., Brzezinski, M. A., Windecker, L. A., Nelson, C. E., 2015a. Synchronous shifts in dissolved organic carbon bioavailability and bacterial community responses over the course of an upwelling-driven phytoplankton bloom. Limnology and Oceanography 60, 657–677.

Wear, E. K., Carlson, C. A., Windecker, L. A., Brzezinski, M. A., 2015b. Roles of diatom nutrient stress and species identity in determining the short- and long-term bioavailability of diatom exudates to bacterioplankton. Marine Chemistry 177, 335–348.

Wetz, M. S., Wheeler, P. A., 2004. Response of bacteria to simulated upwelling phytoplankton blooms. Marine Ecology Progress Series 272, 49–57.

Wilken, S., Soares, M., Urrutia-Cordero, P., Ratcovich, J., Ekvall, M. K., Van Donk, E., Hansson, L. A., 2018. Primary producers or consumers? Increasing phytoplankton bacterivory along a gradient of lake warming and browning. Limnology and Oceanography 63, S142–S155.

Wilken, S., Yung, C., Hamilton, M., Hoadley, K., Nzongo, J., Eckmann, C., Corrochano Luque, M., Poirier, C., Worden, A. Z., 2019. The need to account for cell biology in characterizing predatory mixotrophs in aquatic environments. Philosophical Transactions B 374, 20190090

Wilken, S., Choi, C. J., Worden, A. Z., 2020. Contrasting Mixotrophic Lifestyles Reveal Different Ecological Niches in Two Closely Related Marine Protists. Journal of Phycology 56, 52–67.

Wood, A., Van Valen, L., 1990. Paradox lost? On the release of energy-rich compounds by phytoplankton. Marine Macriobial Food Webs 4, 103–116.

Worden, A., Nolan, J., Palenik, B., 2004. Assessing the dynamics and ecology of marine picophytoplankton: the importance of the eukaryotic component. Limnology and Oceanography 49, 168–179.

Worden, A. Z., Follows, M. J., Giovannoni, S. J., Wilken, S., Zimmerman, A. E., Keeling, P. J., 2015. Rethinking the marine carbon cycle: Factoring in the multifarious lifestyles of

microbes. Science 347, 1257594.

Zohary, T., Robarts, R. D., 1992. Bacterial numbers, bacterial production, and heterotrophic nanoplankton abundance in a warm core eddy in the Eastern Mediterranean. Marine Ecology Progress Series 84, 133–137.

Zohary, T., Robarts, R. D., 1998. Experimental study of microbial P limitation in the eastern Mediterranean. Limnology and Oceanography 43, 387–395.

Zohary, T., Herut, B., Krom, M. D., Fauzi, R., Pitta, P., Psarra, S., Rassoulzadegan, F., Stambler, N., Tanaka, T., Frede Thingstad, T., Malcolm, E., 2005. P-limited bacteria but N and P co-limited phytoplankton in the Eastern Mediterranean - A microcosm experiment. Deep-Sea Research Part II: Topical Studies in Oceanography 52, 3011–3023.

Zubkov, M. V., Tarran, G. A., 2008. High bacterivory by the smallest phytoplankton in the North Atlantic Ocean. Nature 455, 224–226.